

University of Nottingham
UK | CHINA | MALAYSIA

High Sulphur Activated Carbon Regeneration

Christopher James Powell, MChem

Thesis submitted to the University of Nottingham

for the degree of Engineering Doctorate (EngD)

March 2023

Abstract

Companies such as CPL Ltd, who specialise in the production and regeneration of activated carbon, are looking at ways in which they can reduce their impact on the climate by switching to greener methods for their operations. At current, their aim is to move towards producing more regenerated activated carbon rather than procuring virgin carbonaceous material such as coal. However, their current regeneration method, a conventional thermal method, entails long processing times which require vast amounts of fossil fuels and consume large quantities of energy. Additionally, the regeneration of spent sulphurous activated carbon via thermal regeneration results in the production of sulphuric and sulphurous acids, which cause structural damage to their equipment and present a health & safety issue with their workforce. The company have been looking into possible replacement methodologies including the use of microwave technology, with the hope that the volumetric and selective heating involved can reduce their carbon footprint and reduce/eliminate the production of unwanted by-products.

The aim of this research was to study the effects if microwave heating on spent sulphurous activated carbons and whether a process could be developed that would provide a suitable replacement for their current method. This would go on to become a matter of process development as the study was carried out.

The effects of exposing the spent sulphurous activated carbon samples directly to microwaves via a high-density electromagnetic field were studied and found to cause localised overheating. The microwave energy absorbed by the adsorbates was converted into heat energy, which resulted in damage to the surrounding carbon structure. However, the butane activity of this initial method was found to return adsorptivity to a relatively high degree, being 33.43 % (+/- 0.87 std) compared to the thermal methods 40.88 % (+/- 0.92 std). This was achieved over the course of 360s as opposed to upwards of 6 hours needed for thermal regeneration. There were no signs of sulphuric or sulphurous acid having been produced which was a result of being able to remove the steam activation stage needed for thermal regeneration methods.

The next stage of process development involved exposing the spent sulphurous activated carbon samples directly to microwaves via a low-density electromagnetic field to reduce the

localised overheating. With this, the idea being that the more chaotic way low-density fields interact with a target would allow for a slower rate of heating, thus reducing the damage caused by the heat energy emitted from the desorbing sulphurous adsorbates. However, although to a lesser extent than seen in the initial study, the technique still led to damage to the carbon structure, resulting in a loss of potential returned adsorptivity. Additionally, the use of a multimode waveguide cavity also resulted in a different heating profile. The butane activity was also found to be lesser than that of high-density field exposure (32.78 % (+/- 0.03 std) at best – at 800 W over 360s), due to reduced number of incidents between microwaves and the samples. Extended irradiation times did show that certain sulphurous adsorbates desorb before others, and that damage to the carbon structure increased as irradiation time increased. This suggested that the rate at which the desorbing material was desorbing and exiting the activated carbon was determining how much damage was being caused to the carbon structure – exiting at a rate at which emitted heat energy could cause more damage.

A third iteration of microwave processing was established which utilised an inert gas flow directly over the samples during irradiation to control the rate of mass transfer. This design resulted in butane activities surpassing that seen in thermal regeneration, reaching 48.34 % (+/- 1.20 std), and greatly reduced the damage being caused to the overall activated carbon structure. This was achieved by increasing the rate at which material desorbed during the initial stages of irradiation, and by increasing the rate at which desorbed materials were removed from the activated carbon pores. Additionally, the heating rate could be controlled via controlling the microwave power, which gave rise to higher internal pressure and vapor velocity, promoting more efficient removal of adsorbates from the carbon surface. Moreover, the increasing vapor velocity and internal pressure served to perpetuate removal of adsorbates with stronger chemical interactions.

The final method was found to be more efficient than the currently used thermal methods: reducing the processing time from several hours of a matter of minutes; eliminating the production of unwanted acidic by-products; and, increasing the achievable adsorptivity level.

Acknowledgements

I would like to first thank the Faculty of Engineering at the University of Nottingham for providing me with the opportunity to undertake this doctorate in chemical engineering. I would also like to thank CPL Ltd for sponsoring my research project and making the opportunity available.

I would like to express my deepest gratitude to my EngD supervisors, Dr Will Meredith, Dr Andrew Gill and Professor John Robinson for their continuous support, patience, motivation, and immense knowledge. Their guidance and friendship over the years helped to keep me going even when times were tough. Many thanks to my assessors for their constructive comments and valuable feedback.

My appreciation extends to the researchers, technicians, and fellow postgraduate research students belonging to both my research group (the Biomass Research Group), and to my centre for doctoral training (the Carbon Capture and Storage & Cleaner Fossil Energy Group). All of whom supported me through this journey.

Finally, a special thanks to my family for their love, support, and constant encouragement. And, to the family I found at the University of Nottingham, the researchers of Coates C3/4 offices (the Johnson Arms crew), without whom I would have surely lost the will to finish.

Table of Contents

Abstract 2
Acknowledgements 4
Table of Contents 5
List of Figures 8
List of Tables 13
1. Introduction 17
2. Literature review 20
2.1 Activated Carbon 20
2.1.1 Historical and current applications of activated carbons 20
2.1.2 Physical properties of activated carbons 22
2.1.3 Adsorption mechanisms 25
2.1.4 Production methods and activation of activated carbons 38
2.2 Regenerating activated carbons 40
2.2.1 Finical incentives for regeneration 41
2.2.2 Established regeneration methods 43
2.3 Microwave technology and regeneration 50
2.3.1 Conventional radiant heating process 50
2.3.2 Microwave heating process 51
2.3.3 Microwave structure 59
2.3.4 Regeneration of activated carbons by microwave heating 62
2.4 Regenerating spent sulphurous activated carbon 63
2.4.1 Adsorption mechanics of sulphurous compounds 63
2.4.2 The issues with regenerating spent sulphurous activated carbon 67
2.5 Literature conclusions 71
3. Experimental methodologies 73
3.1 Activated carbon materials involved in this study 73
3.2 Material characterisation 74
3.2.1 Sample preparation 74
3.2.2 Sample analysis 75
4. Method development 79
4.1 Adsorption capability 79
4.2 Sulphur species identification and distribution 79
4.3 Electron Micropore Analysis 81
4.4 Thermal Regeneration 83
4.5 Processing options for microwave heating 85

5. Microwave heating of spent sulphurous activated carbon: initial process design . 87
5.1 Introduction 87
5.2 Properties influencing microwave heating of porous carbon 88
5.3 High Field Density 89
5.3.1 Single-mode cavity – Preliminary experiments 90
5.3.2 Single-mode cavity – Reducing Overheating 100
5.4 Conclusions 114
6. Low-density electric field processing 115
6.1 Introduction 115
6.2 Background 115
6.3 Multimode waveguide cavity design 117
6.4 Effects of low-density electromagnetic field on microwave regeneration of spent sulphurous activated carbon 119
6.4.1 Preliminary study of microwave irradiation time when using a low-density electromagnetic field 119
6.4.2 Preliminary study of microwave power on desorption when using a low-density electromagnetic field 122
6.4.3 In-depth studies of low-field density effects on microwave regeneration of spent sulphurous activated carbon 123
6.5 Conclusions 131
7. Manipulating mass transfer mechanics via inert gas flow 133
7.1 Introduction 133
7.2 Background 133
7.3 Mass transfer experimental design 135
7.4 Manipulating mass transfer of sulphurous compounds desorbing from activated carbon – preliminary experiments 137
7.4.1 High-density field 137
7.4.2 Low-density field 144
7.5 Manipulating mass transfer of sulphurous compounds desorbing from activated carbon – heated gas flow 150
7.5.1 Gas flowrate 151
7.5.2 Gas temperature 152
7.5.3 Microwave power 155
7.5.4 Irradiation time 157
7.5.5 Effects on sulphur chemistry and distribution 160
7.6 Conclusions 164
8. Conclusions & Future Work 166
8.1 Effects of MW irradiation 166
8.2 Low-density field 167
8.3 Mass transfer manipulation mechanism 169

8.4 Future work 170
9. References 174
10. Appendix 196
10.1 Appendix A – Methods 196
10.2 Appendix B – All data for tables 200
10.3 Appendix C – Additional EPMA data 219

List of Figures

Figure 1. Different pore structures of activated carbon [52]. 24
Figure 2. Adsorption onto a solid (a) Physisorption: weak, long range Van der Waals forces, multilayer adsorption (b) Chemisorption: strong, short-range forces involving orbital overlap and electron exchange [61]. 26
Figure 3. The change in potential energy for the adsorbate molecule as the size of slit-shape molecules decrease from left to right [64]. 27
Figure 4. Nitrogen adsorption-desorption plot for a porous structure [29] [61] [62].....28
Figure 5. Primary adsorption and desorption isotherms hysteresis loop [68]. 29
Figure 6. The six major types of isotherms in BDDT classification [29]. 30
Figure 7. The hysteresis loop classification by IUPC [69]. 31
Figure 8. Pores with similar internal surface area, but different adsorption capacities [61]....34
Figure 9. Characteristic t-plot curves [61].....35
Figure 10. SEM micrographs of walnut char activated with lower doses of KOH (left) and higher doses of KOH (right) [81]. 39
Figure 11. Comparison of ROI as a function of AC sales prices [88]. 43
Figure 12. Comparison of NPV for 10-Year Investment life as a function of AC sales price [88]. 43
Figure 13. Methylene Blue adsorption/desorption study on (a) activated carbon, and (b) Fe-impregnated activated carbon (H2SO4 as desorbing agent) [106]. 49
Figure 14. The difference in temperature distribution and direction of heat transfer between conventional and microwave heating: (A) conventional heating – heat is transferred from the outside of the material inwards by conduction, (B) microwave heating – MWs penetrate the material and heat volumetrically. Energy is uniformly dissipated throughout the material [108]. 51
Figure 15. Mechanisms of polarisation: (a) dipole, (b) atomic, (c) electronic, (d) Maxwell-Wagner (interfacial) polarisation [129]. 54
Figure 16. Travelling Electromagnetic wave through a dielectric loss [132].....55
Figure 17. Phase diagrams for (a) an ideal dielectric where the energy is transmitted without loss; (b) where there is a phase displacement, δ, and the current acquires a component I 3

sinδ in-phase with the voltage and consequently there is a dissipation of energy. In (c) the relationship between ε*, ε' and ε'' is illustrated; tanδ = ε''/ε' [133].....56
Figure 18. The relation between power absorbed per unit volume and dielectric loss [130]...57
Figure 19. Schematic diagram of mechanical structure for a typical microwave oven [136]....60
Figure 20. Schematic diagram of a magnetron [137]. 60
Figure 21. Horizontal mode structure in microwave cavity using infrared thermal imaging, while heating thin layer of water on a glass plate [138]. 62
Figure 22. ISO corrosion chart for H2SO4 [162][163].....69
Figure 23. Proposed mechanism for H2S corrosion of Fe [165].....70
Figure 24. Spent activated carbon samples – (left to right) pellet, large granule, small granule, moderately fine powder. 74
Figure 25. Carbon tetrachloride activity versus butane activity [170] 75
Figure 26. The experimental setup for CTC activity analysis of spent activated carbon.....76
Figure 27. XRD diffractogram of spent sulphurous AC pellet surface. 81
Figure 28. (top) EPMA scan of a cross section of non-regenerated spent sulphurous activated carbon with sulphur percentages shown at randomly selected areas across the pellet. 82
Figure 29. XRD diffractogram of thermally regenerated AC pellet surface.....84
Figure 30. EPMA scan of a cross section of the edge of a of thermally regenerated sulphurous activated carbon. 85
Figure 31. Experimental setup for spent sulphurous AC regeneration in custom-built MW rig. 90
Figure 32. EPMA scan of a cross section of the edge of a of MW regenerated sulphurous activated carbon at 400 W for 360s. 94
Figure 33. Cold trap and activated carbon trap used in the experimental setup to trap sulphurous compounds being desorbed from the sample sulphurous activated carbon. 97
Figure 34. XRD diffractogram of preliminary MW regeneration experiments: base sample - black; 200 W– red; 400 W – pink; 600 W – blue; and 800 W – green.....98
Figure 35. EPMA scan of a cross section of the edge of MW regenerated sulphurous activated carbon at 400 W for 360s intermittently.....103
Figure 36. XRD diffractogram of intermittent irradiation MW regeneration experiments: base sample – black; 200 W– red; 400 W – pink; 600 W – blue; and 800 W – green. 104

Figure 37. Experimental setup for spent sulphurous AC regeneration, using a solvent bathing method, and the custom-built MW rig. 106
Figure 38. EPMA scan of a cross section of the edge of a of hexane-bathed MW regenerated sulphurous activated carbon at 400W for 360s. 110
Figure 39. EPMA scan of a cross section of the edge of a of kerosene-bathed MW regenerated sulphurous activated carbon at 400W for 360s. 111
Figure 40. Schematic drawing of the electromagnetic field density distribution in a single-mode MW waveguide [198]. 116
Figure 41. Schematic drawing of the electromagnetic field density distribution in a multimode MW waveguide [198]. 116
Figure 42. Experimental setup for spent sulphurous AC in custom-built MW rig using multimode waveguide reactor cavity. 118
Figure 43. Increase in the degree of achieved butane activity with the specific energy input, with respects to increasing microwave irradiation time, for spent sulphurous activated carbon regenerated using a single-mode waveguide cavity reactor versus using a multimode waveguide cavity 121
Figure 44. Increase in the degree of achieved butane activity with the specific energy input, with respects to increasing microwave power, for spent sulphurous activated carbon regenerated using a single-mode waveguide cavity reactor versus using a multimode waveguide cavity reactor. 123
Figure 45. Increase in butane activity with the increase in microwave irradiation time for spent sulphurous activated carbon regenerated using a multimode waveguide cavity reactor. 127
Figure 46. Butane activity versus specific energy input, with respects to increasing irradiation time, using a multimode waveguide cavity reactor. 128
Figure 47. EPMA scan of a cross section of the edge of a of sample regenerated at 800 W over 360s using a multimode waveguide cavity reactor. 130
Figure 48. Experimental setup for spent sulphurous AC regeneration in custom-built MW rig utilising inert gas flow directly over the samples to aid in mass transfer of desorbing material. 136
Figure 49. Increase in butane activity with the increase in specific energy input for spent sulphurous activated carbon regenerated using a single-mode waveguide cavity and inert gas flow directly over the samples. 140

Figure 50. Increase in butane activity with the increase in irradiation time for spent sulphurous activated carbon regenerated using a single-mode waveguide cavity and inert gas flow directly over the samples.....141
Figure 51. EPMA scan of a cross section of the edge of a of sample regenerated at 200 W over 1200s using a single-mode waveguide cavity reactor and continuous inert gas flow over the sample bed.....142
Figure 52. XRD analysis of sample regenerated at 200 W over 360s using a single-mode waveguide cavity and inert gas flow directly over samples. 143
Figure 53. XRD analysis of sample regenerated at 200 W over 960s using a single-mode waveguide cavity and inert gas flow directly over samples. 143
Figure 54. Increase in butane activity with the increase in specific energy input for spent sulphurous activated carbon regenerated using a multimode waveguide cavity and inert gas flow directly over the samples.....146
Figure 55. Increase in butane activity with the increase in irradiation time for spent sulphurous activated carbon regenerated using a multimode waveguide cavity and inert gas flow directly over the samples.....147
Figure 56. EPMA scan of a cross section of the edge of a of sample regenerated at 200 W over 1200s using a multimode waveguide cavity reactor and continuous inert gas flow over the sample bed.....148
Figure 57. XRD analysis of sample regenerated at 200 W over 360s using a multimode waveguide cavity and inert gas flow directly over samples. 149
Figure 58. XRD analysis of sample regenerated at 200 W over 960s using a multimode waveguide cavity and inert gas flow directly over samples. 150
Figure 59. Effect of increasing inert gas flow temperature on the butane activity achieved during MW regeneration. MW power set to 200 W, with a N_2 flowrate of 2 $L.min^{-1}$.....154
Figure 60. Comparison of butane activity – specific energy input relationship when utilising inert gas flow at 160 ^{O}C as opposed ambient temperature. MW set to 200 W, with the N_2 flowrate at 2.0 $L.min^{-1}$.....159
Figure 61. EPMA scan of a cross section of activated regenerated at 200 W over 960s using a single-mode waveguide cavity reactor that utilised inert gas flow (N_2 at 2.00 $L.min^{-1}$, 160 ^{0}C) directly over the sample. 160

Figure 62. XRD analysis of sample regenerated at 200 W over 360s using a single-mode waveguide cavity and heated inert gas flow directly over samples. The gas flowrate was 2.00 $L.min^{-1}$, at 160 .C. 162
Figure 63. XRD analysis of sample regenerated at 200 W over 960s using a single-mode waveguide cavity and heated inert gas flow directly over samples. The gas flowrate was 2.00 $L.min^{-1}$, at 160 ^{0}C. 163
Figure 64. XRD analysis of sample regenerated at 200 W over 1200 using a single-mode waveguide cavity and heated inert gas flow directly over samples. The gas flowrate was 2.00 $L.min^{-1}$, at 160 ^{0}C. 163

List of Tables

Table 1. Properties of some raw materials used in the manufacturing of activated carbons [49]. 23
Table 2. Costs and economic evaluation of an activated carbon production plant, US $, producing 4.5t a day via chemical activation and zero raw materials cost [87]. 41
Table 3. Costs and economic evaluation of an activated carbon production plant, US $, producing 4.5t a day via physical activation and zero raw materials cost [87].....42
Table 4. Effects of MW irradiation time on AC butane activity and specific energy input using 400 W power. Standard deviation (+/- x.xx) shown was calculated for each result from the corresponding results in Appendix B. 92
Table 5. Effects of MW power on AC butane activity and specific energy input. Standard deviation (+/- x.xx) shown was calculated for each result from the corresponding results in Appendix B. 95
Table 6. Effects of intermittent MW irradiation time on AC butane activity and specific energy. Standard deviation (+/- x.xx) shown was calculated for each result from the corresponding results in Appendix B. 102
Table 7. [a] obtained from Green and Perry [191], [b] obtained from the safety data sheet provided by the supplier [192] [193]. 106
Table 8. Table 8. Effects of MW irradiation time on AC butane activity and specific energy input using 400 W power whilst samples were bathed in hexane or kerosene. Standard deviation (+/- x.xx) shown was calculated for each result from the corresponding results in Appendix B. 108
Table 9. Effects of MW power on AC butane activity and specific energy when AC samples were bathed in hexane or kerosene. Standard deviation (+/- x.xx) shown was calculated for each result from the corresponding results in Appendix B. 112
Table 10. Effects of MW irradiation time on AC butane activity and specific energy input using 400 W power in a multimode waveguide reactor cavity. Standard deviation (+/- x.xx) shown was calculated for each result from the corresponding results in Appendix B. 119
Table 11. Effects of MW power on AC butane activity and specific energy using a multimode waveguide reactor cavity. Standard deviation (+/- x.xx) shown was calculated for each result from the corresponding results in Appendix B. 122

Table 12. In-depth study of the effects of MW power on AC butane activity and specific energy input using a multimode waveguide reactor cavity. Standard deviation (+/- x.xx) shown was calculated for each result from the corresponding results in Appendix B. 124
Table 13. In-depth study of the effects of MW irradiation time on AC butane activity and specific energy input using 400 W power in a multimode waveguide reactor cavity. Standard deviation (+/- x.xx) shown was calculated for each result from the corresponding results in Appendix B. 126
Table 14. Preliminary study of the effects of MW power and irradiation time on regeneration when utilising inert gas flow directly over the AC samples in a single-mode waveguide cavity. Standard deviation (+/- x.xx) shown was calculated for each result from the corresponding results in Appendix B. 138
Table 15. Preliminary study of the effects of MW power and irradiation time on regeneration when utilising inert gas flow directly over the AC samples in a multimode waveguide cavity. Standard deviation (+/- x.xx) shown was calculated for each result from the corresponding results in Appendix B. 145
Table 16. Analysis of the effects of flowrate of heated inert gas on butane activity and mass loss from MW regeneration of the spent sulphurous AC. The MW being set to 200W, irradiated over 180s, with the N2 temperature being 160 ^{o}C. Standard deviation (+/- x.xx) shown was calculated for each result from the corresponding results in Appendix B. 152
Table 17. Analysis of impact of inert gas flow temperature on the mass change and butane activity. Experiments run at 200 W MW power, with a N_2 flowrate of 2.00 L.min^{-1}. Standard deviation (+/- x.xx) shown was calculated for each result from the corresponding results in Appendix B. 153
Table 18. Effects of MW power on mass change, butane activity, and specific energy input when utilising heated inert gas flow. The gas flowrate was at 2 L.min^{-1} and the gas temperature was at 160 ^{o}C. Standard deviation (+/- x.xx) shown was calculated for each result from the corresponding results in Appendix B. 156
Table 19. Effects of irradiation time on mass change, butane activity, and specific energy input when utilising heated inert gas flow. The gas flowrate was at 2 L.min^{-1} and the gas temperature was at 160 ^{o}C. Microwave power was kept constant at 200 W. Standard deviation (+/- x.xx) shown was calculated for each result from the corresponding results in Appendix B. 158

Abbreviations

AC	Activated carbon
MW	Microwave
CTC	Carbon tetrachloride analysis (modern day approach uses butane gas)
CPL	Coal Products Ltd (the sponsors of this research project)
EPMA	Electron Probe Microanalysis
XRD	X-ray Powder Diffraction
std	Standard deviation

Terminology

Impregnate	Compound bedded into AC to aid in
Spent	Activated carbon with little-to-no adsorption sites available for adsorption as they are taken by adsorbents
Regeneration	The process by which adsorbents are removed from the surface of activated carbon to allow for adsorption of new adsorbents

Nomenclature

ϑ	The number of adsorption sites of the surface which are covered with gaseous molecules
V	Volume of Gas adsorbed, m^3
V_m	Volume of gas adsorbed forming a monolayer, m^3
P	Pressure at equilibrium
K	Langmuir empirical constant (equilibrium constant of the adsorption and desorption rates for the adsorbate)
p	Partial saturation pressure of the adsorptive gas in equilibrium with surface
p_o	Saturation pressure of gas at temperature of measurement
p/p_o	Relative pressure
C	BET constant

A	Monolayer capacity
A_m	The adsorbate molecular projected area (0.162 nm^2 for nitrogen at 77K)
N_A	Avogadro's constant (6.023 x 10^{23} mol^{-1})
t	Average thickness of the adsorbate layer
σ	Average thickness of a single layer of gas molecules
q_e	Amount of solute adsorbed per unit weight adsorbed
C_e	Equilibrium concentration of solute
K_f	Constant related adsorption capacity
$1/n$	Constant related to adsorption intensity (the higher this value, the more favourable the adsorption ~ n<1 or 1/n>1
n	Energy heterogeneity of the adsorption intensity of affinity
Q_o	Amount of solute adsorbed per unit weight of adsorbent required for monolayer coverage
K	Langmuir empirical constant (equilibrium constant of the adsorption and desorption rates for the adsorbate)
E	Electric field intensity, $V.m^{-3}$
E_0	Amplitude of the electric field
γ	Propagation factor
ε	The material's permittivity
μ	Permeability
ε^*	Dielectric constant for a real dielectric expressed in terms of permittivity
ε'	Relative dielectric constant
ε''	Effective dielectric loss factor
δ	Loss angle
P_A	Power adsorbed per unit volume
f	Frequency, Hz
ε_0	Free space permittivity (8.854 x 10^{-12} $F.m^{-1}$)
E_{rms}	The root mean square of the electric field strength in the material (V/m)
D_p	Penetration depth, m
C	Speed of light in a vacuum

1. Introduction

Activated carbon (AC) is a generic term used to describe any carbonaceous material subjected to controlled thermal treatments, to increase the level of porosity. Due to its high internal surface area and pore volume, AC is a powerful adsorbent [1] [2]. First recognised by the ancient Egyptians, the properties of ACs have seen them used as a contaminant removal tool for thousands of years. In modern times, AC has become a commodity chemical of significant importance to many sectors of industry. For example, the most common uses are for the separation/purification of liquid and gases and the recovery of solvent, with newer applications such as catalyst support, super-capacitors, batteries and electrodes [3] [4] [5].

Once AC has been applied to the intended environment, and the contaminant has been adsorbed, a few key issues present themselves. Having adsorbed as much of the contaminant compound onto the carbon's surface as possible, the user is left with waste in the form of spent AC. Historically, this spent AC would be disposed of; potentially incurring expensive financial costs if the adsorbed material was a health or environmental hazard [6]. Also, owing to the high temperatures and energy demand required to produce ACs from raw carbonaceous materials, the other major issue being that ACs are financially expensive to produce [7]. This high cost of production would then pass onto the consumer. However, the costs of production, and the consequent cost of purchase, for ACs can be reduced via regeneration methods.

Several methods for the regeneration of AC have been established, such as thermal, chemical, electrochemical, and many more. The two most common forms of regeneration are thermal and chemical. Thermal involves first drying the spent AC at 200 ^{o}C to remove moisture and light volatiles, then pyrolysis at 400-600 ^{o}C to remove more volatile compounds, and finally the reactivation at 800-1000 ^{o}C in carbon dioxide and/or steam to remove the last of the volatile compounds [8]. Chemical regeneration utilises suitable chemical reagents that will react with the adsorbed material and remove it from the surface of the AC [9]. Reagents used in chemical regeneration tend to be either oxidising agents, or solvents chosen specifically because they solubilise the adsorbed material [9]. Both popular methods of regeneration are well proven and are considered mature technologies at this point. However, both do present significant disadvantages to their use.

Both thermal and chemical regeneration have several disadvantages in their use, with some incurring costs verging towards that of producing of virgin ACs. The biggest issue with thermal being that it requires extremely high temperatures (up to 1000 ^{o}C), which require a large energy input, often a long period of time to reach the required temperature, and a resultant high financial cost in terms of kWh per tonne of AC produced [10]. The financial costs of thermal regeneration's energy usage are comparable to the production of virgin ACs, which also requires the use of extremely high temperatures over a prolonged period [11]. With chemical regeneration the major issue is also the financial cost; often the chemical reagents are expensive, required in large volumes, and create a health and environmental hazard when used [12] [13] [14].

Sulphurous compounds are often present in water and gas streams, and many industries wish to remove them due to their smell and because they present a health hazard. The most common forms of sulphurous contaminants found in both water gas streams are hydrogen sulphide (H_2S) and sulphur oxides (SO_x) [15]. ACs impregnated with caustics (i.e., KOH, NaOH, etc) or transition metal compounds have been proven extremely effective at adsorbing both H_2S and SO_x onto their surface [15]. And regeneration of spent sulphurous ACs via thermal regeneration has proven possible. However, there are issues with using conventional forms of regeneration on these spent sulphurous ACs, with the adsorbed gasses being converted into H_2SO_4 and elemental sulphur [16] [17]. Both of which are corrosive towards certain metal-alloys and often damage the metal framework of the regeneration oven in which they are being produced. Additionally, the reaction taking place during the regeneration that produces the H_2SO_4 and elemental sulphur is exothermic and had often led to fires [17]. As such, industries and research groups specialising in AC regeneration have begun to look elsewhere.

One potentially viable replacement for the more conventional methods of regeneration is MW heating. The principle being that microwaves heating can heat a material volumetrically; each element of the material being heated individually, and ideally at a similar rate [18]. When compared to conventional heating, the volumetric heating provided by microwaves allows for a much faster heating rate; often requiring minutes rather than hours to reach temperatures required to achieve pyrolysis and reactivation, reducing the energy required for regeneration substantially [19]. Additionally, like conventional heating, no chemical treatment, such as that carried out in chemical regeneration, is required. However, the MW regeneration of AC is not

a field that has had vast amount of research carried out in it, especially in the regeneration of spent sulphurous ACs. Hence, this literature review will seek to explain what is currently known and ACs, conventional methods of regeneration, MW technology relevant to regeneration, and the issues currently present in the removal of sulphurous compounds from ACs.

Research Approach

Although the upcoming work involves experimentation to understand the effects of microwave irradiation on spent sulphurous AC - with the aim of developing a method by which adsorbed species could be removed from the surface - the main goal of this EngD project was to help develop a technique with the potential to replace the existing regeneration method used by CPL Ltd. The aims of each section of research were to not only further understanding of the science behind a new technique, but also the development of laboratory-scale setup that could act as precursor to a pilot scale facility. Essentially, the work involves process development as well as research and understanding.

The thesis will be broken down into 10 chapters. Chapter 1 (this chapter) will serve as an introduction to the work and the aims & objectives. Chapter 2 will explore the prior research conducted by others that pertains to the key areas of the project: activated carbon, widely used regeneration techniques for spent activated carbon, microwave technology, and regeneration of spent sulphurous activated carbon. Chapter 3 will outline the experimental methodologies that will be used throughout the research. Chapter 4 will explain the method development. Chapters 5, 6 and 7 will act as the results chapters, documenting all the work carried out in this project. Chapter 8 will show the conclusions and explore further work to be carried out after the completion of the project. Chapter 9 will contain details of materials referenced throughout the thesis. And Chapter 10 will serve as the appendix - containing any additional data that is not directly shown in the thesis itself.

2. Literature review

2.1 Activated Carbon

2.1.1 Historical and current applications of activated carbons

Evidence shows that the use of ACs stretches further into the past than one might imagine. The earliest documentation of use being in medical treatments and as industrial adsorbents, in the form of charcoal; with recorded use as odour extractors in ancient Egypt [20], as water purification mediums in the form of charcoal in 400 B.C. India [21], and Hippocrates' early attempts at epilepsy treatments in ancient Greece [22].

Activated carbons would continue to be used throughout history, but it wasn't until the 18th century that research into why charcoal had these adsorptive properties truly began. In 1773, chemist Carl Wilhelm Scheele would quantify the adsorption capability of porous carbon by measuring the volume of gases adsorbed by the material [23]. Only three years later, Johann Tobias Lowitz would demonstrate charcoal's adsorptive ability to remove coloured dyes from a series of test solutions [24]. However, the big breakthrough for AC research in the 17th century was conducted by and English sugar refinery, who had discovered how to decolourise their product, producing a pure-white sugar (white being seen as a colour associated with wealth and status at the time), which consequently also sparked the boom in mass AC usage across Europe [25].

After research into charcoal's applications began in the 18th century, it carried on throughout the 19th century, resulting in several major discoveries. Now that its adoptive properties were better understood by scientists, research was conducted to understand if it could be applied to human body to adsorb toxic materials, including the famous test conducted by Gabriel Bertrand in which he swallowed a slurry of arsenic and charcoal to prove how effective the latter could be at treating poison [26]. Fortunately for Bertrand, the charcoal adsorbed the arsenic, and he was left unharmed. Away from medicinal research, it would also be during this century that Frederick Lipscombe would commercialise the use of activated carbons as a method to purify potable drinking water [27].

In the early 20th century, the demand for AC in both the water and sugar industries of Europe was becoming so widespread that the first industrial-scale AC production companies would

be formed [28] [29]. In the purist of meeting demand, these companies would start to turn to other carbonaceous materials as sources from which they could produce their products, including Eponite (made from wood in 1909), and Norit (made from peat in 1911) [28] [29].

Modern day applications

Although many of the medicinal uses of ACs are contested in their legitimacy, there are two main areas that have proven success. The first of which being absorbance of toxic materials within the body such as arsenic (as mentioned in Section 2.1) [26], and the other being the treatment of chronic kidney disease [30]. ACs have been popularised in the treatment of chronic kidney disease because of their ability to adsorb urea, indoxyl sulphate, and other urinary toxins, from the body, enhancing the effectiveness of dialysis [31] [32] [33]. Further studies into AC use in the treatment of chronic kidney disease and other illnesses continues.

Due to ACs' porous nature, it has been used heavily in environmental remediation operations, including groundwater filtration, spill clean-up, air purification, and volatile organic compound capture [34] [35].

In the production of vodka and whiskey, organic impurities that affect the colour, taste and odour of the final product at filtered out using ACs [36]. The process does not affect the alcohol content of the beverage, but instead increases the organic purity in terms of odour and taste [36] [37].

In recent years the storage of natural gas in ACs as absorbed natural gas (ANG), rather than the traditional compression storage (CNG), has risen in prevalence [38] [39]. The reason for which being that ANG requires a smaller volume for containment and it does not require a high-pressured environment, unlike CNG, and it reduces the overall bulkiness of the storage equipment [39]. Not only does this cut costs for storage and transportation facilities, but it also reduces risk of accidents usually associated with highly pressurised environments [28] [40].

As well as natural gas, fuel storage in ACs is also being utilised for fuel hydrogen. In short, the gas is first adsorbed into the AC, and then desorbed when subjected to higher temperatures for either combustion of storage in hydrogen fuels cells [24]. When storing hydrogen in ACs the achievable bond energy has been recorded to be as high as 5-10 kJ mol^{-1} [42].

AC gas filters are usually embedded into the filtration systems and work much in the same way as other filtration systems are used for the removal of oil vapours, odours and other hydrocarbons from the gasses that pass through [43].

AC filters are often used in nuclear plants to adsorb radioactive gas from the boiler water reactor turbine condensers before they decay into non-radioactive solid species [44]. These solids are trapped in the ACs whilst filtered can be passed out of the chamber. They can then be desorbed from the AC bed and reused.

ACs infused with sulphur or iodine are often used for the removal of mercury emissions from coal-fired power stations (flue gas), medicinal incinerators, and natural has well-heads [45] [46]. Although it is an extremely efficient method of mercury removal, the spent mercury-laden AC can be hard to dispose of and often results in the mercury being desorbed and the AC being burnt [45].

2.1.2 Physical properties of activated carbons

Raw materials used for production

ACs are derived from wide variety of carbonaceous sources, with preference to fossil materials i.e., coal, wood, peat, coconut husks, etc [1] [2]. The following criteria are seen as the most desirable aspects when choosing a raw material from which the AC is going to be constructed: Potential for obtaining high-quality ACs, presence of minimum inorganics, volume and cost of raw material, storage of the raw material, a high carbon density, low volatility, and the workability of the raw material [1].

One of the most important of the criteria being a low level of inorganics. The reason being that the higher the level of inorganics, the higher the ash content. A higher ash content in the raw material leads to a higher ash content in the product post-activation. The ash can then settle in the pores, reducing their size and decreasing overall surface area of the activated carbon [47].

Arguably, the two most important criteria of a potential raw material are density and low volatility. If the material is of a higher density, the overall structural strength of the carbon is increased and thus it can withstand excessive particle crumbling during use [47] [48]. Low-density materials produce ACs with large pore volume, but can suffer from structural issues,

leading to them usually being used for liquid phase applications (unsuitable for vapour applications). Low-density materials also tend to contain more volatiles that can affect the adsorption rate and permanently interact with adsorbed materials [48] [49] (see Table 1 below). And so, a balance must be struck in terms of the density so that the structure can withstand the majority of particle crumbling during use, have acceptable pore volume, and to try and have a few volatiles present as possible. However, it should be noted that the quality of these carbons can be improved via densification of the carbon by reconstitution or compression during carbonisation [48].

Table 1. Properties of some raw materials used in the manufacturing of activated carbons [49].

Raw material	Carbon, %	Volatiles, %	Density, kg/L	Ash, %	Texture of activated carbon	Application of activated carbon
Soft wood	40.0 - 45.0	55.0 - 60.0	0.40 - 0.50	0.3 - 1.1	Soft, large pore volume	Aqueous phase adsorption
Hard wood	40.0 - 42.0	55.0 - 60.0	0.55 - 0.80	0.3 - 1.2	Soft, large pore volume	Aqueous phase adsorption
Lignin	35.0 - 40.0	58.0 - 60.0	0.30 - 0.40	-	Soft, large pore volume	Aqueous phase adsorption
Nutshells	40.0 - 45.0	55.0 - 60.0	1.40	0.5 - 0.6	Hard, large micropore volume	Vapour phase adsorption
Lignite	55.0 - 70.0	25.0 - 40.0	1.00 - 1.35	5.0 - 6.0	Hard, small pore volume	Wastewater treatment
Soft coal	65.0 - 80.0	20.0 - 30.0	1.25 - 1.50	2.0 - 12.0	Medium hard, medium micropore volume	Liquid and vapour phase adsorption
Petroleum coke	70.0 - 85.0	15.0 - 20.0	1.35	0.5 - 0.7	Medium hard, medium pore volume	Wastewater treatment
Semihard coke	70.0 - 75.0	10.0 - 15.0	1.45	5.0 - 15.0	Hard, large pore volume	Gas vapour adsorption
Hard coal	85.0 - 95.0	5.0 - 10.0	1.50 - 1.80	2.0 - 15.0	Hard, large pore volume	Gas vapour adsorption

Porosity

Activated carbons are known for having a high degree of microporosity which afford them an extremely large surface area for their size i.e., a single gram of activated carbon can have a surface area more than 500 m^2 due to the numerus pores [50] [51]. There are three general terms used to describe pore sizes: macropores - radius greater than 50 nm; mesopores - radius 2 – 50 nm; and micropores - radius less than 2 nm (see Figure 1 below) [52]. The different pore sizes allow for selectivity when adsorbing i.e., certain larger molecules may not be able to fit into the micro or sub-micropores and can be removed from the AC before the smaller molecules.

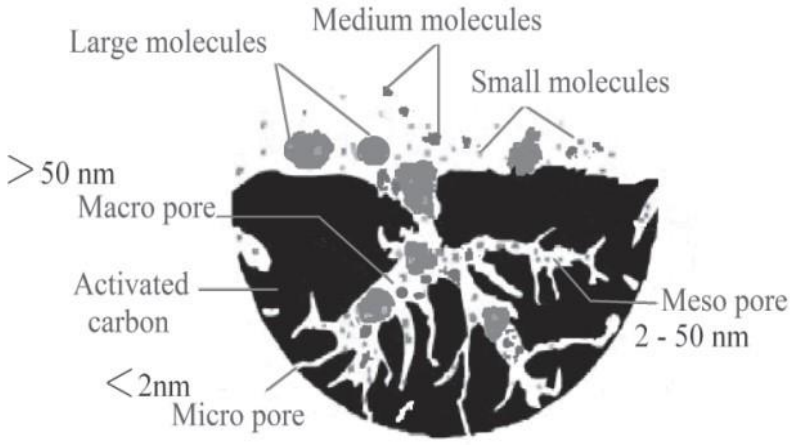


Figure 1. Different pore structures of activated carbon [52].

Various types of pores can be seen on a single activated carbon sample. This can include flat graphite-like surface running parallel to one another – pores like these provide good adsorbing conditions because the adsorbing material can interact with several surfaces at once [50].

Different forms of activated carbon

PAC (powdered activated carbon) consists of fine carbon particles able to pass through an 80-mesh sieve (0.18 mm diameter holes), usually with a diameter less than 0.1 mm [53]. The small size of the particles allows for a large surface to volume ratio and a small diffusion distance during adsorption [53] [54]. However, the size of the particles can also present problems as it allows for the creation of dust, and, when adsorbing liquid or vaporous volatile, sludge. Additionally, PAC cannot be regenerated as structural integrity is lost upon heating. Thus, it must be removed and disposed of often, increasing running costs of a large-scale operation. [53] [54] [55].

GAC (granular activated carbon) has relatively large particle size ranging between 0.2 to 5 mm, and a subsequently smaller external surface [56]. Unlike PAC, GAC can be regenerated as the smaller surface size allows for fast diffusion times of vapour or liquid adsorbent. And, as GAC can be regenerated, the ability to desorb contaminants quickly allows for a quick turn over and re-use [57].

PAC or powdered char can be mixed with a binder and formed into cylindrical pellets known as extruded activated carbon (EAC). The benefit being that dust creation is minimised, and it has a high mechanical strength, making it ideal for gas phase adsorption [58].

2.1.3 Adsorption mechanisms

The term "adsorption" was first coined by Heinrich Kayser in 1881 to describe the enrichment of one or more of the components in the region between two bulk phases or interfacial layer [59]. With an "adsorbent" being a solid onto which adsorption takes place, and an "adsorbate" being the compound retained by the adsorbent [60]. It is by the following mechanisms that ACs adsorb compounds onto their surface, removing them from their initial medium.

Physisorption

Physical adsorption (physisorption) takes place because of short range intermolecular forces known as Van der Waals, and London Dispersion, forces. Both of which are generated between the adsorbent and adsorbate by the intense electron density fluctuation within each atom; these fluctuations induce an electrical dipole moment in the neighbouring species, resulting in an attraction between the two atoms [60]. Due to its non-specificity, physisorption can take place across an entire surface of a solid compound. And, once the surface of the solid is covered by the initial layer of the adsorbate molecules, another layer may adsorb directly on to that initial layer – this is known as multi-layer adsorption (see Figure 2) [60]. Physisorption is the most common form of adsorption of most gases onto porous solids.

Chemisorption

Chemisorption refers to adsorption in which intramolecular forces i.e., polar covalent bonding, are formed between surface molecules of the adsorbent and adsorbate. It is for this reason that chemisorption is stronger than physisorption, as more energy is required to remove the adsorbate. Unlike, physisorption, chemisorption on takes place in specific sites on the adsorbent, and only mono-layer adsorption occurs at these sites (see Figure 2) [51].

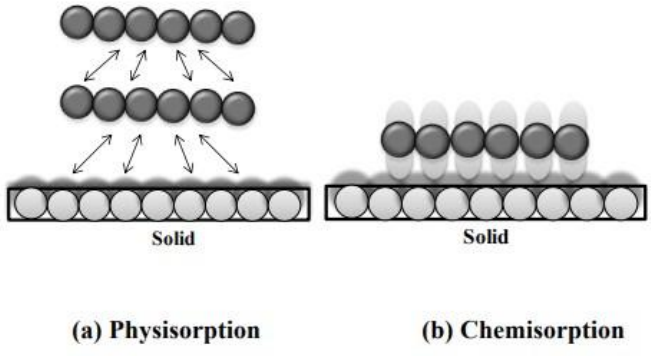


Figure 2. Adsorption onto a solid (a) Physisorption: weak, long range Van der Waals forces, multilayer adsorption (b) Chemisorption: strong, short-range forces involving orbital overlap and electron exchange [61].

Adsorption in gas-solid phase

The form of adsorption mostly commonly observed with gases adsorbing onto porous solids is physisorption. The amount adsorbed onto the solid is directly dependent on its mass, temperature, partial pressure of the gas and the specific chemical characteristics of the gas and solid. Thus, the quantity of gas adsorbed at constant temperature per unit quantity of solid can be expressed as a function of pressure, $V_{ads} = f$ (P). This being the fundamental principle of adsorption isotherms – volume of gas adsorbed over a range of pressures [61]. Although, it should be noted that in adsorption isotherms, adsorbed amounts are plotted against relative pressure, p/p_o; where p indicates the partial pressure of the gas in equilibrium, and p_o represents the saturation pressure of the adsorbate at the temperature of measurement [62].

Characterising porous structures through their adsorption-desorption isotherms helps to provide a detailed dataset on adsorption capacity, surface area, type of porosity, and pore size. The most reliable method of obtaining adsorption isotherms is to use adsorbates with molecules of a differing sizes to the porous structure. The two most used gases for this form of isotherm determination are nitrogen at 77K, and carbon dioxide at 273K. Nitrogen is often used because of its relatively small molecular size allowing adsorption to both macro- and the far small mesopores. But, with its kinetic restrictions taking place at such a low temperature, narrow micropores are often not accessible to nitrogen, in which case carbon dioxide is used as a suitable substitute [62]. However, neither nitrogen or carbon dioxide adsorption are usual

contaminants that are adsorbed by industrial AC use, but their ease of use and worldwide application has made adsorption tests involving them common place during research [63].

Mechanism of adsorption in porous solids

Initially, gas molecules will fill pores with the highest potential energy. Gas-solid interaction energy is considerably higher when the pores narrow, as the potential energy from neighbouring pore walls overlap towards the centre of the pore. Thus, adsorptions initiate in the narrowest of micropores and subsequently continues as the pore becomes wider [64].

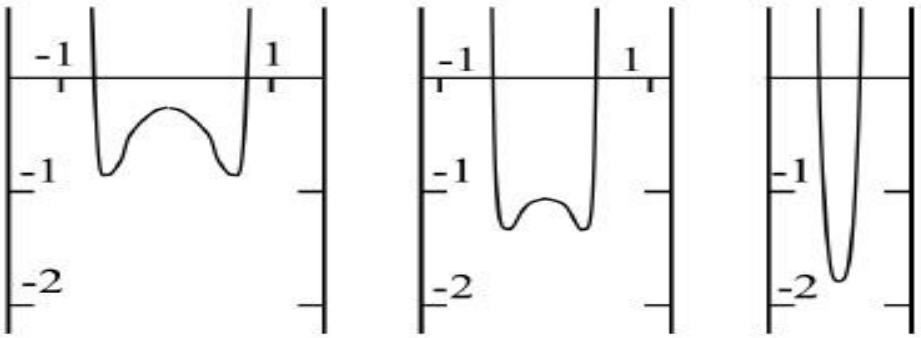


Figure 3. The change in potential energy for the adsorbate molecule as the size of slit-shape molecules decrease from left to right [64].

The mechanism of adsorption is considered to have three distinct phases: the primary micropore filling, then secondary (or "super-") micropore filling, followed by the mesopores filling. The primary phases take places at extremely low relative pressure of $p/p_o < 0.01$ in highly energetic *ultra*-micropores. In the next phase, in secondary-micropores (width less than 2nm), the gas-solid interaction energy decreases significantly, and so the adsorption takes place at a higher relative pressure ($p/p_o = 0.2$-0.3). The mechanism for super-micropore filling differs from primary micropore filling as there is a cooperative effect between the adsorbate molecules [65]. Once both micropore filling stages are complete, less energetic pores with a width between 2 – 50 nm (the mesopores) will be filled at a relative pressure greater than 0.3. As with the micropore filling phases, the mesopore filling phase begins with surface coverage of the pore walls, however multilayer adsorption then begins to take place until the pore is filled [66].

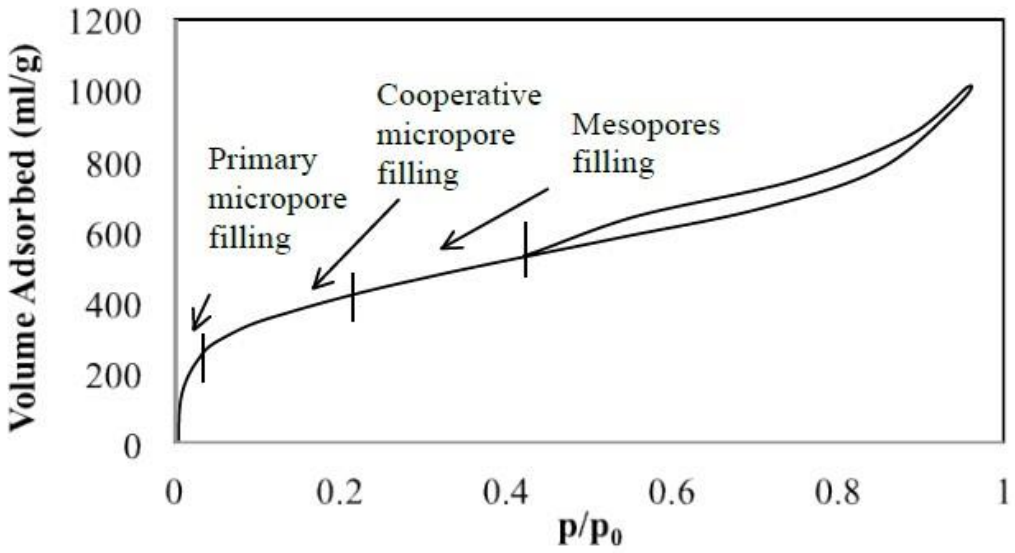


Figure 4. Nitrogen adsorption-desorption plot for a porous structure [29] [61] [62].

In the mesopores, in addition to multilayer adsorption, there is strong evidence to suggest that capillary condensation also occurs. Capillary condensation implies that the pore is filled through single layer adsorption, followed by multilayer, up until a point where the amount adsorbed by the pore does not correspond to the level of multilayer formation. Instead, the adsorbent layers are condensed on the pore walls [29] [61]. That is to say, the gas molecules being adsorbed are condensed to liquid-like state before the saturation pressure of gas is reached.

When the adsorption system's pressure is reduced desorption can occur, however, it occurs at much slower rate than adsorption itself as the required activation energy is far higher. For a non-mesoporous solid the desorption occurs on the adsorption isotherms, but for mesoporous solids the adsorption-desorption curves are not coincident [67]. In other words, the adsorbent loading and regeneration follow different paths in the adsorbed phase concentration versus partial pressure space (shown below as X [-] in Figure 5). When this occurs is it known as hysteresis.

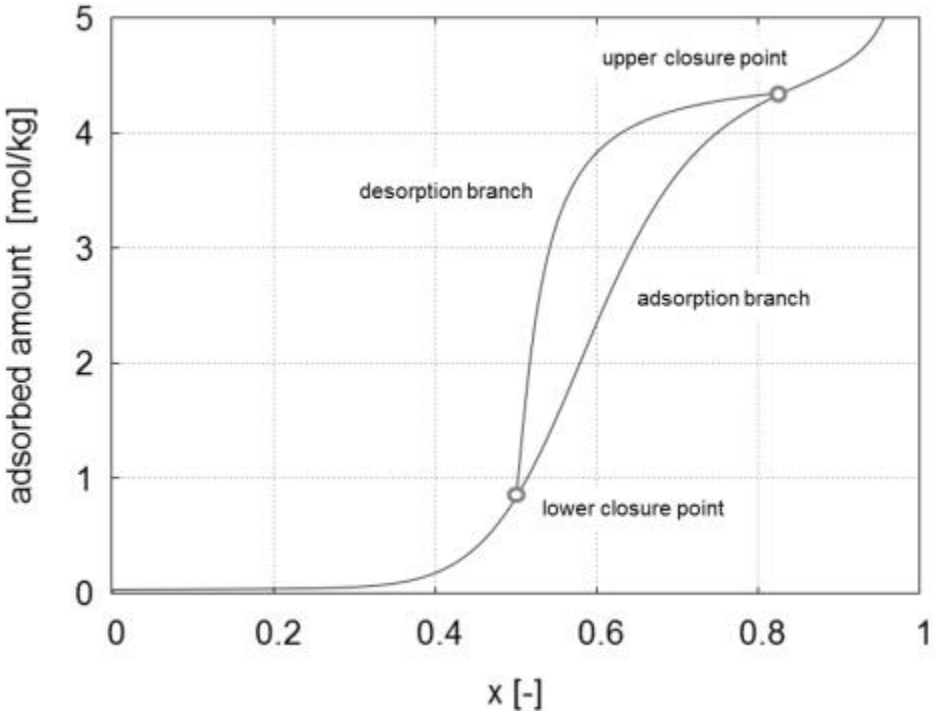


Figure 5. Primary adsorption and desorption isotherms hysteresis loop [68].

The lag between adsorption-desorption isotherms under certain pressures is attributed to liquid in a capillary system exhibiting a greater vapour pressure when filled than when being emptied, because the radius of the meniscus is less during the filling process due to incomplete wetting [61] [62].

Classification of adsorption isotherms

The shape of adsorption isotherms helps to provide in-depth information regarding the extent of adsorption and porous structure of a solids. Although there have been a multitude of isotherms reported on through literature, the majority can be placed into six classes (see Figure 6). Isotherm I is most observed when chemisorption or physisorption is taking place in highly micropores materials. For I, the plateau represents the maximum monolayer capacity of micropores. The gradient of the initial linear section is indicative of the dimensions of micropores, which increases with narrower microporosity. Due to the high interaction energy within narrow micropores, complete filling of the pores at low relative pressures can be achieved in highly microporous materials, giving rise to a Type I isotherm [29] [61] [62].

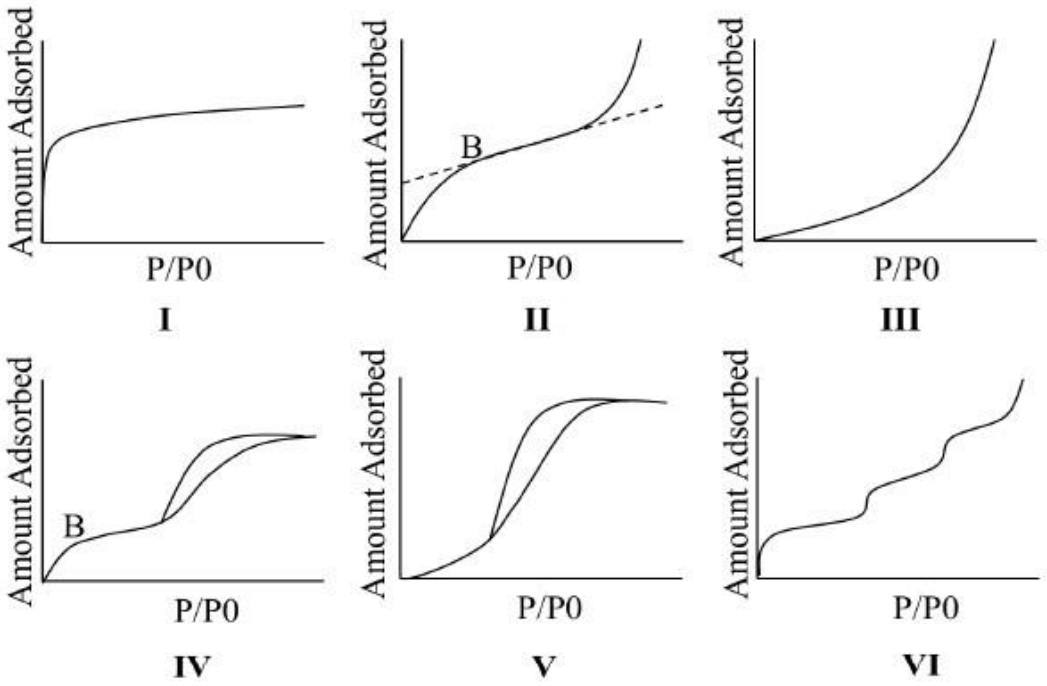


Figure 6. The six major types of isotherms in BDDT classification [29].

From I, the limiting value of the monolayer adsorption is indicative of micropores which can only accommodate monolayer adsorption. Isotherm II are indicative of multilayer physisorption on a non-porous solid; the limiting value being indicative of monolayer completion (represented by B) [29]. Both III and V show a convex shape towards the pressure axis, indicative of cooperative adsorption in which there is a strong adsorbate-adsorbate interaction which contributes to the further adsorption of more molecules [29]. Type III isotherms are obtained from nonporous or highly microporous materials during adsorption of vapours, whereas V type isotherms (with a hysteresis loop) can be observed from mesoporous or microporous adsorbents [29]. Typed VI is for surfaces with extremely homogenous structure. IV isotherms are obtained for mesoporous materials with the capability of both mono- and multilayer adsorption with capillary condensation, hence the occurrence of a hysteresis loop. Hysteresis loops are classified, as shown in Figure 6, by the IUPAC system: H1 for solids with spheroidal, uniformed particle size, H2 for some silica gels, and H3 & H4 in solids with slit- or plate-shaped pores [60] [61].

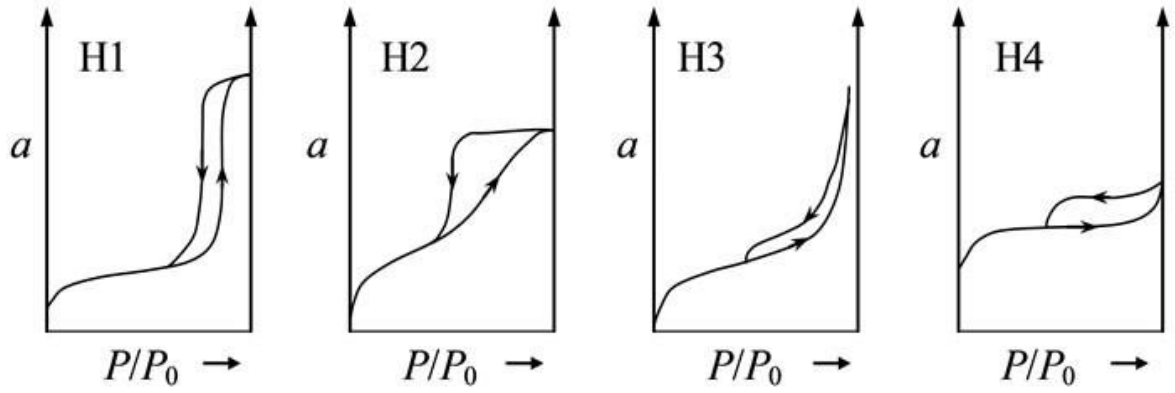


Figure 7. The hysteresis loop classification by IUPC [69].

The interpretation of adsorption isotherms is possible through several models, each of which express monolayer coverage and thus allows for the determination as parameters such as surface area and pore size distribution. The mostly commonly used are the Langmuir, BET and t-plot models, which will be explained subsequently [29].

Langmuir model

Developed in 1918, the Langmuir model assumes that adsorption is limited to monolayer adsorption, and that multilayer adsorption does not occur. To this theory there are three main assumptions: (1) adsorption occurs at a definite localised site, (2) each site can only accommodate one adsorbate molecule, and (3) the energy of the adsorbate molecule is the same on all sites regardless of the presence of other molecules, implying there is no adsorbate-adsorbate interactions [29]. The equation for the Langmuir model for the adsorption of gas onto a porous solid is as follows:

Equation 1.

$$\theta = \frac{\mathrm{V}}{\mathrm{V_m}} = \frac{\mathrm{KP}}{\mathrm{KP} + 1}$$

Where: θ = Fractional occupancy of the adsorption sites

V = Volume of gas adsorbed onto the solid

V_m = Volume of gas adsorbed forming a monolayer

K = Pressure at equilibrium

P = Langmuir empirical constant

At low pressure KP is so small, that the factor (1+KP) in denominator can almost be ignored. Langmuir reduced the equation to θ = KP. However, at high pressure KP is so large that the factor (KP + 1) in denominator is nearly equal to KP, so the equation can be reduced to θ = KP/KP =1. Thus, the equation can still be applied to me type isotherms for microporous materials, as pores can attain a maximum capacity at certain pressures; the pores being so narrow that they cannot allow in multilayer adsorption [29].

In terms of analysing isotherms, the Langmuir equation applies to Figure 4, directly before point B. For ACs, the limit of using the Langmuir equation would be $p/p_o < 0.15$, where the monolayer coverage takes place [61]. The main criticism of this model is that it assumes adsorption sites are energetically homogeneous, with no adsorbate-adsorbate interactions. For ACs, none of those assumptions are applicable [70].

BET model

Using the Langmuir model as a foundation, but changing assumptions that were made, the BET model was developed in 1938 by Brunnauer, Emmet and Teller. It observes that only the first layer of adsorbate molecules is attached to the solid surface by adsorbate-adsorbent adsorption forces and that these forces were not strong enough to affect the formation of further layers of adsorbate. The belief being that subsequent layers of adsorbates that adsorb are instead facilitated by the same kinds of forces involved in the condensation of vapours in the liquid state [71]. Three key assumptions were made regarding the adsorption of the second and third layers of adsorbate: (1) adsorption energy in all layers, except the first, is equal to the molar heat of condensation; (2) in all layers, except the first, evaporation and condensation conditions are identical; (3) an infinite numbers of layers can be built up at the saturation pressure ($p = p_o$) [61] [62] [70]. As such, the BET equation for the adsorption of gas onto a porous solid was derived:

Equation 2.

$$\theta = \frac{V}{V_m} = \frac{CP}{(p_o - p) \times [1 + (C - 1)(p/p_o)]}$$

Where: θ = Fractional occupancy of the adsorption sites

V = Volume of gas adsorbed onto the solid

V_m = Volume of gas adsorbed forming a monolayer

p = Pressure of gas

p_o = Saturation pressure of gas at temperature of measurement

C = BET constant

Although the value of C is proportional to the heat of adsorption, it does not measure the energy quantitatively. For reference, if this method were to be used, IUPAC have recommended that it only be used when the equation becomes linear; in general, the for microporous solids the best fit is restricted to p/p_o >0.15 [61] [72].

In contrast to the BET theory assumptions, ACs have groupings of surface sites, each of which is homogenous to themselves, but different from the others. Thus, the applicability of BET at pressures lower than the B value is dubious due to the high heterogeneity of adsorption energy on the surface. Additionally, at relative pressure passed the linear range, the model loses its legitimacy because capillary condensation occurs [29].

Assuming that the adsorption of molecules onto a pore surface were the same as adsorption onto a non-porous surface, the specific area of pores can be estimated from the value of the monolayer capacity, A, from the BET monolayer adsorption equation seen below:

Equation 3.

$$A = a_m \times N_A \times V_m$$

Where: A = Surface area of pores

a_m = Adsorbate molecular projected area (0.162nm^2 for nitrogen at 77K

N_a = Avogadro's number (6.0221 x 10^{23} mol^{-1})

V_m = Volume of gas adsorbed forming a monolayer

The BET surface area is calculated based on the area of adsorbate molecule projection on a flat surface [61] [71]. However, part filling of porosity (as seen in Figure 8), and the density of molecular filling within said porosity being a function of the size and shape of the adsorbate molecules, influences the overall calculation of surface area. Namely, the amount of adsorbate is retained by a pore is not always proportional to the pore surface area. As such, it would be advisable to take it as an indication of what the adsorption capacity is likely to be, and not as an expectation of definite data on where and how adsorption is taking place on the surface site [72] [73].

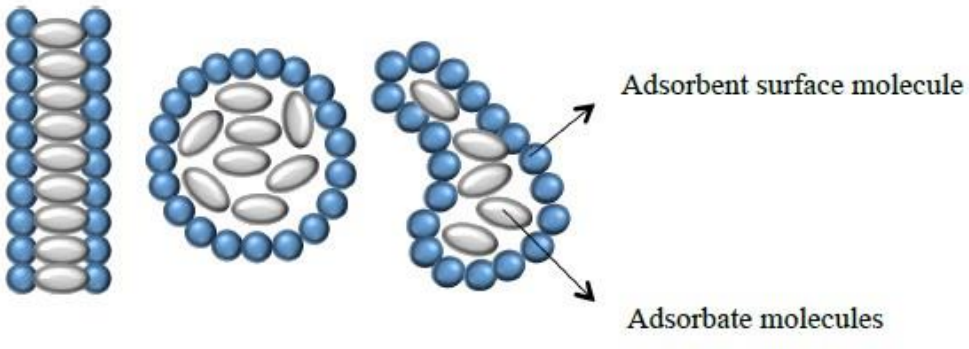


Figure 8. Pores with similar internal surface area, but different adsorption capacities [61].

T-plot model

The t-plot model assumes that the adsorption of gases by homogeneous non-porous solids occurs due to a perfect mechanism of surface coverage, followed by multilayer adsorption; employing isotherms derived from plotting the amount of gas adsorbed, V, against the film thickness, t [66] [74]. From this assumption, the t-plot equation for the adsorption of a gas against the film thickness was developed based on the linearity of the plot for the adsorption of a gas on a non-porous solid:

Equation 4.

$$V = \frac{V_m \mathrm{t}}{\sigma}$$

Where: t = Average thickness of the adsorbate layer

σ = Average thickness of a single layer of gas adsorbed gas molecules

V = Volume of gas adsorbed onto the solid

V_m = Volume of gas adsorbed forming a monolayer

Any deviation from the linear form of Equation 4 suggests the presence of different types of porosity. As shown by Figure 9, there are four t-plots for solids: (i) linear t-plot (with a zero intercept), for non-porous and macroporous solids, suggesting layer-by-layer adsorption mechanism, (ii) linear t-plot (with a non-zero intercept) for microporous solid, indicative of more adsorption capacity at lower pressures due to higher surface area of micropores, (iii) mesoporous solids with an upward deviation from non-porous solid t-plot, caused by the capillary condensation in mesopores, and (iv) micro and mesoporous solid plot which is a combination of type ii and iii, indicating the subsequent adsorption in micropores followed by meso- and macropores [66] [74] .

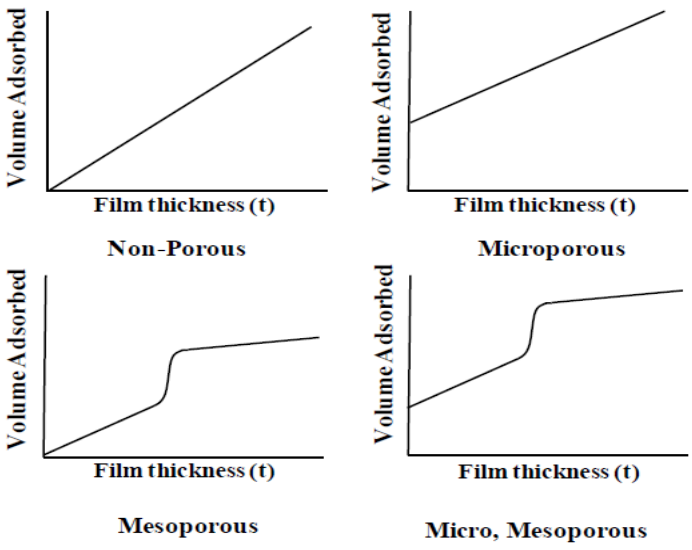


Figure 9. Characteristic t-plot curves [61].

The surface area and micropore volume can also be gathered from the t-plot. For a porous solid such as AC, the t-plot should contain two distinct linear regions: the first representing micropore filling and surface coverage of larger pores; and the second being the multilayer adsorption in meso- and macropores [74]. Obtaining the slope of the line for the first linear region will result in total surface area, and the slope of the second linear section will determines the external surface area unrelated to the micropores [66] [74]. Additionally, extrapolating the second linear region of the plot to the vertical axis gives the total micropore volume [74].

Liquid-phase adsorption

As to be expected with the amount of use ACs have seen in liquid-phase adsorption (i.e., detoxification of water), characterisation of adsorption via isotherms is key. The study of liquid-phase adsorption is segregated into two categories – adsorption of solutes with restricted solubility, and the adsorption of solutes which are highly soluble within the solvent in which they are present [75]. Of all the various models that have been developed to describe adsorption from solution, the two most popular are the Freundlich model, and the liquids-phase version of the Langmuir.

Freundlich model

Used to interpret the adsorption from solutions, the Freundlich model represents the increase in adsorption capacity as being related to the concentration of the adsorbate in solution [76]. The non-linear form of the equation to calculate solute adsorption per weight of adsorbent is shown below:

Equation 5a.

$$q_{e= k_f C_e^{1/n}}$$

Where: q_e = Amount of solute adsorbed per unit weight of adsorbent

C_e = Equilibrium concentration of solute

K_f = Constant related to adsorption capacity

N = Constant related to adsorption intensity

* Data from the Freundlich model is often required in a linear fashion, as such; the equation can be expressed logarithmically as follows [76]:

Equation 5b.

$$\log q_e = \log k_f + \frac{1}{n} \log C_e$$

Where the values of n and k_f are obtained from the slope and intercept of the linear plot of log q_e vs log C_e. As such, steep slopes represent high affinity capacity at high equilibrium concentrations, with rapid reductions at lower concentrations [76] [77].

Langmuir model for liquid-phase adsorption

Overall, the assumptions made in the gas-phase version of the Langmuir are like that which are made for the liquid-phase [78]. This is echoed in the liquid-phase versions' equations other than the substitution of gas pressure for solution concentration at equilibrium:

Equation 6.

$$\frac{q_e}{Q_o} = \frac{KC_e}{1 + KC_e}$$

Where: q_e = Amount of solute adsorbed per unit weight of adsorbent

Q_0 = Amount of solute adsorbed per unit weight of adsorbent required for complete monolayer coverage

C_e = Equilibrium concentration of solute

K = Langmuir model constant related to rate of adsorption

When using a Langmuir liquid-phase model for adsorption testing, the value of $1/q_e$ is plotted against $1/C_e$, resulting in the straight line having the slope of $1/bQ_o$ and intercept of $1/Q_o$ [61]. Q_o acts as the monolayer adsorption capacity based on the assumption that only a single layer can form on the surface of the pore walls. Additionally, Q_o can also be used to determine the specific area of the adsorbent by using a solute of which the molecular area is already known. Whereas b represents of the interaction energy between adsorbate and the surface of the adsorbent.

2.1.4 Production methods and activation of activated carbons

The activation of carbonaceous species happens in two main stages: carbonisation and activation. This section will outline in detail the processes involved in each, and the effect on the carbon source itself.

Carbonisation/pyrolysis

Carbonisation, the first stage producing an AC, takes place when a carbonaceous material is converted into char via heating at high temperatures up to 800 ^{o}C in an oxygen deprived environment; also known as pyrolysis [78] [79]. The process itself seeks to remove volatile elements such as oxygen, hydrogen, nitrogen and sulphur, from the carbon source. The newly pyrolyzed carbon has a proto-graphitic structure and is often referred to as an elementary crystallite. The amount of char produced from carbonisation is dependent on the amount of carbon being removed with the other elemental species i.e., in the form of oxides and hydrocarbons [78].

Overall, the mechanisms behind conversion into char are complex, but can be simplified into three main stages. Initially, moisture and some light volatiles are removed. The char begins to form in the second step as liquid fraction evolution starts to occur. After the initial devolatisation that has occurred in the first two stages, further carbonisation takes place in the final step. During this third step, cracking, depolymerisation, recondensation of the liquid fraction, and a slow condensation of the char structure occurs, from which a carbon-rich solid residue is exposed following the removal of volatiles [79] [80].

At the end of the carbonisation step, the final product is a structure of disordered, cross-linked aromatic sheets which forms the initial carbon structure. But the pore structure is not fully developed, and often filled with remnants of unpyrolysed materials. At this point, the char has a low adsorptive capacity, hence why the activation stage is required [78] [79].

Activation

As well as the raw materials used as the initial carbon source, the actual process of activation greatly effects the properties of an AC, especially the method of activation that has been chosen. An example of which is shown Figure 10 below; the AC on the right was treated with a higher dose of activating agent (KOH) than the AC on the left. The difference in the number

of pores on the surface is clearly visible. However, the reliability of SEM is questionable as there is no guarantee that the image area represents the entirety of the material under study.

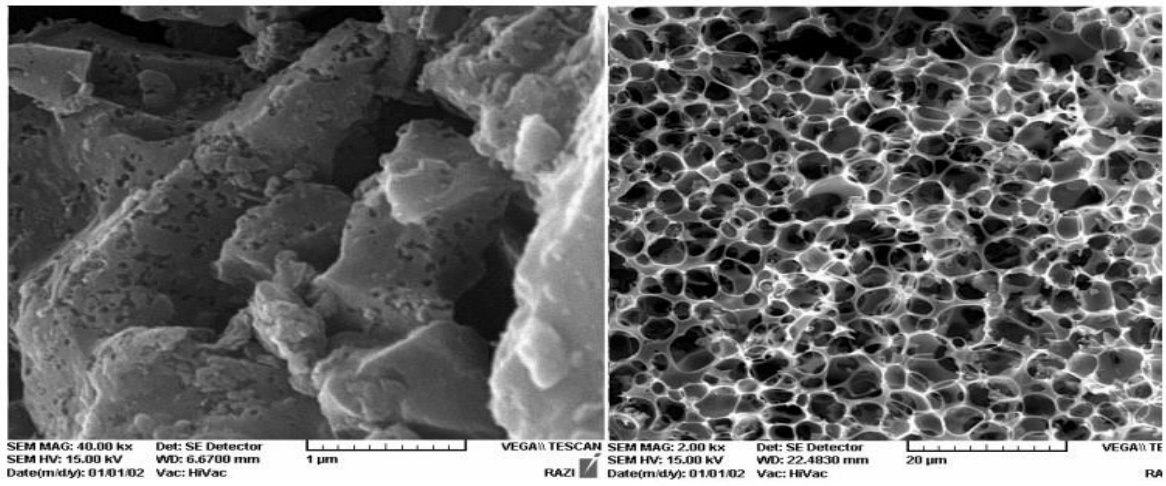


Figure 10. SEM micrographs of walnut char activated with lower doses of KOH (left) and higher doses of KOH (right) [81].

The activation process starts with the removal of disordered carbon produced from carbonisation to clear out the pores. After that, the aromatic sheets are exposed to activating agent(s) to further enhance pore structure – it is at this stage that micropores are formed, and the pores themselves are widened [29] [49]. These two stages are indicative of the temperature at which the activation is being conducted [81].

When it comes to activation methods there are two distinct categories most chosen – physical and chemical. In chemical activation the raw material being used is impregnated with a chemical agent; usually an acid, strong base or salt i.e., phosphoric acid (H_3PO_4), potassium hydroxide (KOH), copper oxide (CuO), or zinc chloride (ZnCl) [12] [64] [65]. The impregnated raw material will then undergo carbonisation whilst also going through activation at the same time (usually at 400 – 600 ^oC) [29] [82]. The impregnated species help to reduce the required temperatures due to their ability to take up sites in the carbon matrices, and bond with the carbon, more readily. The impregnated species will also take part in the chemisorption of adsorbates when the AC is in use later.

Physical activation is carried out at much higher temperatures (800-1100 °C) and utilises gases for oxidation (usually steam and/or CO_2) [83]. During activation with steam and CO_2, the reactions between gas-carbon and water-gas are simultaneous [84], as seen below:

$C_{(s)} + H_2O_{(g)} \rightarrow CO_{(g)} + H_{2(g)}$	$\Delta H = 130$ kJ mol^{-1}	steam activation, water-carbon phase
$C_{(s)} + CO_{2(g)} \rightarrow 2CO_{(g)}$	$\Delta H = 159$ kJ mol^{-1}	carbon dioxide activation, water-carbon phase
$CO_{(g)} + H_2O_{(g)} \leftrightarrow CO_{2(g)} + H_{2(g)}$	$\Delta H = -41$ kJ mol^{-1}	water-gas equilibrium at >800 °C

Both steam and carbon dioxide activation are endothermic reactions, with carbon-steam showing lower reaction enthalpy. This would suggest that a higher activation temperature is required for the CO_2 activation of char [84].

Whilst the activation step is happening, the reaction between carbon and steam and CO_2 can be inhibited by products from the activation itself; CO from CO_2 and H from steam can adsorb onto the active sites of the carbon surface [85]. But this is not always unfavourable as it can prohibit fast oxidation from occurring, and thus control the formation of the porous structure [86]. When choosing between the two, it must be noted that CO_2 has a slower reaction rate due to its geometry; CO_2 is linear, and its overall size is larger than that of H_2O [85].

2.2 Regenerating activated carbons

Regenerating ACs is a form of recycling a carbon source to reduce the costs associated with production from virgin carbon sources. These costs can be financial in terms of the high costs of producing activated carbons, and environmental with regards to the removal of carbon source from the earth and the associated effects on the surroundings of an excavation site. This section seeks to give a detailed reasoning for AC regeneration, and to show what established methods of regeneration are currently being used.

2.2.1 Finical incentives for regeneration

In 2009 Stravopoulos and Zabaniotou conducted a study regarding the production costs of ACs with regards to both running costs and raw materials. The pair found that there was a significant difference in the costs of production dependent on whether chemical of physical (thermal) activation methods had been used for production (see Tables 2 & 3), with chemical activation being financially more viable [87]. This was because chemical activation produced far higher yields than physical, especially in coal and lignite. The study also revealed that production of ACs from materials such as wood proved to be unfavourable, with returns on investment being extremely low [87]

Table 2. Costs and economic evaluation of an activated carbon production plant, US $, producing 4.5t a day via chemical activation and zero raw materials cost [87].

	Used tires	**Wood**	**Pet coke**	**Carbon black**	**Charcoal**	**Lignite**
Total investment cost	6,858,693	6,295,651	4,097,285	3,447,736	4,152,362	5,829,895
Total operating cost	2,329,024	2,234,747	1,558,365	1,372,354	1,574,440	2,085,729
Total production cost	2,843,394	2,729,971	1,915,351	1,690,988	1,934,733	2,550,636
Production cost (US$/kg)	1.92	1.84	1.29	1.14	1.30	1.72
Production cost (10^{-7} US$/m^2)	27.4	22.9	4.29	22.7	6.52	7.81
Income	4,073,639	2,851,960	2,851,200	2,851,200	2,850,566	2,851,200
Income [a]	*3,218,427*	*2,281,568*	*8,553,600*	*1,425,600*	*5,701,133*	*6,272,640*
Return on investment, %	18.7	1.9	22.8	33.7	22.1	5.2
Return on investment, % [a]	*5.7*	*<0*	*>100*	*<0*	*90.7*	*63.8*
Net present value, $	<0	<0	39.167	1,680,415	<0	<0
Net present value, $ [a]	*<0*	*<0*	*25,243,846*	*<0*	*12,495,171*	*10,621,409*
Discounted pay-back, %	23.4	-	13.7	7.17	14.8	-
Discounted pay-back, % [a]	-	*<0*	*1.14*	*<0*	*2.13*	*3.17*
Pay-out period, years	9.63	<0	6.88	3.94	7.27	<0
Pay-out period, years [a]	*<0*	*<0*	*0.65*	*<0*	*1.21*	*1.8*

Capacity: 4.5t/day, chemical activation, zero raw materials cost.
[a] *Items refer to costs per m^2 of carbon BET surface area.*

Table 3. Costs and economic evaluation of an activated carbon production plant, US $, producing 4.5t a day via physical activation and zero raw materials cost [87].

	Used tires	**Wood**	**Pet coke**	**Carbon black**	**Charcoal**	**Lignite**
Total investment cost	7,301,682	8,145,760	3,086,328	3,656,307	3,777,027	7,130,948
Total operating cost	2,762,118	3,088,436	1,324,303	1,498,209	1,535,940	2,697,5561
Total production cost	3,306,734	3,691,853	1,606,124	1,812,264	1,856,967	3,230,516
Production cost (US$/kg)	2.34	2.49	1.08	1.22	1.25	2.18
Production cost (10^{-7} US$/m^2)	44.5	31.1	10.8	24.4	13.9	27.2
Income	4,482,720	2,851,200	2,850,858	2,850,994	2,851,200	2,850,592
Income [a]	*3,057,120*	*2,280,960*	*2,850,858*	*1,425,497*	*2,566,080*	*2,280,473*
Return on investment, %	16.1	<0	40.3	28.4	26.3	<0
Return on investment, % [a]	*<0*	*<0*	*40.3*	*<0*	*18.8*	*<0*
Net present value, $	<0	<0	2,415,412	934,893	617,493	<0
Net present value, $ [a]	*<0*	*<0*	*2,415,412*	*<0*	*<0*	*<0*
Discounted pay-back, %	-	<0	5.59	9.27	10.5	<0
Discounted pay-back, % [a]	*<0*	*<0*	*5.59*	*<0*	*22.9*	*<0*
Pay-out period, years	12.8	<0	3.12	4.97	5.55	<0
Pay-out period, years [a]	*<0*	*<0*	*3.12*	*<0*	*9.55*	*<0*

Capacity: 4.5t/day, chemical activation, zero raw materials cost.
[a] *Items refer to costs per m^2 of carbon BET surface area.*

In 2017 Santadkha and Skolpap conducted a comparative research assessment of the profitability of AC plants who produced ACs from virgin sources of carbon, regenerated ACs from spent sources, and those who operated an integrated system which featured both. These assessments were based on the costs of running each type of plant when compared to one another, and the effects that had on the overall profitability [88]. At low AC sales price, return on investment (ROI) of generation and integrated cases were negative representing greater annual cost than annual revenue (Figure 11). When the sales price of AC was increased from 514 to 686 USD/t of AC, ROI of generation (G), regeneration (R), and integrated (G&R) plants were achieved 2.20, 33.94, and 11.02%, respectively [88].

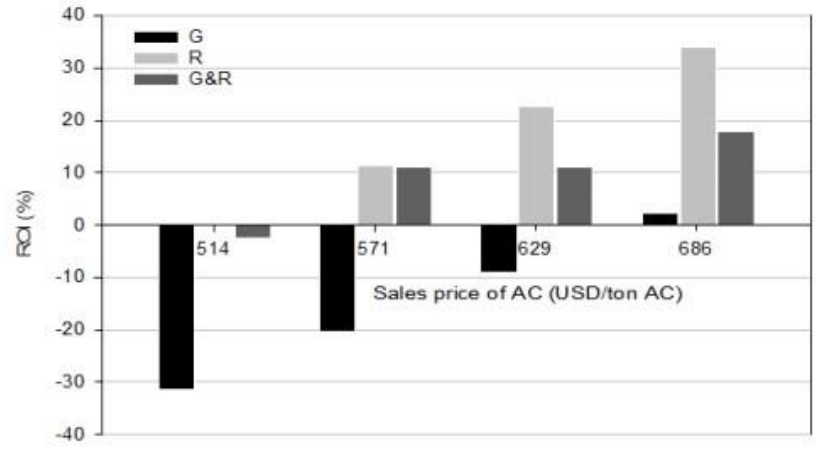


Figure 11. Comparison of ROI as a function of AC sales prices [88].

Similarly, Santadkha and Skolpap showed that the net present value (NPV) for 10-year investment life obtained from all projects were proportional to AC sales price, as shown in Figure 12 [88]. Evidently, all positive NPVs of the regeneration case suggested the most profitability of the project for the entire studied sales price range.

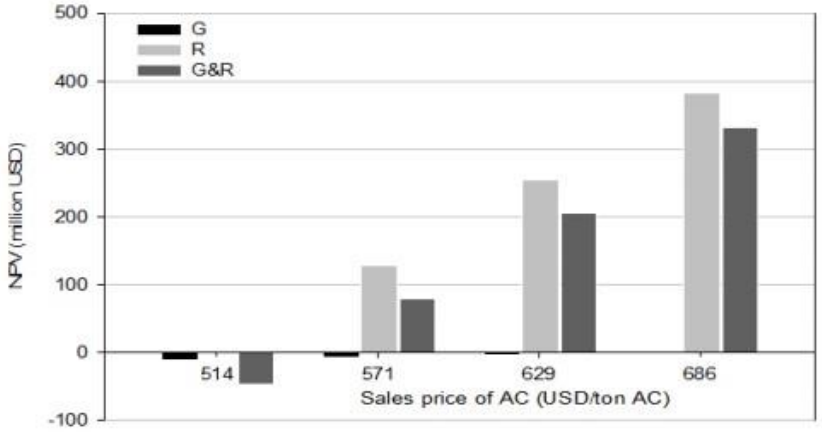


Figure 12. Comparison of NPV for 10-Year Investment life as a function of AC sales price [88].

2.2.2 Established regeneration methods

The main goal of regenerating ACs is to desorb the accumulated adsorbates and restore the porous structure with a little damage as possible to the carbon matrix [89]. There are several established methods by which ACs can be regenerated, and they all include subjecting the spent species to conditions that shift the adsorption equilibrium towards desorption [89] [90].

The ease of regeneration for an AC is dependent on the type of adsorption that took place during the loading – physisorption or chemisorption. If the adsorption that place in the

loading of the AC was physisorption, desorption can usually be achieved with heating, lowering the pressure, or washing with a solvent [89] [90]. However, if the AC was loaded via chemisorption, energy greater than the adsorptive force that created the covalent or ionic bonds during adsorption is required.

Thermal regeneration

Thermal regeneration of ACs shares similarities with the original activation process. Split into three steps, thermal regeneration is typically carried out as follows:

- the temperature is initially raised to approximately 200 ^{o}C for the drying and release desorption of the light volatiles.
- The AC is then pyrolyzed between 400 – 600 ^{o}C to remove reversibly adsorbed substances and to decompose irreversibly adsorbed substances (creating more char residue)
- For the following reactivation stage, the carbon will be heated to temperatures between 800 – 1000 ^{o}C in an CO_2 and/or steam-rich atmosphere, oxidising the char [91]. The detention time and amount of CO_2 and/or steam used is dependent on the adsorbate(s).

Advantageously, thermal regeneration can be used on a sample of ACs with a variety of adsorbates housed inside the pores. As expected, these heterogeneous adsorbates will react in a different manner to one another. These are categorised into three groups: type (1) compounds are volatile organics that are not irreversibly bound and thus they can be removed with ease in the initial stages of the regeneration; type (2) compounds are tightly bound to the AC (usually via strong covalent or ionic bonds) and do not undergo thermal regeneration and are instead undergo thermal cracking, forming volatile fragments; type (3) are those which undergo pyrolysis and leave behind carbonaceous residue [10] [92]. Types (2) and (3) require a controlled oxidation step to remove carbonised residue. The reactions that occur in the reactivation stage are identical to those in the activation step of AC production. Combustion conditions in the furnace are controlled to limit oxygen content to effect oxidation of the adsorbate rather than the carbon [10].

Steam and CO_2 are commonly used reactivating gases and use the following reactions [85]:

$C_{(s)} + H_2O_{(g)} \rightarrow CO_{(g)} + H_{2(g)}$	$\Delta H = 130$ kJ mol^{-1}	steam activation, water-carbon phase
$C_{(s)} + CO_{2(g)} \rightarrow 2CO_{(g)}$	$\Delta H = 159$ kJ mol^{-1}	carbon dioxide activation, water-carbon phase
$CO_{(g)} + H_2O_{(g)} \leftrightarrow CO_{2(g)} + H_{2(g)}$	$\Delta H = -41$ kJ mol^{-1}	water-gas equilibrium at >800 ^oC

As both reactions are endothermic, they can be manipulated into oxidising the pyrolyzed adsorbate without damaging the surface of the carbon [90]. Although, it is difficult to control the process conditions at such high temperatures, and so oxidation of the carbon surface can also occur. For reactivation 950 ^oC and above, even short residence times can lead to excessive oxidation of the carbons on the surface with potential carbon losses of 5-10% [10].

The biggest disadvantage with thermal regeneration is the potentially for loss of adsorption capacity due to the changes in pore structure of the carbon when heated to such high temperatures for a prolonged period. In the literature, it has been reported that the initial heating period of 10 minutes saw a marked increase in macro- & micropores due to further activation, but heating over the next 50 minutes saw a reduction in micropore volume of 44%, and an increase in meso- & macropore volume of 66% and 50%, respectively [10]. The physical changes that occurred were attributed to the burning out of the walls between the micropores. The loss of micropores contributed to an overall reduction in surface area and thus adsorption capacity.

Other disadvantages associated with thermal regeneration include extremely high energy requirements, air pollution issues associated with the release of off-gasses, and incompatibility with some adsorbates regarding the high operations temperature i.e. TNT [11].

Chemical & solvent regeneration

Chemical regeneration is the process by which adsorbates are removed from spent ACs by way of reactions with suitable chemical reagents. In literature there are two main groups of

reagents used for the regeneration process: those with oxidising ability (inorganics) and those with solubilising ability (organics) [12].

In literature there have been many attempts to regenerate ACs with suitable chemical regenerates, often with mixed results. In a 1984 study, Martin and Ng studied the effectiveness of various organic regenerates on the chemical regeneration of ACs via organics such as carboxylic acids, amines and chloromethanes. They discovered that there was a marked decrease in the effectiveness in regenerating the ACs with as the molecular weight of the organic regenerate increased. They surmised that the smaller regenerates could travel deeper into the micropores, displacing the adsorbates more effectively [93]. Leng and Pinto conducted a study in 1996 that explored the effects of the solubility of the organic adsorbates bound to spent ACs, and how the AC's surface characteristics could influence attempts at chemical regeneration. By using reactive inorganic reagents and controlling the surface charge characteristics through pH they were able to enhance the solubility of selected organic adsorbates in aqueous solution. The pair attempted this with phenol, an adsorbate that is notoriously difficult to solubilise and binds strongly to the AC surface, and they achieved a reduction affinity for the surface by changes in surface charge [12].

There are several advantageous aspects to chemical & solvent regeneration of ACs, such as: (1) The process can be conducted *in situ*, meaning that the unloading, transporting, and repacking of adsorbents is eliminated. (2) The loss of carbon and potential destruction of the parts of the porous network can be avoided. (3) It may be possible to fully recover valuable adsorbates. (4) Post-treatment, the chemical regenerate may be recovered and reused [12] [13].

However, this form of regeneration also comes with several disadvantages, such as: (1) Often the regenerates are required in large volumes and can be extremely costly. (2) If the chemicals being used are pollutants, which can be common, it can result in a dangerous working environment for those conducting the regeneration and be subjected to numerous legislative issues. (3) The level of regeneration is often dependent on the solubility of the adsorbate in the regenerate solution. (4) Multiple adsorbates may be adsorbed onto the surface of the AC, and each of which may require a different regenerate solution. AS such, chemical regeneration required extensive study of identity of adsorbates adsorbed onto the surface before it can be carried out [12] [13] [14].

Electrochemical regeneration

Upon reaching adsorptive capacity, ACs can be transferred to an electrochemical cell (anode or cathode) in which electrochemical regeneration can occur [95]. The principle behind electrochemical regeneration is that ions generated at the electrodes of the cell can change the local pH conditions, affecting the adsorption equilibrium, and in so doing organic adsorbates begin to desorb [95] [96]. Additionally, alternate methods include reactions between ions generated and the adsorbed pollutants resulting in the formation of a species with a lower adsorptive affinity for activated carbon, causing subsequent desorption, or oxidative destruction of organic adsorbates on the AC surface [97].

In cathodic electrochemical cells the cathode acts as a reducing electrode, producing OH^- ions which increase the pH of the local environment. With this, adsorbates migrate towards the anode where they are subjected to oxidation, destroying the migrated adsorbates [98]. In anodic regeneration the anode acts as an oxidising electrode, resulting in a lower localised pH during electrolysis, which also prompts desorption of some organic adsorbates [98] [99].

Both techniques hold several advantages, including: (1) the ability to be performed *in situ*. (2) Can be performed at room temperature, as opposed to the extreme high temperatures of thermal regeneration. (2) The treatment can be stopped in a matter of seconds, rather than having the issue of having to wait for a heated system to decrease in temperature before removing the ACs. (3) The energy consumption is far lower (0.20 – 1.80 kWh/kg) than that of thermal regeneration (220 – 250 kWh/kg) [98] [100] [101].

However, there are drawbacks to the use of electrochemical regeneration of ACs: (1) in cathodic regeneration, due to mass transfer limitations between the cathode and the anode, there is often residual desorbed adsorbate left in the cathode. (2) The technique has only been applied successfully to organics compounds. (3) The regeneration is not as efficient as other techniques, with typical cathodic regeneration being 85% at best, and anodic regeneration being between 65-80% [98] [100] [101].

Effects of impregnation on regeneration

As previously discussed in this literature review, ACs are sometimes purposefully impregnated with specifically chosen compounds to increase selectivity in adsorption [102]. Impregnates can alter the surface charge, the temperature required for initial production, and the overall adsorptive capacity of the ACs [82] [93].

It stands to reason that when impregnated ACs are subjected to similar environments as they were under production, with several types of regeneration being like production methods, there may be adverse effects. In 2015, Gibson *et al* noted that thermal regeneration temperatures caused the impregnate, triethylenetetramine (TETA), to leach away from the AC bed and form carboxylate, carbamate, and urea complexes [103]. This was believed to be due reactions between the TETA and the carbon bed were more favourable at higher temperatures than that of TETA and the CO_2 it was supposed to be adsorbing [103] [104]. After the first regeneration cycle, 20% of the adsorptive capacity was lost. However, the use of chemical regeneration on CO_2 spent ACs impregnated with similar amino compounds does not suffer with the amine leaching issues Gibson *et al* faced with their experiment, as found by Khalil in 2018. Instead, Khalil found that the regenerated amino-impregnated ACs achieved a faster breakthrough time when being loaded with CO_2 than virgin non-regenerated ACs [105].

Khalil did however find that after multiple regeneration cycles of the amino-impregnated ACs, there was a significant decrease in adsorptive capacity [105]. Conversely, ACs impregnated with metals that undergo chemical regeneration have been documented as having retained a high level of absorptivity and desorptivity after multiple regeneration cycles (as seen in Figure 13) [106] [107]. This would suggest that certain regeneration methods may be suitable for types of spent impregnated ACs, but other may require a different form of regeneration, especially those carrying out multiple cycles.

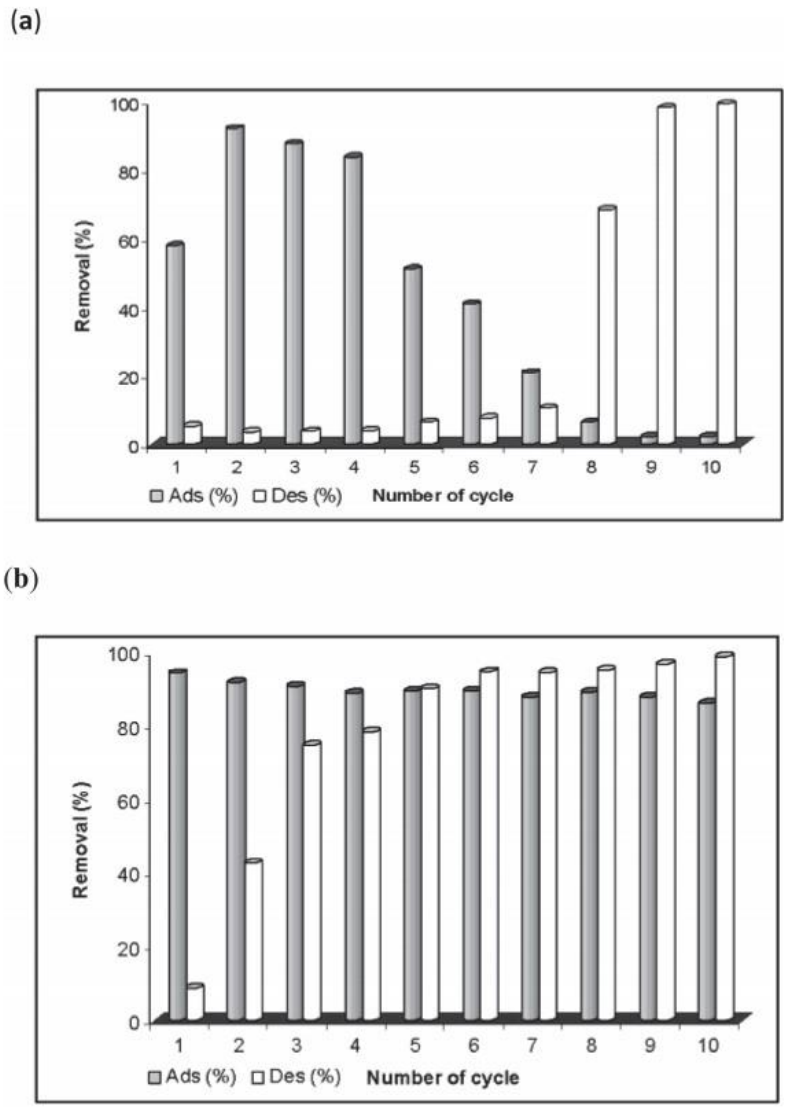


Figure 13. Methylene Blue adsorption/desorption study on (a) activated carbon, and (b) Fe-impregnated activated carbon (H2SO4 as desorbing agent) [106].

2.3 Microwave technology and regeneration

Microwaves (MW) are a form of electromagnetic energy located on the electromagnetic spectrum between 300-300,000 MHz; in the region between infrared and radio frequencies and have corresponding wavelengths of 1 cm-1 m [108] [109] [110]. Because telecommunication and cellular frequencies also operate in the same area of the electromagnetic spectrum as microwaves, most mw reactors and domestic MW ovens operate at a frequency of 2.45 GHz, or around 900 MHz Other frequencies are reserved by the likes of the Federal Communications Commission for industrial, scientific and medical purposes [108] [111].

2.3.1 Conventional radiant heating process

Conventional heating relies on three basic heat transfer concepts: conduction, convection and radiation. Through it long established usage in human society, conventional heating has become a highly adaptable technology with a multitude of uses in both domestic and industrial applications.

Conventionally heated electrical furnaces use heating elements which are usually made from resistance wires. The basis for the heat production in these furnaces is the resistance from the element material against the flow of the electric current [112]. The heat generated from this process is then transferred to the surface of the material by means of conduction, convection or radiation through intermediate media. After the material in question receives the heat, it is transferred from the surface towards the centre of the material's body, primarily via conduction (see Figure 14) [112]. During the conventional heating of the material, a large heat gradient is formed from the surface to the core of the material. However, due to thermal inertia of the system, the temperature of the material is always lowers than the furnace itself, which can often lead to areas inside the material being unable to reach the desired temperature without prolonged exposure to the heat source [113].

Despite being the favoured heating method for many years, conventional heating is problematic due to its slow and imprecise heating of the workspace surface. Even when assuming that surface temperature is controlled precisely, the rate at which heat is transferred from the surface into the body is highly limited by the physical properties of the material, such as specific heat, thermal conductivity & density, plus thermal diffusivity of the

workspace. Additionally, a larger workspace implies a longer time to heat the workspace by conventional methods and is also much more difficult, as well as non-uniform [113] [114].

2.3.2 Microwave heating process

In brief, the use of MWs for heating purposes originated in the 1940s with the inception of the first magnetrons, initially for military radar purposes [115]. The invention of the magnetron sparked vastly increased levels of research into MW technology, including the development of the first commercial MW oven in 1950, and its subsequent use in industry from 1962 [116]. Since 1962, MW heating has been successfully used in various industrial and domestic applications such as food industry, vacuum drying, crude oil exploration and processing, and many more [115] [116].

Unlike conventional heating, MW heating heats both *volumetrically* and *selectively*, resulting in a more efficient heating of material. MW heating is achieved throughout the volume of the material by the conversion of electromagnetic waves energy to heat as waves penetrate the substrate (as seen in Figure 14) [108]. Consequently, the heating is not limited by thermal diffusion through the material, thus uniform heating of the material is achieved. The selectivity of MW heating comes from the fact electromagnetic wave energy is only dissipated as heat in materials with dielectric properties (and not necessarily everything that meets them) [108] [117].

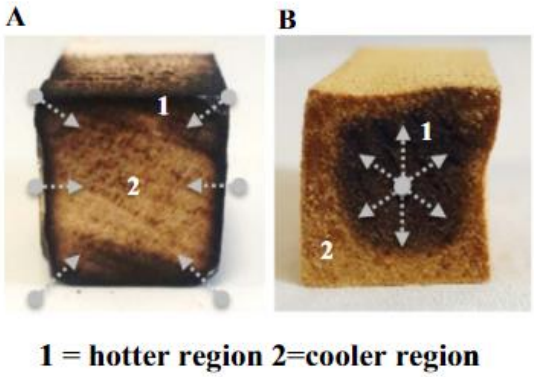


Figure 14. The difference in temperature distribution and direction of heat transfer between conventional and microwave heating: (A) conventional heating – heat is transferred from the outside of the material inwards by conduction, (B) microwave heating – MWs penetrate the material and heat volumetrically. Energy is uniformly dissipated throughout the material [108].

By enabling high heating rates, utilising MW energy may lead to significant savings in total energy consumption and process times. In recent times, MW heating has been used in the processing of municipal waste, sewage sludge, contaminated soil, plastic, rubber waste and many other dielectric materials, proving its versatility [118] [119] [120] [121] [122]. However, although MW heating is seen to be an advantageous alternative for conventional heating techniques in waste management and conversion processes, it's worth noting that it is not without its limitations. A few examples of this being: often the knowledge of a material's dielectric properties is lacking; lack of control over the accelerated heating (thermal runaway); transfer of MW energy to the workplace is not always efficient, and many other [120] [123].

Microwave heating efficiency

When comparing MW heating to more conventional heating methods, efficiency is key. There have been notable recordings in the literature of MW heating achieving greater efficiency than conventional methods, namely in the chemical, food and extraction industries [124] [125] [126]. However, MW heating efficiency depend greatly on the type of application and material being heated. In his work on comparing MW and conventional heating being used to run meso scale organic reactions, Moseley argued that the efficiency of conversion of electrical energy into MW energy was approximately 50-60% (assuming that all MW energy is adsorbed by the material), and it would not result in a dramatically increased overall efficiency when compared to conventional techniques [124].

The type of material being heated has a profound influence on the on the efficiency of MW heating process; in other words, some materials cannot be efficiently heated by MWs. Materials being hit by MWs are placed into three general categories: (1) MW transparent/insulator – MWs pass through the material without any losses (e.g., glass and ceramics); (2) MW-conducting – MW do not penetrate and are instead reflected (e.g. metals); or (3) MW-adsorbing – MW are adsorbed and converted into heat (e.g. polar molecules such as water) [107] [127]. As such, the benefits of heating with MWs can be substantial only when applied to suitable material; this is of more significance when heating times is a crucial factor, as the slow heating rates achievable by conventional methods have a far higher energy consumption.

Microwave heating mechanism

As stated earlier in this review, a significant aspect of MW heating is its ability to heat a material volumetrically; each element of the material being heated individually, and ideally at a similar rate. In his 1998 book on the engineering applications of MW heating, Meredith explained that there were four methods by which volumetric can be achieved: (1) conduction/induction for materials with a low resistivity – achieved at electrical frequencies of DC to 60 Hz for conduction and 50 Hz to 30 kHz for induction (usually used in annealing and/or hardening processes in metallurgy); (2) ohmic heating of conduction f heating liquids and solutions – achieved at frequencies in the range of 50 or 60 Hz; (3) radio frequency heating of materials with high resistivity – achieved at frequencies ranging between 1-100 MHz; and (4) MW heating [128].

To understand the principals of MW heating, the definition of specific terms is required, most importantly of all are *dielectrics* and *dipoles*. An electric dipole consists of two equal and opposite charges, located at a certain distance. A host of molecules intrinsically carry dipoles due to their non-uniform distribution of positive and negative charges on various atoms. Molecules holding a permanent dipole are termed as polar molecules. Dielectric materials are electrical insulators (or partial insulators) which do not intrinsically contain dipoles but can be polarised when placed in an electrical field. This form of polarisation takes place when minute changes in the charges of the molecules in insulating or partially insulating materials occur. The difference between conductors and dielectric materials comes from the charges in the dielectric materials being held by atomic or molecular forces and their inability to move en masse (as occurs in conductors) when passing an electric current.

In Figure 15, the polarisation of permanent dipoles under an electric field can be seen. Additionally, three other mechanisms of dipole induction and polarisation under an external electric field are shown: (b) atomic polarisation takes place through the displacement of atomic nuclei due to the unequal distribution of charges in a molecule; (c) electronic polarisation occurs when electrons around the nuclei are displaced generally to one side under due to the effects of a n external electrical field; and (d) Maxwell-Wagner (interfacial) polarisation occurs in areas where charge has built up in the interfaces between components in heterogeneous materials (or due to imperfect arrangement of atoms, ions or molecules) [128] [129].

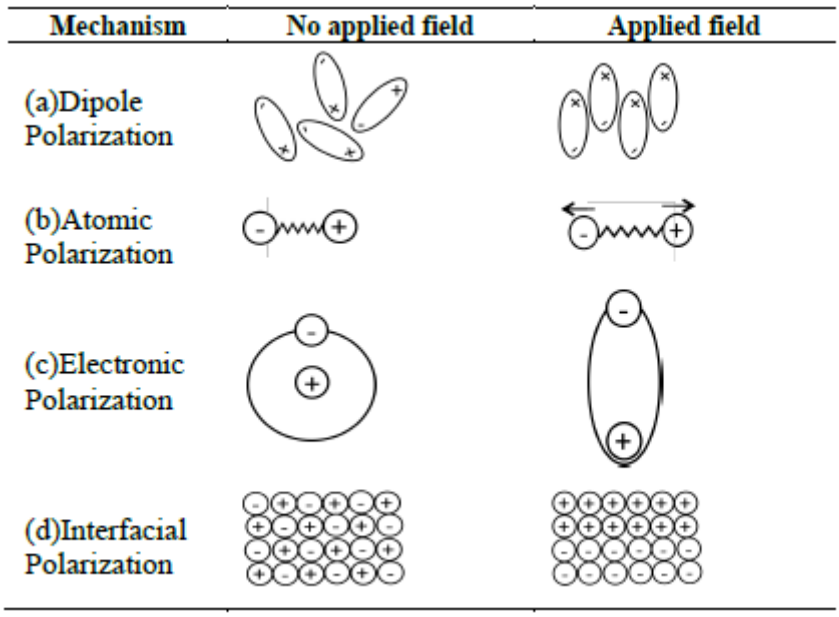


Figure 15. Mechanisms of polarisation: (a) dipole, (b) atomic, (c) electronic, (d) Maxwell-Wagner (interfacial) polarisation [129].

Dipolar components tend to tend to physically align with the electric field once introduced to an electromagnetic field. MW frequencies are low enough to provide sufficient time for dipoles to realign to the field, and high enough to stop re-orientation taking place simultaneously with the field oscillations. Phase lag between the field charges and dipole re-orientation (i.e., *relaxation time*) is attributed to heat generation through molecular friction and collision; the amount of heat produced (power dissipation) is directly related to MW frequency [128] [130] [131].

Permittivity and permeability

MWs, as with all electromagnetic waves, consist of an electric (X component) and a magnetic (Y component) field, oscillating perpendicular to each other, as shown in Figure 16. The fields are expressed thusly:

Equation 7.

$$E = \mathrm{E}_0 \, \mathrm{e}^{-\gamma z} \hat{\mathrm{x}}$$

Equation 8.

$$H = \frac{\mathrm{E}_0}{\sqrt{\mu/\varepsilon}}\, \mathrm{e}^{-\gamma z}\hat{\mathrm{y}}$$

Where: E_0 = Amplitude of the electric field

γ = Propagation constant

ε = The material's permittivity

μ = The material's permeability

$\hat{x}$ = Electric field

$\hat{y}$ = Magnetic field

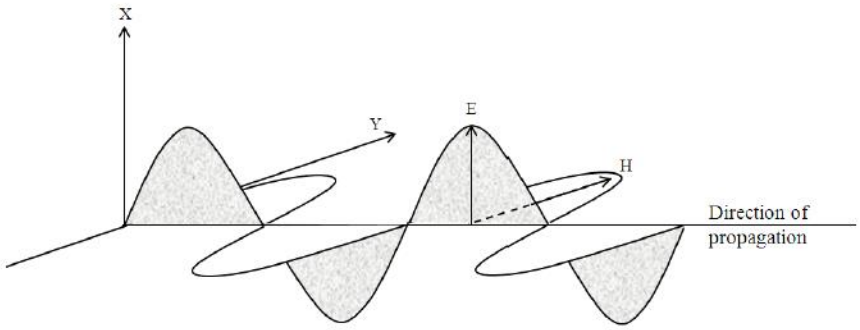


Figure 16. Travelling Electromagnetic wave through a dielectric loss [132].

Permeability is the ability for a material to support the formation of a magnetic field within itself. Although, it should be noted that the effect of permeability in non-magnetic materials is negligible, and so it plays a less significant role in the heat conversion throughout MW heating. And so, the capability of materials in adsorbing the MWs and heat conversion is more governed by their dielectric properties in terms of their real dielectric constant or permittivity (ε), relative dielectric constant (ε'), effective dielectric loss factor (ε''), and loss angle (δ). With the relative dielectric constant, ε', being the permittivity of material relative to that of free space and represents the ability of a dielectric to store the potential electric energy if placed in an electric filed. And the effective loss factor, ε'', being representative of the efficiency of conversion of adsorbed energy to heat [108] [130] [132]. To account for loses, the dielectric constant for a real dielectric is expressed in terms of permittivity, ε* [121]:

Equation 9.

$$\varepsilon^* = \varepsilon' - j\varepsilon''$$

Characterisation of dielectric material is usually done with their loss angle, which is expressed as the ratio of real permittivity and the loss factor [133]:

Equation 10.

$$\tan\delta = \frac{\varepsilon''}{\varepsilon'}$$

Where: ε = Real dielectric constant

ε' = Relative dielectric constant

ε'' = Effective dielectric loss factor

δ = Loss angle

ε* = Dielectric constant for a real dielectric is expressed in terms of permittivity

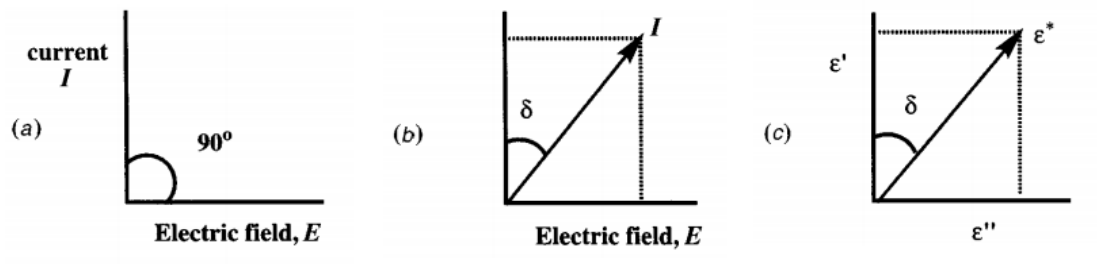


Figure 17. Phase diagrams for (a) an ideal dielectric where the energy is transmitted without loss; (b) where there is a phase displacement, δ, and the current acquires a component I 3 sinδ in-phase with the voltage and consequently there is a dissipation of energy. In (c) the relationship between ε, ε' and ε'' is illustrated; tanδ = ε''/ε' [133].*

When a dipole is placed in an electric field, it will try to reorient to the variations of the alternating voltage of the electric field. This results in an electric current known as the Maxwell displacement current. The parameter δ represents the phase displacement caused by the dipole lag the electric field i.e., the lag between the re-orientation of dipoles with the electric field oscillation.

As seen above in Figure 17, when an ideal dielectric is placed in an oscillating electric field, there is no lag between the electric field and variations of voltage in the electric field. Which would imply that displacement current is at a 90° angle with the electric field and energy is transmitted without loss due to absence of a component of the current in phase with the field. However, in a real dielectric, the phase displacement (δ) acquires a component I x sin δ

in phase with the electric field, resulting in the energy dissipation and heat production through internal resistance rotation i.e., resistive heating [133]. As such, in addition to heat capacity and density of the material, the dielectric loss is helpful in allowing for comparisons between materials in terms of their heating rates under the influence of an electromagnetic field.

The suitability for microwave heating

As mentioned in Section 4.2.1, not all materials can be heated via the use of MWs, and the ability to do so is usually dependent on dielectric properties of the materials being heated. There are two quantitative terms indicative of the suitability of materials to be MW processed; power absorbed per unit volume (P_A), and depth of penetration (D_P). According to the power adsorbed per unit volume of the materials, they can be identified to be suitable for MW heating as MW receptors [130], as shown in Figure 18 below.

Equation 11.

$$P_A = 2\pi f \, \varepsilon'' \varepsilon_0 {E_{rms}}^2$$

Where: P_a = Power absorbed per unit volume

f = Frequency, Hz

ε'' = Effective dielectric loss factor

ε_0 = Permittivity of free space

E_{rms} = The Root mean square of electric field strength in material

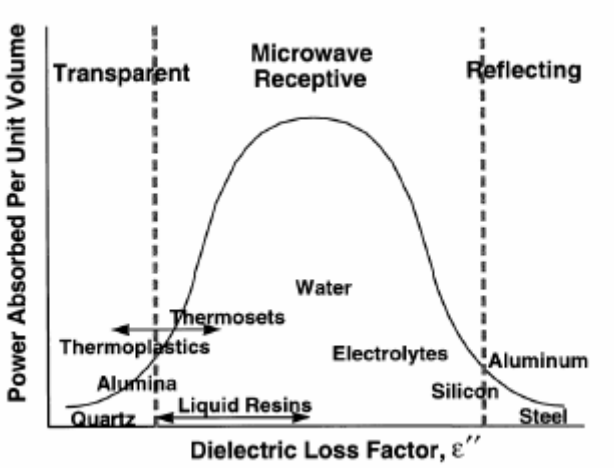


Figure 18. The relation between power absorbed per unit volume and dielectric loss [130].

However, it should be known that Equation 11 is only valid for very thin materials, where the electric field can be constant, due to the electric field losing its influence as distance from the surface increases. As such, the D_P value is defined as distance from the surface of the sample, where the absorb3ed material is as the specific ratio (I/e) of the power at the surface of the material. A simplified version of MW penetration depth is given in Equation 12b [130]. However, in their 1995 paper, Thostenson and Chou used the real loss factor (ε'') rather than the relative or effective loss factor [118], thus the equation is modified from Equation 12a, to 12b:

Equation 12a.

$$D_P = \frac{C\varepsilon_0}{2\pi f\, \varepsilon''}$$

Equation 12b.

$$D_P = \frac{C}{2\pi f\, \varepsilon''}$$

Where: D_p = Penetration depth

C = Speed of light in a vacuum

ε'' = Effective dielectric loss factor

ε_0 = Permittivity of free space

f = Frequency, Hz

Equation 12b helps to process particularly thick materials as, if the penetration depth of the MW is much less than the material thickness, the rest of the material is heated by conduction.

Microwave heating of non-coupling materials

For those materials with a low MW heating capacity, there are techniques to allow MW heating to occur. A famous example being the 1996 research conducted by Clark and Sutton, in which they increased the temperature of the material being heated until MW adsorption reached a point at which self-heating was possible, and more uniform heating could be achieved [134]. Another example being the introduction of MW heating to non-responsive materials whilst said material is coupled with a highly responsive material, such as carbon. This can be highly favourable if the additives and mixing ratios are selected properly.

Although, it should be noted that heating non-susceptible materials using responsive additive materials does not necessarily enable the energy transfer benefits of the MW heating (such as volumetric heating) to be realised as the heat is initially transferred from one material to the other through conventional thermal conduction from receptors with the associated inefficiencies. Additionally, as seen with MW heating in general, the heating can cause excessive increase in radiation adsorption ability of additives at higher temperatures, which may lead to thermal runaway. Under these conditions the temperature of the material raises uncontrollably, often irreversibly damaging the material [123].

When it comes to the MW processing of biomass the poor dielectric properties are not the controlling factor of the heating process. Instead, the selective heating process of MWs allows for the heating of the water stored inside the biomass source. Once the water has been removed, the biomass often becomes completely MW transparent though. Heating the biomass through water molecules is generally not enough to cause initiate pyrolysis, and so MW heating receptive additives such as char or inorganic matter are added. However, as mentioned above, this brings with it a set of new potential problems [135].

2.3.3 Microwave structure

The structure of a MW oven, as well as the output power, has a significant effect on the heating of objects. If any changes occur in the configuration of the system, such as single or multimode MW ovens, shape and size of the cavity, shape and type of the reactor and its position within the MW cavity, could cause considerable changes in the heating behaviour of the materials inside. This characteristic of MW heating can make the process receptive to uncontrollable changes, it also provides an element of versatility to the production method through making simple adjustments to the above factors. Thus, understanding the mechanism through which electromagnetic waves are produced and delivered to the material in a MW heating system is indispensable.

The overall mechanical structure of a MW oven consists of a high voltage power supply, MW source, transmission lines, cooling system, and applicator (see Figure 19 below). With the power system producing high voltage current which is later converted to electromagnetic waves through charge acceleration in the MW source. This section will seek to explain the key parts of a MW oven in detail.

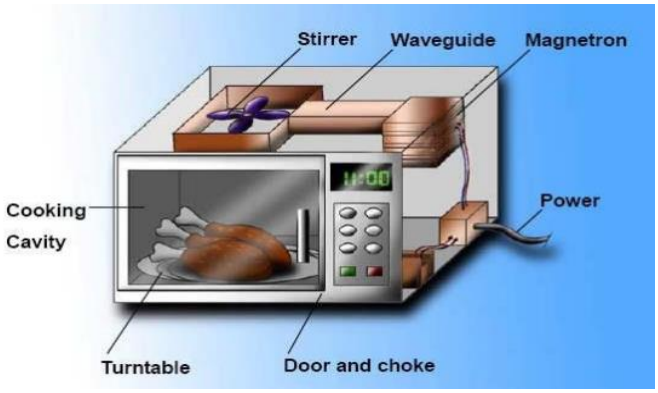


Figure 19. Schematic diagram of mechanical structure for a typical microwave oven [136].

Microwave sources and transmission lines

The most common MW sources used in MW heating are magnetrons and klystrons. Of the two, magnetrons tend to be favoured due to their frequency ability, higher efficiency, and lower cost due to mass production. However, klystrons can produce higher powers and their lifespan can be up to eight times that of magnetrons [130].

Magnetrons produce MWs ranging between 1-40 GHz at ~80% efficiency and have an average lifespan of 5000 hour. As shown in Figure 20, magnetrons structures consist of a cylindrical cathode placed on the axis of a circular copper anode, in a vacuum tube. The high-density magnetic field given off by magnetrons is produced by a permanent magnet (or electromagnet) placed around the anode [138].

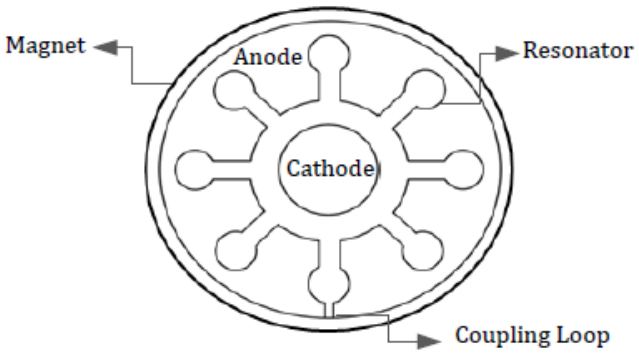


Figure 20. Schematic diagram of a magnetron [137].

Applying a high voltage between the electrodes causes loosely bound electrons to be ejected from the tip of the cathode under a strong electric field. However, the high density magnetic created by the magnet can cause electrons to follow a spiral path, resulting in a swirling cloud

of electrons [130] [139]. When this occurs, cavities inside the anode act as resonators, resulting in an acceleration of electrons. And so, the electron cloud starts to swirl more vigorously by entering the resonant circuit. Oscillation frequency is dependent on the size of these cavities. The high frequency swirling electrons produce electromagnetic waves, which are directed to the transmission lines (waves guides), and eventually to the applicator [130] [139] [140]. The transmission lines can be made from conductive materials such as copper, brass, silver, aluminium, or other similar materials with low bulk resistivity [130].

Applicator

The MW applicator refers to the space in which MW energy is coupled with the subject material. MW coupling with the subject material is strongly influenced by the size and geometry of the applicator, as well the material size and location, and the size and shape of the subject material relative to the applicator, plus the subject material's dielectric properties [141].

The geometry of the cavity can determine how electromagnetic waves resonate in the applicator to produce *standing waves*. These standing waves are produced from the reflection of waves off the cavity walls, where they will begin to form a three-dimensional stationary pattern with high and low-density (known as *modes*) [131]. As such, cavities are designed to operate in single- or a multi- mode manner. Single-mode applicators are made in the size of one order of wavelength, which can be calculated by solving Maxwell equations with one resonance mode. Single-mode cavities contain non-uniform, but well-defined and predictable electromagnetic fields, implying that high and low points of standing waves can be closely located. Knowing the location of hot spots in the MW cavity can help with optimisation of heating efficiency [130] [139].

Although single-mode applicators provide higher power densities, their limited cavity size can only be used for small samples, especially those with low effective loss factors. Multimode applicators (i.e., MW ovens) on the other hand can are built with at least one dimension much larger than one wavelength in free space, meaning they can be used on much larger samples. However, multimode applicators can result in a non-uniform electromagnetic field and multiple heating locations (see Figure 21 below). But, an increased length of the cavity, the more uniform the heating is expected to be in multimode cavities [130] [138] [141].

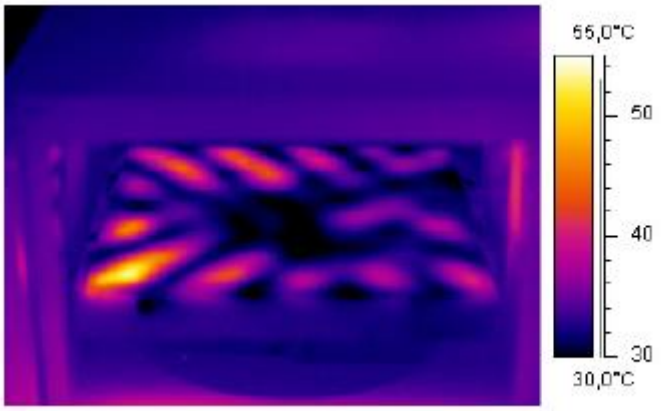


Figure 21. Horizontal mode structure in microwave cavity using infrared thermal imaging, while heating thin layer of water on a glass plate [138].

In the literature, there have been recorded uses of domestic MW ovens in initial stages of experimental work concerning MW heating, often with experiment-specific modifications. However, such experiments are often limited by the domestic MW oven drawback i.e., not being designed for high temperatures (>~150^{o}C) and having no provision for temperature control [142] [143]. Domestic MW ovens also tend to produce multiple hotspots on their subject material. There have been some solutions to achieve more uniform heating in the material, one of which is the use of *mode stirrers*; metallic rotating vanes fans with a speed of 1-10 Rev/s that can be placed near the waveguide input [142].

2.3.4 Regeneration of activated carbons by microwave heating

Microwaves have been used in the production, modification, and regeneration of activated carbons, however, the level of research into the latter is significantly less than the other two. But this does not mean that the research conducted has not been of relevance to this thesis.

Ania *et al*'s 2005 paper on the effects of MW and conventional regeneration on the microporous & mesoporous network, and the adsorptive capacity of AC, is of note. The research group found that the use of MW energy in the regeneration process shortened the time required significantly when compared to the thermal regeneration of spent ACs from the same source. Additionally, MW heating achieved preservation of the porous structure with a higher efficiency than that than those regenerated thermally. Both forms of regeneration were cycled several times, with microporosity reducing with each successive cycle. However, thermal regeneration shifted the micropore size distribution to pores of

narrower size. And the apparent BET surface areas were also reduced significantly over the regeneration cycles. A loss of the adsorptive capacity of the carbon material was observed after six adsorption-desorption cycles in both systems [144].

In other studies, rather than conducting the entirety of the regeneration process using MW heating, the technique has been paired with conventional thermal heating. This is known as MW-assisted regeneration. Although rather than being run in tandem, the ACs are first carbonised thermally, before MW are employed for the activation step to remove any latent organic volatiles [145]. In studies by the likes of Coss *et al* and Foo *et al*, MW-assisted regeneration has been carried out with the conventional method being chemical (due to the ACs being impregnated). In both studies, the use of MWs in the activation step of regeneration allowed for not only removal of volatiles, but also the reclamation of active sites. Neither study saw a drop in impregnate number by more than 5% after multiple regeneration cycles [146] [147].

However, the purpose of this study is to apply and study the ability of MW regeneration on sulphurous spent activated carbons. This area represents a significant gap in the literature where MW regeneration is concerned. But, to address any potential issues, the next section will explain the adsorption mechanics of sulphurous carbons and their absorptivity regarding ACs.

2.4 Regenerating spent sulphurous activated carbon

Sulphur is a multivalent compound that's widely abundant in nature, and often a component of common compounds found in the emissions of industrial processes. Sulphurous compounds are one of the major groups of contaminants ACs are used to remove.

2.4.1 Adsorption mechanics of sulphurous compounds

Sulphurous compounds such as H_2S and SO_x have become a key issue in industrial operations. Thus, the use of adsorbate materials such as ACs being used to remove them has become increasingly popular. As previously discussed in Section 2.4, there are two main forms of adsorption that take place when ACs are used as an adsorbate: physisorption and chemisorption. This is seen for both sulphurous species groups in question, as well as oxidation on the surface of the AC post-adsorption. The following section will go into the

mechanisms of how ACs adsorb sulphurous materials, and the issue that arise in the regenerations processes.

Sulphur oxides' reaction mechanism

The physisorption of SO_2 onto ACs is greater at lower temperatures, as shown in reactions 1 and 2; with SO_2 producing (sulphurous acid) H_2SO_3 when reacting with H_2O only, and sulphuric acid (H_2SO_4) produced when reacting with water and oxygen [148].

(1) $SO_{2\,(g)} + H_2O_{\,(ads)} \rightarrow H_2SO_{3\,(ads)}$

(2) $SO_{2\,(g)} + ½\ O_{2\,(ads)} + H_2O_{\,(l)} \rightarrow H_2SO_{4\,(ads)}$

Additionally, in the presence of O_2, SO_2 can be adsorbed directly onto AC before oxidation to SO_3, as shown in reactions 3, 4, and 5 [149] [150].

(3) $SO_{2\,(g)} \rightarrow SO_{2\,(ads)}$

(4) $O_{2\,(g)} \rightarrow O_{2\,(ads)}$

(5) $SO_{2\,(ads)} + ½\ O_{2\,(ads)} \leftrightarrow SO_{3\,(ads)}$

Theoretically chemisorption should be favoured in the adsorption of SO_2 due to it having a *trigonal planar* geometry, unconducive of the layered packing one might expect in multilayer physisorption. As such, higher temperatures would be expected to be conducive to good adsorptivity as it would allow the SO_2 to overcome the activation barrier and raise the collision fraction of sufficient collision energy to react with impregnated alkali metal oxides i.e., potassium hydroxide (KOH) [15]. However, literature has shown that the adsorptivity has decreased as the temperature increased. In fact, at lower temperatures (300 K), the following occurs:

(a) The H_2O produced by the reaction between KOH and SO_2 on the surface of the KOH impregnated AC ($KOH_{(IAC)}$) becomes adsorbed to the surface, reacting with SO_2 and O_2 to produce H_2SO_4, which then goes on to react with KOH to form K_2SO_4 (a stable crystalline solid). At temperatures higher than 600 K decomposition occurs, and so the majority of the H_2SO_4 will remain on the surface at lower temperatures. This is due to SO_2 being more soluble than H_2SO_4 at lower temperatures, and the reaction between KOH and H_2SO_4 is superior to the direct reaction between SO_2 and KOH [149] [150].

(b) The equilibrium of the SO_2 reaction with O_2 shifts towards the production of SO_3 with decreasing temperature [151]. Thus, the oxidation of SO_2 to SO_3 will occur.

(c) Research by the likes of Lisovskii *et al*, and Mochida *et al*, shows that although chemisorption is favoured, physisorption does occur at lower temperatures on ACs adsorbing sulphurous compounds. So, whilst K_2SO_4 and $KOH_{(IAC)}$ are formed are formed simultaneously through chemisorption, physisorption is expected to occur at the same time [152] [153].
And so, at low temperatures, the following reactions are expected to occur as the dominant mechanism. The reaction between KOH and SO_2 forms K_2SO_3 and H_2O. The formed H_2O adsorbed to the surface is converted into H_2SO_4 by reacting with SO_2 and O_2. Then, with 2 mol of KOH, K_2SO_4 is formed, simultaneously producing 2mol of H_2O, circulating mechanism (8), and thus creating a repetitive reaction [15].

(6) $2\ KOH_{(IAC)} + SO_{2\ (ads)} \rightarrow K_2SO_{3\ (ads)} + H_2O_{\ (ads)}$

(7) $K_2SO_{3\ (ads)} + ½\ O_{2\ (g)} \rightarrow K_2SO_{4\ (ads)}$

(8) $SO_{2\ (ads)} + ½\ O_{2\ (ads)} + H_2O_{\ (ads)} \rightarrow H_2SO_{4\ (ads)}$

(9) $2\ KOH_{(IAC)} + H_2SO_{4\ (ads)} \rightarrow K_2SO_{4\ (ads)} + 2\ H_2O_{\ (ads)}$

When adsorption takes places at higher temperatures (340-370 K), the following occurs:

(a) Instead of staying adsorbed to the AC surface, the reaction between KOH and SO_2 vaporises contrary to the low-temperature temperature reaction, oxidation into K_2SO_4 by adsorption of SO_2 following reaction between KOH and SO_2 will take place, which is contrary to low-temperature cases (reaction mechanism 10) [15].

(b) Regardless of H_2O being present, SO_2 does not readily become H_2SO_4 (reaction mechanism 8) as its solubility for H_2O at higher temperatures is low [154].

(c) Because chemisorption of oxygen takes place on the surface of ACs at high and low temperatures, oxidation of K_2SO_3 into K_2SO_4 is facilitated (reaction mechanism 12), producing an O_2 by-product which goes on to facilitate SO oxidation [151]. The adsorptivity will show large variances from that at low temperature.

(10) $2\ KOH_{(IAC)} + SO_{2\ (g)} \rightarrow K_2SO_{3\ (ads)} + H_2O_{\ (ads)}$

(11) $K_2SO_{3\ (ads)} + ½\ O_{2\ (g)} \rightarrow K_2SO_{4\ (ads)}$

(12) $K_2SO_{3\ (ads)} + 2\ SO_{2\ (g)} \rightarrow K_2SO_{4\ (ads)} + 2SO_{\ (g)} + ½\ O_{2\ (g)}$

In summary, the reaction mechanism at higher temperature is as follow: no source of H_2SO_4 is produced, K_2SO_3 is formed instead and takes up the selective adsorption sites of K-IAC in the form of K_2SO_4. Reaction mechanisms 6, 7, 10, and 11 are the only mechanism that occur at both high and low temperatures.

Hydrogen sulphide reaction mechanism

Another particularly common sulphurous contaminant that warrants the use of ACs is hydrogen sulphide (H_2S). The mechanism for the adsorption of H_2S onto AC is somewhat simpler than that of SO_2, and research literature explains that it is less temperature dependent [144]. Due to its two sets of electron pairs producing a greatly electronegative force on the bonded hydrogen, the molecular geometry of H_2S is *bent*. The bent formation of the molecule allows for an easier layer packing than the likes of SO_2, meaning physisorption acts as the dominant type of surface adsorption [155] [156].

In the physisorption, H_2S adsorbs directly onto the surface (reaction 1), before dissolution into the water/steam film (reaction 2), followed by dissociation of the H_2S in an adsorbed in the water/steam film (reaction 3).

(1) $H_2S_{(g)} \rightarrow H_2S_{(ads)}$

(2) $H_2S_{(ads)} \rightarrow H_2S_{(ads\text{-}liq)}$

(3) $H_2S_{(ads\text{-}liq)} \rightarrow HS^-_{(ads)} + H^+$

Additionally, surface oxidation reactions with adsorbed oxygen (reaction 5 and 6), or transition metal oxide catalysts (i.e. Fe, Zn, and Cu in carbons) will occur, converting H_2S into either elemental sulphur (S) or SO_2. Further oxidation of the SO_2 to H_2SO_4 will also happen if the reaction system has water/steam present (reaction 7) [16] [156].

(4) $O_{2\,(g)} \rightarrow O_{2\,(ads)}$

(5) $HS^-_{(ads)} + ½\ O_{2\,(ads)} \rightarrow S_{(ads)} + OH^-$

(6) $HS^-_{(ads)} + 1\ ½\ O_{2\,(ads)} \rightarrow SO_{2\,(ads)} + OH^-$

(7) $SO_{2\,(ads)} + ½\ 2O_{2\,(ads)} + H_2O_{(ads)} \rightarrow H_2SO_{4\,(ads)}$

(8) $H^+ + OH^- \rightarrow H_2O$

Although physisorption may be the more dominant form of adsorption of H_2S onto AC, chemisorption still takes place. H_2S requires an alkali earth metal hydroxide such as KOH to

be present for chemisorption. The resulting reactions convert the H_2S into either adsorbed KHS or K_2S, with by-products of H_2O (reactions 9 and 10). Moreover, the H_2O produced from both reactions can aid the oxidation of the SO_2 (formed in the physisorption) into H_2SO_4 (see reaction 7) [157].

(9) $H_2S_{(g)} + KOH_{(IAC)} \rightarrow KHS_{(ads)} + H_2O_{(ads)}$

(10) $H_2S_{(g)} + KOH_{(IAC)} \rightarrow K_2S_{(ads)} + 2\ H_2O_{(ads)}$

However, there are notable disadvantages to chemisorption being used for the adsorption of H_2S: (1) at low temperatures self-ignition can occur due to the exothermic nature of reactions between KOH and naturally occurring CO_2 in the air, (2) the capacity for simultaneous physisorption is limited due to the filling of the pore system with the impregnate, (3) H_2SO_4 produced during oxidation is corrosive and can damage equipment, (4) the cost of alkali earth metal hydroxides is high and the costs for impregnating ACs with them further increases running costs [158] [159]. In summary, the two forms of adsorption happen simultaneously, with chemisorption helping to propagate further oxidation reactions from those first achieved because of the physisorption.

2.4.2 The issues with regenerating spent sulphurous activated carbon

As discussed in Section 3.2.1, during the conventional regeneration of spent sulphurous ACs the system is heated to high temperatures of 400-600 ^oC for the pyrolysis stage, before being heated up to 1000 ^oC during the reactivation stage [91]. The purpose of which is to convert the adsorbed sulphurous compounds into gases so that they can be removed. However, heating the removal of the adsorbed compounds present several issues, as will be discussed below.

Gaseous H_2S removed from the AC is an extremely odorous and very toxic gas. In terms of its toxicity, prolonged exposure to low levels of the gas can induce nausea, tearing at the eyes, headaches, or loss of sleep, as well as bronchial constriction in those who suffer from asthma. As concentrations increase, exposure can inflict more dangerous effects on persons in its vicinity, including loss of smell and even death [160]. However, post-adsorption, some of the H_2S has been converted to S, which is also an extremely pungent and toxic compound. There are also issues pre-regeneration with storage of large quantities of the spent AC: if the storage facility for the spent sulphurous ACs is in a close vicinity to members of the public (i.e. residential) then the health hazard may be passed along, potentially causing entanglements

with and even financial punishments from local governing bodies and/or councils [160]. H_2S is also extremely flammable, and even explosive. And, when oxidised (shown below), it will convert into sulphur dioxide (SO_2) exothermically, a gas that causes as many problems as H_2S in terms of health and safety [161]. Thus, storing the spent sulphurous ACs pre-regeneration can become a major problem.

Additionally, in terms of post-regeneration, SO_x and other sulphurous compounds adsorbed from the initial sulphur capture (HS^-, S, H_2S), or produced from heating to high temperatures during regeneration, provide their own set of health hazards in a working environment: the release of gases into the air which are toxic by inhalation (can cause death), extremely corrosive to skin (causing extensive chemical burns), and it is also extremely corrosive upon contact with eyes.

Additionally, although SO_2 is not corrosive towards metals or metal alloys, it readily reacts with atmospheric water to form H_2SO_3, which in turn reacts with oxygen molecules to form H_2SO_4 (in this case, *acid rain*), hence the classification as a greenhouse gas [17] [162]. Plus, H_2SO_4 adsorbed onto the AC will also desorb under high temperatures. The metal corrosion rates of H_2SO_4 are not problematic in an industrial setting until the temperature is raised to over 150 ^oC, or if the concentration levels are high (shown below in Figure 22). This is due to the H_2SO_4 returning to a liquid phase at this temperature as intermolecular attractions between sulphurous species and the AC begin to diminish with the increasing temperature. As the H_2SO_4 approaches 337 ^oC it will begin to turn into a gas and thus the area in which corrosion can occur begins to increase [17].

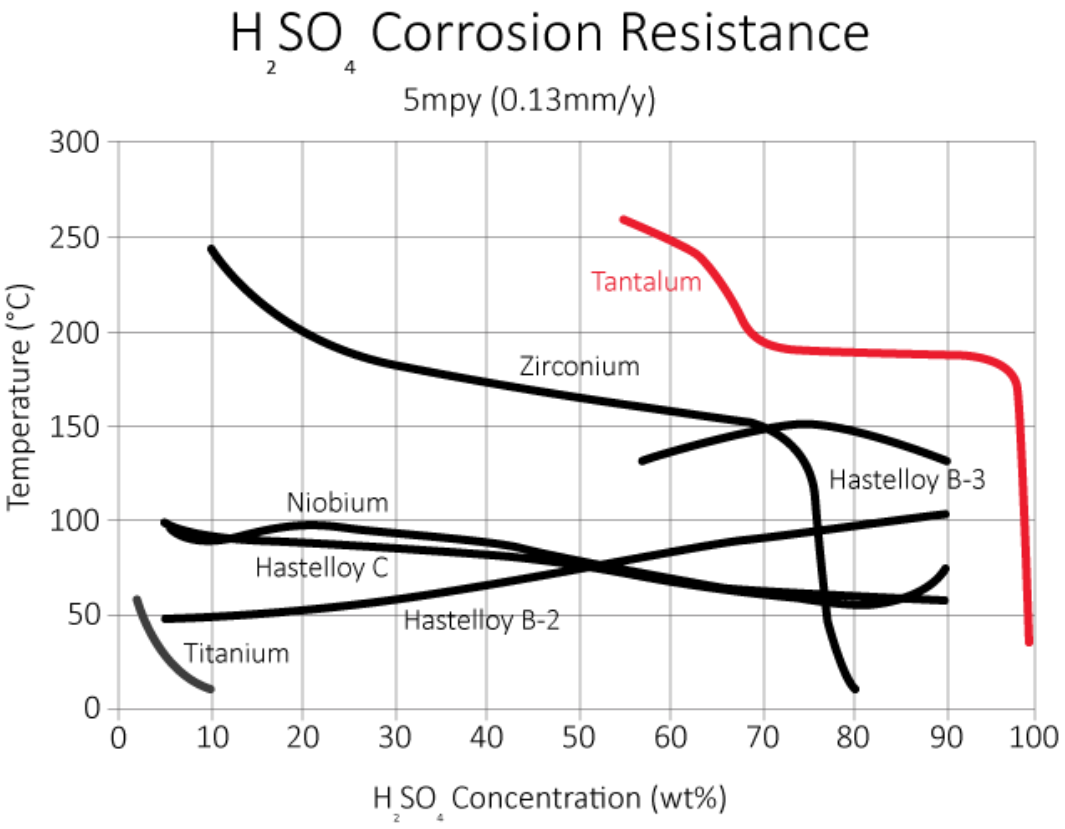


Figure 22. ISO corrosion chart for H2SO4 [162][163].

However, in addition to H_2SO_4 acting as a corroding material, H_2S itself also influences metal-alloy framework, especially that which contains iron. Corrosion due to H_2S is mainly electrochemical in nature; products of dissociation of the H_2S gas are aggressive and can catalyse electrochemical reactions, especially the dissolution of Fe [164]. Surface scale formation is one of the important factors governing the corrosion rate. The scale growth depends primarily on the kinetics of scale formation. In contrast to relatively straight forward iron carbonate precipitation in pure CO_2 corrosion, in an H_2S environment many types of iron sulphide may form such as amorphous ferrous sulphide, mackinawite, cubic ferrous sulphide, smythite, greigte, pyrrhotite, troilite and pyrite, among which mackinawite is considered to form first on the steel surface by a direct surface reaction [165] [166]. The poorly known mechanism of H_2S corrosion makes it difficult to quantify the kinetics of iron sulphide scale formation. A probable mechanism for iron dissolution in aqueous solutions containing H_2S based on the formation of mackinawite film (see Figure 23 below).

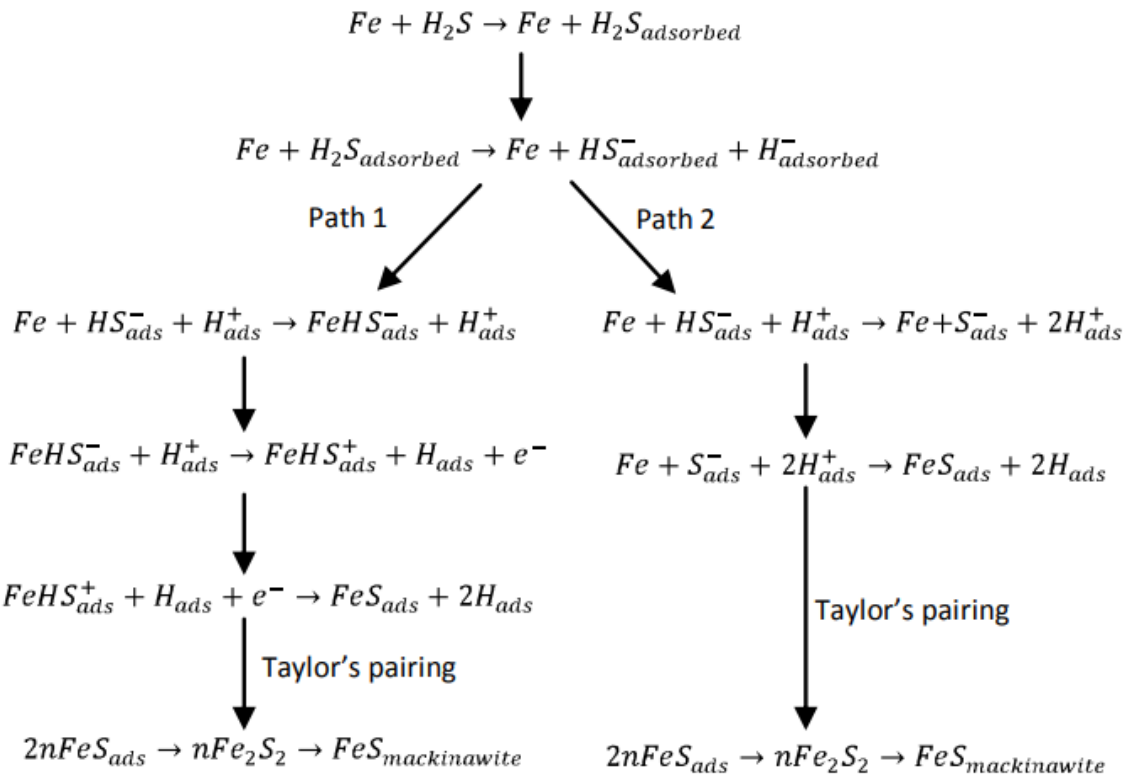


Figure 23. Proposed mechanism for H2S corrosion of Fe [165].

As discussed in Section 3.2.1, he other major issue with conventional thermal regeneration of AC the potentially for loss of adsorption capacity due to the changes in pore structure of the carbon when heated to such high temperatures for a prolonged period. Often resulting in the widening of micropores, reducing the total surface area [91]. This was found by in research by Zain *et al*, and Feng *et al*, who used different impregnates (ferric chloride hexahydrate ($FeCl_3.6H_2O$), and Zinc, respectively) for the regeneration of ACs used previously to adsorb H_2S , and both sets of research found pore widening and destruction during their post-regeneration analysis [167] [168]. However, in the study by Bagreev *et al*, concerning the thermal regeneration of spent ACs impregnated with caustics (KOH and/or NaOH) which had been used to adsorb H_2S, the issue was not the destruction of pore structure, but instead the loss of adsorptivity. Interestingly the loss of adsorptivity in ACs usually attributed to pore damage/destruction, but the study found that pore structure could be regenerated 100%. However, the cause of the loss of adsorptivity was discovered to be a change in surface chemistry; the oxidation and/or incorporation of sulphur into the carbon matrix itself. It was believed that this adoption of the sulphur into the matrix had reduced the number of active

sites on which further adsorbents could be adsorbed [169]. This was evident after reduction in the percentage of total sulphur removed.

And so, although regeneration provides an alternative to purely disposing of spent sulphurous ACs, it does also come with several major disadvantages. The purpose of this study is to examine if the regeneration spent sulphurous ACs will not only be possible via MW technology, but whether it will abate the issues discussed above.

2.5 Literature conclusions

The regeneration of AC has been investigated in numerous works, some of which have been summarised in this literature review. The objective of these works was mainly to provide an alternative to the production of virgin AC with regeneration methods; increasing access to a valuable filter and adsorbent, decreasing the amount of wasted spent materials, and reducing the financial costs associated with the production process for both the customer and supplier.

A plethora of research regarding the adsorption of sulphurous compounds onto AC was studied, owing to the growing demand for removal of compounds such as H_2S and SO_x from industrial water and gas streams. The literature showed that the use of AC for the adsorption of these sulphurous compounds has been extremely effective. Due to the growing demand for ACs as a source of sulphur compounds removal, research regarding the regeneration spent sulphurous ACs was studied. The typical methods of regeneration being carried out on spent sulphurous ACs were found to be chemical and thermal, with thermal being the favoured option by far. Thermal regeneration has been proven to be effective at removing adsorbed sulphurous species from AC, although, it has also presented its own problems i.e. corrosive and toxic materials produced on the surface of the AC during adsorption are undergoing phase change during the regeneration process and being released in a gaseous form.

This literature review emphasised the importance of the efficiency of heating methods in the reduction energy and time requirements for the regeneration of AC. Previous research has shown that the unique properties AC (i.e. the high surface area, porosity, and adsorption capacity) are strongly affected by the by regeneration conditions such as temperature, reactivation time and activating agents. As such, the use of MW heating on AC properties was studied in preparation for the research into whether MW heating could act as a suitable regeneration method for spent sulphurous AC. Accordingly, the properties of MW heating

were studied in comparisons with the traditional conduction-convection heating methods, alongside the adsorption and desorption of specifically sulphurous compounds to provide a platform for this thesis. The next chapter will introduce the methods by which the research was conducted throughout the course of this thesis.

3. Experimental methodologies

3.1 Activated carbon materials involved in this study

The AC used in this study were identified and selected by this project's sponsor company, CPL. CPL specialise in both the production and regeneration of AC. A large portion of CPL's clientele use AC to remove high levels of sulphurous compounds from waste streams before returning the spent AC for regeneration. This presents a problem, as the adsorbed sulphurous materials are often desorbed in such a way that they will undergo chemical reactions that lead to the production of other materials, such as sulphuric and sulphurous acid. As such, most studies presented in this thesis will pertain to activated carbon that has been loaded with sulphurous compounds typical to industrial waste processing systems, including hydrogen sulphide and sulphur dioxide.

The samples provided were loaded with high levels of sulphur to emulate the typical returned spent sulphurous ACs that CPL receive from customers. In other words, these samples had sulphurous compounds adsorbed onto the surface by CPL that are typical of the sulphurous adsorbates on AC received by CPL for regeneration. The provided spent sulphurous ACs had an average sample sulphur percentage of 41.51 % (+/- 0.93 std). It should be noted that the samples provided were taken from the same batch to allow for a fair representation of desorption and reducing the possibility of stark AC composition changes leading to alternate effects when processed during experimentation. Other adsorbates have been desorbed/processed using the same microwave-based methods to allow for study on whether the methods developed are viable for a wider usage in the industry.

The AC used in this study were produced from several carbonaceous feedstock materials, with the majority coming from the same base source of charcoal. This charcoal itself is known to have significant iron levels that can be seen in the XRD later. Additionally, the ACs used were impregnated with sodium hydroxide and potassium hydroxide during their initial production to allow for adsorbate targeting when used in waste stream remediation.

Additionally, the ACs used were provided in several forms with regards to their shape – pellets, large granules, small granules, and powders. The reason for this being that users of the AC have different needs and different types of waste streams that may require larger or

smaller AC particle size. Thus, the method needed to be tested on different particle sizes to understand whether it would be a viable regeneration process for all types of spent sulphurous AC being returned to CPL.

3.2 Material characterisation

The aim of the experiments described in this section was to study the effects of MW heating on spent activated carbon and whether it provided a viable alternative to traditional regeneration methods. Material characterisation involved butane analysis to show the returned adsorption capacity, XRD analysis to identify adsorbate molecules before and after regeneration, and EPMA scanning to help visualise the concentration, location, and movement of adsorbed materials before and after analysis.

3.2.1 Sample preparation

As previously mentioned, the spent sulphurous activated carbon samples were provided directly by CPL. The cylindrical pelletised samples were 5-8 mm in length with a diameter of 3mm. the large granular samples were more varied in their size distributions, with individual granule dimensions being, on average, 8 mm x 6 mm x 4 mm. The small granular samples used exclusively for experiments regarding non-sulphurous adsorbates were approximately 0.8 mm x 0.5 mm x 0.1 mm. The powdered samples were classified as *moderately fine*, meaning the powder particles passed through a sieve with a nominal mesh of 355 microns. Examples of the AC particle sizes are shown below in Figure 24.



Figure 24. Spent activated carbon samples – (left to right) pellet, large granule, small granule, moderately fine powder.

3.2.2 Sample analysis

Adsorption quantification

Originally the intention had been to measure the adsorption capacity of samples pre- and post-regeneration using Brunauer-Emmett-Taylor analysis (BET analysis). BET analysis is traditionally used to characterise surface area, morphology, and subsequent adsorption capacity in adsorbents such as AC. However, the sulphurous adsorbates involved in this research made it impossible to use BET. The reason being that during the initial phases of BET analysis, a sample must be put under a vacuum to allow for accurate pore analysis. The multi-layered packing of some of the physiosorbed adsorbates had weak intermolecular interactions that caused them to be removed into the vacuum line quickly, clogging the lines, and causing critical technical errors. After several attempts of trying to avoid this phenomenon, it was decided that the technique would not be viable for these samples.

Carbon tetrachloride analysis was employed as a replacement for BET analysis. CTC being a method in which bulk adsorption capacity is characterised by measuring sample mass before and after carbon tetrachloride gas is passed over the sample. However, due to CTC's ozone damaging nature, butane gas is used as a replacement. Butane gas is a suitable replacement to CTC for the analysis when it comes to analysing AC adsorption ability, correlating to CTC activity by a factor of 2.55, with an R_2 value of 0.935 [170].

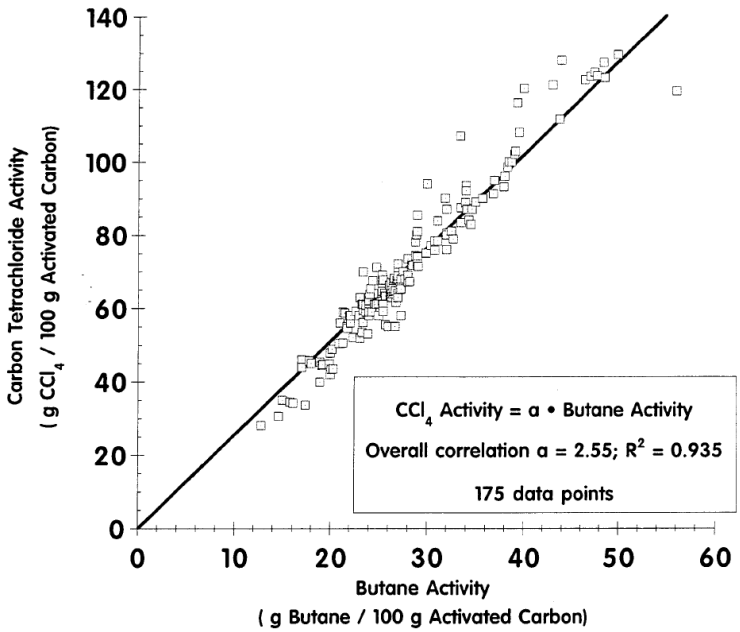


Figure 25. Carbon tetrachloride activity versus butane activity [170]

CTC gas activity is calculated using butane gas as shown below:

Equation 13.

$$CTC\ activity, \% = 2.55\ \times \left(\frac{(D - C) \times 100}{(C - M)} \right)$$

Where: M = Mass of the sample tube and stoppers

C = Mass of unsaturated (butane) activated carbon + M

D = Mass of butane saturated activated carbon + C + M

The process itself is setup as shown in Figure 26: a rubber hose links the butane cylinder to a flowmeter, which is then linked to a second rubber hose that attaches directly to the sample tube. With this, a controlled flowrate of 250 ml/min of butane over a period of 1200s ensures a complete saturation of the sample. The sample itself was dried at 105°C in a muffle oven before being placed into a specialised glass sample tube that has a sintered disc base on which samples can be places and gas can flow out into a fume cupboard, avoiding pressure build-up.



Figure 26. The experimental setup for CTC activity analysis of spent activated carbon.

X-ray Diffraction

Concerning surface adsorbate identification and characterisation, X-ray diffraction (XRD) has been employed widely when analysing the change to adsorbate species via processing, and the effects of desorption processing on the adsorbent itself [171] [172]. The XRD device used for this research was a Bruker D8 Advance Series 2 with a Cu x-ray tube, parallel beam function, and a scintillation counter detector. A key advantage also being that not only can adsorbate species be identified pre- and post-regeneration; the molecular geometry and crystalline state can be identified. This can be key in identifying whether a molecule has remained adsorbed to a surface during heating or has taken part in a reaction and has changed state, such as sulphurous compound adsorption and desorption discussed previously.

In this study, XRD was performed to determine the identity of sulphurous adsorbates and to study how the effects of MW heating had changed the geometry of said adsorbents, as well as identifying compounds formed during the heating/regeneration of the spent activated carbon. For this analysis the sample size was kept consistent for activated carbon forms, and a selection of carbons were analysed from each experiment to eliminate anomalous results.

Additionally, samples were run over longer periods than typical for the instrument – 10 hours rather than 20 minutes – to gain a better signal-noise ratio. Essentially, longer scans ensured more accurate results as opposed to quicker scans which would be useful only in giving a brief impression of the potential compounds available.

Electron Microprobe Analysis

Electron microprobe analysis is an x-ray spectrometry based quantitative determination of elemental composition for solid samples. It is a non-destructive technique that allows for the mapping of concentration distribution for elements and compounds. It is like an SEM (scanning electron microscope) and includes electron imaging capabilities, but it is optimized for chemical determination. Low-energy electrons are emitted from a tungsten filament and before acceleration by an anode plate at 3-30 electron volts [175]. The anode plate has a central opening through which electrons pass and are collimated via a series of magnetic lenses. This results in an electron beam which can then be rastered across samples to produce several several effects: phonon excitation (heat), cathodoluminescence (visible light

fluorescence), continuum x-ray radiation, characteristic x-ray radiation, secondary electrons, backscattered electron production, and Auger electron production [175].

Upon the electron beam interaction with the bound electron shells of the target atoms, they scatter the bound electrons producing vacancy and thus ionize the atoms. This ionized atom is unstable and must be filled by unbound electrons of low energy. The difference in binding energy between electron shell in which the vacancy was produced and the shell from which the electron comes to fill the vacancy is emitted as a photon [176]. The energy of this photon is on the x-ray region of the electromagnetic spectrum. With each electron structure of each element being unique, the x-ray line energies produced from the interaction differ for each element [176] [177]. These x-rays can then be analysed and used to identify the elements present. Additionally, in the case of EPMA, the number of x-rays produced from each quadrant areas can be analysed to show the concentration of the element when compared to the quadrants across the rest of the target site [175]. EPMA scans can also be used comparatively for samples before and after they have undergone processing to show changes in structure – loss of the structure is visible on the scans [175] [176] [177].

With this technique the element of sulphur can be selected as a target element and the EPMA scan will identify if it is present and what the concentration dispersion is. This technique was selected for part of the analytical methodologies to help understand the movement of sulphur across the AC before and after processing. This would help to identify the effects MW processing had on adsorbed sulphur and to what degree desorption was occurring.

The electron microprobe analysis was carried out using the EPMA function of the NMRC's FEI Quanta 200 3D Dual Beam FIB-SEM. This use of the device and the techniques required for this particular use were supervised by Elizabeth Steer.

4. Method development

The aim of the experimental and analytical techniques outlined in this section was to study the chemical makeup and adsorption capacity of the spent AC, and identify the adsorbed sulphurous compounds, before and after conventional thermal regeneration. The thermal regeneration performed on the spent AC is detailed in Section 4.4. Conducting the thermal regeneration would not only give a standard to which later MW regenerated samples could be compared, but also help to identify the reactions taking place when adsorbed sulphur species were being heated and oxidised during said regeneration process.

4.1 Adsorption capability

Roughly 10 kg of spent sulphurous AC was provided by CPL. The sample provided was provided as a representation of the typical spent sulphurous AC the company regenerates daily for clients. Following the companies preferred method of testing adsorption capability, butane activity analysis was utilised. The samples provided came in two forms: compressed cylindrical pellets, and large granules, with approximate dimensions stated in Section 3. Each butane analysis run was conducted with 10.00g (+/- 0.02 std) to allow for a fair representation. The AC was found to have a butane activity of 2.01 % (+/- 0.11 std). The less uniform construct of the granules was believed to have led to less adsorption taking place during industrial use. These two numbers would go on to help characterise how much regeneration capacity had been regained during any form of regeneration as CPL stated that an average thermal regeneration of spent sulphurous AC would yield AC with a butane activity of 40-50%.

4.2 Sulphur species identification and distribution

XRD is an analytical method used to identify the compounds adsorbed to the surface of AC before and after all methods of regeneration to help clarify the physical and chemical transformations of the adsorbates. It has been widely used for study of AC adsorbates undergoing pyrolysis [178]. XRD can also show changes in the overall carbon structure that occur during heating processes such as pyrolysis as the appearance of amorphous humps on the diffractogram indicate charring, which is typically indicative of loss of overall structure [179].

The main sulphurous compounds adsorbed to the surface of CPL's ACs are H_2S, CS_2 and SO_2. XRD was used to confirm the presence of these adsorbates on the surface of the spent AC, as well as the presence of impregnates used in these ACs to aid adsorption: the likes of FeOH, NaOH, KOH. For SO_2, as described by Young-Wahn *et al*, the adsorption mechanics are relatively simple, with SO_2 chemisorbing to the surface of the AC via bonds being formed between the metal oxide ions from the impregnates and the SO_2 directly, resulting in potassium sulphite [180]. This potassium sulphite interacts with atmospheric oxygen ions to form potassium sulphate.

$$2\ KOH_{(IAC)} + SO_{2\ (ads)} \rightarrow K_2SO_{3\ (IAC)} + H_2O_{(ads)}$$
$$K_2SO_{3\ (IAC)} + ½\ O_{2\ (g)} \rightarrow K_2SO_{4\ (IAC)}$$

H_2S can chemisorb to the surface of the ACs in much the same way as SO_2, reacting metal oxide impregnates to form metal sulphates.

$$H_2S_{(g)} + KOH_{(IAC)} \rightarrow K_2S_{(ads)} + 2\ H_2O_{(ads)}$$

However, owing to its molecular size, H_2S also can physisorb directly onto the surface carbon via intermolecular forces such as Van Der Waals and London dispersion forces [181]. Additionally, the physiosorbed H_2S can then react with the metal oxide impregnates to form metal hydrosulphides, such as potassium hydrosulphide, allowing for chemisorption to also take place [182].

$$H_2S_{(g)} \rightarrow H_2S_{(ads)}$$
$$H_2S_{(ads)} \rightarrow H_2S_{(ads\text{-}liq)}$$
$$KOH_{(IAC)} + H_2S_{(ads\text{-}liq)} \rightarrow KHS_{(ads)} + H_2O_{(ads)}$$
$$H_2S_{(g)} + KOH_{(IAC)} \rightarrow KHS_{(ads)} + H_2O_{(ads)}$$

With CS_2, both chemi- and physisorption can take place similarly to that seen with K_2S, resulting in the formation of metal thiocarbonates and metal carbonates being formed on the surface [183]. However, the linear geometry of CS_2 also allows for multilayer packing to take place, increasing the strength of intermolecular interactions and thus promoting higher rates of adsorption.

$$6\ KOH_{(IAC)} + 3\ CS_{2\ (g)} \rightarrow 2\ K_2CS_{3\ (ads)} + K_2CO_{3\ (ads)} + 3\ H_2O$$

$$CS_{2\ (g)} \rightarrow CS_{2\ (ads)}$$

The XRD analysis showed signs of all the compounds shown above in the adsorption formulas, with particularly intense peaks for sodium sulphate/sulphate analogues, and potassium sulphate ions. XRD analysis was performed of both the surface of the pellets and granules, and of cross sections to give a fair representation of distribution of adsorbed species. There was no discernible difference between the identities of compounds found on the scans taken between the adsorbed materials found inside the ACs and those found at on the outside. However, there were differences in the peak intensities, suggesting the compounds were distributed unevenly throughout the AC.

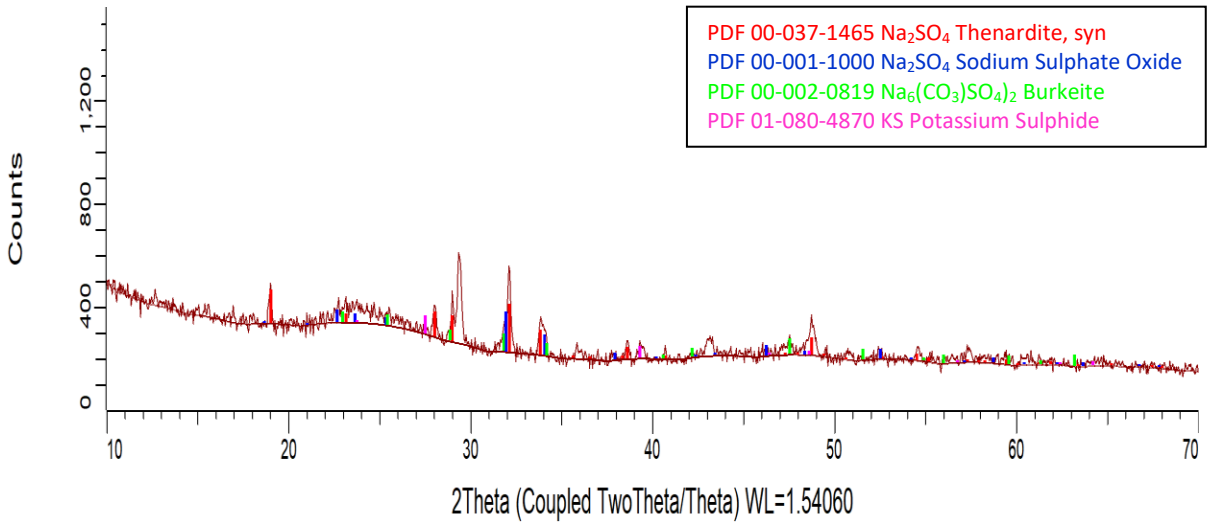


Figure 27. XRD diffractogram of spent sulphurous AC pellet surface.

4.3 Electron Micropore Analysis

The experimental methods for EPMA are detailed in Section 3. Figure 28 shows an EPMA scan of the distribution of sulphurous materials across breadth of one of the spent AC pellets. In addition to this, Appendix C shows the intensity profile of the scan created using ImageJ – this allowed for a more quantitative gauging of the sulphur distribution across the AC. The EPMA scans show an uneven distribution of sulphurous compounds, with higher concentrations on the outer edges of the pellet. Additionally, the corresponding intensity profile showed an uptick in the gray value at the edges of the pellet. This mirrored what was shown with the peak intensity in the XRD diffractograms: compounds being more common on the outside of

the AC as opposed to being inside. Additionally, as seen in the study by Li *et al*, impregnates tend to be in higher concentrations on the outer edges of AC pellets/granules due to the way by which they are implanted into the AC during pyrolysis of carbonaceous materials [184]. With the concentration of impregnates decreasing towards the centre of the AC, the number of sites onto which chemisorption can occur with the adsorbates decreases, leading to an overall decrease in the level of adsorption occurring.

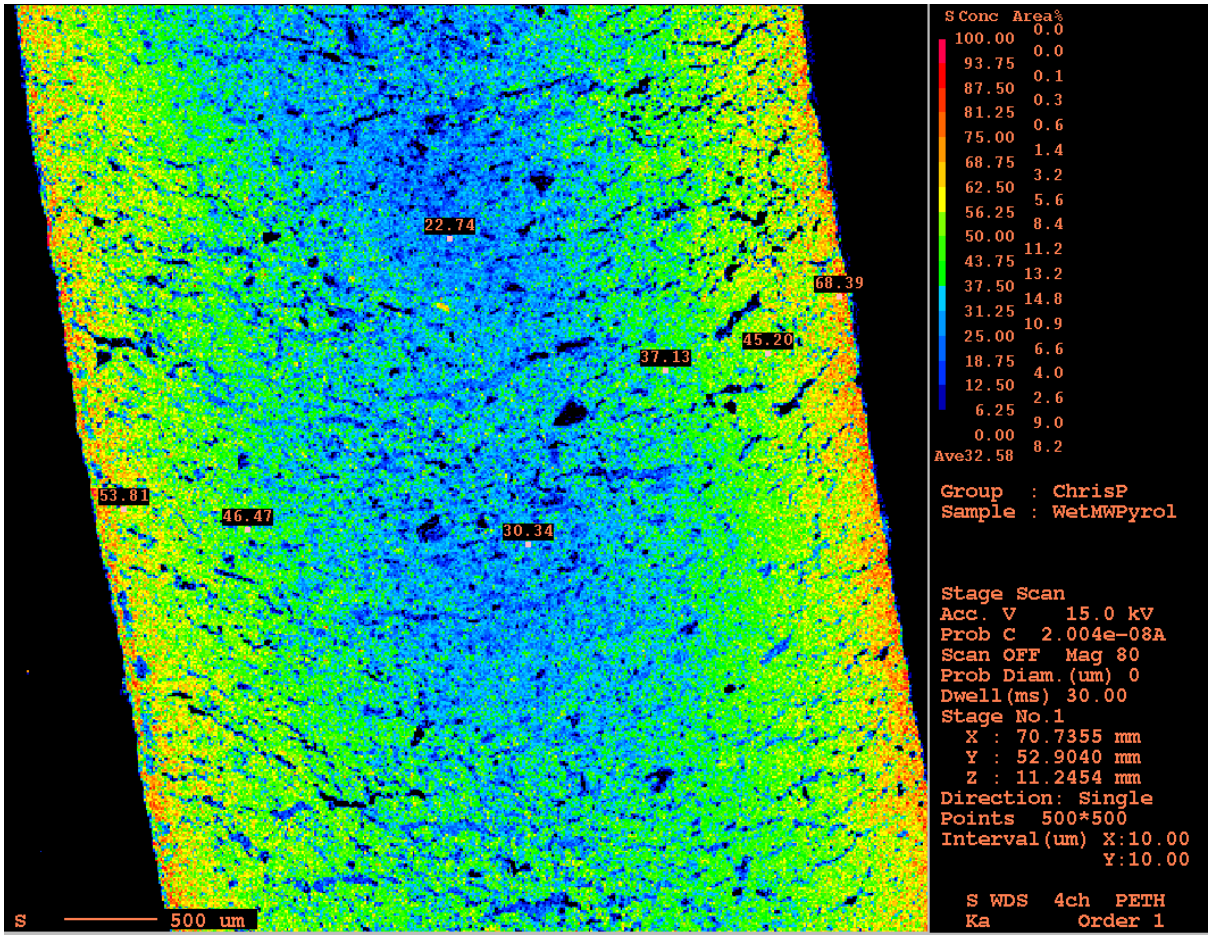


Figure 28. (top) EPMA scan of a cross section of non-regenerated spent sulphurous activated carbon with sulphur percentages shown at randomly selected areas across the pellet.

The distribution of sulphurous compounds could also be indicative of the overall pore distribution on these particular AC. As stated in Section 2.1, ACs pore classification is characterised by decreasing diameter: Macro (greater than 50 nm); Meso (2 – 50 nm); and Micro (less than 2 nm) [52]. CS_2 has a linear geometry which allows for molecular packing on ACs impregnated with metal oxide impregnates when physisorbing and could allow for multilayer adsorption onto the surface of pores with a smaller diameter. However, H_2S and

SO_2 cannot form packed layers in the same way owing to their V-shaped molecular geometry causing, promoting weaking interactions intermolecularly. Additionally, as pore size decreases, the overall molecular radius effects the ability of molecules to adsorb next to one another as they begin to compete for adsorption site space.

4.4 Thermal Regeneration

The aim of the thermal regeneration experiments was to create representation of conventional regeneration that could be used as a comparison for microwave-based regeneration experiments. Additionally, analysing the thermally regenerated samples would give information about how thermal regeneration affects the chemical makeup of the sulphurous adsorbates – high temperatures and oxidation phase causing the formation of by-products such as sulphuric and sulphurous acid [15] [16] [156].

Spent sulphurous ACs samples were regenerated thermally using the method described in Section 2.2.2 . This method was designed to mimic the setup used by CPL at their Immingham facility, albeit a scaled down version that allowed for 5.00g of the sample to be regenerated at oner time. The use of a lab scale, as opposed to the full-scale facility, was to allow for a more comparable set of results to those from the upcoming MW regeneration experiments.

The butane activity for both for thermally regenerated samples came to 40.88 % (+/- 0.92 std), and the mass loss was 50.31 % (+/- 0.95 std) for the granules. This was to be expected as the thermal regeneration method has been an industry standard in the removal of sulphurous adsorbents from AC for decades.

When analysing the regenerated samples via XRD there were signs sulphuric and sulphurous acid analogues in the form of sodium hydrogen sulphate and potassium sodium sulphate, as well as sulphuric acid found on the surface. The formation of sulphuric acid and its analogues echoed the information provided by CPL, who themselves had witnessed acid production during their industrial regeneration. The reaction for which is well documented by the likes of Perry *et al* in 'Perry's Chemical Engineering Handbook', and several others [181][182][183].

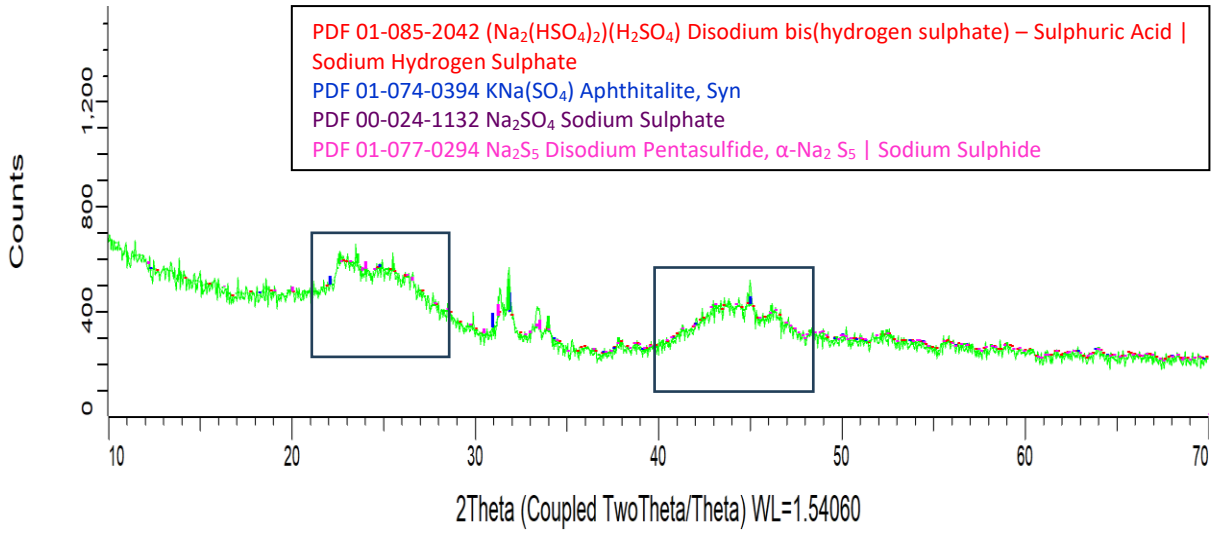


Figure 29. XRD diffractogram of thermally regenerated AC pellet surface.

However, the prevalence of sodium sulphide analogues indicates carbothermic reactions between adsorbed sulphates and elemental carbon that has been charred and removed from a larger carbonaceous body (as shown below) [185][186]. This was confirmed with the EPMA scans taken of the regenerated granule which shows large dark areas where there previously were non and fraying around the edges. The intensity profile (Appendix C) also showed a larger number of dark spots in the form of very low gray values, symptomatic of very low sulphur concentration areas, or areas of missing carbon because of heat damage. The general trend in the intensity profile of vastly decreased gray values showed the decrease in sulphur concentration: sulphur concentration originally depicted as blue in EPMA scans indicate a lower concentration in the highlighted area and a darker (blue) colour corresponds to a lower gray value. Additionally, the XRD diffractogram also showed amorphous humps in the regions of 22-27 and 41-47 2Theta (highlighted on diffractogram). This likely occurred due to the high temperature required to allow for pyrolysis and reaction to occur. With MW heating being volumetric, this requiring lower temperatures to ensure that the entirety of a material is heated to the same extent, this should be something that can be avoided. Localised heating that comes with MW heating should allow for bonds and interactions between carbon and non-carbon species due to polar interactions being present rather than between carbon-carbon bonds which are not dipolar [128]. However, localised heating with MWs can also overheating and what is termed as thermal runaway. This effect occurs when dipolar molecules such as H_2S exert excessive thermal energy whilst they themselves are being heated, leading to thermal damage to surrounding non-polar molecules bonds [129].

$$Na_2SO_{4\,(ads)} + 2\,C_{(s)} \rightarrow Na_2S_{x\,(ads)} + 2\,CO_{2\,(g)}$$

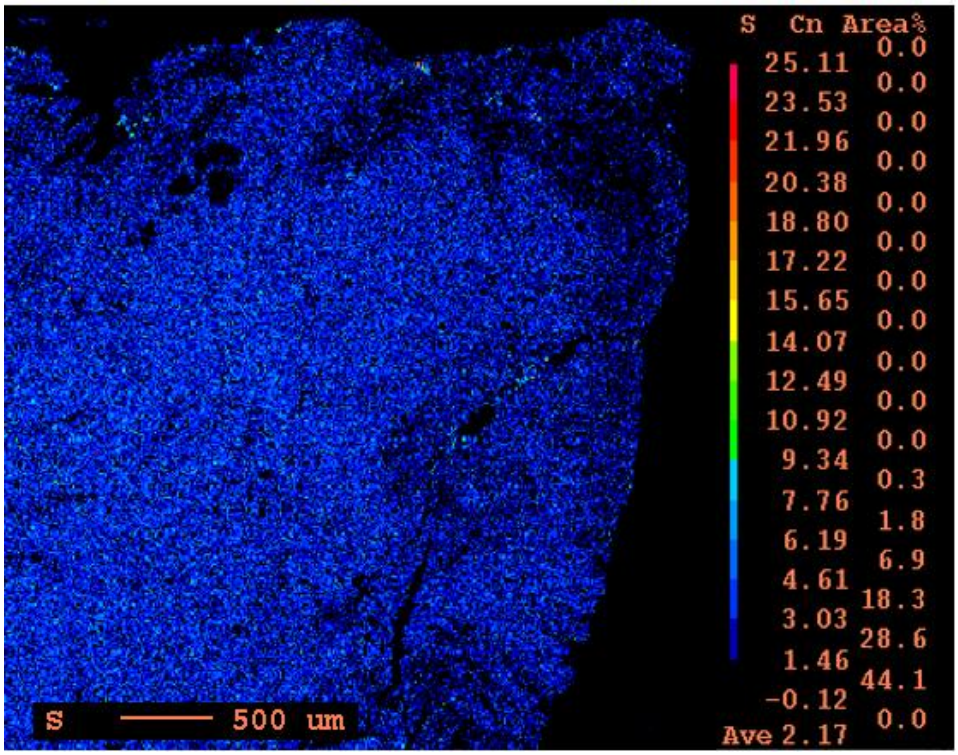


Figure 30. EPMA scan of a cross section of the edge of a of thermally regenerated sulphurous activated carbon.

4.5 Processing options for microwave heating

As discussed in Sections 2.2 and 2.4, one of the main challenges facing MW heating is the heterogeneity, which can lead to thermal runaway and localised overheating. Heating heterogeneity issues arise because of the nature of standing waves inside the applicator which create areas of high electric field intensity and others of low electric field intensity. It was theorised that using a narrow waveguide cavity would give a high field intensity and thus reduce the likelihood of localised overheating. Additionally, as shown earlier in Section 4.4, ACs are susceptible to structural damage when exposed to high temperatures for long periods, but a high energy input is required to allow for desorption to occur. With a single-mode cavity creating a high field intensity, the period of heating can be relatively quick as it allows for high energy input quickly. Plus, with short, sharp periods of heating that target only the adsorbates, an oxidation step may not be required, eliminating the risk of acid production that has been previously discussed with regards to thermal regeneration.

Essentially, a balancing act between the energy input and period of exposure had to be struck to allow for maximum adsorbate desorption while avoiding overheating that leads to structural damage of the AC. The details of a proposed MW-based regeneration system for spent sulphurous ACs will be discussed in the following chapters. This will include the initial design, and modification made over time to the process and rig design that helped to identify the optimum setup required for MW regeneration of spent sulphurous ACs.

5. Microwave heating of spent sulphurous activated carbon: initial process design

5.1 Introduction

The aim of the work reported in this chapter is to develop an initial design for overcoming the issues with conventional thermal regeneration of spent sulphurous AC via MW heating. Heating via MWs differs from conventional heating in that the process material heats volumetrically due to interactions with the electric field. There are several mechanisms by which heating can occur, and the overall extent to which a particular component or phases will heat depends on the electric field intensity and the dielectric properties [108] [117]. In the case of AC with adsorbed contaminants such as adsorbed sulphurous compounds, the adsorbed material, carbon and any water that is present will all interact individually with the electric field, meaning that the levels of energy dissipation will be different for each component. If the thermal conductivity/diffusivity is low, then it is possible for all three components to attain different desorption temperatures (i.e. selective heating). Additionally, the volumetric nature of this kind of heating can greatly reduce the time required for processing, improving the overall energy efficiency, and reducing the potential for by-product formation.

A move away from traditional thermal regeneration provides a benefit from an industrial standpoint. In the case of CPL's regeneration of spent sulphurous AC, the main issues that arise are sulphurous acid compounds being formed from interactions between the adsorbed sulphurous species (SO_2, H_2S, C_2S) and steam used in the activation step; the length of time required to regenerate (upwards of 10 hours per ton); and the energy & financial costs incurred from heating at such high temperatures over long periods. Several previous studies have reported microwave-based regeneration processes. Numerous key advantages have been highlighted such as vast reduction in time required for regeneration, the ability to generate favourable levels of returned adsorptivity when processing over short periods, and the ability to regenerate without needing further activation with steam/carbon dioxide [145]. Coss *et al.* utilised MW heating as a replacement for the activation step in thermal regeneration, resulting in a reduced overall regeneration time whilst maintaining the final adsorption capacity [146]. If adsorption capacity could also be restored to the AC by removing

the adsorbed material whilst leaving the porous carbon structure intact, MW heating would offer a step-change for regeneration and will promote a move away from traditional thermal regeneration processes.

It should be noted here that there are no published studies specifically addressing the use of MW heating as replacement for the entire regeneration process, rather only documenting the replacement of certain steps such as Coss *et al's* work on activation step replacement, and the likes of Ao *et al,* and Liu *et al,* who worked specifically on the formation of AC from carbonaceous sources. The latter of these studies providing insight into the issues that arise with overheating when forming a porous network, but do not specifically address MW heating effects on pre-standing porous networks, spent or otherwise [173] [174].

5.2 Properties influencing microwave heating of porous carbon

Volumetric heating and deep energy penetration for MW heating is the founding principle behind the uniform heating inside materials that Meredith reported in his seminal book, 'Engineers Handbook of industrial Microwave Heating' [128]. However, successful MW heating of a material is strongly dependent on power, irradiation time and cavity design, as well as the dielectric properties of the materials. These parameters must be controlled to allow for efficient MW heating to occur. If they are not controlled then hot spots could occur in which areas of a material are heated at a higher rate than others, leading to a reduction in an overall efficiency of the process.

Non-uniformity in MW heating of some materials correlates with dielectric properties such as penetration depth (D_p). Additionally, hotspots/overheating can occur when polar molecules are in a higher concentration in certain areas as opposed to being spread evenly across a larger host material such as a non-polar porous material. As such, even at higher MW irradiation powers, power will be at its highest density on the surface of a material, whilst still at relatively lower levels towards the centre. Thus, the surface of the material heats, often exponentially, whilst transferring to the centre of the material more slowly [143]. As documented in section 4.2, the spent sulphurous AC provided by CPL were shown to have most of their sulphurous adsorbate concentrated around the edges of the pellet rather than having a more even distribution. This was seen to be key to understanding the how the MW heating would affect the samples.

As such, the following sections of this chapter will seek to analyse the effects of power and field intensity on the provided samples, the ability to heat uniformly, and how these factors affect the adsorption capability.

5.3 High Field Density

Up until the early 2000s commercial scale microwave processing was limited to multimode units owing to industrially viable single-mode units being unavailable to industrial practises – single-mode units tend to be small and only able to process very limited samples sizes at any one time [187]. During the past few decades, the availability and viability of small, fast processing single-mode units has expanded after research and development of unit direct temperature control via IR sensor probes and software enabled on-line temperature/pressure control via microwave power output [188] [189]. The major merit to single-mode cavity MW heating is the ability to selectively heat components of materials with a relatively low energy input and achieved optimal heating rates within a short period [130 [131]. This is achieved due to the high electromagnetic field density generated and carried through a narrow cavity to the target sample, which will be bombarded with a high level of incidence, as discussed in Section 2.3. However, one of the main drawbacks to using a single-mode waveguide cavity is the limitation that comes with such targeted heating in the form of overheating occurring as energy passes from MW-absorbing polar molecules (which redistribute the adsorbed MW energy as heat energy) to surrounding non-polar molecules via conduction (in this case resulting in surrounding carbon charring).

In the initial work it was decided to start the studies by using a custom-built single-mode microwave rig to investigate the effects of single-mode cavity viability as well as the effects of power and irradiation time. This was followed alternating irradiation exposure via a pulsed method and using solvent bathing to cool samples and avoid overheating. The results of which are presented throughout this chapter, with the first being the effects of just the single-mode cavity setup.

5.3.1 Single-mode cavity – Preliminary experiments

Design

The initial stage of the MW heating of the spent sulphurous ACs took place inside a 3.2 cm quartz glass tube (the reactor). The quartz tube was then inserted into the cavity via a 40 cm long metallic tube with an internal diameter of 5.0 cm, acting as a choke for the electromagnetic power. MW power was supplied by a custom-built microwave rig consisting of a 2.0 kW generator (~2.45 GhZ) which supplied MWs to the single-mode cavity through WR340 aluminium waveguide together with E-bends as shown in Figure 31. An automatic three-stub tuner was attached to the waveguide for power analysis.

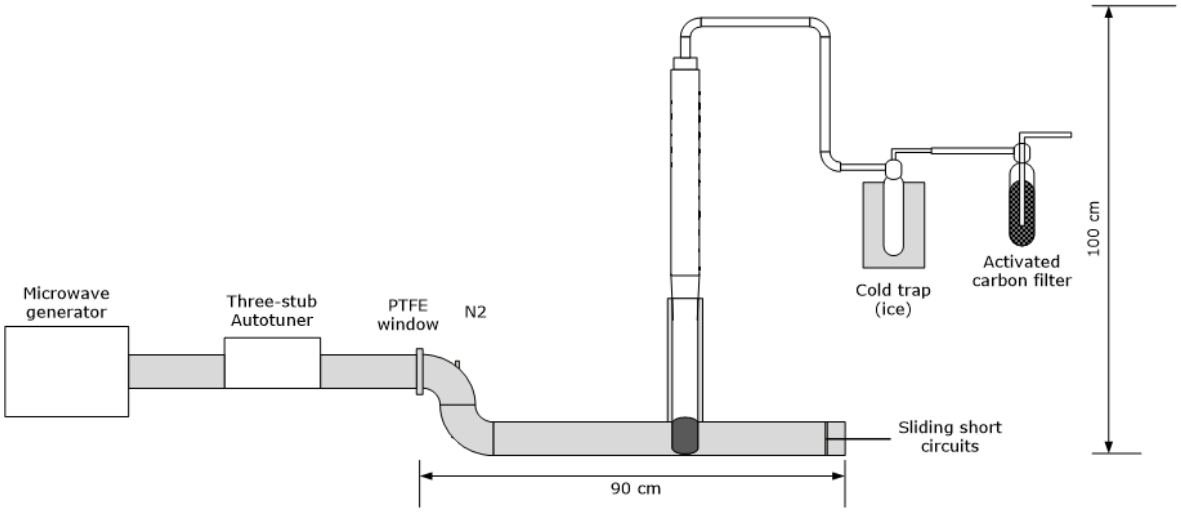


Figure 31. Experimental setup for spent sulphurous AC regeneration in custom-built MW rig.

For each of the heating experiments, a weighted quantity of the spent sulphurous AC (10.00g (+/- 0.2 std)) was placed in the reactor. During the heating of samples, the cavity was inerted using a continuous flow of nitrogen at 2 $L.min^{-1}$ as a safety feature to avoid fire in case of failure in the system such as electric breakdown and/or any breaks in the quartz tube. The flow of nitrogen was turned on 3 minutes before experiments took place and remained on for 5 minutes after. This was to ensure that the oxygen content inside the cavity was less than 5%, per the calculated inerting levels shown in Appendix 10.1. A PTFE window was attached to the waveguide to ensure nitrogen and any vapours would not flow directly into the generator. Off-gases were collected via a cold trap and activated carbon trap, with any excess gases being vented out of the building.

The MW power was set to various levels (200 W, 400 W, 600 W, 800 W) before the MW was turned on. A stopwatch was used to track heating times as well as an automated timer on the MW generator itself. At the end of each experiment the MW power was turned off.

After each experiment a period of 10 minutes was allowed for sample and reactor cooling to allow for safe manual handling. The samples were then weighed to allow for a quick look at how much sulphurous compounds may have been removed before thorough analysis via methods outlined in Section 3.

Experiments

The preliminary MW regeneration experiments of spent sulphurous AC were run at varying powers and over various periods to establish the effects each would have, respectively, on the level of heating, sulphur removal, and overheating that may lead to damage to the overall AC. In addition to this, the specific energy input for each experiment was calculated using the adsorbed energy data recorded from each experimental run to show the efficacy of the method when compared to the laboratory scale thermal regeneration. This was done using equations 14a and 14b, shown below. Analysing the specific energy input allowed comparisons between differing irradiation time, powers, and samples masses in a single parameter.

Equation 14a

$$\mathrm{E_{nea}} = \frac{\mathrm{Pr_{Avg}} \times \mathrm{t}}{1000}$$

Equation 14b

$$e = \frac{\mathrm{E_{nea}}}{m}$$

Where: E_{nea} = Net energy absorbed, KJ

Pr_{Avg} = Average reflected power, KJ

t = Time, s

e = Specific energy input, KJ. g^{-1}

m = Mass change in sample, g

Irradiation time

As shown in Table 4, the increase in MW irradiation did lead to overall increases in the butane activity for the AC samples, with those running for 360s achieving 33.43 % (+/- 0.87 std). Although this does not match the levels of butane activity seen achieved in the lab-scale thermal regeneration experiments for AC granules, 40.88 % (+/- 0.92 std), the level of butane activity symbolised significant value with regards to the time taken for regeneration processing. Thermal regeneration in the laboratory set-up required roughly 1 hour (+/- 5 minutes) to reach the temperature suitable for the oxidation step (600 ^{o}C). Once at the correct temperature, a 30-minute dwell time with the addition of steam was required to allow for a complete oxidation of the samples, followed by roughly 1-1.5 hours for the furnace (and samples) to cool to a temperature at which they could be handled. As stated in Section 4.4, this follows the procedures conducted by CPL with their current industrial scale thermal regeneration unit. As such, although the level of butane activity was lower than that achieved thermally, the reduction in processing time represents a significant saving for the project's intentions to scale to industrial processing at this early stage of development.

Table 4. Effects of MW irradiation time on AC butane activity and specific energy input using 400 W power. Standard deviation (+/- x.xx) shown was calculated for each result from the corresponding results in Appendix B.

Time (s)	Mass change (%)	Butane activity (%)	Specific energy input (kJ.g $^{-1}$)
120	45.58 +/- 2.32	24.65 +/- 1.52	3.75 +/- 0.04
180	47.11 +/- 2.19	29.63 +/- 1.38	6.26 +/- 0.09
240	49.34 +/- 2.05	30.86 +/- 1.83	9.37 +/- 0.31
360	51.43 +/- 2.58	33.43 +/- 0.87	12.90 +/- 0.23
Thermal	50.31 +/- 0.95	40.88 +/- 0.92	-

However, the initial set of data from the first run also hinted at a significant problem with the level of heating occurring inside the MW cavity. More specifically potential overheating.

When samples were regenerated thermally a typical mass loss to the samples was 51.43 % (+/- 2.45 std), symbolising a rough estimate of sulphur/adsorbate removal that had occurred during processing as well as carbon charring/loss. With the MW-regenerated samples, the level of mass loss was significantly higher, yet the butane activity did no surpass that of thermal regeneration. As an initial impression this implied that the mass loss percentage loss was indicative of carbon loss at a higher level than that seen in thermal regeneration. It was theorised that this would likely be due to overheating - an issue that had been theorised would likely be a negative effect of MW regeneration. And it was theorised that the overheating was likely taking place on the edges of the pellets due to the higher concentration of sulphurous adsorbates being situated there – energy given out in the form of heat energy can lead to hotspots and cause damage to surrounding structures such as the surrounding carbon porous network in these AC granules.

Upon examination of the sulphur distribution using the electron micropore analyser, the suspicion of localised overheating was confirmed. Although the level of sulphur around the edges of the pellets had had been significantly reduced by the MW heating (see Figure 32), there were clear signs of fraying, and damage. The same could be seen in the intensity profile (Appendix C), where there were noticeable sharp peaks to very low gray values which indicated an absence of colour, or, in this case, a lack of sulphur concentration in areas previously saturated with sulphurous compounds. The distribution of sulphurous compounds was more consistent and homogenous across the entirety of the granules than that seen in post-thermally regenerated pellets (relatively flat gray value distribution in intensity profile), but the level of sulphur was much higher. This suggested that most of the sulphur being desorbed was from the surface of the granule as opposed to the interior. The sulphurous compound removal was taking place primarily around the edges of the pellet owing to the high sulphurous adsorbate concentration pre-regeneration.

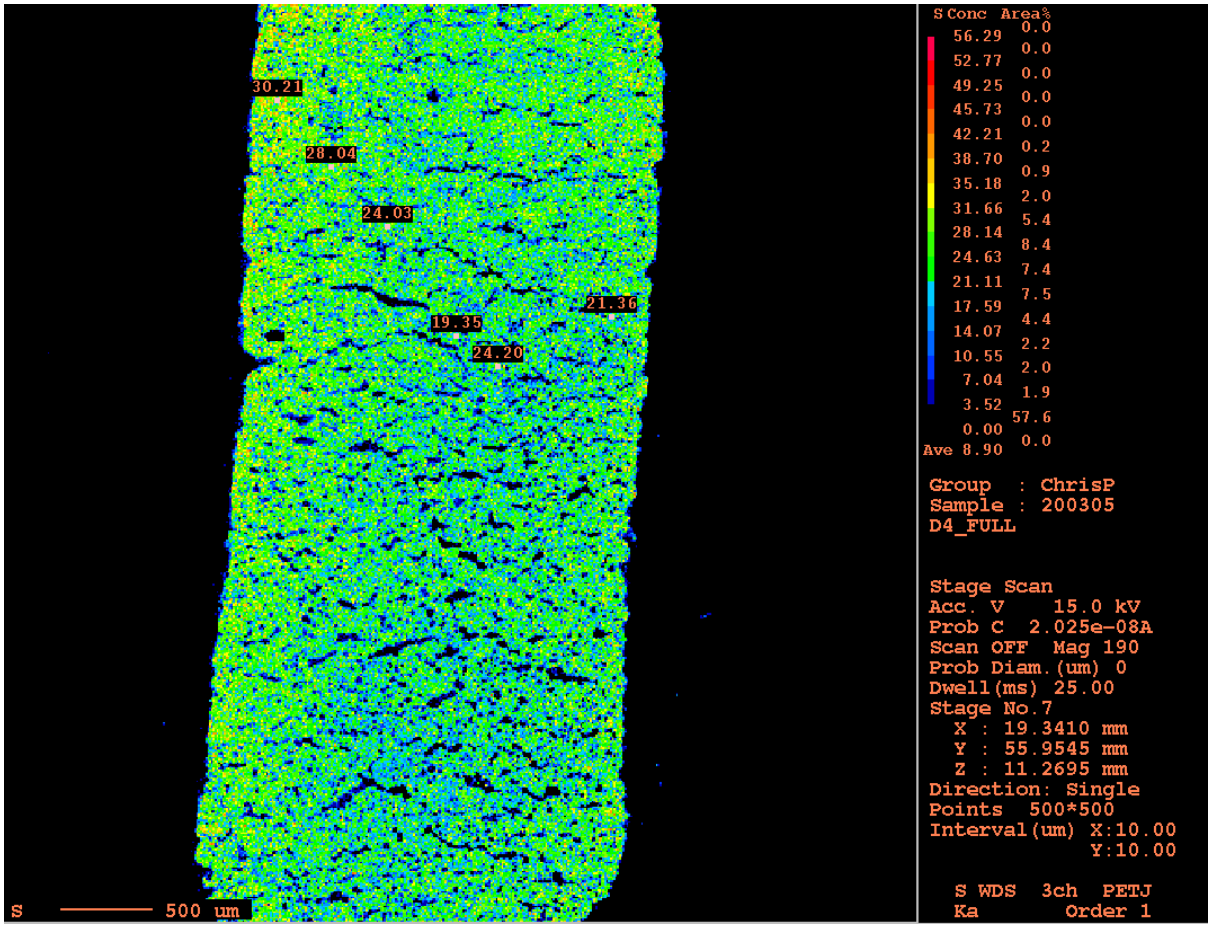


Figure 32. EPMA scan of a cross section of the edge of a of MW regenerated sulphurous activated carbon at 400 W for 360s.

It should be noted that the level of mass loss, butane activity and specific energy input all increased as irradiation increased. The latter being significant in that it confirmed what may be seen as obvious – the longer the irradiation time, the more energy being absorbed by the adsorbates, thus the higher the level of MW energy being converted into heat energy and thus the higher the level of damage being caused to the carbon structure. With this, the next step of this first study was to monitor the effects of MW power on adsorbate desorption, but also how it would also be impacted by time: could a high MW power over a shorter irradiation time lead to higher level of desorption without causing as much damage to the overall surrounding carbon?

Microwave Power

With this second part of the initial study the aim was to understand the relation MW power had to the desorption of sulphurous adsorbates from the AC samples. In addition, this part of

the study also sought to explore whether increasing the power would allow for a reduction the irradiation required to remove significant levels of the adsorbate. For this a selection of runs were conducted using the same set-up as the first part of the study but running the experiments at different MW powers. As the MW power was increased in steps of 200 W, the irradiation time was reduced by 60s. This was done to compensate for the damage exhibited by increased irradiation time seen in the first step of the study.

Table 5. Effects of MW power on AC butane activity and specific energy input. Standard deviation (+/- x.xx) shown was calculated for each result from the corresponding results in Appendix B.

Power (W)	Time (s)	Mass change (%)	Butane activity (%)	Specific energy input (kJ.g $^{-1}$)
200	240	29.32 +/- 1.20	15.42 +/- 1.49	3.47 +/- 0.02
400	180	47.39 +/- 1.01	29.50 +/- 0.46	6.23 +/- 0.03
600	120	31.68 +/- 1.60	16.75 +/- 2.16	5.10 +/- 0.12
800	60	44.94 +/- 1.26	22.36 +/- 3.02	3.93 +/- 0.16
Thermal		50.31 +/- 0.95	40.88 +/- 0.92	-

The first point of note with the data shown above is there appears to be a trade-off with MW power and time. The results for 200 W MW power showed a reduction in butane activity when comparing to the result for the run of the same irradiation time seen in Table 4. With this, one could have concluded that an increase in power leads to a definite increase in adsorbate desorption. This could further be supported by the fact that the specific energy input, the energy absorbed by the MW-absorbing molecule/compound, was relatively similar. With this information, it was initially theorised that MW power was the determining step for the rate of energy dispersed as heat energy from the adsorbate into surrounding non-MW absorbing materials, and thus a linear trend for the butane activity could have been predicted. However, this was not the case. With the run at 600 W the butane activity decreased in comparison to the run at 400 W, as did the mass change. Both of which were closer to that seen in the 200 W run than that seen in the 400 W, with the determining factor appearing to

be the MW irradiation time, which had been reduced from 240s to 180s and then to the 120s for the 200, 400 and 600 W runs, respectively. What this showed was that there was a trade-off between the MW power and the MW irradiation time in which an increase in power did lead to an increase in overheating, but the irradiation time reduced the level of desorption taking place in the form of butane activity achieved. Additionally, although the mass change and butane activity were similar between the runs at 200 and 600 W, the latter saw a significant increase in specific energy input. This seemingly confirmed that although the MW energy absorbed by the sulphurous compounds was higher, with a higher MW power, a longer irradiation would be required to remove more sulphurous compounds. But, as shown in the first stage of this study, that would lead to overheating and damage to the carbon structure.

With the run at 800 W, the theory that a power-time trade-off was present was confirmed, with results in butane activity and mass change being closer to that seen in the 400 W run than that seen in the 600 W run. This would suggest that increasing the power to 800 W had increased the rate at which the adsorbate was being removed, considering it had an irradiation time of 60s. The specific energy input was smaller than that seen in the 400 and 600 W runs, which, when paired with the high mass percentage change, suggested overheating from MW energy having been absorbed and redistributed as heat energy to the surrounding carbon was already taking place.

Change in sulphur chemistry

As stated earlier in this section, not all the sulphurous compounds were removed from the surface of the AC when regenerated using MW irradiation. This represented a challenge for progressing MW regeneration later in this project as optimisation was key for surpassing the sulphur removal seen with traditional methods. However, for these preliminary experiments the main objective (in terms of sulphur compound chemistry) was to induce the removal of adsorbed sulphurous compounds without desorption resulting in the production of acids.

As shown in Figure 31, the MW rig setup utilised a cold, and an AC trap that caught gaseous sulphurous compounds being removed during the process. Figure 33 shows these traps in action during the preliminary runs.



Figure 33. Cold trap and activated carbon trap used in the experimental setup to trap sulphurous compounds being desorbed from the sample sulphurous activated carbon.

XRD was used on the surface of the sample ACs to identify which compounds were being pulled out of the ACs during the MW regeneration. It was noted that the base sample (non-regenerated) showed peaks corresponding to SO_2, CS_2 and H_2S, the compounds CPL Industries declared as the main target compounds of their customers for adsorption, thus the most likely to be found on the base sample. As, discussed in Chapter 2, these compounds are those that are oxidised to acidic species during the steam/oxidation step.

In every sample that was regenerated there were no signs of CS_2 or H_2S, meaning they had either been removed or had reacted with other compounds on the surface to produce new compounds. Additionally, although compounds such as Fe_2SO_4 and $K_2Fe(SO_4)_3$ were found on the surface, there were no peaks indicating the presence of sulphuric or sulphurous acid. Essentially, the change in sulphur compounds seen in thermal regeneration pre-oxidation had occurred.

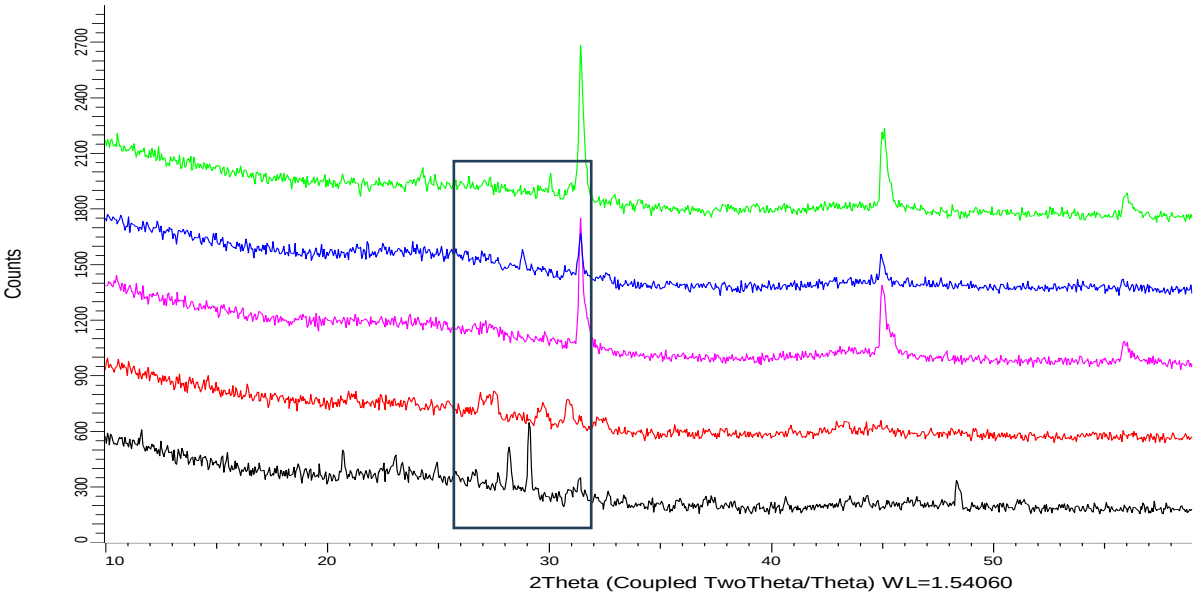


Figure 34. XRD diffractogram of preliminary MW regeneration experiments: base sample - black; 200 W– red; 400 W – pink; 600 W – blue; and 800 W – green.

When irradiated at a lower MW power, intense clusters of peaks between 26 and 32 2theta appeared, matching potassium sulphate, sodium peroxide and potassium iron sulphate. As the power is increased this cluster disappears and the intensity of peaks matching these compounds lessens. This was because the heating at 200 W was insufficient to force these compounds out of the pores, they could also be formed at lower temperatures.

The XRD of AC in the AC trap confirmed that no sulphur-based acids were produced during the process. However, the sulphur compound deposited in the cold trap is S_8, pure elemental sulphur – a side-effect of the surface water having been vaporised via MWs interacting with the dipolar O-H bonds. H_2S can adsorb directly onto the surface, before dissolution into the water/steam film, followed by dissociation of the H_2S in an adsorbed in the water/steam film.

$$H_2S_{(g)} \rightarrow H_2S_{(ads)}$$

$$H_2S_{(ads)} \rightarrow H_2S_{(ads\text{-}liq)}$$

$$H_2S_{(ads\text{-}liq)} \rightarrow HS^-_{(ads)} + H^+$$

$$O_{2\,(g)} \rightarrow O_{2\,(ads)}$$

$$HS^-_{(ads)} + \tfrac{1}{2}\, O_{2\,(ads)} \rightarrow S_{(ads)} + OH^-$$

Surface oxidation can occur with the metal hydroxide impregnates (i.e., $FeOH_2$), forming SO_2 or S_8. However, unlike that of the thermal regeneration process, no further oxidation to acids occurs as a steam phase is not required to agitate compound desorption. The formed elemental sulphur is physiosorbed to the surface, being desorbed via continuous MW irradiation, before being turned into subsequent liquid and solid phases with the cooling atmosphere of the cold trap.

$$HS^-_{(ads)} + 1\,½\ O_{2\ (ads)} \rightarrow SO_{2\ (ads)} + OH^-$$

$$FeOH_{(IAC)} + HS^-_{(ads)} \rightarrow FeS_{(ads)} + H_2O_{(g)}$$

$$8FeS_{(ads)} + 12H_2O_{(ads)} + 6O_{2\ (g)} \rightarrow 8Fe(OH)_{3\ (ads)} + S_{8\ (ads)}$$

$$S_{8\ (ads)} \rightarrow S_{8\ (g)}$$

Conclusions

Examining the nature and identity of the sulphur species still adsorbed on the surface, as well as that removed, revealed that the use of MW irradiation had stopped the need for a steam oxidation phase, eliminating the production of sulphur-based acid compounds. With this, one of the most important goals for the project was achieved. However, there were several issues relating to the AC structural integrity.

Although the preliminary MW setup reduced the time and energy requirements for the regeneration, it had a negative effect on the reusability of the AC integrity and reusability of the carbon. The results of the preliminary study confirmed that the predicted localised overheating did occur, resulting in damage to the overall carbon structure. With this, a significant mass loss to the sample's mass was seen. Analysing the effects of MW power and irradiation time revealed that both were rate determining steps for both the level of sulphur adsorbate being removed and the damage to the overall structure. With this knowledge, the foundations were set for the next stages of the research project.

5.3.2 Single-mode cavity – Reducing Overheating

5.3.2.1 Intermittent microwave irradiation

After the first two stages of study, it was clear that MW power and irradiation time were key determining factors in localised overheating and manipulating these factors could be key to achieving suitable sulphurous adsorbate removal. MW power was controlled and kept steady via the use of the three-stub autotuner in previous experiments which changes tuning positions to keep at a constant power output. But MW irradiation time had only been analysed in so far as keeping irradiation constant over a set period. The purpose of the next study was to analyse whether the use of intermittent MW irradiation over set periods would reduce the localised overheating.

Design

Much like the design MW rig outlined in Section 5.3.1, the MW heating of the AC samples took place inside a 3.2 cm quartz glass tube. This quartz tube was inserted into the MW cavity via the 40 cm metallic tube choker, which had a length of 40 cm and an internal diameter of 5 cm. The MW power was supplied by the custom-built MW rig consisting of the 2.0 kW generator (~2.45 GhZ) which supplied MWs to the single-mode cavity through WR340 aluminium waveguide together with E-bends as shown in Figure 31. The automatic three-stub tuner was used to keep the MW power input consistent and for analysis.

Weighted quantities of spent sulphurous AC (10.00g (+/- 0.20 std)) were placed inside of the quartz reactor. A continuous flow of nitrogen, at 2 $L.min^{-1}$, was introduced into MW waveguide 3 minutes prior to each experimental run, remained flowing during the run, and continued to flow for 5 minutes after the run had concluded, to ensure that the oxygen content inside the cavity was less than 5%, per the calculated inerting levels shown in appendix 10.1. A PTFE window was attached to the waveguide to ensure nitrogen and any vapours would not flow directly into the generator. Off-gases were collected via a cold trap and activated carbon trap, with any excess gases being vented out of the building.

The MW power was set to 400 W before the MW was turned on – this experiment examined the effects of intermittent MW irradiation and so only a single set power was used. The intermittent irradiation was achieved by conducting each experiment over a period double that of the intended irradiation time, in which the MW irradiation was controlled by turning

it on and off at the 2.0 kW generator for periods of 10s. For example, a 120s irradiation experiment would run over 240 s: 10 seconds of MW power on, followed by 10 seconds of MW power off, followed by 10 seconds on, and so on until the total experimental time of 240s (120s irradiation time) was completed. A stopwatch was used to track heating times as well as an automated timer on the MW generator itself. At the end of each experiment the MW power was turned off.

After each experiment a period of 10 minutes was allowed for sample and reactor cooling to allow for safe manual handling. The samples were then weighed to allow for a quick look at how much sulphurous compounds may have been removed before thorough analysis via methods outlined in Section 3.

Experiment

The MW regeneration experiments of solvent spent sulphurous AC were run at varying over various periods of intermittent MW irradiation (120s, 180s, 240s, 360s) to establish the effects on the level of heating, sulphur removal, and overheating that may lead to damage to the overall AC. The MW irradiation times were kept at the same increments as those in the previous studies to allow for reasonable comparison. As with the previous studies, the specific energy input for each sample was calculated using equations 14a and 14b.

Results

As shown in Table 6, and much like the preliminary MW regeneration experiments described in Section 5.3.1, an increase in irradiation time did lead to an increase in butane activity for the AC samples, with those running for 360s achieving 33.62 % (+/- 0.76 std). However, the increase in butane activity over with increased irradiation time was much more dramatic, with the incremental increase between 120s to 180s being 16.38 %, compared to the analogous runs (which were not irradiated intermittently) being 4.98 %. There was a similar, albeit to a lesser degree, difference in the increase of butane activity between the samples intermittently irradiated over 180s and those intermittently irradiated over 240s, with a 3.95% increase, compared to the analogous results of the non-intermittently irradiated samples which saw an increase in butane activity of 1.23%. Yet, both the intermittently irradiated and non-intermittently irradiated samples saw a butane activity increase of approx. 3% between 240s to 360s. The larger increase in butane activity over initial MW irradiation

suggested that the adsorbate removal was linked to not only time, but how much MW energy had been absorbed by the dipolar adsorbates and redistributed as heat energy to surrounding adsorbates (leading to further desorption). Continuous MW irradiation appeared to have caused the point at which excess heat energy exertion caused a cascade of desorption to occur. Essentially, the more frequently the samples were exposed to incidents of electromagnetic energy in the form of MWs, the more desorption and heat energy exertion would occur.

Table 6. Effects of intermittent MW irradiation time on AC butane activity and specific energy. Standard deviation (+/- x.xx) shown was calculated for each result from the corresponding results in Appendix B.

Irradiation time (s)	Mass change (%)	Butane activity (%)	Specific energy input ($kJ.g^{-1}$)
120	19.23 +/- 0.92	8.00 +/- 0.05	18.40 +/- 0.51
180	40.21 +/- 0.26	26.38 +/- 0.26	20.02 +/- 1.13
240	44.16 +/- 0.26	30.33 +/- 1.26	22.45 +/- 0.97
360	44.41 +/- 2.41	33.62 +/- 0.76	25.97 +/- 1.71
Thermal	50.31 +/- 0.95	40.88 +/- 0.92	-

However, much like the samples regenerated via MWs non-intermittently in the first study of this chapter, the mass loss was an initial indicator that localised overheating was occurring in these runs as well, with the samples irradiated over 360s having a mass loss of 44.41% (+/- 2.41 std). The mass loss was not quite as high as that seen in the non-intermittently irradiated samples, but still significantly high considering the butane activity had not reach that seen in the thermal regeneration. However, as shown below in Figure 35, when examining the EPMA scans for the samples irradiated intermittently over 360s, it showed a much different distribution of sulphurous compounds inside the pellet to that seen in the analogous non-intermittently irradiated sample. Although the distribution of sulphurous compounds echoed that shown in Figure 32 – a more even spread across the sample with the pre-regeneration high concentrations around the outer edges of the sample having decreased – many of the samples showed patches of low concentration within the individual granule. This same

samples showed many large areas of structural damage (represented by the black cracks inside the pellet) in areas where more sulphurous compounds had been desorbed. This suggested that the intermittent heating led to high sulphur removal in some areas, but not others, and that the areas which had seen large level of sulphur removal had succumbed to carbon structural damage.

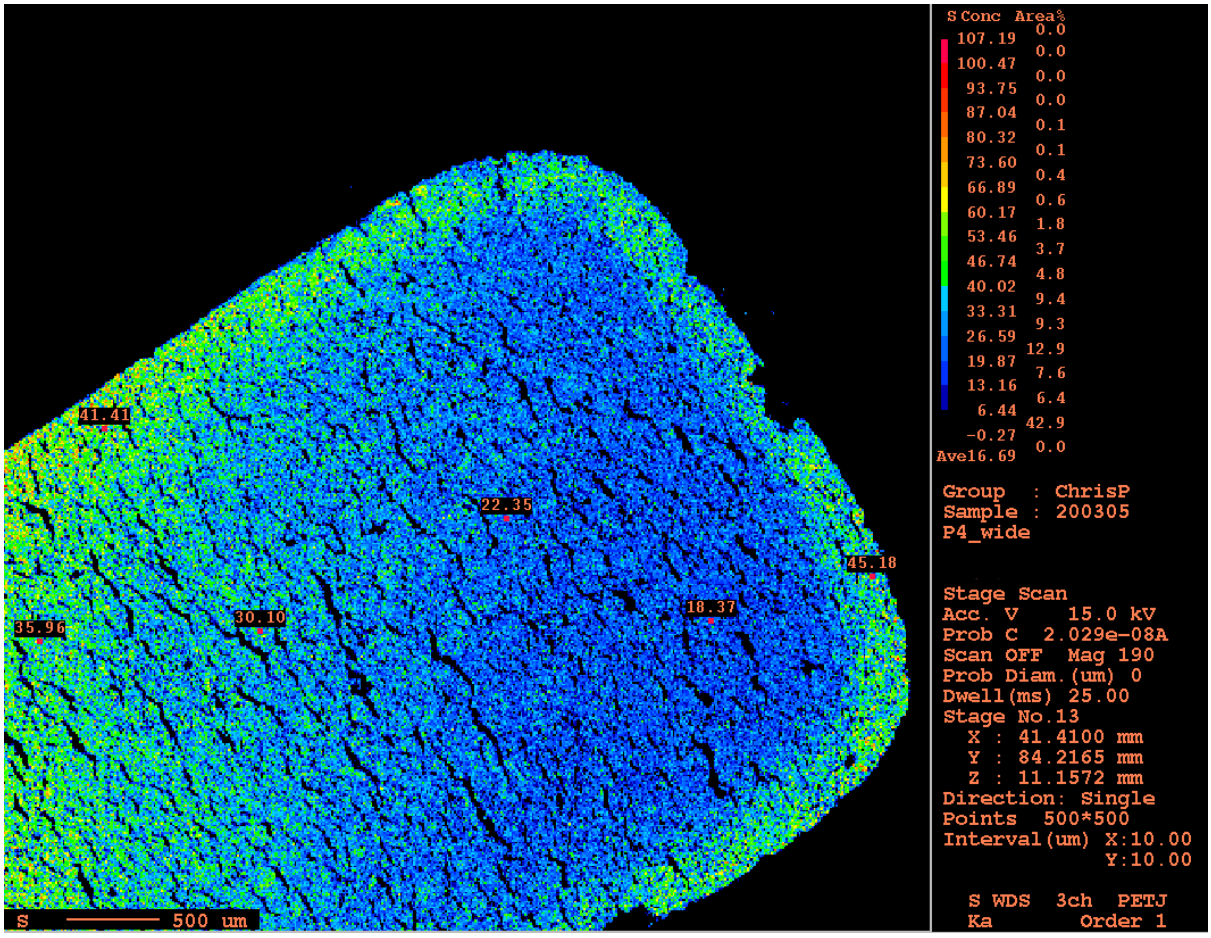


Figure 355. EPMA scan of a cross section of the edge of MW regenerated sulphurous activated carbon at 400 W for 360s intermittently.

When examining the intensity profile (Appendix C), there is a noticeably large number of sharp peaks at lower gray values, indicative of either lower sulphur levels or damage to the carbon. Considering other results show the sulphur concentration had not decreased dramatically owing to the lower density of electric field, this suggested excessive damage to the AC. Additionally, the gray value trend was still mainly between 100-150 – the same area as base value – seemingly confirming that the concentration had not decreased dramatically across the AC.

As shown in Table 6, the specific energy input of the intermittently irradiated samples and the analogous non-intermittently irradiated samples is vastly different, with the intermittently irradiated samples requiring far more energy to desorb the sulphurous adsorbate. This is likely due to the sample cooling between periods of irradiation, and bond vibration decreasing, resulting in more energy being required per heating step [194]. Additionally, it should be noted that although the experiments were run as outlined, the intermittent process (turning the power on and off in relatively quick succession) did cause the 2.0 kW generator to begin to heat up. This would be an operational obstacle if this process were to be scaled-up as a much larger generator would be required and may result in electrical faults.

Change in sulphur chemistry

As one might suspect, the XRD analysis was strikingly like that of the non-intermittently irradiated samples, with each analogous run's diffractogram being able to overlay and show the exact same peaks. With this, it was established that the same desorption mechanics (in terms of the sulphur compounds transitions and desorption) were happening. The exception to this was the samples run for 120s, which did see low intensity peaks for CS_2, suggesting that time under intermittent irradiation was not sufficient to trigger desorption mechanisms for all members of this species that had been previously adsorbed. However, there were no signs of CS_2 in samples regenerated over longer periods of time.

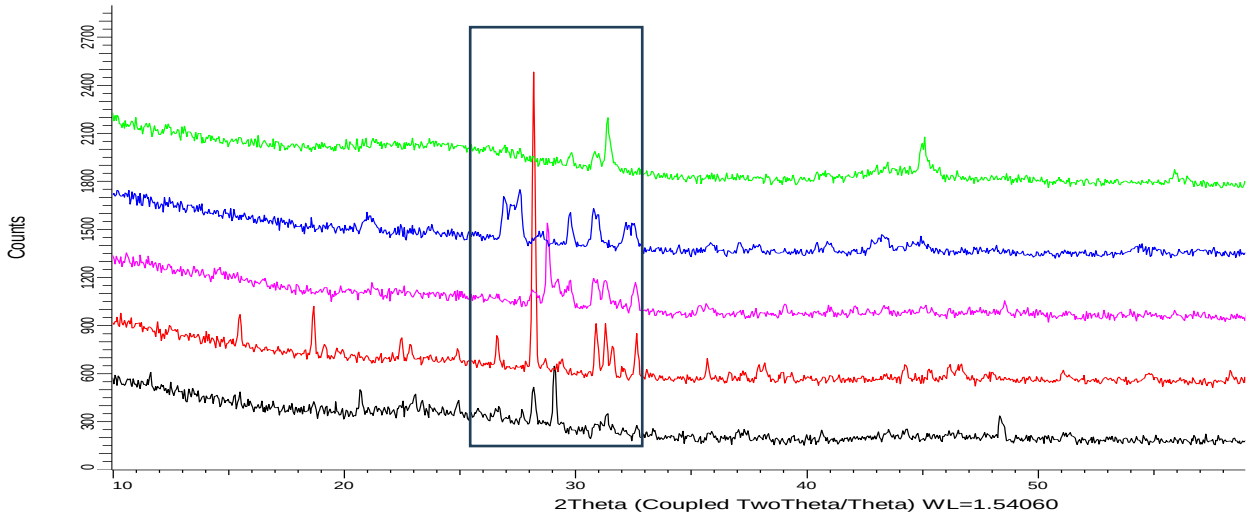


Figure 36. XRD diffractogram of intermittent irradiation MW regeneration experiments: base sample – black; 200 W– red; 400 W – pink; 600 W – blue; and 800 W – green.

Conclusions

The samples subjected to intermittent MW irradiation reacted in much the same way as those irradiated continuously in terms of increasing irradiation time leading to higher levels of butane activity being achieved. As with the continuously irradiated samples, increased irradiation time also led to an increase in mass loss and structural damage to the AC itself. The intermittently irradiated samples also showed no signs of acid production, having not required a further steam oxidation step to cause desorption of adsorbates adsorbed to the surface via stronger interactions with the AC itself.

However, it should be noted that the level of energy required for adsorbate removal was significantly higher than that of the analogous samples that had been continuously irradiated. This would likely prove to be an issue if the project had been moved forward in this direction when it came to scaling up to an industrial level regeneration operation.

5.3.2.2 Solvent-bathing

Due to the overheating of the AC samples seen in the preliminary experiments, a study was conducted that involved attempting to regenerate samples whilst they were bathed in inert solvents. These experiments were conducted to show the effects of heating during regeneration whilst the surface temperature was cooled. This method was first shown by Dr Mohamed Adam in his thesis regarding optimisation of MW pyrolysis of biomass materials [190]. As Mohamed is a colleague in my research group during my research project, he guided me through designing the process.

Materials

The AC samples used for this experiment were from the same overall batch as the experiments outlined in Section 5.3.1. Two hydrocarbon solvents with different boiling points were used for these experiments: hexane and kerosene. Table 7 shows the chemical formula, molecular weight, and boiling points of both solvents.

Table 7. [a] obtained from Green and Perry [191], [b] obtained from the safety data sheet provided by the supplier [192] [193].

	Hexane [a]	Kerosene [b]
Formula	$CH_3(CH_2)_4CH_3$	A mixture of C10-C14 naphthenes, iso- and n- paraffins [c]
Molecular weight	86.18	
Boiling point (°C)	69	200-250

Design

The experimental setup was identical to that used in Section 5.3.1, with the key difference being that the samples were submerged in solvent inside of the reactor (quartz tube), shown below in Figure 37.

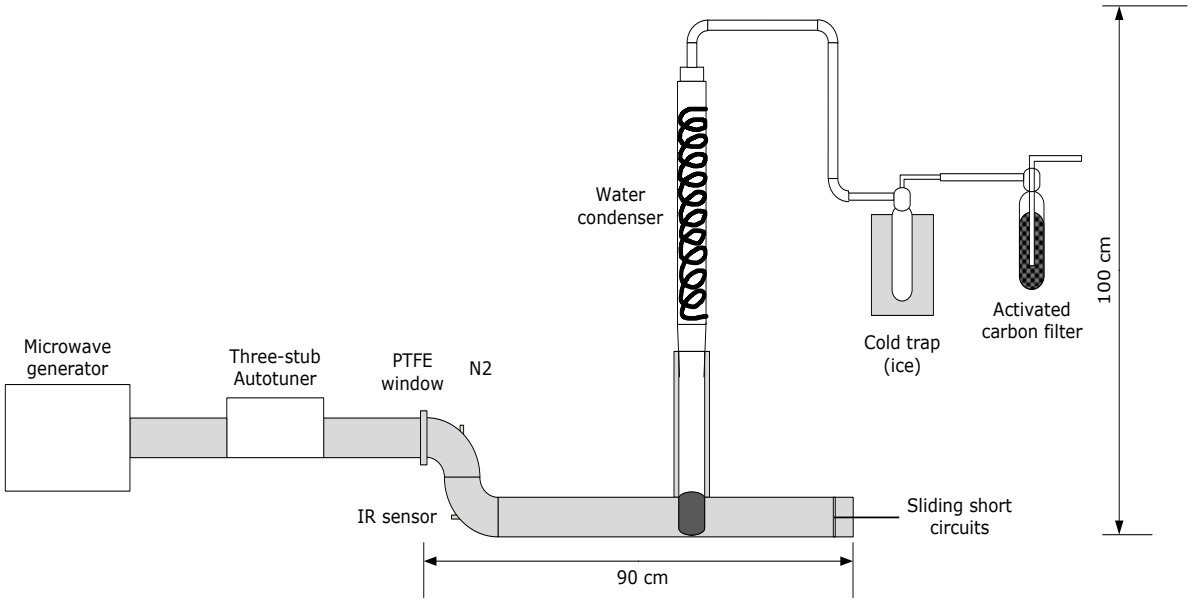


Figure 377. Experimental setup for spent sulphurous AC regeneration, using a solvent bathing method, and the custom-built MW rig.

As with the first experimental setup, the quartz tube was then inserted into the cavity via a 40 cm long metallic tube with an internal diameter of 5.0 cm. Atop the quartz reactor a condenser was stattioned to reclaim any solvent boiled off during the heating process. Again, the MW power was supplied by a 2.0 kW generator (~2.45 GhZ) which supplied MWs to the

single-mode cavity through WR340 aluminium waveguide together with E-bends. An automatic three-stub tuner was attached to the waveguide for power analysis.

For each of the heating experiments, a weighted quantity of the spent sulphurous AC (10.00 (+/- 0.20 std)) was placed in the reactor. The samples were bathed in solvent for 24 hours prior to experimentation to ensure any tapped air could bubble off. The quantity of solvent used was calculated using the method described in appendix A (10 ml of hexane per gram, 20 ml kerosene per gram, respectively).

As the MW rig was setup in the same manner as the preliminary experiments, the nitrogen flow used to inert the waveguide cavity was calculated and implemented in the same way. the off gases were also collected in a carbon and cold trap.

To allow for comparison between the experiments that utilised solvent bathing, various levels of MW power were used (200 W, 400 W, 600 W, 800 W), as well as the same increments of MW irradiation. Both were monitored in the same fashion as described for the preliminary experiments.

After each experiment a period of 10 minutes was allowed for sample and reactor cooling to allow for safe manual handling. Once the samples were at a comfortable handling temperature, they were extracted from the reaction vessel using a sieve. They were then dried over 8 hours in a muffle oven at 60 ^{o}C to remove the last of the solvent. The samples were then weighed to allow for a quick look at how much sulphurous compounds may have been removed before thorough analysis via methods outlined in Chapter 3.

Experiments

The MW regeneration experiments of solvent spent sulphurous AC were run at varying powers and over various periods to establish the effects each would have, respectively, on the level of heating, sulphur removal, and overheating that may lead to damage to the overall AC. As with the preliminary experiments, the specific energy input for each sample was calculated using equations 14a and 14b.

Results - Irradiation Time

Table 8 shows that, much like the preliminary MW regeneration tests, an increase in irradiation time lead to an increase in the butane activity for the samples bathed in solvents.

However, the level of returned absorptivity, shown by the butane activity, was significantly lower than that seen in both the preliminary MW experiments and that of the thermally regenerated samples. Also, a much lower level of mass loss was recorded, which represented an early indicator of low levels of sulphur compounds desorption before further analysis. This is paired with extremely high specific energy inputs.

Table 8. Table 8. Effects of MW irradiation time on AC butane activity and specific energy input using 400 W power whilst samples were bathed in hexane or kerosene. Standard deviation (+/- x.xx) shown was calculated for each result from the corresponding results in Appendix B.

	Time (s)	Mass change (%)	Butane activity (%)	Specific energy input ($kJ.g^{-1}$)
Hexane	120	14.40 +/- 2.30	2.36 +/- 0.13	21.81 +/- 2.62
	180	15.92 +/- 1.40	2.50 +/- 0.25	36.31+/- 5.22
	240	16.69 +/- 2.01	2.48 +/- 0.28	53.79 +/- 3.68
	360	17.40 +/- 0.90	2.39 +/- 0.07	65.05 +/- 5.26
Kerosene	120	14.28 +/- 2.48	2.09 +/- 0.02	20.16 +/- 1.86
	180	15.75 +/- 0.67	2.29 +/- 0.08	36.31 +/- 5.05
	240	17.14 +/- 2.20	2.32 +/- 0.04	65.28 +/- 5.71
	360	17.43 +/- 2.34	2.44 +/- 0.23	69.89 +/- 7.87
Thermal		50.31 +/- 0.95	40.88 +/- 0.92	-

When comparing the three MW regeneration methods for the samples irradiated over 360s, the mass change for the non-bathed AC was 51.3 % (+/- 0.95 std) (albeit a result from overheating), whereas the solvent-bathed samples were 17.40 % (+/- 0.90 std) and 17.43 % (+/- 2.34 std) for hexane and kerosene, respectively. The butane activity of the solvent-bathed samples was dramatically lower than what had been expected, with the hexane-bathed samples only reaching 2.39 % (+/- 0.07 std) and the kerosene-bathed samples recorded at 2.44 % (+/- 0.23 std). The pre-regenerated spent AC samples butane activity was recorded as having been an average of 2.01 % (+/- 0.11 std). This low level of Butane activity increase suggested that potentially barely any sulphur has been removed from the surface of the AC. Moreover, the cold and AC traps appeared to contain no visible signs of sulphur compounds

having been deposited with a distinct lack of a yellow hue. However, the solvents themselves did show some signs of sulphur, having changed from clear colourless solutions to clear yellowish fluids. With this, it appeared that at least some of the adsorbed sulphurous compounds had been desorbed into the solvent during the process.

When analysing the hexane-bathed sample's EPMA scans (Figure 38) it showed that the distribution of sulphur had changed, with a more even spread across the sample, but the high levels of sulphur compound build-up on the edges of the sample no longer present. However, the intensity profile (Appendix C) suggests that there was a slight dip in the gray value in the centre of the AC, echoing the trend seen in Figure 28 for the base sample, albeit with lower intensity on the edges of the AC. But the level of sulphur was still exceedingly high across the AC. It was theorised that some form for desorption had taken place, hence the lower concentrations of sulphur around the outside of the samples, and the yellowish tinge to the solvent, but that this was to a much lesser extent to that seen in the preliminary MW experiments. Additionally, there were signs of less damage having been caused by the process than that seen in the preliminary experiments, with less fraying around the edges of the sample and a less cracks having been formed internally.

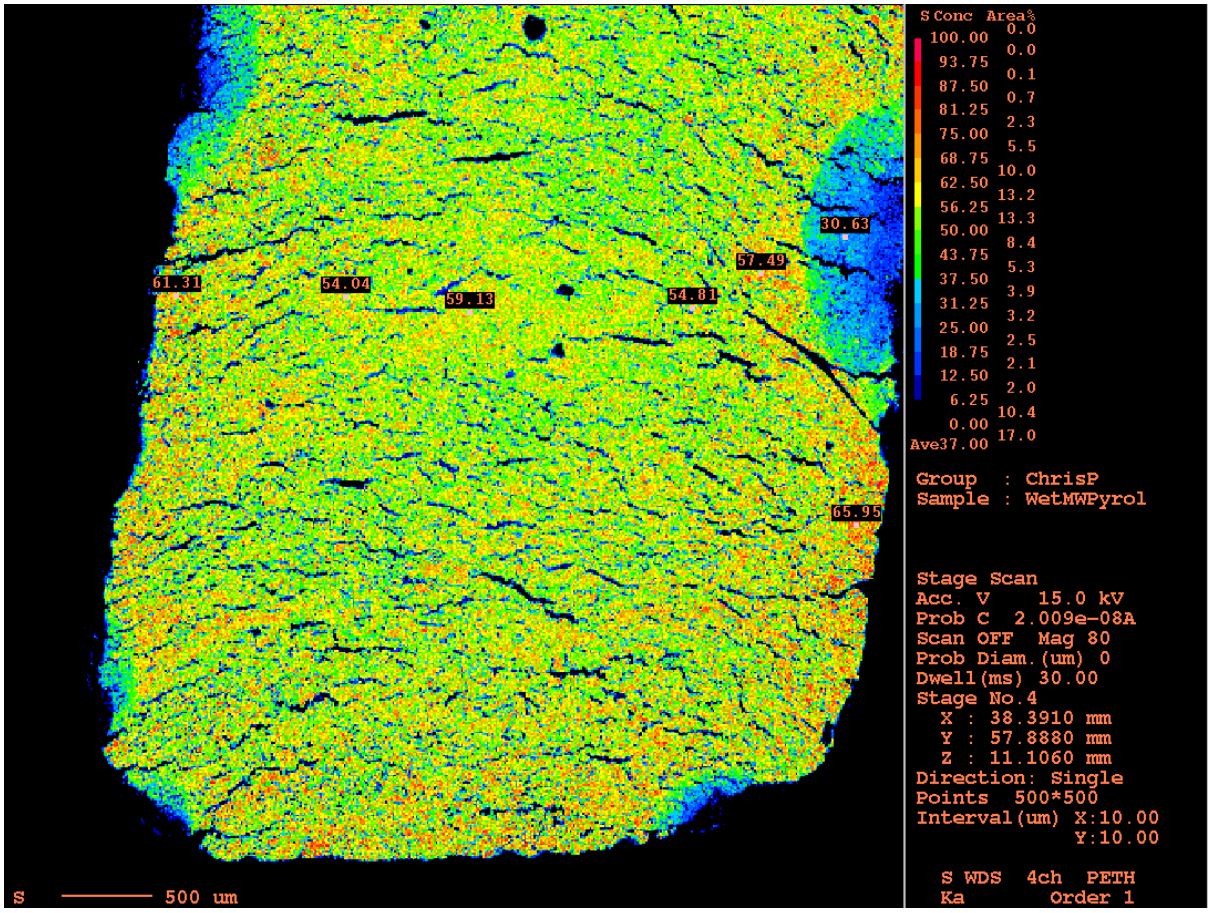


Figure 38. EPMA scan of a cross section of the edge of a of hexane-bathed MW regenerated sulphurous activated carbon at 400W for 360s.

With the kerosene-bathed samples, although the numerical data appeared to be analogous to that of the hexane-bathed samples, the visible changes were different. The solvent itself appeared to be closer to its original colourless hue than to the yellow seen with the hexane post-regeneration. When examining the sample irradiated over 360s, the EPMA scan appeared more like that of the AC pre-regeneration, suggesting that less desorption from the edges of the samples, and subsequent reactions had taken place during the MW process. The intensity profile (Appendix C) did show large dips to low gray values, indictive of the damaged areas (black gaps), as seen in other prior regeneration attempts i.e., Figures 30, 32, 35.

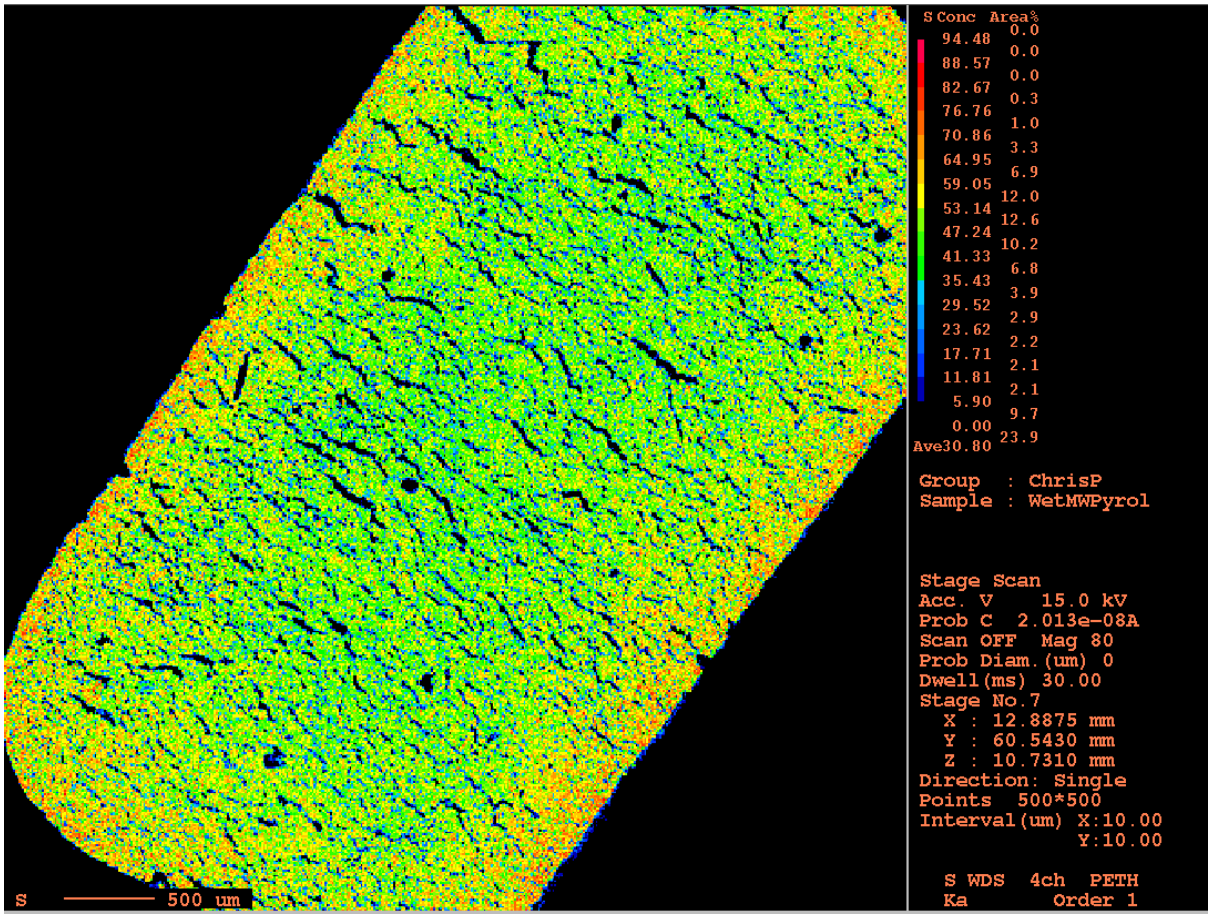


Figure 39. EPMA scan of a cross section of the edge of a of kerosene-bathed MW regenerated sulphurous activated carbon at 400W for 360s.

In terms of the specific energy input, as predicted with the solvents being in place to cool the surface, far more energy was required to remove even small amounts of sulphur from the surface. However, it was not predicted before the experiments that it would take upwards of 67 $kJ.g^{-1}$ to remove as smaller amount of sulphur as was removed over 360s. When comparing the results with that of Dr M Adam, the effects of solvent-bathing samples that are to be processed with MWs appears to have had a similar effect, albeit to a much more significant degree [190]. It was theorised that low level of sulphur materials had been due to the solvents clogging the pores of the carbon, reducing the mass transfer of desorbed materials closer to the surface of the carbon (or those chemisorbed) as those further away on packed physiosorbed beds could not move away as quickly and heat transfer through the solvent was not as efficient as heat transfer through air.

Results – Microwave Power

The next step of the solvent-bathed AC sample regeneration experimentation was to analyse the effects of MW power and whether a similar trade-off between MW power and irradiation time, as seen in the preliminary experiments, would be apparent. For this selection of runs the same set-up and method was used as that used for the MW power study in Section 5.3.1, with incremental steps of 200 W.

Table 9. Effects of MW power on AC butane activity and specific energy when AC samples were bathed in hexane or kerosene. Standard deviation (+/- x.xx) shown was calculated for each result from the corresponding results in Appendix B.

	Power (W)	Mass change (%)	Butane activity (%)	Specific energy input (kJ.g $^{-1}$)
Hexane	200	15.78 +/- 0.95	2.19 +/- 0.09	27.34 +/- 1.15
	400	16.24 +/- 3.44	2.37 +/- 0.13	33.71 +/- 0,52
	600	18.13 +/- 0.87	2.41 +/- 0.26	22.62 +/- 1.44
	800	17.41 +/- 3.01	2.28 +/- 0.07	22.62 +/- 1.44
Kerosene	200	17.11 +/- 3.32	2.25 +/- 0.03	23.01 +/- 1.52
	400	15.43 +/- 0.72	2.30 +/- 0.03	38.43 +/- 1.55
	600	18.40 +/- 2.39	2.33 +/- 0.04	36.26 +/- 0.72
	800	18.43 +/- 3.26	2.28 +/- 0.08	25.34 +/- 3.73
Thermal		50.31 +/- 0.95	40.88 +/- 0.92	-

As with the experiments in Section 5.3.1, the trade-off between power and time was apparent. Both parameters act as rate determining steps for desorption of the sulphurous adsorbates – as the power was increased by 200 W, the irradiation time was reduced by 60s, resulting in lower butane activity percentages. When the irradiation time decreased too much, even after an initial increase with power increase from 200 to 400 W, there was a reduction in butane activity achieved between 600 to 800 W. this pattern was echoed by the specific energy input.

Changes in sulphur chemistry

As previous, XRD was used on the surface of the sample ACs to identify what sulphurous compounds were being formed during the desorption process. Much like the previously analysed MW-regenerated samples, there were no signs of the adsorbed H_2S, CS_2, or SO_2, indicating that although the level of sulphurous compounds removed was low, desorption had started to occur. Additionally, as with the 5.3.1 study, there were no signs of sulphuric or sulphurous acid on the surface of the ACs.

With the kerosene and hexane series, there were similarities with the compounds being identified in the previous study. Specifically, finding potassium sulphate and sodium iron sulphate. However, the sodium iron compounds' peaks are found in different 2theta positions and were classified on the XRD EVA database as having different geometrical positioning. Those found in the non-solvent were in orthorhombic crystal structures rather than Tetragonal (as was found here), suggesting that although present, they were formed in different ways as shown by their differing lattice structures.

Conclusions

Much like the preliminary experiments conducted in Section 5.3.1, the MW irradiation of solvent-bathed spent sulphurous AC resulted in the desorption of some (not all) of the adsorbed sulphurous species. However, the use of solvent-bathing resulted in a dramatically reduced level of sulphur adsorbate removal from the outer surface of the AC and even greater reduction in the levels of removal from that which was adsorbed within carbon pores. But the use of a technique to reduce localised overheating (cooling the surface via solvents in this case) did aid in the reduction of localised overheating.

Although the level of returned AC adsorptivity was poor in relation to other methods tested, the idea of reducing carbon structural damage proved to be useful and would inform the direction of the project going forward.

5.4 Conclusions

An initial study was undertaken to understand the viability of MW heating/processing for the regeneration of spent sulphurous AC. A systematic approach was followed for the process design that considered the requirements outlined by the research project's sponsors, CPL Ltd. In this, the ability to reduce the overall time required for regeneration, the reduction/elimination of unwanted by-product production, and the returned level of adsorption capabilities (in the form of butane activity) for the AC, were studied.

Initial experiments with various MW powers and irradiation times were conducted to establish the effects of systems utilising high density electric fields as a mechanism by which sulphur adsorbate desorption could be achieved. It was found MW irradiation did achieve regeneration of the spent sulphurous ACs, desorbing much of the material and returning absorptivity to a significant degree with considerable butane activity levels being achieved. However, MWs caused localised overheating in areas with higher concentrations of sulphurous compounds on/in the AC, leading to damage to the overall carbon structure.

The MW processing did achieve regeneration of the spent ACs in far smaller period than that seen in thermal regeneration, and it did eliminate the need for late-stage oxidation steps used in thermal regeneration, eliminating the production of acids. The oxidative steps that did take place resulted in the production of elemental sulphur molecules via interactions between adsorbed materials reacting with adsorbed water molecules when heated.

Further studies were conducted with the goals of stopping the localised overheating from occurring via the use of solvent bathing target samples and using intermittent heating. The former proved to drastically reduce the regeneration efficiency of MW processing, whilst the latter did not reduce the overheating when being used at MW powers required for desirable butane activity achievement.

Although the initial studies presented promising results in certain regards (reduced processing time, elimination of unwanted by-product production, a degree of regeneration), the reduction in localised overheating represented challenges that would be investigated further during the development of an adequate process.

6. Low-density electric field processing

6.1 Introduction

Following on from the work conducted in the previous chapter, the aim of the work documented in this chapter was to develop an understanding of the effects of electromagnetic field density on AC during regeneration via MW processing. The work in the previous chapter established that although MW processing presented positive attributes in the form of reducing the overall regeneration processing time (when compared to thermal methods), eliminating the production of unwanted by-products, and desorption of adsorbed sulphurous species, the localised overheating resulted in damage to the overall carbon structure and had not reached the butane activity levels seen in traditional methods.

There are several published studies on the effects of microwave field density, such as those by Qiao *et al*, Kesbi *et al*, and Hassani *et al*, which document the effects of manipulating microwave field desnity and how it affects the heating process as well as structural integrity of targeted materials [195] [196] [197]. With each case documenting that the heating rate is lowered by decreasing the MW field intensity, but the reduction in heating rate reduces the level of localised overheating and thus damage to surrounding materials.

At the time of experimentation there were no publications detailing the effects of field density on spent ACs. The reason being that high field density MW processing units are achieved via the use of a narrow waveguide cavity typical of lab-scale units. Field density is reduced with the increase in size of the waveguide cavity. One of the overall goals for this project was to move towards replacing an industry-scale thermal processing unit. Thus, the following studies were justified in that the viability of a large-scale unit could be approximated by using a larger waveguide cavity in laboratory experiments.

6.2 Background

The localised overheating was due to the density of the MW field being high, owing to the use of a single-mode waveguide cavity. Single-mode waveguide cavities are narrow, often narrow enough that only a single wavelength can be achieved, thus a directly focused irradiation of the target reaction vessel, as shown in Figure 40. This focused irradiation is termed as a high MW field density, and effectively results in results in exceedingly fast heating rates, as the

faster rates of incidents of MW interaction with dipolar molecules lead to more heat energy being dispersed from said dipolar molecules to the surroundings [128] [130] [131]. As was the case with spent sulphurous ACs, the fast-heating rates, and thus high levels of heat dispersion, proved to be detrimental to the overall carbon structure.

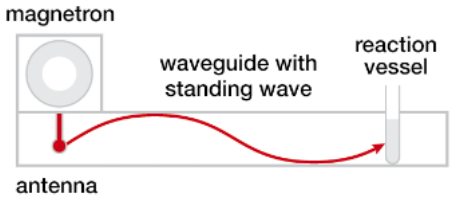


Figure 40. Schematic drawing of the electromagnetic field density distribution in a single-mode MW waveguide [198].

With multimode waveguide cavities, the cavity in which the reaction vessel is housed is much larger so to create slower rates of moments of incidence. Essentially, the purposeful avoidance of generating a standing wave pattern inside the cavity, as is the case with single-mode reactors, results in much greater dispersion on MW radiation in many directions. With this the waves can bounce off the walls of the cavity several times before interacting with the samples inside the reaction vessel, and it may take more time before each wave does interact with the reaction vessel [199] [200] [201] [202]. This can be seen in Figure 41. With the rate of MW incidence reduced, the rate of heating is reduced.

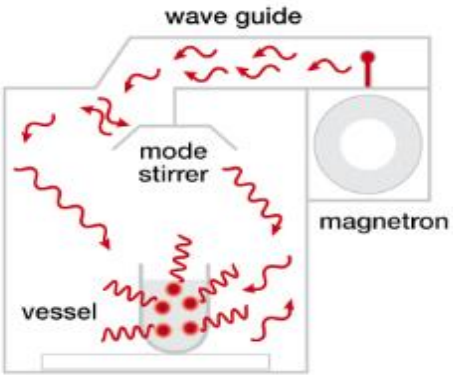


Figure 41. Schematic drawing of the electromagnetic field density distribution in a multimode MW waveguide [198].

To allow for comparisons with the work in the previous chapter, studies regarding the effects of MW power and irradiation time were carried out. With analogous results, the difference in field density could then be studied to establish issues that could be encountered if methods such as the initial set-up in the previous chapter were to be scaled-up to use a multimode for industrial operations. The following study studies a potential method to avoid localised overheating seen in the single-mode experiments of the previous chapter.

6.3 Multimode waveguide cavity design

The experiments of the previous chapter confirmed that MW power and irradiation time were key in controlling the localised overheating. However, these factors alone did not permit enough control to heat the samples in such a way that achieved satisfactory butane activity levels without causing structural damage to the AC. These experiments utilised a high-density MW field, meaning that the moments of incidence of MW interaction with the ACs was high, leading to fast heating rates, and localised overheating. The purpose of the next set of experiments was to analyse whether the localised overheating could be controlled/reduced by reducing the intensity of the MW electric field via the use of a multimode waveguide reactor cavity instead. This would be done by using a multimode waveguide reactor cavity instead of a single-mode reactor cavity.

Design

The following experiments for the study pertaining to the effects of low-density electric field fields were conducted as follows:

The regeneration of the spent sulphurous ACs took place inside a 3.2 cm diameter quartz reaction vessel. The quartz vessel was then inserted into the cavity via a 40 cm long metallic tube with an internal diameter of 5.0 cm, acting as a choke for the electromagnetic power. MW power was supplied by a custom-built MW rig consisting of a 2.0 kW generator (~2.45 GhZ) which supplied the MWs to a multimode waveguide reactor cavity (measuring 30 cm x 24 cm x 24 cm) through a WR340 aluminium waveguide together with E-bends, as shown in Figure 42. An automatic three-stub tuner was attached to allow for analysis and control for MW power.

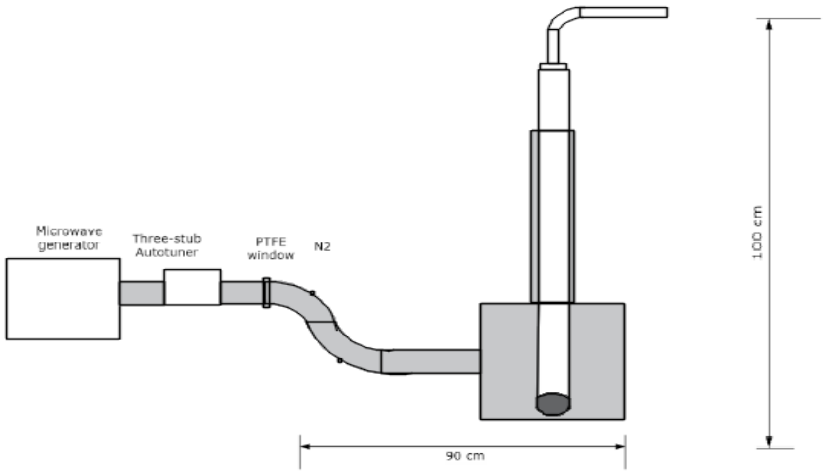


Figure 42. Experimental setup for spent sulphurous AC in custom-built MW rig using multimode waveguide reactor cavity.

For each of the heating experiments, a weighted quantity of the spent sulphurous AC (10.00g (+/- 0.20 std)) was placed in the reactor. During the heating of samples, the cavity was inerted using a continuous flow of nitrogen at 10 $L.min^{-1}$ as a safety feature to avoid fire in case of failure in the system such as electric breakdown and/or any breaks in the quartz tube. The flow of nitrogen was turned on 3 minutes before experiments took place and remained on for 5 minutes after to ensure that the oxygen content inside the cavity was less than 5%, per the calculated inerting levels shown in Appendix 10.1. A PTFE window was attached to the waveguide to ensure nitrogen and any vapours would not flow directly into the generator. Off-gases were collected via a cold trap and activated carbon trap, with any excess gases being vented out of the building.

The MW power was set to various levels (200 W, 400 W, 600 W, 800 W) before the MW was turned on. A stopwatch was used to track heating times as well as an automated timer on the MW generator itself. Increments of time were 120s, 180s, 240s, 360s. At the end of each experiment the MW power was turned off.

After each experiment a period of 10 minutes was allowed for sample and reactor cooling to allow for safe manual handling. The samples were then weighed to allow for an initial gauge of how much sulphurous compounds may have been removed before thorough analysis via methods outlined in Chapter 3.

6.4 Effects of low-density electromagnetic field on microwave regeneration of spent sulphurous activated carbon

The multimode MW regeneration experiments of spent sulphurous AC were run at varying powers over various irradiation times to create results that could be compared to those runs using the single-mode in the previous chapter's studies. In addition to this, as was done for previous experiments, specific energy input was calculated using equations 14a and 14b (page 94) using absorbed energy data recorded from each experimental run to show the efficiency of the method.

6.4.1 Preliminary study of microwave irradiation time when using a low-density electromagnetic field

The initial study into the effects of MW irradiation time when using a multimode waveguide cavity reactor are shown below in Table 10. The results of the study showed that increasing irradiation time used for the regeneration process resulted in an increase in mass change, butane activity and specific energy input, echoing the pattern of results detailed in the previous chapter when a single-mode cavity reactor was used.

Table 10. Effects of MW irradiation time on AC butane activity and specific energy input using 400 W power in a multimode waveguide reactor cavity. Standard deviation (+/- x.xx) shown was calculated for each result from the corresponding results in Appendix B.

Irradiation time (s)	Mass change (%)	Butane activity (%)	Specific energy input (kJ.g $^{-1}$)
120	15.32 +/- 0.17	18.89 +/- 0.10	4.56 +/- 0.03
180	17.73 +/- 0.08	20.73 +/- 0.19	6.64 +/- 0.12
240	19.77 +/- 0.55	21.01 +/- 0.12	9.67 +/- 0.05
360	22.49 +/- 0.44	22.94 +/- 0.04	13.60 +/- 0.13
Thermal	50.31 +/- 0.95	40.88 +/- 0.92	-

As can be seen from the table, the use of a multimode waveguide cavity decreased the mass loss when comparing analogous results from the single-mode study detailed in the previous chapter. This trend is also seen with the decrease in achieved butane activity. This is likely due

to the decrease in field density having caused a decrease in the moments of incidence in which MWs interact with the ACs inside the quartz reactor. With this, the overall heating rate would likely decrease and level of heating, leading to less sulphurous adsorbate desorption having occurred. Additionally, the visible decrease in elemental sulphur having been deposited in the cold trap, and sulphurous compounds having been taken up in the AC trap, were a confirming indicator that less desorption had taken place.

Although less sulphurous compounds were desorbed during the multimode regeneration experiments, it was clear that less damage was occurring to the overall carbon structure. The preliminary indicator being the reduced mass loss, but also the lack of ash and carbon dust that had been seen after the analogous single-mode regeneration processing.

The specific energy input was marginally higher for samples regenerated using the multimode setup than those regenerated using the single-mode, as shown by Figure 49. However, the butane activity was significantly less for each comparable run, suggesting that the reduced rate and level of heating had reduced the amount of adsorbate desorption. This may be due to the localised overheating having been averted, but that the reduced moments of incidence rate had led to less desorption having taken place. This was attributed to the desorption that had taken place being the desorption of molecules adsorbed via physisorption, and those chemisorbed to the surface with weaker bonds that required less energy to break.

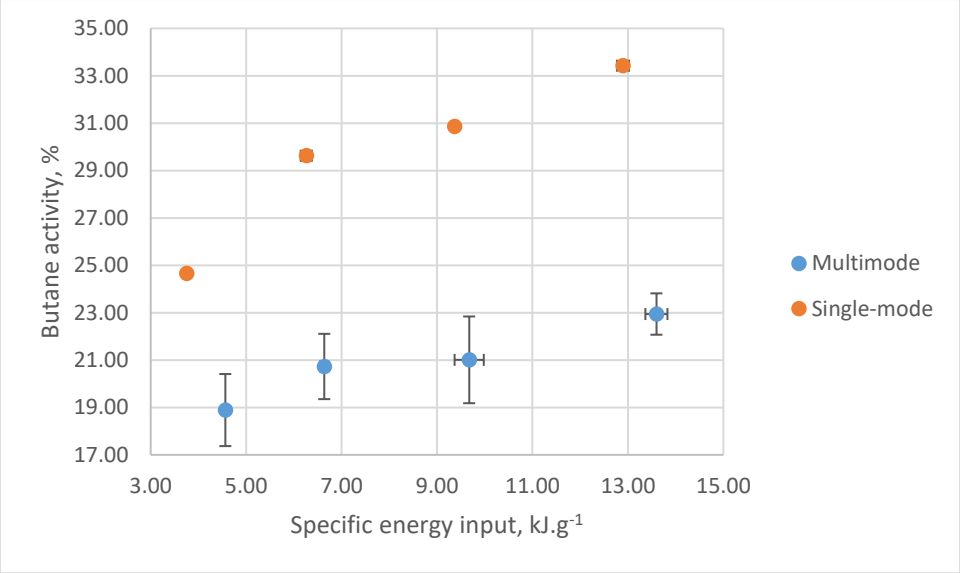


Figure 43. Increase in the degree of achieved butane activity with the specific energy input, with respects to increasing microwave irradiation time, for spent sulphurous activated carbon regenerated using a single-mode waveguide cavity reactor versus using a multimode waveguide cavity.

6.4.2 Preliminary study of microwave power on desorption when using a low-density electromagnetic field

The initial study into the effects of MW power when using a multimode waveguide cavity reactor are shown below in Table 11. The results of the study showed that MW power used for the regeneration process results in an initial increase in mass change, butane activity and specific energy input, echoing the pattern of results detailed in the previous chapter when a single-mode cavity reactor was used.

Table 11. Effects of MW power on AC butane activity and specific energy using a multimode waveguide reactor cavity. Standard deviation (+/- x.xx) shown was calculated for each result from the corresponding results in Appendix B.

Power (W)	Mass change (%)	Butane activity (%)	Specific energy input ($kJ.g^{-1}$)
200	8.69 +/- 0.04	10.53 +/- 0.23	3.42 +/- 0.20
400	17.76 +/- 0.20	20.88 +/- 0.77	6.70 +/- 0.17
600	12.18 +/- 0.46	21.19 +/- 1.19	6.74 +/- 0.08
800	14.38 +/- 0.34	20.18 +/- 0.17	7.02 +/- 0.09
Thermal	50.31 +/- 0.95	40.88 +/- 0.92	-

As with the analogous experiments that utilised a single-mode waveguide cavity reactor, a decrease in irradiation time in incremental steps of 60s (240s for 200 W, 180s for 400 W, 120s for 600 W, 60s for 800 W) was used to reduce the localised overheating that would occur with the increase in MW power. Much like the single-mode runs, this helped to show the trade-off between MW and irradiation time: even at higher powers, a reduced irradiation time led to a reduction in achievable butane activity. And, as with the irradiation time experiments, the use of a multimode cavity served to greatly reduce the mass loss during the experiments as the energy absorbed by the adsorbates was lower than that of the single-mode runs due to the decreased field density. This ran in conjunction with the butane activity achieved being lower than that of the single-mode runs – less energy absorbed resulting in less desorption of adsorbates. This was backed up by the large increase in specific energy input required to achieve much reduced butane activity levels for comparable runs.

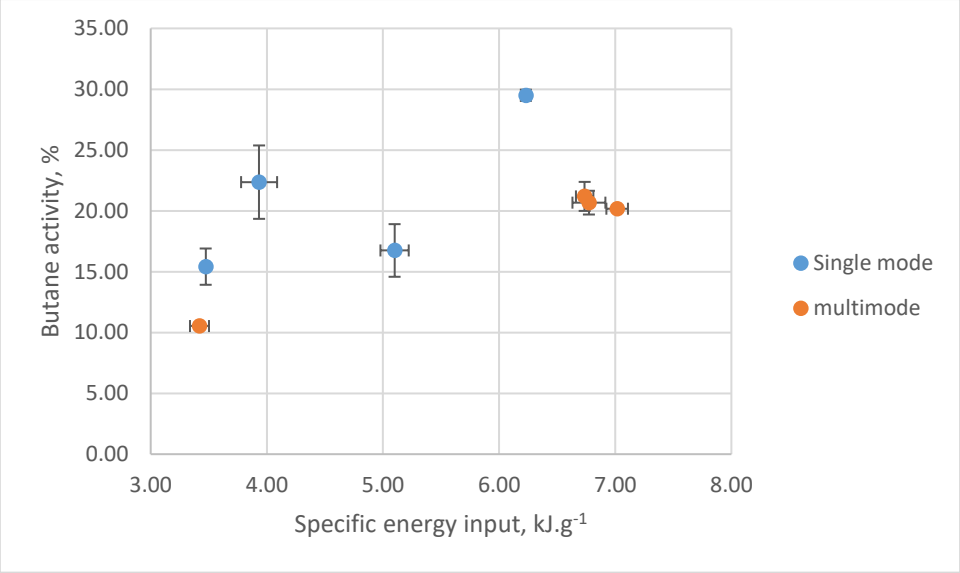


Figure 44. Increase in the degree of achieved butane activity with the specific energy input, with respects to increasing microwave power, for spent sulphurous activated carbon regenerated using a single-mode waveguide cavity reactor versus using a multimode waveguide cavity reactor.

6.4.3 In-depth studies of low-field density effects on microwave regeneration of spent sulphurous activated carbon

Further studies were required into a wider range of MW power and irradiation times to establish whether the implementation of a low-density field could allow for an increase in MW power that would allow for increased butane activity. This helped to understand what a scaled-up MW regeneration process may look like as multimode cavities are far easier to use in industrial settings than single-mode waveguide cavities owing to the size restrictions for the latter.

Microwave power

With this more in-depth study into the effects of MW power on spent sulphurous AC regeneration using a multimode waveguide cavity, each experiment was replicated a total of 3 times to ensure that anomalous results could be identified and that true patterns in the data could be identified. As with previous studies on MW power, this was studied in increments of 200 W, ranging from 200 – 800 W. Previous experiments had shown that a trade-off between MW power and irradiation time factored into butane activity and heating levels, so two sets of irradiation times were studied. The results are shown in Table 12.

Table 12. In-depth study of the effects of MW power on AC butane activity and specific energy input using a multimode waveguide reactor cavity. Standard deviation (+/- x.xx) shown was calculated for each result from the corresponding results in Appendix B.

Power (W)	Time (s)	Mass change (%)	Butane activity (%)	Specific energy input (kJ.g $^{-1}$)
200	120	4.69 +/- 0.05	10.38 +/- 0.03	1.41 +/- 0.08
	240	5.76 +/- 0.13	12.32 +/- 0.11	3.60 +/- 0.10
400	120	17.64 +/- 0.54	19.54 +/- 0.13	4.72 +/- 0.15
	240	22.84 +/- 0.19	21.84 +/- 0.06	9.23 +/- 0.14
600	120	18.21 +/- 0.10	21.16 +/- 0.13	6.22 +/- 0.10
	240	28.21 +/- 0.24	24.03 +/- 0.03	12.62 +/- 0.13
800	120	18.76 +/- 0.21	21.25 +/- 0.09	8.04 +/- 0.04
	240	32.29 +/- 0.09	29.30 +/- 0.08	15.90 +/- 0.05
Thermal		50.31 +/- 0.95	40.88 +/- 0.92	-

As with the previous studies conducted using a single-mode cavity, the increase in MW power did result in an increased mass loss paired with an increase in butane activity. This was to be expected as the increase in MW power output results in an increase in the level of MW energy absorbed by the target – more energy absorbed leads to more kinetic energy being converted into heat energy at a faster rate and thus the level of desorption will increase as that heat energy aids in the breaking of inter- and intramolecular interactions between adsorbate and adsorbent. Too much power (and subsequently too much heating) would result in similar localised overheating effect that had been seen in the previous studies. However, the use of the multimode cavity counteracts this to a degree as the more chaotic way the MWs are dispersed works to reduce the overall heating rate, as previously discussed. And, when comparing the mass losses of the sample to those of samples run in the single-mode at lower powers, the multimode ran samples mass loss is significantly less, giving an initial indicator that less damage may have been done to the carbon structure during the processing of the sample.

Additionally, the increase in butane activity to levels close to that achieved at 400 W using a single-mode cavity were achieved when increasing the power used to 800 W. In terms of a commercial scale unit, more power may be needed for larger samples sizes as the penetration depth would be decreased as the size of the cavity increased – a larger cavity would be required for the kinds of target sizes required for the regeneration output desired by CPL in their daily operations. The butane levels themselves are not at the levels seen with the traditional thermal regeneration (see Section 4.4) but are considerably high when the time of irradiation is considered.

The specific energy input significantly increased each time the power was increased by 200 W. This was not unexpected as the lower density of the magnetic field does mean that energy absorbed by the sample is lesser over a set period when compared to the single-mode experiments. If the design were to be scaled to a commercial level this could present an issue though as the energy cost involved would likely be higher than that of conventional thermal regen over shorter periods as the energy for the lab-scale thermal regen was found to be 1.50 $kJ.g^{-1}$ (+/- 0.23 std). However, when discussing the energy input required it should be noted that the MW regeneration process has been conducted across 120s or 240s here as opposed to the 7200s required for thermal regeneration on a lab scale. In addition, when considering the time taken for the experiments, it was found that the specific energy input required effectively doubles with time. With a larger unit for commercial use likely being much larger than the unit used in these experiments, and penetration depth coming becoming a factor with larger samples sizes, theoretically the energy input required would increase substantially. The MW-based regeneration may be substantially faster than that of thermal regeneration, but it would still require a large energy input which could lead to high financial costs.

Irradiation time

Regarding the in-depth study into the effects of MW irradiation time on spent sulphurous AC regeneration using a multimode waveguide cavity, a range of times were studied at a range of powers to help better solidify the trade-off between MW power and time of exposure. As with the MW power experiments outlined above, each regeneration experiment was performed 3 times to ensure anomalous results could be identified and to establish patterns in the data collected. The results for the extended irradiation studies are shown in Table 13.

Table 13. In-depth study of the effects of MW irradiation time on AC butane activity and specific energy input using 400 W power in a multimode waveguide reactor cavity. Standard deviation (+/- x.xx) shown was calculated for each result from the corresponding results in Appendix B.

Power (W)	Time (s)	Mass change (%)	Butane activity (%)	Specific energy input (kJ.g $^{-1}$)
200	120	8.12 +/- 0.08	10.54 +/- 0.11	2.13 +/- 0.06
	180	9.96 +/- 0.12	11.24 +/- 0.12	3.06 +/- 0.10
	240	8.72 +/- 0.17	12.40 +/- 0.07	3.53 +/- 0.35
	360	10.43 +/- 0.12	13.15 +/- 0.17	5.35+/- 0.26
400	120	15.57 +/- 0.48	18.63 +/- 0.43	4.51 +/- 0.31
	180	17.65 +/- 0.11	20.79 +/- 0.16	6.55 +/- 0.38
	240	19.82 +/- 0.06	21.07 +/- 0.24	7.53 +/- 0.24
	360	22.46+/- 0.21	22.84 +/- 0.08	13.43 +/- 0.32
600	120	16.44 +/- 0.13	21.62 +/- 0.11	7.62 +/- 0.19
	180	20.02 +/- 0.42	22.93 +/- 0.17	10.74 +/- 0.09
	240	22.36 +/- 0.27	29.36 +/- 0.25	14.53 +/- 0.31
	360	27.70 +/- 0.12	32.78 +/- 0.03	24.23 +/- 0.14
800	120	16.44 +/- 0.13	21.62 +/- 0.11	7.62 +/- 0.19
	180	20.02 +/- 0.42	22.93 +/- 0.17	10.74 +/- 0.09
	240	22.36 +/- 0.27	29.36 +/- 0.25	14.53 +/- 0.31
	360	27.70 +/- 0.12	32.78 +/- 0.03	24.23 +/- 0.14
Thermal		50.31 +/- 0.95	40.88 +/- 0.92	-

Echoing the single-mode studies conducted on the effects of MW irradiation time, the increase in time in which the sample was exposed to MWs led to increases in the percentage mass loss, which coincided with an increase in butane activity. Although not all the mass loss can be completely attributed to adsorbate desorption, it acted as an initial indicator of the level of desorption having taken place. In the case of this study, the butane activity did increase as the irradiation time increased for each specific MW power setting. This was to be expected as the increase in irradiation time leads to more moments of incidence in which the

samples are interacted with by the MW being emitted into the waveguide cavity. Additionally, the increase in butane activity after 180s is greater than before it (as shown in Figure 45), indicating that although MWs heat volumetrically, time is required for the sample to reach a temperature at which more desorption can occur. This is due to the heat energy being released from the sulphurous adsorbates being dispersed to such a degree that the heat energy aides/starts the chemical reactions compounds adsorbed via stronger interactions to begin. In other words, the amount of heat energy required for the severing of intermolecular interactions, such as Van der Waals forces in place during physisorption, is less than those required for intramolecular interactions in the form of chemisorbed compounds.

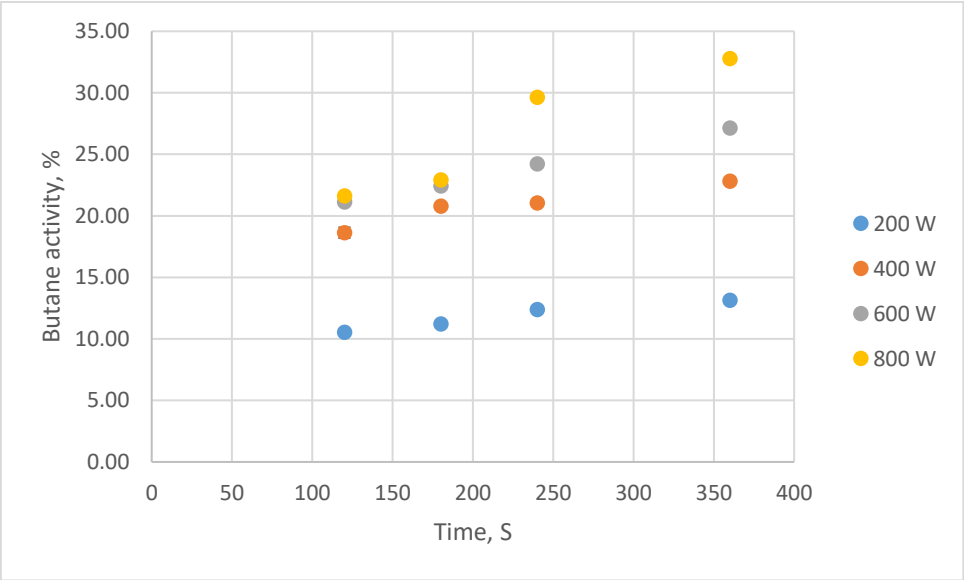


Figure 45. Increase in butane activity with the increase in microwave irradiation time for spent sulphurous activated carbon regenerated using a multimode waveguide cavity reactor.

When comparing the butane activity with the specific energy input for each experiment it became clear that more energy was required to increase the butane activity achieved over time. As was to be expected, the longer the irradiation of the sample, the more energy was absorbed, leading to higher level of butane activity being achieved, as shown in Figure 46. Effectively, if localised overheating could be avoided by reducing the heating rate, as was achieved via the use of a multimode cavity, longer runs at higher MW powers could yield butane activity closer to that seen in the single-mode runs (33.43 % (+/- 0.87 std) at 400 W

over 360s), such as the runs at 800 W for 360s which achieved butane activity of 32.78 % (+/- 0.03 std).

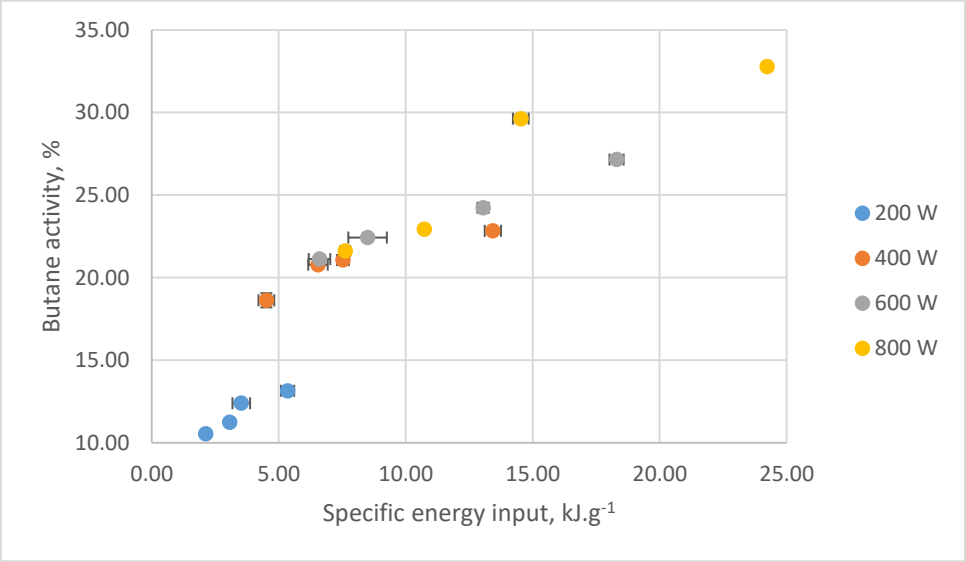


Figure 46. Butane activity versus specific energy input, with respects to increasing irradiation time, using a multimode waveguide cavity reactor.

However, as noted in the previous study regarding the effects of increasing MW power, when increasing the MW irradiation time, the specific energy input increases dramatically. When the project was scaled-up to a commercial-scale unit it would require more time per regeneration as larger target batches would be desired to ensure that daily quotas could be met. Although the time required for MW-based regeneration is much less than that required for conventional thermal regeneration, the amount of energy per run would be considerable. This would need to be factored in, alongside the penetration depth capabilities of a multimode processing cavity, when deciding upon how much AC could be processed in each batch, and how many batch would need to be processed each day.

Sulphur distribution

When examining the sulphur distribution using the electron micropore analyser it showed an altogether different removal of the sulphur than that seen in the experiments conducted using a single-mode waveguide cavity. As previously discussed, most of the sulphurous adsorbates were situated around the edges of the pellet rather than the interior. With the single-mode regeneration experiments conducted in Section 5.3.1, the high concentrations of sulphur around the edges were reduced, and the EPMA scans showed that less sulphur was

situated in the centre of the AC than the surrounding areas (see Figure 32), showing more blue concentration readings than green. This was to be expected as the volumetric and selective nature of MW heating means that all the materials with dielectric properties heat at the same time as it is not limited by thermal diffusion [108] [117]. With the dispersion of the sulphurous compounds across the AC being a far higher concentration on the edges with a lower concentration being situated in the centre of the AC, a similar distribution would be seen when the volumetric effects of the MW heating take place [108].

However, when examining the sulphur distribution of the samples regenerated in a multimode waveguide cavity using the electron micropore analyser it showed an altogether different desorption profile. Rather than decreasing the concentration of sulphur in all areas across the granule, maintaining a higher concentration on the edges and lower concentration in the interior, the concentration distribution became more homogeneous (see Figure 47). Although, there were many black spots symbolising damage to the AC during the regeneration process. This was echoed by the gray value distribution on the intensity profile (Appendix C) which saw sharp drops/peaks to low gray values evenly spread across the AC. The overall butane activity for the multimode runs, at best, reached 32.78 (+/- 0.03 std) for runs at 800 W over 360s, compared to the single-mode runs 33.43 % (+/- 0.87 std). at 400 W over 360s. This would suggest that the decrease in the field density from the use of the multimode reduced the level of sulphur being desorbed from the interior of the AC granule even when using a much higher MW power. Essentially, the exterior of the AC was affected by the MWs far more, resulting in a reduction of sulphur adsorbates on the edges of the AC, but the sulphur adsorbates at the centre of the pellet were likely to be affected to a far lesser degree. The intensity profile confirmed this with the gray value being somewhat flat bar the sharp peaks symbolising the damage/broken off carbon areas.

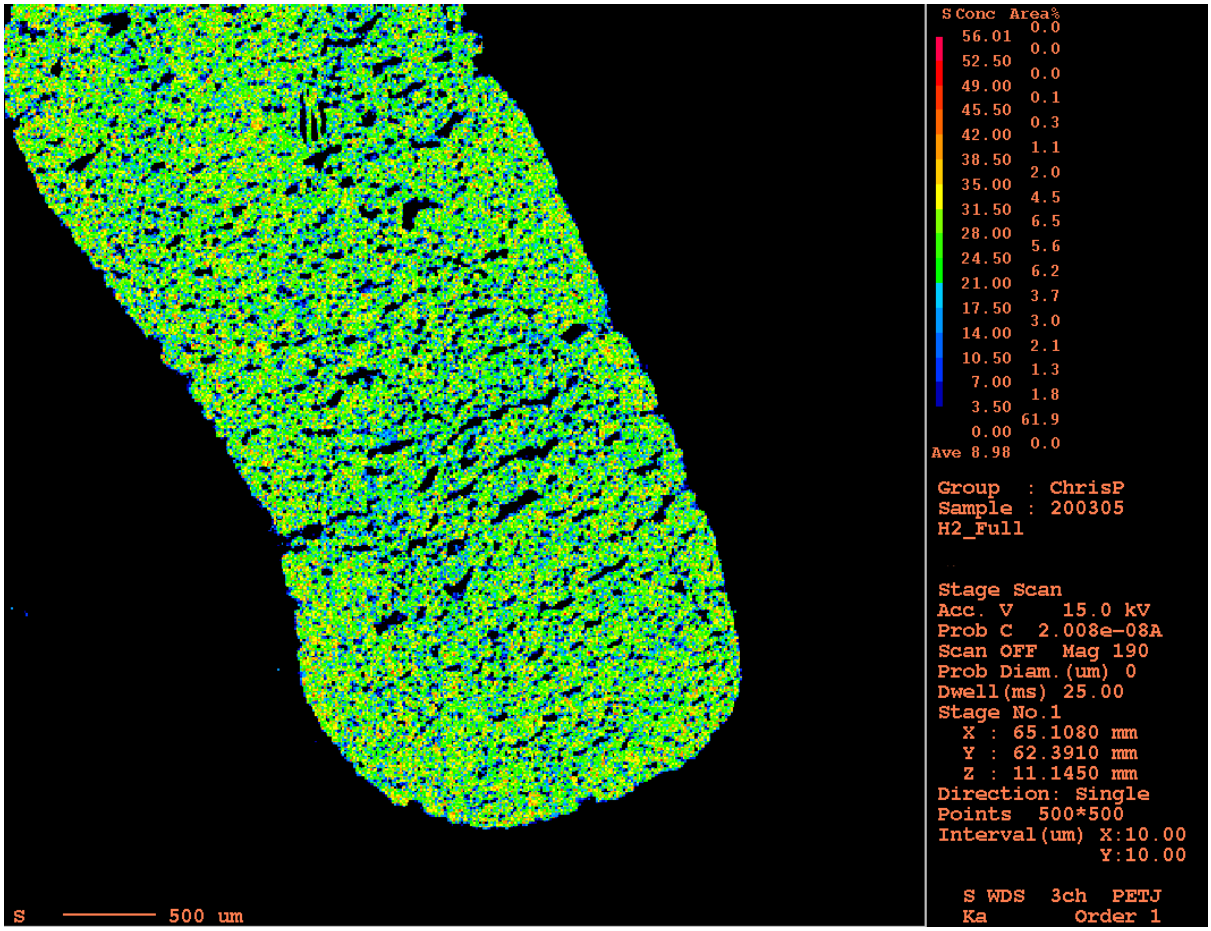


Figure 47. EPMA scan of a cross section of the edge of a of sample regenerated at 800 W over 360s using a multimode waveguide cavity reactor.

Additionally, when comparing the mass changes of those specific single-mode and multimode runs (51.43 % (+/- 2.58 std)) and 27.70 % (+/- 0.12 std)), respectively) the initial impression was that less damage had been caused by using a lower density field even though a higher power was used. This looked likely to be the case when the butane activities for the two samples were relatively similar. However, when examining the carbon structure via the EPMA scans, many black crevasses/fractures had formed, representing destruction of carbon areas. Interestingly these fractures were situated more towards the centre of the AC. The single-mode run also saw a large degree of damage in the interior of the AC. It was theorised that heat energy being dispersed inside the AC was still enough to cause damage if it could not be dispersed out of the pellet quickly enough to reduce the damage. If desorbing materials were not transferring out of the AC at a fast enough rate, then they were causing damage to the interior. With this information, it was discovered that a key factor in damage to the AC was

the rate of desorbed material mass transfer. This would lead to subsequent reduction in butane activity after carbon structure destruction resulted in pore channels, and subsequent surface area available for later adsorption, decreasing.

It should be noted that the level of damage to the exterior of the AC was less than that seen with the single-mode. The decrease in field density having reduced the overheating to an extent, but not having reduced the damage seen to the interior of the AC.

Sulphur chemistry

In terms of the sulphurous compound desorption the multimode MW regeneration process, the chemical changes were like that seen in the single-mode regeneration runs. The adsorbed SO_2, H_2S, and CS_2 were not found on the surface of the AC in XRD scans, having reacted to form the likes of metal sulphate and sulphides representative of the target adsorbates having been reacted with the impregnate molecules before being desorbed. As with the single-mode experiments, S_8 was deposited in the cold trap. Additionally, there was no sign of sulphuric or sulphurous acid having formed. This would have been unlikely given the lack of steam oxidation phase required for MW-based regeneration. The XRD confirmed that the use of a low-density field did not affect the chemical reactions occurring during desorption, but instead effected the level of desorption having occurred.

6.5 Conclusions

A study was carried out to understand the effects the use of a low-density MW field would have on MW-based regeneration of spent sulphurous AC. A systematic approach was followed for the process design which allowed for comparisons between the results from the previous study that documented the use of a single-mode design. This study was also carried out with the explicit goal of not only meeting the criteria for a thermal regeneration technology replacement outlined by the sponsor company, CPL Ltd, but also reducing the damage caused by localised overheating which had been documented in the single-mode waveguide study.

For this study, initial small-scope studies were first carried out that followed the same parameters for studies of the single-mode waveguide cavity in terms the MW powers and irradiation times being studied. Following on from this, extended in-depth studies were carried out with larger ranges of irradiation time and MW power. During these initial studies

it was found that, like the high-density field studies, regeneration was achievable. Sulphurous materials were desorbed from the AC surface, albeit to a lesser degree than during the high field density studies. Adsorptivity (documented in the form of butane activity) was returned to the ACs, again, to a lesser degree than that of the high field density experiments. This being a result of heating rates being slower and penetration depth being less than that seen in the high-density field study.

Utilising extended irradiation times for increased MW power (800 W) yielded similar butane activity to the best of the high-density field experiments. However, this led to a different heating profile in which the desorption mainly occurred on the edges of the AC as opposed to throughout - linked to the reduced penetration depth associated with low field density irradiation. Additionally, the high MW power also led to similar carbon structure damage/loss in the AC interior as that which had been seen with the high field density. It was theorised that this was due to a mass transfer issue in which the desorbed material was moving out of the AC at a rate where the energy being dispersed was damaging the surrounding carbon structure. This is likely a factor in internal carbon structure damage seen in the high field density experiments as well.

Following the findings of this study it was decided that a method would be designed to increase the rate of mass transfer with the goal of reducing internal carbon structural damage.

7. Manipulating mass transfer mechanics via inert gas flow

7.1 Introduction

The results from the previous chapter suggested that part of the reason for the damage towards the interior of the AC during MW regeneration was due to mass transfer rates – desorbed material emitting heat energy causing damage to the overall carbon structure. The aim of this next study was to establish whether that was the case, and, whether mass transfer could be controlled/manipulated. In addition, it was theorised that if material desorbed at lower temperatures earlier in the process it could aid in the removal of those chemisorbed to the surface as there would be a reduced influence of intermolecular forces brought on by physiosorbed material packed on top.

Most of the literature pertaining to the effect of mass transfer involving activated carbon pertains to the adsorption. Research such as that conducted by the likes of Díaz-Blancas *et al* and Eder *et al* discuss how the use of an inert gas flow, like nitrogen or carbon dioxide (in some cases) can aid the rate of movement of adsorbates to active sites, resulting in faster rates of complete adsorption [203] [204]. In converse studies, such as those by Junjie *et al* and Cai *et al*, gas flow systems were used during regeneration to great effect, reducing the damage to the carbon structure during a thermal regeneration process by increasing the rate at which adsorbates desorb and move out of the micropore system of the AC [205] [206]. It is the latter two of these studies which served as a basis for the following work, with the idea being to mimic the introduction of an inert gas flow seen in their experiments.

If the work proposed could aid in the reduction of damage to the interior of the AC, as well as maintain the short irradiation periods, and avoid the production of acidic by products, it would represent the basis for a scaled-up unit that could replace the existing thermal units used by CPL Ltd.

7.2 Background

The rate at which the adsorbates were moving out of the AC following desorption is determined by the MW power input as well as irradiation time, or, in other words, the power density effect. In which the power absorbed per unit volume, Pd (in Wm^{-3}) is calculated thusly [207] [208]:

Equation 15.

$$P_d = \rho C_p \frac{\Delta T}{\Delta t} = 2\pi f \varepsilon_0 \varepsilon'' E^2$$

Where: Pd = Power absorbed per unit volume, Wm^{-3}

ρ = Density of the heated material, kg/cm^3

C_p = Specific heat capacity of the heated material in J/kg ^oC

t = Time, s

ΔT/Δt = Heating rate

f = Frequency of applied field, Hz

ε_0 = Permittivity of free space (8.854×10^{-12} F/m)

ε'' = Effective dielectric loss factor

E = Root mean square of field intensity, $V\ m^{-1}$

Using equation 15, the heating rate of a specific material is determined by the dielectric component as well as the electric field intensity, which is increased by increasing the power input at equivalent energy. This in turn gives rise to a higher internal pressure and vapour velocity, further promoting efficient removal of adsorbates from the carbon surface, creating new adsorption capacity without adversely affecting the mass loss. Moreover, the increasing of vapour velocity and internal pressure serves to perpetuate removal of other adsorbates with stronger chemisorption interactions [209] [210]. This has been the reason for successful desorption with high butane activity being achieved in earlier studies documented in this report.

However, as previously discussed, the flow of desorbing materials is not fast enough to avoid damage to the interior of the AC. This is due to the Biot number (B_i), which reflects the ratio of internal and external transfer resistances of the adsorption/desorption process [204]. The Biot number for porous media such as activated carbon can be defined by the following:

Equation 16.

$$B_I = \frac{k_F r_p C_0}{DpC_0 + Ds\rho_{.p} q_{eq}}$$

Where: B_I = Biot's number

K_F = External mass transfer coefficient

r_p = Adsorbent particle radius, cm

C_o = Adsorbent initial concentration

Dp = Damköhler number

D_s = Surface diffusion coefficient

ρ = Density of the heated material, kg/cm^3

q_{eq} = Equilibrium concentration on adsorbent, g/g

The rate of film diffusion in comparison to the intraparticle diffusion resistance becomes faster as the B_i value increases. And the way in which the B_i value can be increased is to increase the velocity of desorbing material by increasing liquid, or gaseous in this case, media flow within the pores. Thus, introducing an inert gas flow that will not chemically interact with the AC, the desorbing material, or the MWs. Effectively, an inert gas used in this way will help to carry the desorbing material out of the porous network at a faster rate.

7.3 Mass transfer experimental design

The following experimental MW rigs were designed with the intention of increasing the rate of mass transfer of desorbing materials from inside the AC with the desired effect being the reduction of latent emitted heat energy causing damage to the surrounding carbon structure. The design of the of the MW rig that would utilise inerting gas to aid mass transfer. All the variations of the rigs described over the following chapter are like those that have been used before baring changes that allow for the inerting gas to flow directly over the AC samples during the regeneration process. This includes both the high-field density and low-field density waveguide cavity rigs.

Design

The first change to the original design is the quartz tube. Although being the same diameter and length, it was re-designed to include a sintered disc 2 cm from the main base with a porosity grade of 1 (allowing for gas dispersion). The sample would be placed on the sintered disc. The rounded base/bottom included a spout to which a direct nitrogen inlet line could be attached. This allowed for nitrogen to pass directly over the AC samples before, during and

after experimentation. The nitrogen line was passed through a flowmeter with a range of 0-5 $L.min^{-1-}$ (with 1 $L.min^{-1}$ increments). Most experiments were carried out at 2 $L.min^{-1}$, but a second flowmeter was used in place of the first with a range of 0-2 $L.min^{-1}$ (0.25 $L.min^{-1}$ increments) when analysing the effects of flowrate. An initial flowrate of 2 $L.min^{-1}$ was used to not only test how the use of an inert gas could aid regeneration, but also purge the environment. The gas was allowed to flow for 3 minutes before each experiment ran, during the entirety of each experiment, and for 5 minutes afterwards to help purge the system.

As with the original MW design, the quartz tube was then inserted into the waveguide cavity via a 40 cm long metallic tube with an internal diameter of 5.0 cm, acting as a choke for the electromagnetic power. However, the waveguide had a second choke directly below the original that allowed for the spout of the quartz tube to be fitted to the nitrogen line. MW power was supplied by the 2.0 kW generator (~2.45 GhZ) which supplied MWs to the single-mode cavity through WR340 aluminium waveguide together with E-bends as shown in Figure 48. An automatic three-stub tuner was attached to the waveguide for power analysis.

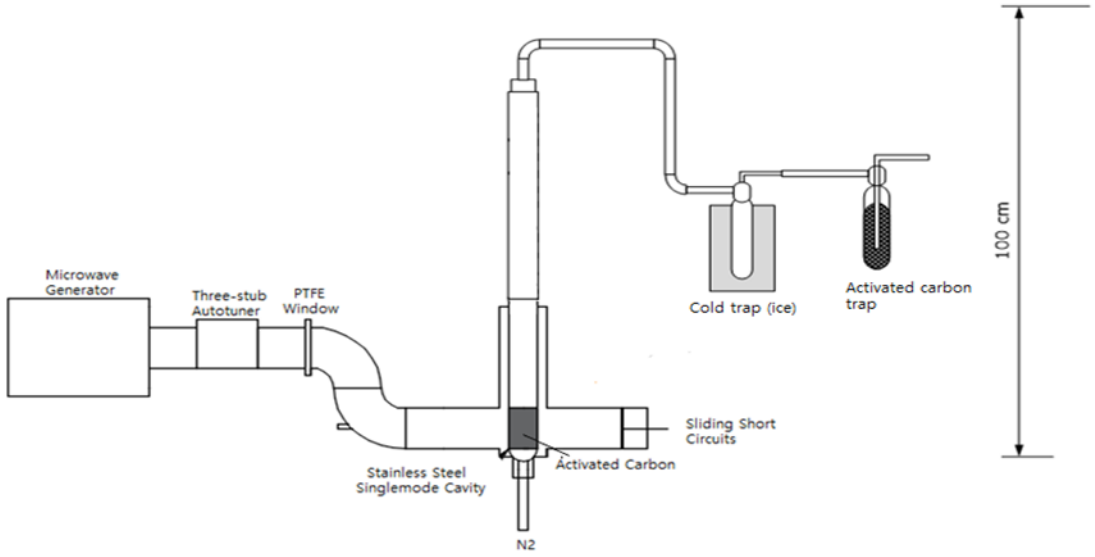


Figure 48. Experimental setup for spent sulphurous AC regeneration in custom-built MW rig utilising inert gas flow directly over the samples to aid in mass transfer of desorbing material.

For experiments involving the multimode waveguide reactor the exact same design was followed in terms of the same quartz reactor being used, the same flowrates, the same MW

powers, and MW irradiation times. This was done to allow for a fair comparison between results between the two waveguide designs.

As with before, for each experimental run a weighted quantity of spent sulphurous AC (10.00g (+/- 0.20 std)) was placed in the reactor (on the sintered disc). A PTFE window was attached to the waveguide to ensure nitrogen and any vapours that accidentally escaped from the reaction vessel would not flow directly into the generator. Off-gases were collected via a cold trap and activated carbon trap, with any excess gases being vented out of the building.

As before, the MW power was set to various levels for testing (50-400 W). after each experiment was completed, the MW was immediately turned off. A stopwatch was used to track irradiation times as well as an automated timer on the MW generator itself.

After each experiment a period of 10 minutes was allowed for sample and reactor cooling to allow for safe manual handling. The samples were then weighed to allow for a quick look at how much sulphurous compounds may have been removed before thorough analysis via methods outlined in Section 3.

7.4 Manipulating mass transfer of sulphurous compounds desorbing from activated carbon – preliminary experiments

The MW regeneration of spent sulphurous AC utilising inert N_2 gas flow directly over the samples were run at varying powers and over various irradiation times. This was done to allow comparison with previous experiments from previous chapter, analysing the difference that the gas flow would make. And, as previously, specific energy input was calculated using calculations 14a and 14b using absorbed energy data recorded from each experimental run to show the efficiency of the method.

7.4.1 High-density field

Microwave power and irradiation time

It was theorised that the use of the inert gas flow would aid the regeneration to such a degree that MW powers previously used (i.e., 400+ W) would be too high and could lead to overheating where adsorbates were still adsorbed to the surface. As such, a much lower power range was used. Each sample run was conducted in triplicate to reduce the impact anomalous results could have on the data patterns. The initial study into the effects of MW

power and irradiation time on the regeneration process whilst using a single-mode waveguide and utilising inert gas (N_2) flowing directly over the AC samples is shown below in Table 14.

Table 14. Preliminary study of the effects of MW power and irradiation time on regeneration when utilising inert gas flow directly over the AC samples in a single-mode waveguide cavity. Standard deviation (+/- x.xx) shown was calculated for each result from the corresponding results in Appendix B.

Power (W)	Time (s)	Mass change (%)	Butane activity (%)	Specific energy input (kJ.g $^{-1}$)
50	360	5.05 +/- 0.07	5.46 +/- 0.03	1.59 +/- 0.18
	480	6.17 +/- 0.24	10.19 +/- 0.08	2.00 +/- 0.10
	960	7.38 +/- 0.27	12.90 +/- 0.12	4.23 +/- 0.13
	1200	7.97 +/- 0.28	13.04 +/- 0.06	5.43 +/- 0.43
100	360	12.45 +/- 0.29	10.68 +/- 0.26	2.81 +/- 0.35
	480	14.34 +/- 0.47	16.49 +/- 0.26	3.56 +/- 0.11
	960	14.01 +/- 0.17	17.21 +/- 0.23	6.12 +/- 0.13
	1200	13.11 +/- 0.30	21.45 +/- 0.30	7.62 +/- 0.24
150	360	18.32 +/- 0.49	20.67 +/- 0.18	3.45 +/- 0.08
	480	20.58 +/- 0.14	27.13 +/- 0.11	4.74 +/- 0.04
	960	21.33 +/- 0.04	31.43 +/- 0.03	9.92 +/- 0.09
	1200	21.77 +/- 0.32	31.65 +/- 0.32	13.94 +/- 0.05
200	360	29.24 +/- 0.12	33.81 +/- 0.16	6.34 +/- 0.05
	480	24.72 +/- 0.07	34.09 +/- 0.14	7.89 +/- 0.39
	960	28.69 +/- 0.09	40.31 +/- 0.13	16.26 +/- 0.20
	1200	28.97 +/- 0.10	40.73 +/- 0.11	19.31 +/- 0.22
Thermal		50.31 +/- 0.95	40.88 +/- 0.92	-

As seen with the experiments that did not involve the use of inert gas flow directly over the samples, increasing the MW power and irradiation time resulted in increased mass change, butane activity and specific energy input. This was not unexpected. However, the extent to which the butane activity increased whilst utilising a relatively low MW power setting (200

W) was incredibly positive in terms of reaching the levels seen in conventional thermal regeneration (40.88 % (+/- 0.92 std)). This increase in butane activity with MW power and irradiation time was paired with a much lower mass change. When comparing samples run without the inert gas flow at 400 W over 360s resulted in 33.43 % (+/- 0.87 std) butane activity and a mass change of 50.31 % (+/- 0.95 std), those run with the inert gas flow at 200 W over 1200s resulted in 40.73 % (+/- 0.11 std) butane activity with a 28.97 % (+/- 0.10 std) mass loss, the difference was stark. This was the first indicator that the use of an inert gas flow had aided in the rate of mass transfer, reducing the damage to the carbon structure caused by localised overheating.

Before this study it had been theorised that an increase in energy absorbance by the target compounds would result in an increased level of desorption. This would be achieved with an increase in MW power. But, because of the localised overheating from the insufficient mass transfer rate, higher MW powers also presented a problem. However, increasing the rate of mass transfer was theorised to help to reduce the overheating effect, thus allowing for higher rates of energy absorbance, and thus allowing for higher returned adsorptivity in the form of higher butane activity levels. When analysing the results from this preliminary study there is a clear trend in the increase in absorbed energy (shown as specific energy input) leading to an increased level of butane activity. In Figure 49, this was confirmed to be the case.

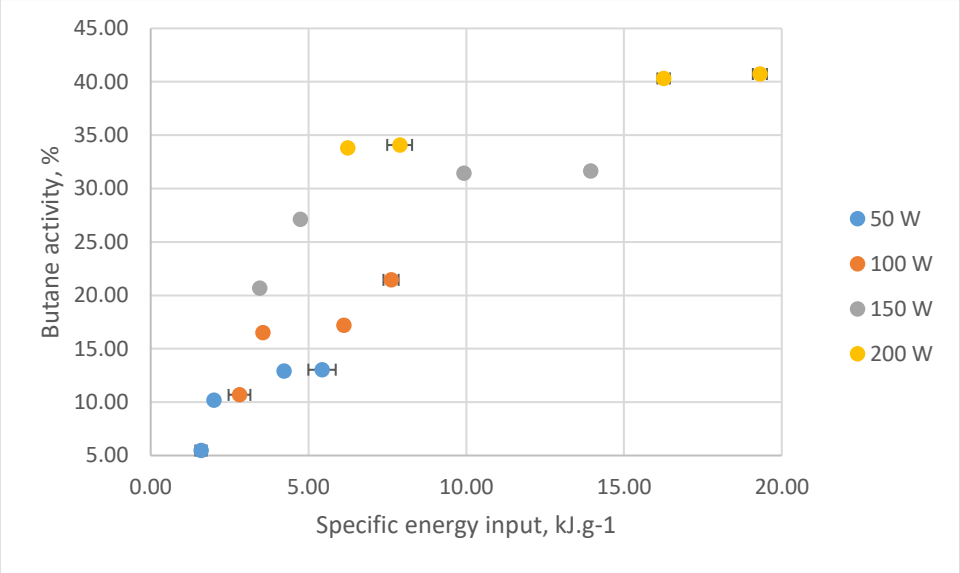


Figure 49. Increase in butane activity with the increase in specific energy input for spent sulphurous activated carbon regenerated using a single-mode waveguide cavity and inert gas flow directly over the samples.

Additionally, this study used longer irradiation times than those that came before as it was believed that this would aid regeneration when using lower MW power settings. The results from Table 14 showed that the increase in time did not increase the mass change too much, but higher butane activities were achieved (as seen in Figure 50). Although the increase in time to obtain the best butane activity results (1200s) was substantial compared to previous MW regeneration studies, it was far less than the time required for thermal regeneration. As such, with times greatly reduced the technology being developed represents a way in which costs can be saved in terms of time and energy required. However, as stated before, the use of a single-mode waveguide cavity would likely be unsuitable for scaling up due to wave dispersion from the MW generator itself.

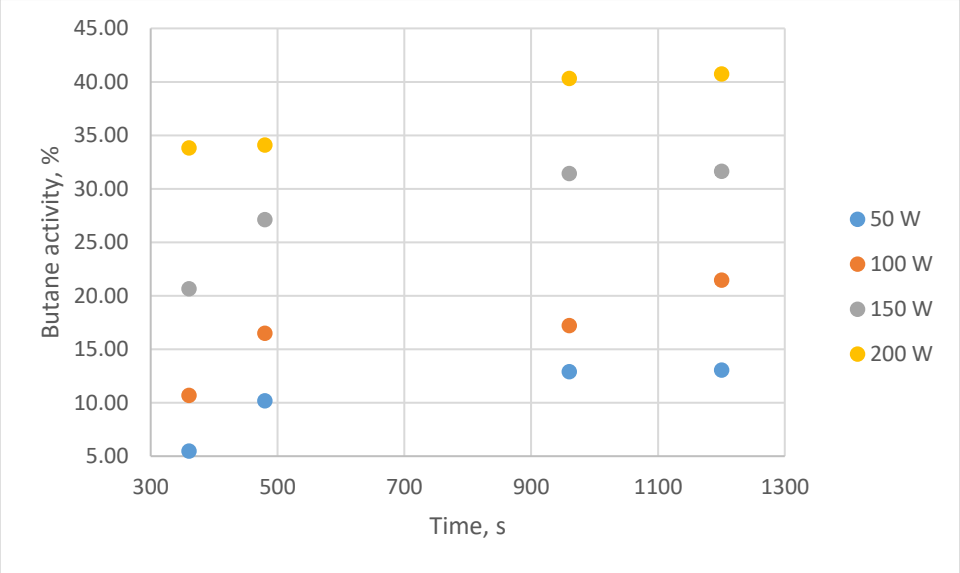


Figure 50. Increase in butane activity with the increase in irradiation time for spent sulphurous activated carbon regenerated using a single-mode waveguide cavity and inert gas flow directly over the samples.

Sulphur distribution

When examining the sulphur distribution using the electron micropore analyser it showed how dramatically the sulphur has been reduced during the regeneration method involving the inert gas flow. Examining the EPMA scan for a run at 200 W over 1200s (Figure 51), the level of sulphur had been reduced to a level not seen before in this research project, with most of the sulphur distribution now being blue, signifying the level of sulphur was now below 10% in most areas, with the average being 7.55%. additionally, the higher levels of sulphur were seen towards the interior of the AC rather than the exterior, suggesting that penetration depth of the MWs was the limiting factor to the sulphur removal. The previously high concentrations of sulphurous compounds from around the edges of the AC were dramatically reduced, often being the lowest areas of concentration. There was, however, signs of damage to the interior in the form of black scars, likely still caused by heat energy being emitted from desorbing materials during the regeneration process, but the level of scarring was much less than that seen before in the MW-based regeneration. This was reflected in the intensity profile (Appendix C) in which the gray value remained relatively flat across the distance measured, apart from occasional sharp peaks to low values, indicating dark/black areas.

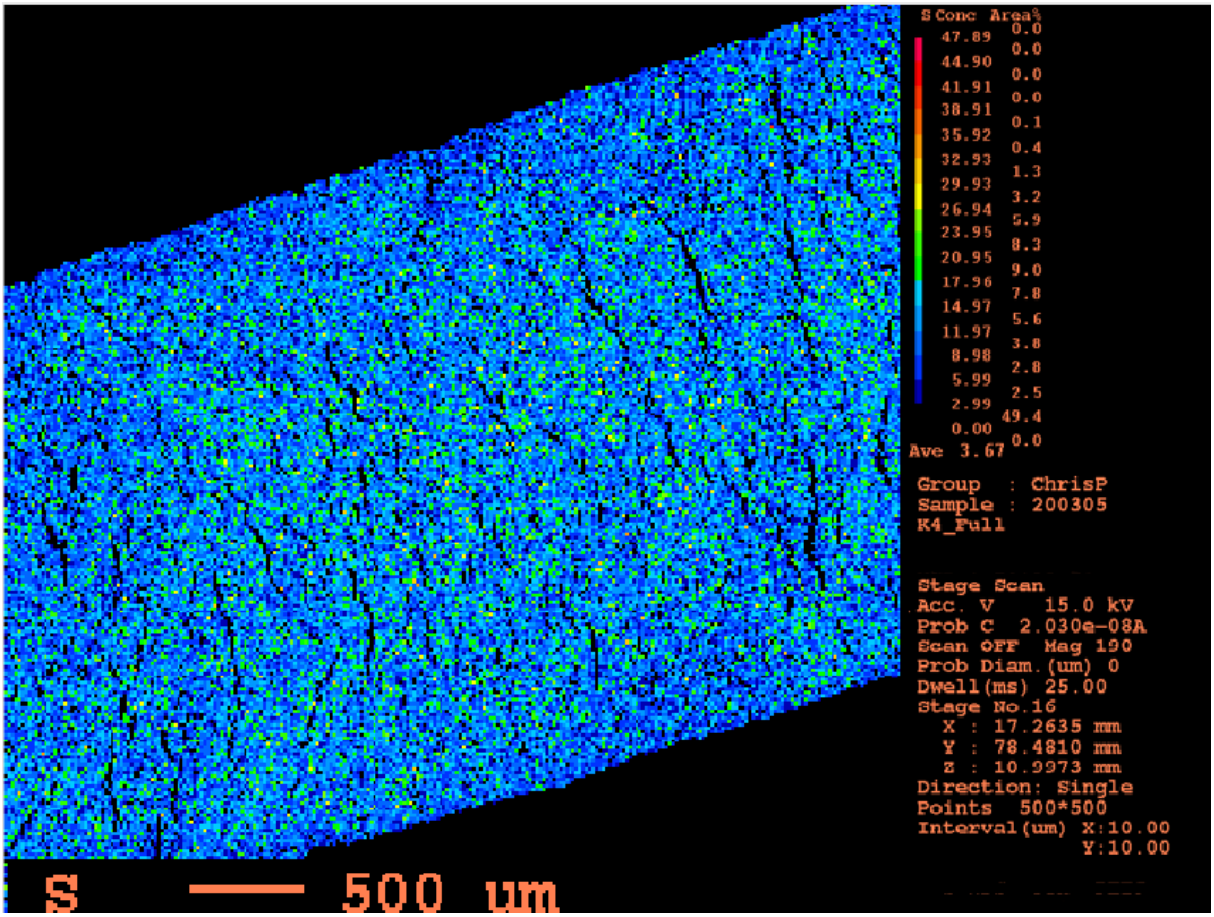


Figure 51. EPMA scan of a cross section of the edge of a of sample regenerated at 200 W over 1200s using a single-mode waveguide cavity reactor and continuous inert gas flow over the sample bed.

Sulphur chemistry

In terms of the sulphurous compound desorption this single-mode regeneration process that utilised the inert gas flow over the samples, the chemical changes were like that seen in the single-mode regeneration runs that did not utilise an inert gas flow. However, being able to reduce the power and thus increase the irradiation time allowed for examination of what compounds were desorbing at what stage of the regeneration. The inert gas flow not only aided mass transfer, it reduced overheating, meaning that the desorption process was effectively being drawn out as it was happening a lower temperature. With this, it was possible to identify which compound desorbed earlier or later in the process. In Figure 52, a run performed at 200 W over 360s, the red peaks indicate sulphur atoms bonded directly to the impregnate in the form of FeS_2, as well as other compounds such as Na_2SO_4. Whereas

Figure 53 (run at 200 W over 960s) shows elemental sulphur and evidence of impregnates which were not bonded to any sulphurous compound, in the form of Na (the blue peak).

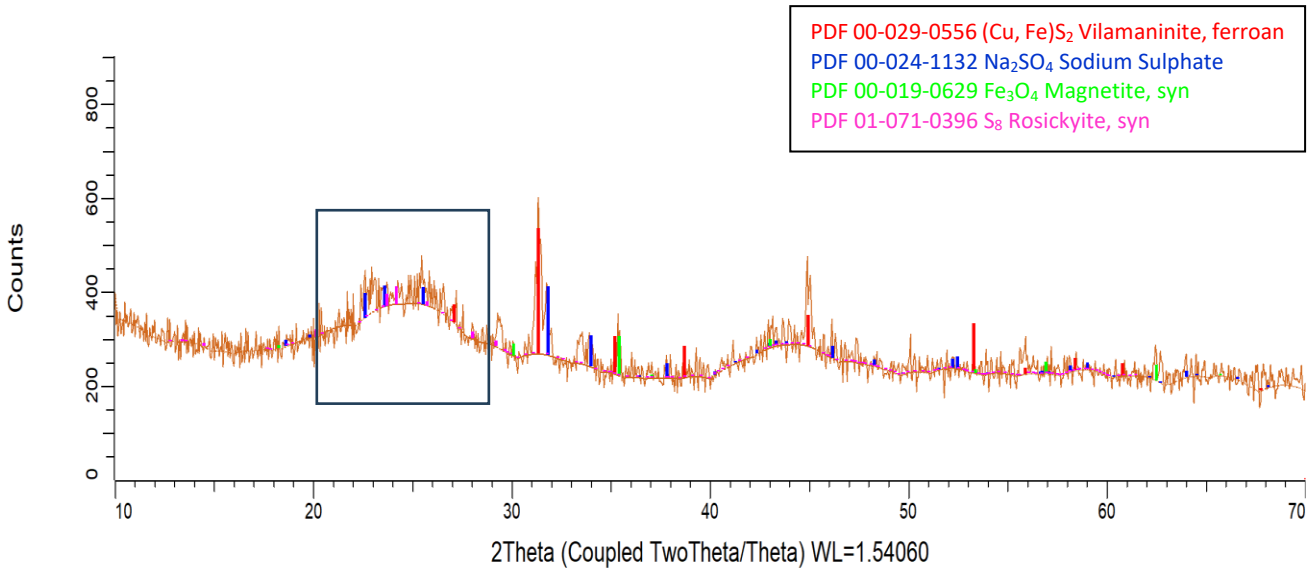


Figure 52. XRD analysis of sample regenerated at 200 W over 360s using a single-mode waveguide cavity and inert gas flow directly over samples.

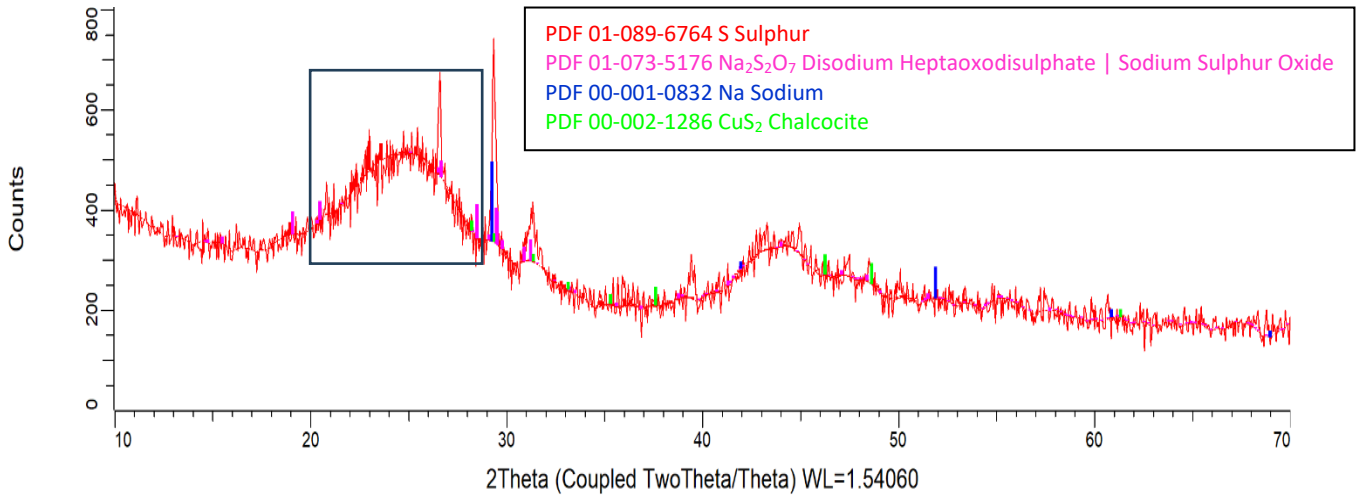


Figure 53. XRD analysis of sample regenerated at 200 W over 960s using a single-mode waveguide cavity and inert gas flow directly over samples.

The XRD analysis also confirmed that, although overheating had been reduced, longer irradiation times did lead to some level of overheating with the emergence and increase in size of an amorphous hump between 20-28 2theta, which signified charring being present on the sample surface.

7.4.2 Low-density field

Microwave power and irradiation time

In previous studies conducted as part of the overall research for this thesis, low-density fields showed potential for reducing the damage to the carbon structure by reducing the heating rate and thus reducing the localised overheating. With this iteration employing the inert gas flow system directly over the samples being regenerated, the aim was to reduce the damage to the interior of the AC whilst maintaining similar levels of butane activity. As with the previous study, each sample parameter was used in triplicate to try to reduce the effects of anomalous results on the dataset. The study into the effects of using a low-density field for MW regeneration with inert gas flow directly over the samples during processing are outlined in Table 15.

In a similar fashion to the studied presented in Section 7.4.1, the increase in MW power and irradiation time mimicked the pattern seen in the analogous study (chapter 6) which did not utilise the inert gas flow directly over the sample, resulting in creases in butane activity, mass change and specific energy increased. Much like the results seen in the 7.4.1 study, the butane activity achieved whilst using relatively low MW power was incredibly positive, reaching 38.72 % (+/- 0.24 std). This was almost as high as that achieved when a single-mode waveguide cavity was used (40.73 % (+/- 0.11 std)). This came with a lower mass change, suggesting that the use of the multimode waveguide cavity may have reduced the damage/loss to the carbon structure during processing. The slightly lower achieved butane activities (compared to those achieved using a single-mode) were attributed to the reduced rate of moments of incidence between the MWs inside the waveguide cavity and the samples themselves. As stated previously, this is due to the distance needed to travel within the cavity being larger with the waveguide cavity reactor being larger. The ability to reach butane activity levels like that of the single-mode cavity were promising even before further analysis had taken place.

Table 15. Preliminary study of the effects of MW power and irradiation time on regeneration when utilising inert gas flow directly over the AC samples in a multimode waveguide cavity. Standard deviation (+/- x.xx) shown was calculated for each result from the corresponding results in Appendix B.

Power (W)	Time (s)	Mass change (%)	Butane activity (%)	Specific energy input (kJ.g $^{-1}$)
50	360	3.64 +/- 0.10	3.97 +/- 0.15	1.19 +/- 0.03
	480	4.40 +/- 0.09	7.32 +/- 0.13	1.45 +/- 0.04
	960	5.35 +/- 0.07	9.59 +/- 0.13	3.08 +/- 0.02
	1200	5.80 +/- 0.09	9.66 +/- 0.07	3.72 +/- 0.08
100	360	10.39 +/- 0.21	8.85 +/- 0.14	2.28 +/- 0.22
	480	11.53 +/- 0.15	13.46 +/- 0.25	2.90 +/- 0.05
	960	11.42 +/- 0.02	14.08 +/- 0.13	5.14 +/- 0.17
	1200	10.49 +/- 0.28	17.62 +/- 0.08	6.18 +/- 0.13
150	360	15.78 +/- 0.20	18.10 +/- 0.11	3.05 +/- 0.07
	480	17.94 +/- 0.11	23.51 +/- 0.10	4.04 +/- 0.14
	960	18.43 +/- 0.11	27.53 +/- 0.33	8.69 +/- 0.11
	1200	18.98 +/- 0.11	27 .59 +/- 0.13	12.34 +/- 0.41
200	360	20.40 +/- 0.15	24.41 +/- 1.70	5.19 +/- 0.08
	480	20.79 +/- 0.14	29.43 +/- 0.13	7.05 +/- 0.12
	960	22.31 +/- 0.13	35.43 +/- 0.44	13.76 +/- 0.08
	1200	24.95 +/- 0.05	38.72 +/- 0.24	17.18 +/- 0.19
Thermal		50.31 +/- 0.95	40.88 +/- 0.92	-

As shown in the previous study with Figure 49, the increase in power absorbed results in the increase in adsorbate desorption - see Figure 54. Essentially, increasing the MW power would increase the level of energy being absorbed by the target materials, allowing for greater level of desorption. Increasing the rate of heat transfer would allow for this to happen without energy being dispersed by the adsorbates which would lead to as much damage happening

to the carbon structure. As with the previous study, the increase in specific energy input leads to an increase in the butane activity achieved.

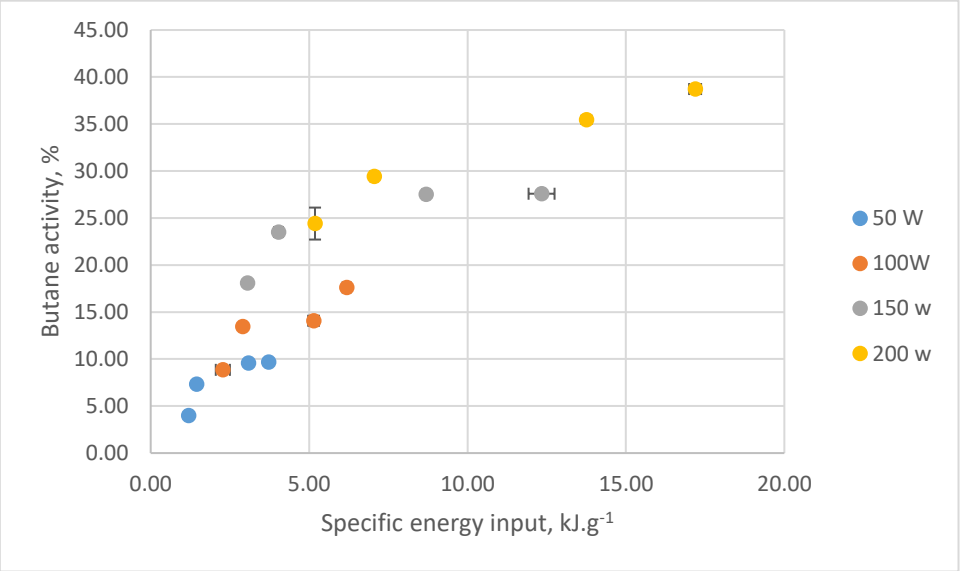


Figure 54. Increase in butane activity with the increase in specific energy input for spent sulphurous activated carbon regenerated using a multimode waveguide cavity and inert gas flow directly over the samples.

Unlike the study conducted using the single-mode waveguide cavity, the effects of increased irradiation time were more apparent after a certain point when using certain MW powers. In Figure 55, those run at 100 W and 200 W saw a significant rise in butane activity when irradiating over 960s, but not for those samples irradiated at 50 or 150 W. This is in contrast with the pattern seen when using a single-mode waveguide cavity. It could symbolise energy inputs at which desorption of specific materials can only be achieved when surpassing 960s. However, it could also signify that triplicating each run was not sufficient and that each run should have been conducted several more times to rule out reduce the impact of anomalous results even further. Further study would be required here.

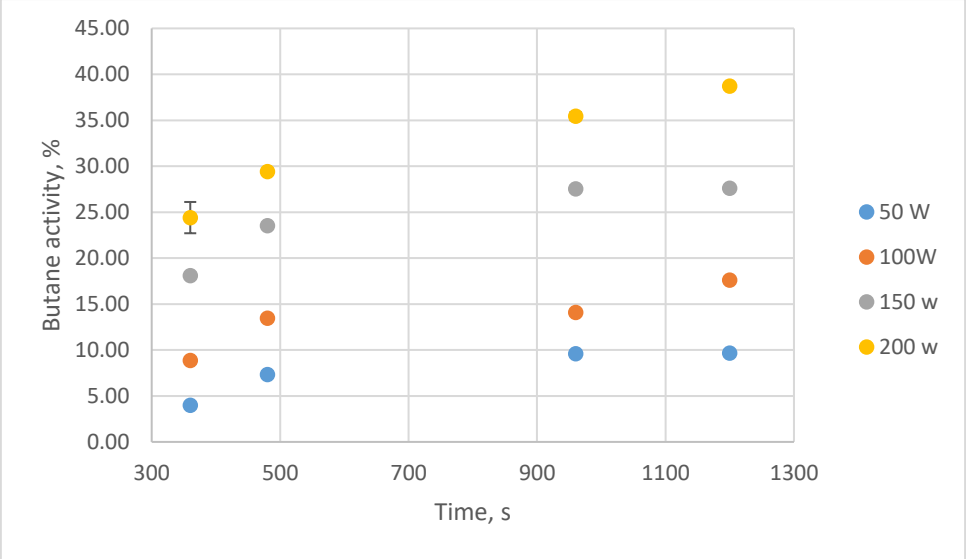


Figure 55. Increase in butane activity with the increase in irradiation time for spent sulphurous activated carbon regenerated using a multimode waveguide cavity and inert gas flow directly over the samples.

Regarding processing time, as with the single-mode generations using inert gas flow directly over the target samples, the butane activity achieved is like that achieved via conventional thermal regeneration in a fraction of the time. With this study having been conducted using a multimode waveguide cavity, a waveguide cavity much more typical of large-scale MW processing, this represents what could be a more realistic starting point for scale-up as a multimode would be far more likely to be used in such large-scale operations.

Sulphur distribution

The sulphur distribution for the samples run at 200 W over 1200s using a multimode waveguide cavity and an inert gas flow directly over the samples was somewhat like that seen in in the previous study when a single-mode waveguide cavity was used. Although the heating rate was slowed via the use of a low-density field, this did not stop all damage to the carbon structure in the interior of the sample, nor did it remove more sulphur compounds in the same area. In fact, the level of scarring appeared to be more so than that using the single-mode waveguide cavity reactor. This is due to the energy input being lower, extending the time required to remove compounds at lower desorption temperatures, allowing heat to emit and resonate for longer periods. The single-mode reactor appears to have removed the samples quickly enough that this kind of damage from slower desorption rates was avoided.

Additionally, as previously discussed, one of the side effects of using a low-density field is the potential reduction in MW penetration depth. This is likely the cause of the concentration being still significant in the centre of the AC. This is also shown by the reduction in energy absorbed which results in a reduced specific energy input, as seen when comparing analogous results from Tables 11 and 12.

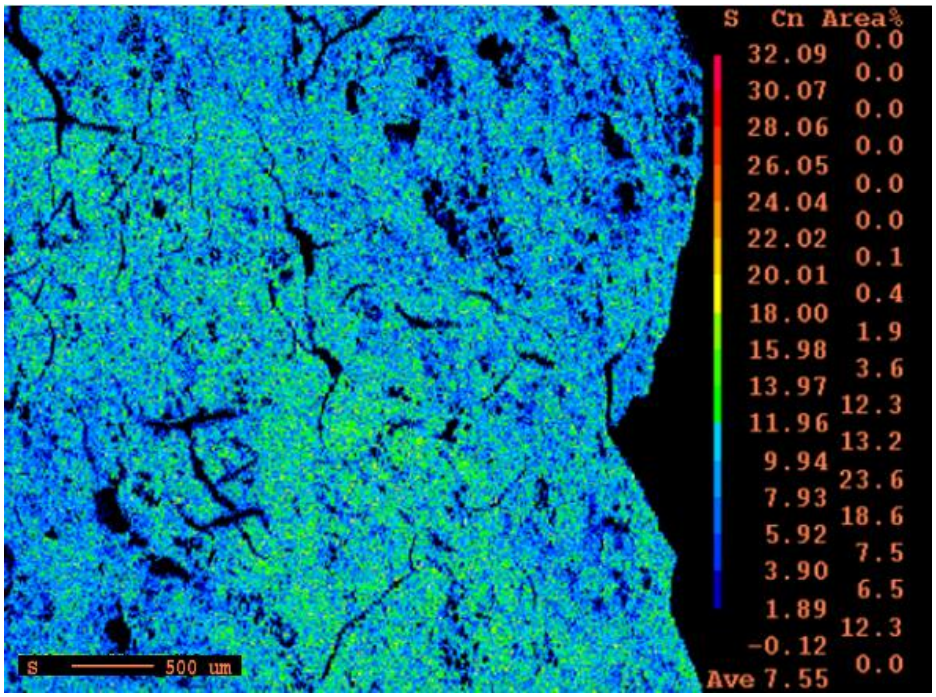


Figure 56. EPMA scan of a cross section of the edge of a of sample regenerated at 200 W over 1200s using a multimode waveguide cavity reactor and continuous inert gas flow over the sample bed.

The corresponding intensity profile (Appendix C) for Figure 56 showed a general reduction in the gray value, with the main trend being 100-140 as opposed to 100-150 seen in the base sample. This was indicative of the reduction in the level of sulphur, as seen in the EPMA scan. However, as had been the case before in previous experiments, there were instances of damage, which was represented by the sharp peaks to low gray values. These lesions are clear in Figure 56, and were a result of the heating method, as already discussed above.

Sulphur chemistry

With the XRD analysis of samples run over 360s and 960s there were differences in the sulphur chemistry, suggesting which compounds were being desorbed at which part of the process. In Figures 57 and 58 the green and brown lines, respectively, signify the presence of Na_2SO_4. However, the intensity of the peaks increases over time, indicating the increased presence of the compound on the surface. This is a result of the Na_2SO_3 (formed from SO_2 adsorbing to the surface via a known impregnate, NaOH) being oxidised into Na_2SO_4 before desorption of SO_2, resulting in NaO_2, Na and Na_2O_2 on the surface, as seen in Figure 58. Additionally, signs of S_8 in the sample run over 960s were not apparent, suggesting that the desorption of the molecule had already happened.

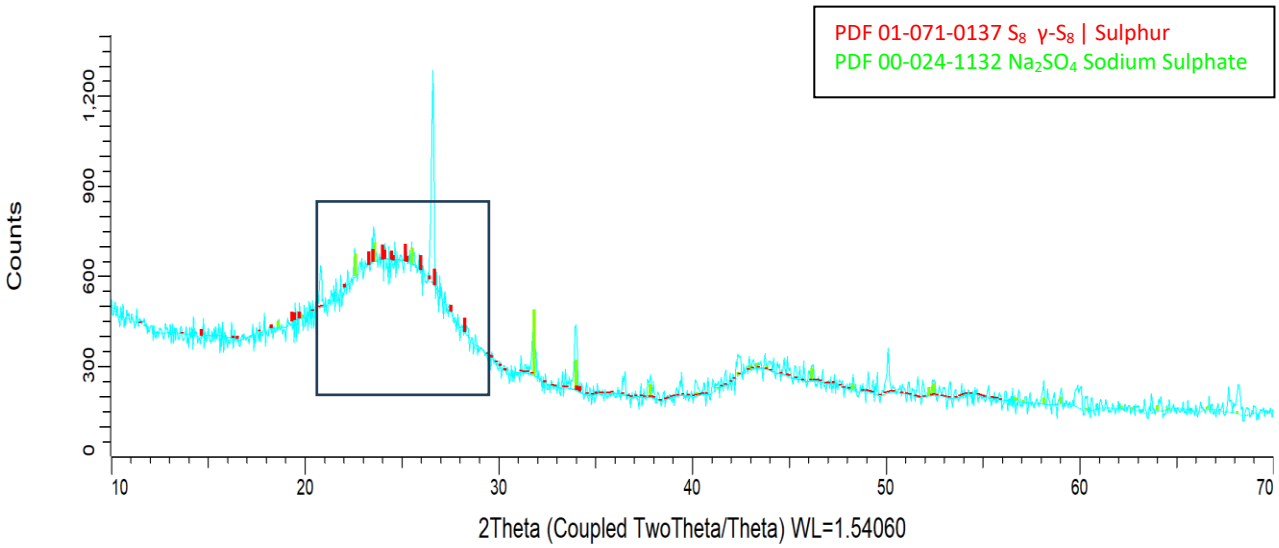


Figure 57. XRD analysis of sample regenerated at 200 W over 360s using a multimode waveguide cavity and inert gas flow directly over samples.

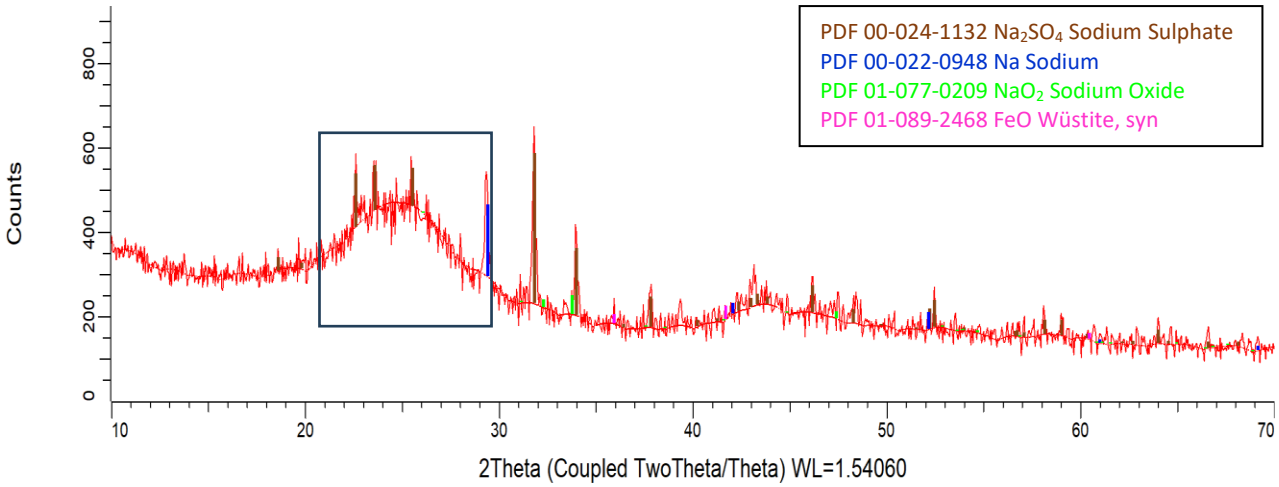


Figure 58. XRD analysis of sample regenerated at 200 W over 960s using a multimode waveguide cavity and inert gas flow directly over samples.

Additionally, as with the single-mode runs, the presence of an amorphous hump between 20-28 2theta shows the signs of charring having occurred where the sample was overheated.

7.5 Manipulating mass transfer of sulphurous compounds desorbing from activated carbon – heated gas flow

Throughout literature concerning mass transfer of particles from one space to another there have been several methods used to aid movement including the use of inert gas and heat. Previously in this chapter, the effects of mass transfer manipulation via inert gas flow through a system have been documented and proved successful in increasing the butane activity of the regenerated sample, as well as reducing the damage to the AC structure from localised overheating. However, there were still issues regarding the damage that can be caused by the heat energy being emitted during the desorption process by adsorbates, and when said desorbed materials exit the porous system. Studies on the Baskakov-Palchonok correlation by the by Leckner *et al* and Ma *et al* document the effects of heating an inert gas flow to aid in the mass transfer effect [213] [214]. In both studies, small compounds physiosorbed to a porous media can be removed at a faster rate when heat energy from a heated gas flow helps to weaken intermolecular interactions, such as Van der Waals, in packed layered scenarios. This is done by first weakening intermolecular forces between the top layer adsorbates and those below, allowing them to desorb, and then progressive layers below can follow suit [214] [215]. When this is applied to a system in which a source of energy is employed for desorption has a heated inert gas/liquid flow over the adsorbent and adsorbate, desorption occurs at a

faster rate [216]. In the case of MWs, the localised energy source is the MWs as they interact only with the target dipolar molecules. A heated gas flow would remove the physiosorbed layer at a faster rate, reducing further the damage caused by heat energy being emitted during the desorption process by the desorbing materials, as well as during the time in which they exit the AC. Essentially, the heating of the inert gas flow would aid in desorption of physiosorbed materials faster than that of the inert gas flow when it not heated.

For this, the inert gas was kept as nitrogen. It would be heated via passing through a coiled copper tube which itself had been heated inside a bath of silicone oil. The temperature of the oil would be taken as representative, albeit not one-to-one, of the gas temperature. The gas was heated for 10 minutes before being allowed to flow through the reactor for 3 minutes before the MW was turned on. The gas flow was continuous, as was the heating of the gas, during the entirety of the process. The oil bath was turned off immediately after the MWs were, but the nitrogen was allowed to flow for a further 5 minutes to allow the system to be purged.

7.5.1 Gas flowrate

When establishing the optimum flowrate for the heated inert gas flow setup a range of flowrates (0.25-2.00 $L.min^{-1}$) were analysed in triplicate. This was done at 200 W, over 180s with the gas temperature being 160 ^{o}C. At lower flowrates the variation between replicated samples was significantly large, with the experiments run at 0.25 $L.min^{-1}$ seeing standard deviation of over 3 for both the mass change and butane activity. As the flowrate was increased the converse was seen, with the standard deviation being significantly lower. This would suggest that lower flowrates may have led to localised overheating and thus damage to the carbon structure which limits the achievable butane activity. Additionally, the variation seen at lower flowrates shows an insufficient control of the processes outcome when gas flow is not used or at a lower rate.

Table 16. Analysis of the effects of flowrate of heated inert gas on butane activity and mass loss from MW regeneration of the spent sulphurous AC. The MW being set to 200W, irradiated over 180s, with the N2 temperature being 160 ^{o}C. Standard deviation (+/- x.xx) shown was calculated for each result from the corresponding results in Appendix B.

N_2 flowrate (L.min^{-1})	Mass change (%)	Butane activity (%)
0.25	22.00 +/- 2.92	31.65 +/- 2.34
0.50	24.93 +/- 2.57	36.50 +/- 3.80
0.75	22.07 +/- 0.73	36.13 +/- 1.28
1.00	23.14 +/- 0.28	36.51 +/- 0.45
2.00	42.50 +/- 0.18	42.50 +/- 0.18

However, the butane activity achieved when using a flowrate at 2.00 L.min^{-1} was 42.50%. This figure provided a reassurance that the technique was going to be important going forward as the runs at this flowrate had already surpassed the butane activity of thermal regeneration at a fraction of the time. When this project was scaled-up, the cost of nitrogen will had to be factored into operational costs, however.

7.5.2 Gas temperature

A study was undertaken to analyse the effect the temperature of the inert gas flow would have one the efficiency or the regeneration process. For this, two irradiation periods were monitored, 360s and 960s. The idea being that increased gas temperature may increase the butane activity and mass change, but as shown in previous studies, it may be marginal or even detrimental to the regeneration after a certain period. To give a wide scope of possible suitable temperatures a range of temperatures between 100-200 ^{o}C was studied. This range was chosen as literature regarding thermal regeneration shows that light volatiles physiosorbed to the surface can be removed in initial heat up phases at low temperatures during heating [15]. Although this process does not mimic the traditional thermal regeneration method, it does emulate the early stages of heating in that a low temperature environment is being introduced by the gas flow which is then followed up by the introduction of a

secondary heating mechanism (MWs in this case). As with other studies, each experiment was performed in triplicate to help eliminate/reduce the impact of anomalous results on the dataset produced. The dataset collected is shown in Table 17.

Table 17. Analysis of impact of inert gas flow temperature on the mass change and butane activity. Experiments run at 200 W MW power, with a N_2 flowrate of 2.00 $L.min^{-1}$. Standard deviation (+/- x.xx) shown was calculated for each result from the corresponding results in Appendix B.

Irradiation time (s)	N_2 temperature (°C)	Mass change (%)	Butane activity (%)
360	100	28.08 +/- 0.13	39.62 +/- 1.53
	120	28.62 +/- 0.53	40.73 +/- 2.20
	140	29.35 +/- 0.20	42.73 +/- 0.34
	160	29.57 +/- 0.46	42.95 +/- 0.92
	180	28.77 +/- 0.19	43.55 +/- 0.23
	200	28.84 +/- 0.62	45.20 +/- 1.15
960	100	29.62 +/- 1.21	46.47 +/- 0.40
	120	29.73 +/- 0.32	45.74 +/- 0.04
	140	30.75 +/- 0.16	46.63 +/- 0.23
	160	30.38 +/- 0.10	47.08 +/- 0.12
	180	29.20 +/- 0.30	47.36 +/- 0.12
	200	30.89 +/- 0.17	47.50 +/- 0.10
Thermal		50.31 +/- 0.95	40.88 +/- 0.92

The overall mass change in the samples did not vary much with an increase in gas flow temperature for both the 360s and 960s studies. The 360s series seeing increase of 0.76 % for the entire dataset, and the 960s series and increase of 1.27 %. There was no linear increase in mass change as temperature increases for either study. There was an increase in the mass change when the irradiation time was increased of around 1.23 %, suggesting, as seen before, that material desorption is dependent on the temperature of the adsorbate and AC – temperature increasing over time as more energy is absorbed.

With regards to the butane activity there was a clear linear progression as the inert gas flow temperature increased (see Figure 59). This followed the findings by Leckner and Ma *et al* in that heated gas flow increased the heat and mass transfer rates of desorbing materials, and increasing the temperature increased the mass and heat transfer rate [214] [215]. Although, it should be said that the increase of butane activity began to level off after 160 °C for both irradiation time datasets. Considering the next stage of this research following the completion of the EngD would been to scale-up and thus factor in operational costs, a costs benefits analysis would have to be conducted. This would establish whether heating the gas to a higher temperature, which would incur higher financial costs associated with the increased energy requirement, would be beneficial for what is a fractional gain in butane activity after this point.

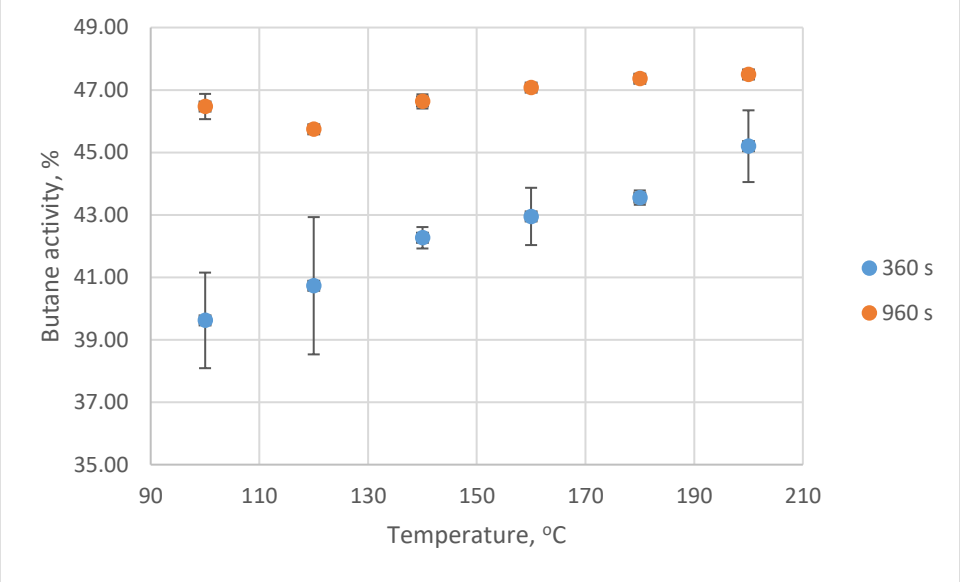


Figure 59. Effect of increasing inert gas flow temperature on the butane activity achieved during MW regeneration. MW power set to 200 W, with a N_2 flowrate of 2 L.min^{-1}.

Finally, it should be noted that the butane activity achieved for the samples run across the range inert gas flow temperatures was much higher than that seen in both conventional thermal regeneration methods and in any of the previous studies conducted as part of this research project – being at least 7% higher than both respectively. This was only improved when an increased irradiation time was used employed. Further study into the true effects of irradiation time are shown later in this chapter.

7.5.3 Microwave power

This study focused on the effects of MW power in the experiments involving heated inert gas flowing directly over the sample during the regeneration process. With this a range of powers between 200 – 800 W were studied at two set irradiation times, 120s and 360s. This power range was chosen over the use of lower power ranges as the study on the effects of power when using an ambient temperature inert gas flow showed 200 W to have been the optimum power setting, and previous studies had shown that increasing power beyond that may yield an even greater butane activity. During each experiment the gas was kept at a constant flowrate of 2 $L.min^{-1}$ with a temperature of 160 ^{o}C. As with previous, each experiment was replicated in triplicate to reduce/eliminate anomalous results from the dataset.

In Table 18, the resulting mass changes, butane activities and specific energy inputs are documented for the MW powers studied. The table shows that mass change increases linearly for runs at corresponding irradiation times as the MW power is increased. This trend is not dissimilar to that seen in previous studies when analysing mass changes of the samples regenerated. However, the mass change reaches levels seen in the experiments conducted without the inert gas flow directly over the samples. Pairing this with the fact that the increase in power sees an initial increase in the butane activity before decreasing to lower levels - the samples run at 800 W recorded average butane activities lower than that of the samples regenerated at 200 W whilst the mass change increased by over 10% - suggested that damage to, and subsequent loss of, carbon structure had occurred. This was not altogether surprising as previous studies in this project had shown that higher MW power resulted in increased heating rates, or increased levels of localised overheating. Although the technique yielded promising results in terms of reach new heights of butane activity, it also reflected that MW power was as much a limiting factor as it had been seen to be in previous studies.

Table 18. Effects of MW power on mass change, butane activity, and specific energy input when utilising heated inert gas flow. The gas flowrate was at 2 L.min^{-1} and the gas temperature was at 160 ^{o}C. Standard deviation (+/- x.xx) shown was calculated for each result from the corresponding results in Appendix B.

Power (W)	Time (s)	Mass change (%)	Butane activity (%)	Specific energy input (kJ.g $^{-1}$)
200	120	28.32 +/- 0.47	40.57 +/- 0.35	2.30 +/- 0.06
	360	30.27 +/- 0.48	43.55 +/- 0.38	6.68 +/- 0.08
400	120	29.14 +/- 0.52	42.72 +/- 0.16	5.50 +/- 0.05
	360	30.69 +/- 0.38	45.52 +/- 0.48	14.60 +/- 0.34
600	120	32.79 +/- 0.29	42.19 +/- 0.84	7.77 +/- 0.09
	360	33.43 +/- 0.77	45.39 +/- 0.63	18.13 +/- 0.17
800	120	38.32 +/- 0.78	41.26 +/- 0.11	9.41 +/- 0.06
	360	40.44 +/- 0.23	40.27 +/- 0.01	22.75 +/- 0.12
Thermal		50.31 +/- 0.95	40.88 +/- 0.92	-

When examining the specific energy input there was a clear trend showing an increase as the MW power increased. Again, this was not unexpected as this had been seen before with extended examinations of MW power in previous studies in this project. However, the rate of increase in specific energy input was much higher than that seen in the studies involving the effects of using a cold inert gas flow were employed (see Tables 14 and 15). Again, this was caused by an increased heating rate provided by the increase in MW power – the increase in MW power caused an increase in energy absorbed by target molecules at a faster rate. This energy would then be dispersed as heat energy during desorption and during the mass transfer itself, causing damage and loss of the carbon structure. The increased specific energy input levels paired with the decreasing butane activity, and increasing mass change, as MW power was increased were indictive of this.

Additionally, although a more expanded study into the effects of irradiation time follows on from this study, there were clear signs that as it increased, the butane activity increased (up until a point). Those samples regenerated at 600 W represented the incidents at which

localised overheating was starting to increase and carbon structural loss was occurring. With those at 400 W it is likely that this would have occurred with longer irradiation times as the absorbed energy beginning to increase dramatically when as irradiation time increased. As such, the next study following on from this, the study regarding an in-depth analysis on irradiation time was set to be studied at 200 W.

7.5.4 Irradiation time

The following study analysed the effects of irradiation time during the MW regeneration process in which the inert gas flowing directly over the samples throughout was heated. As has previously been discussed in this chapter, there was a decline in performance when using MW over 400 W for extended periods and, and it was suspected the same decline in achievable butane activity would be seen if experiments were conducted for longer periods at 400 W. As such, the following experiments were all carried out with the MW power being set at a continuous 200 W. During all the experiments the inert gas flow was kept continuous at 2 $L.min^{-1}$ at a temperature of 160 ^{o}C. As previous, each experiment was replicated in triplicate to reduce/eliminate anomalous results from impacting the dataset to a distinct degree.

Table 16 shows the effects of prolonged irradiation time and how it affects the mass change, butane activity, and specific energy input. Trends that had been seen before in previous studies regarding increasing irradiation time leading to an increase in increases in mass change, butane activity and specific energy input were present. The increase in mass change over time paired with the increase in butane activity signified the desorption happening in stages – as the material heats up over time in conjunction with prolonged exposure to MWs, desorption of different materials occurs. In other words, certain materials desorb when they have absorbed specific amounts of energy from the MW interactions. During the desorption process the energy absorbed is transferred to the surrounding as heat energy, propagating other dipolar materials to reach a level of energy absorbed at which they too can desorb. The inert gas flow helps to remove these desorbing materials before they can transfer enough energy in the form of heat that damages/destroys the surrounding carbon structure. This, in turn, gives rise to higher internal pressure within the pore, which, when paired with the inert gas flow, increases the vapour velocity to further promote removal of adsorbates from the surface. In addition, as previously stated in Section 7.5.2, the heated gas also helps to remove

adsorbates physiosorbed to the surface and in packed layers. Essentially, the mechanisms feed into, and aid one another.

Table 19. Effects of irradiation time on mass change, butane activity, and specific energy input when utilising heated inert gas flow. The gas flowrate was at 2 L.min^{-1} and the gas temperature was at 160 ^{o}C. Microwave power was kept constant at 200 W. Standard deviation (+/- x.xx) shown was calculated for each result from the corresponding results in Appendix B.

Time (s)	Mass change (%)	Butane activity (%)	Specific energy input (kJ.g $^{-1}$)
30	9.10 +/- 3.65	12.45 +/- 1.28	0.53 +/- 0.05
60	13.96 +/- 0.89	23.50 +/- 2.90	1.14 +/- 0.16
90	18.36 +/- 2.37	31.64 +/- 2.41	1.56 +/- 0.09
120	24.62 +/- 0.39	41.92 +/- 1.46	2.10 +/- 0.18
360	29.38 +/- 0.60	43.01 +/- 0.71	6.23 +/- 0.21
960	30.35 +/- 1.26	47.06 +/- 1.71	16.01 +/- 0.21
1200	32.67 +/- 0.61	48.34 +/- 1.20	20.30 +/- 0.28
Thermal	50.31 +/- 0.95	40.88 +/- 0.92	-

When comparing the runs with ambient temperature for the inert gas flowing over the samples during regeneration, and those running the inert gas flow at 160 ^{o}C (as show in Figure 60), that were both run for the exact same irradiation times, the specific energy input is roughly similar, yet the heating of the gas has led to a direct increase in butane activity. This comparison helped to confirm the approach modified from Leckner and Ma *et al*'s approaches regarding the effects heating an inert gas flow through a system and how it aids with desorption of adsorbates directly [213] [214]. Additionally, when comparing the mass changes for the analogous results, the mass changes were marginally higher even though the butane activities had increased dramatically. This would suggest that the increased mass change was due to adsorbate desorption as opposed to damage to the overall carbon structure.

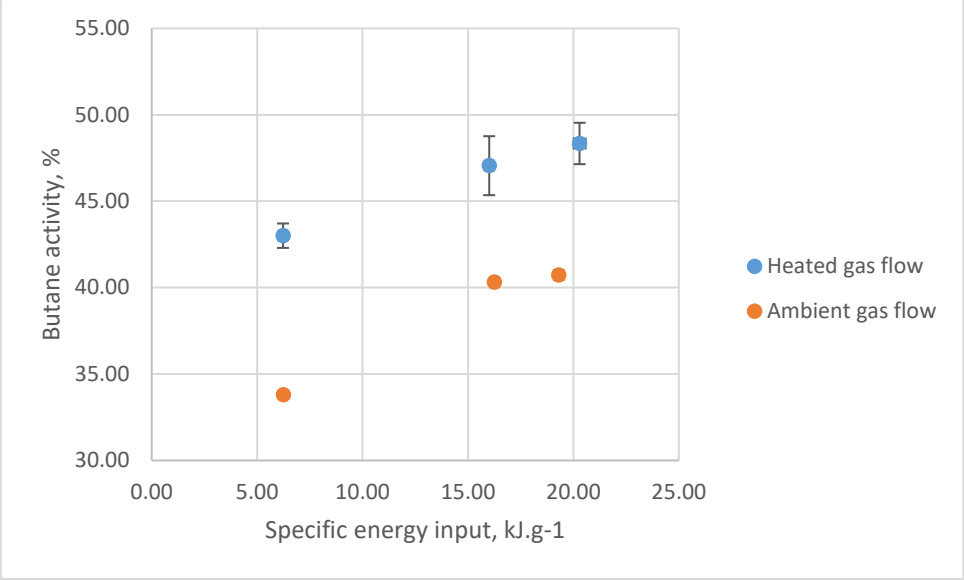


Figure 60. Comparison of butane activity – specific energy input relationship when utilising inert gas flow at 160 ^{O}C as opposed ambient temperature. MW set to 200 W, with the N_2 flowrate at 2.0 $L.min^{-1}$.

The results from this study were seen to be extremely positive in that the butane activity achieved resulted in the highest level seen in any if of the studies recorded during this research project, 48.34 % (+/- 1.20 std) . This level of butane activity is almost 8 % higher than that seen in the thermal regeneration experiments performed as standard to which the MW research could be set against. Additionally, when comparing this result to thermal regeneration, the mass change was reduced dramatically (from 50.31 % (+/- 0.95 std) to 32.67 % (+/- 0.61 std)), signifying that the return of adsorptivity via MW regeneration had not caused significant damage/loss to the overall carbon structure.

7.5.5 Effects on sulphur chemistry and distribution

Sulphurous compound distribution

The EPMA analysis for the regeneration experiments involving the use of heated inert gas flow directly over the samples during the regeneration process showed the distribution of sulphurous compounds across the AC, and how the concentrations of said sulphurous compounds had been greatly decreased. This is shown in Figure 61 – the EPMA scan of a sample regenerated over 960s at 200 W with a continuous N_2 flow of 2.00 L.min^{-1}at 160^{o}C.

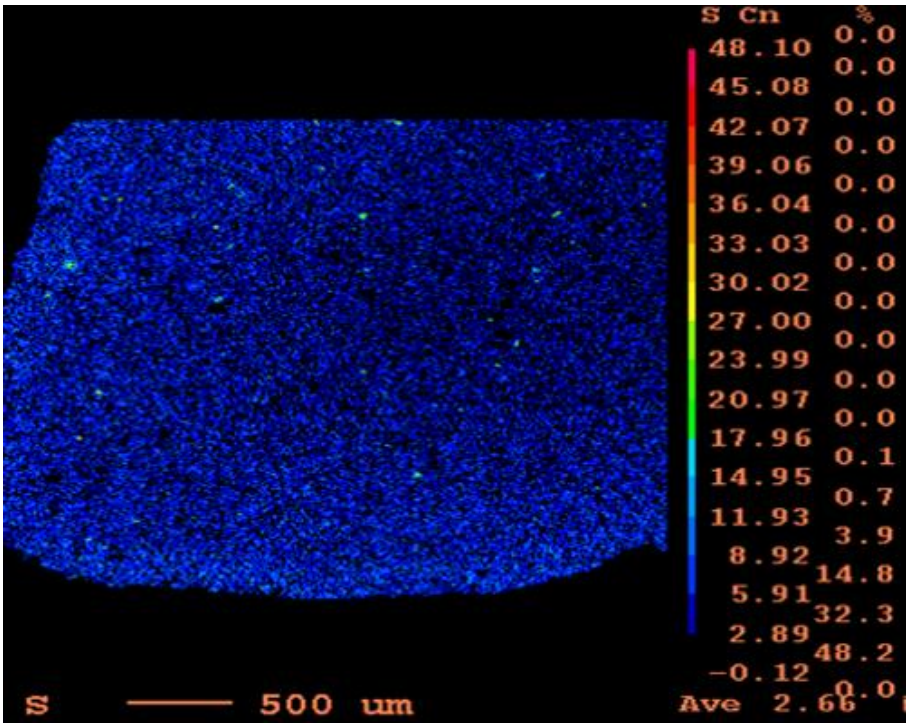


Figure 61. EPMA scan of a cross section of activated regenerated at 200 W over 960s using a single-mode waveguide cavity reactor that utilised inert gas flow (N_2 at 2.00 L.min^{-1}, 160 ^{0}C) directly over the sample.

Unlike previous scans of MW regeneration experiments there was no sign of the distinctly higher concentrations of sulphurous compounds in the interior of the AC, instead it was the exterior that showed a slight increase in concentration – a slightly lighter shade of blue on the scan. Moreover, the damage seen in all pervious regeneration experiments (low- or high-density MW field, or thermal) was not replicated here. This showed that the heating of the inert gas had not only aided the mass transfer of the desorbing materials, but it had also aided in the heat transfer during the process. With this the heat energy being emitted during the

desorption process by the sulphurous compounds desorbing, and by those having already been desorbed that are moving out of the AC, was not overly affecting the carbon structure. The heated gas flow having effectively sped up the rate at which physiosorbed materials were desorbed before they could be overheated via MW interactions that would propagate overheating in localised areas. This in turn then creating increased vapour pressure inside the pore (aided by the flow of the gas), which only served to propagate further desorption.

The intensity profile of Figure 61 (Appendix C) showed a dramatic reduction in the gray value to reflect the reduced sulphur concentration, with all but three peaks being below 100. Unlike previous experiments, these low gray values were clearly not due to damage in the carbon structure. Thus, confirming the success found in the technique.

The reduced/lack of damage to the carbon structure aided the increase return in adsorptivity in the form of a butane activity much higher than even that seen in thermal regeneration (as shown in by the results in Table 16). And, unlike the EPMA scan of thermal regeneration (Figure 30), the edges appear to have been subject to less fraying. This occurring with the exterior edges having been the areas of highest concentration pre-regeneration, and still slightly higher concentrations post-regeneration, suggests that the MW heated the sample volumetrically. Essentially, the sulphurous contingent of the spent AC was heated evenly and at the same rate rather than being subject to thermal diffusion. Thus, the desorption of each specific species occurred at the same rate across the AC. With this and an efficient removal mechanism in the form of the heated inert gas flow, the localised overheating was reduced/eliminated.

It should be noted however that the scans did show small pockets of sulphurous compounds still being present (small green/yellow areas). It is likely that these are sulphurous compounds that would require more energy, or higher temperatures to remove. This is not something that was seen in thermal regeneration. But, the increased level of achievable butane activity, and reduced damage to the carbon structure makes up for this. Additionally, as the thermal regeneration EPMA scans show, the removal of all adsorbed material is all but impossible.

Sulphur chemistry

When analysing the XRD diffractograms of samples run in the single-mode MW waveguide cavity that utilised a heated (160 ^{o}C) inert gas flow directly over the samples during the

regeneration process, the results were somewhat like those of the samples run using ambient temperature inert gas flow directly over the samples. However, at the lower irradiation times (360s) the heated gas samples showed intense peaks for Metal (II) sulphides (shown by the large pink peaks in Figure 62), suggesting that the adsorption reaction in which metal hydroxide impregnates react with adsorbed hydrogen sulphide ions to form the metal sulphide is occurring around this time in the process. This process was not happening to this degree as early into the process with the ambient gas flow samples, with the corresponding peaks being much less intense. Following this, the sulphurous compounds such as metal sulphates and elemental sulphur molecules were present as the irradiation time progressed, as was the case with the samples that had been regenerated using cold inert gas flow directly over the samples (see Figures 63 and 64). These peaks were less intense, suggesting that the concentrations of these compounds may be lower. Essentially, the XRD analysis appeared to confirm that certain desorption reactions were taking place faster, at lower levels of energy absorbed, thus less heat energy was being exerted by the desorbing materials during the desorbing materials which resulted in the destruction/damage to the overall carbon structure. It is this that allowed for a higher butane activity to be achieved as there was more of the carbon structure remaining intact that could be regenerated and contribute to the overall adsorptivity ability.

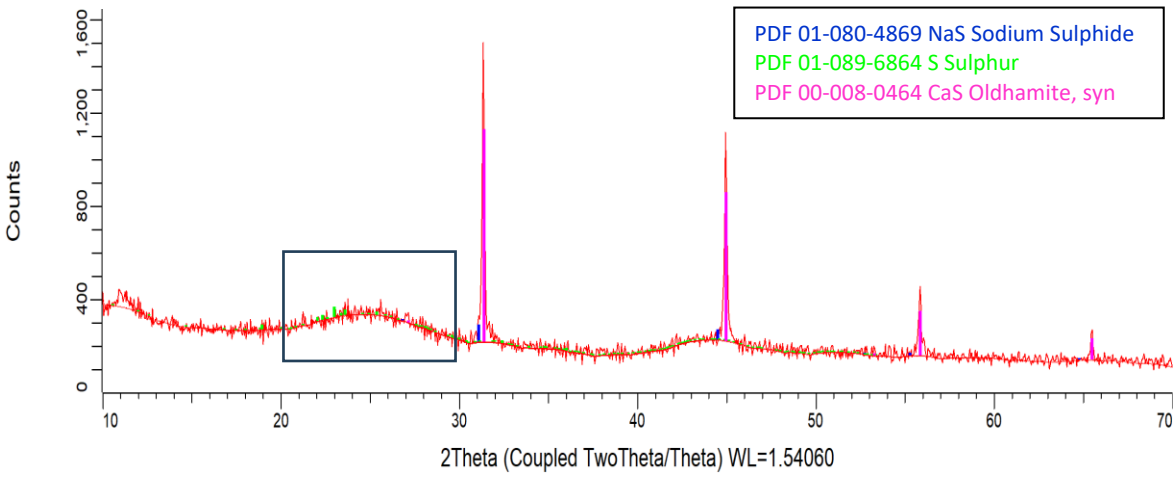


Figure 62. XRD analysis of sample regenerated at 200 W over 360s using a single-mode waveguide cavity and heated inert gas flow directly over samples. The gas flowrate was 2.00 L.min^{-1}, at 160 .C.

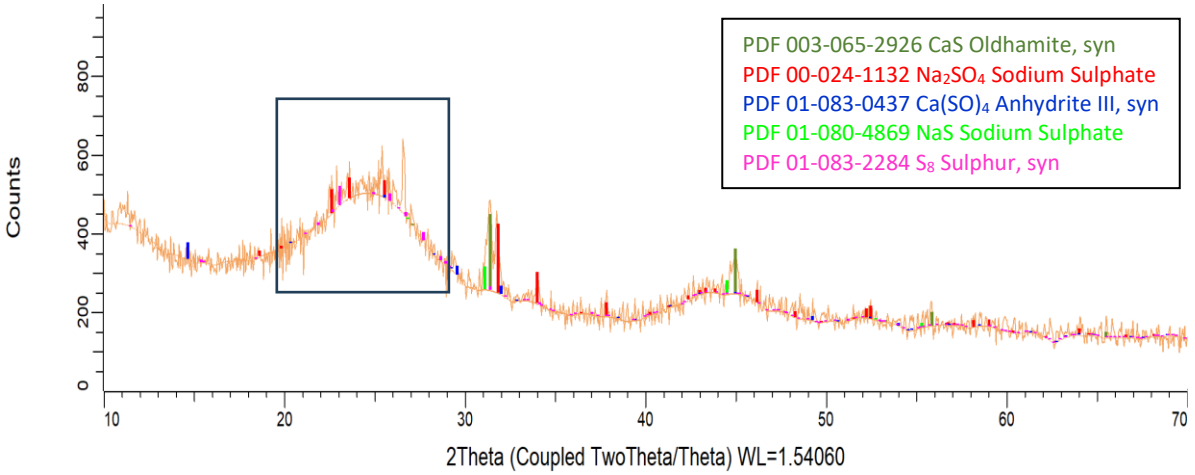


Figure 63. XRD analysis of sample regenerated at 200 W over 960s using a single-mode waveguide cavity and heated inert gas flow directly over samples. The gas flowrate was 2.00 L.min^{-1}, at 160 ^{0}C.

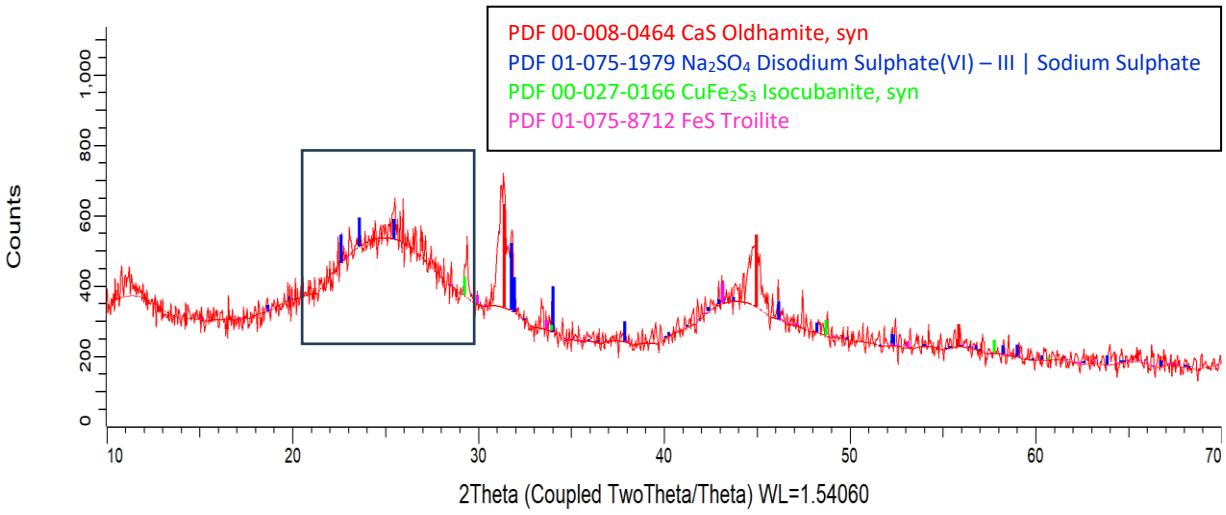


Figure 64. XRD analysis of sample regenerated at 200 W over 1200 using a single-mode waveguide cavity and heated inert gas flow directly over samples. The gas flowrate was 2.00 L.min^{-1}, at 160 ^{0}C.

It should be noted however that at a point after 360s of irradiation a degree of charring had occurred on the carbon itself. This is shown by the emergence of amorphous humps between 20-28 2Theta. This suggests that some degree of damage has occurred to the AC, albeit to a much lesser degree than that seen in previous studies. This would explain why the butane activity, although high, was not even higher – some level of adsorption site loss. It would also suggest that any form of regeneration using a MW system would result in some structural

damage, but that using the heated inert gas flow directly over the samples during the process limits the damage to a degree. And, with the butane activity being as high as was achieved here, and with it having been achieved over such a short period compared to that of thermal regeneration, the level of damage incurred is acceptable at this stage of development.

7.6 Conclusions

The studies outlined in this chapter were conducted to establish the effects of increasing mass transfer rates during MW regeneration, with the intention being that it would reduce the overheating caused by heat energy being emitted to the surrounding carbon structure during the desorption process. This was done inserting a continuous flow of inert gas through the reaction vessel, passing directly over the target samples throughout MW irradiation. A systematic approach was followed to allow for comparisons between previous experiments which had not utilised inert gas flow directly over the samples during processing and those that had. The aim of this approach, and thus this study, was to outline the effects of increasing mass and heat transfer would have on the validity and efficiency of MW-based regeneration for spent sulphurous AC.

The first part of the study outlined the effects of using ambient temperature inert gas flow directly over the samples during processing would have in high-density and low-density microwave fields. Although the low-density field would be more suitable for a scale-up process, lower levels of energy were being absorbed by the target compounds, translating into butane activity lower than that of the high-density field. This was also, in part, due to the low-density field resulting in a shallower penetration depth, thus higher sulphurous compounds concentrations remaining in the interior of the compound. The high-density field study saw higher levels of butane activity achieved due to higher levels of energy having been absorbed during the process. However, both the high- and low-density field experiments saw damage to the carbon structure due to mass transfer rates not being sufficient, and thus a level of heat transfer occurring between the desorbing material and the surrounding carbon structure. This resulted in damage to said carbon structure.

The second half of the study was an in-depth analysis of the effects of heating the inert gas flow, with the express purpose being to increase the speed at which more readily desorbed material were desorbed, and subsequently removed from the AC. The theory being that if physiosorbed layers could be desorbed at a faster rate than the heat energy emitted from

their desorption would not impact the surrounding carbon structure as dramatically. A series of flowrates, inert gas temperatures, MW powers and MW irradiation times were studied. The theory proved to be fruitful and damage to the carbon structure was reduced dramatically, leading to butane activity levels higher than any other experiment and higher than that seen in thermal regeneration methods. Heating the inert gas flow had allowed for an increased vapour pressure and increased mass transfer rate, which reduced the level of heat energy being transferred to the carbon structure as the desorbing material exited the AC at a much faster rate. The process has been deemed a major success, having achieved butane activity of 48.34 % (+/- 1.20 std) and a mass loss of 32.67 % (+/- 0.61 std). This being major improvement on the thermal regeneration, which reached only 40.88 % (+/- 0.92 std) butane activity and mass loss of 50.31 % (+/- 0.95 std).

The study and experimentation into controlling the rate of mass transfer proved to be successful in displaying the efficacy of MW-based processing for the regeneration of spent sulphurous activated carbon. The process reduced the processing time immensely from several hours to 20 minutes. It also yielded higher butane activity levels than possible via thermal regeneration. And, as was seen in previous MW regeneration experimentation in this thesis, it eliminated the need for a steam oxidation phase and thus stopped the production of unwanted acidic by products.

8. Conclusions & Future Work

The aim of this thesis was to study the effects of MW heating on spent sulphurous activated carbon and whether it would provide a sufficient replacement for the traditional thermal regeneration technique used by the project's industrial sponsor, CPL Ltd.

MW heating and MW regeneration was studied with a variety of parameters to understand the efficacy of using an alternate heating source to replace that which is used in current methods. This included: initial testing in which the effects of MW power and irradiation time had on adsorbate desorption mechanics; the effect of high- and low-density MW fields had on adsorbate desorption; and the effects of manipulating mass transfer rates via the use of inert gas flow directly over the target samples during irradiation.

With this a MW regeneration technique was developed capable of achieving greater levels of returned adsorptivity for spent sulphurous AC than that seen with thermal regeneration. This following chapter will offer the conclusions of each chapter studied and what was discovered.

8.1 Effects of MW irradiation

Spent sulphurous AC provided by the project's sponsor company, CPL Ltd, were subjected to irradiation with a variety of MW powers and over a variety of periods of time to analyse the effects MWs would have. The study was funded and pursed owing to the negative side-effects of the thermal regeneration process used by the sponsor in their industrial operations. These included: long processing times which incurred high energy and financial costs; and the production of unwanted by-products in the form of sulphuric and sulphurous acids. The recorded butane activity for which bring 40.88 % (+/- 0.92 std), and the mass loss was 50.31 % (+/- 0.95 std).

It was found that exposure to MWs caused the dipolar sulphurous compounds emit energy in the form of heat, which resulted in damage/loss to the surrounding carbon structure. Butane activities recorded for MW regenerated samples were relatively high (33.43 % (+/- 0.87 std)) when compared to those recorded for thermal regeneration, but not at the same level. It was discovered that increased MW power and irradiation time was a key parameter in the level of energy absorbed, which in turn increased the butane activity. However, if the MW power

was too high, or if irradiation time was too long, this resulted in an increase in detrimental effects to the carbon structure.

However, the processing times recorded for these experiments were significantly lower (minutes rather than hours), and the lack of a need for a steam activation stage, which is required in thermal regeneration, resulted in no sulphurous or sulphuric acids being produced (as had was the case with the traditional thermal method).

Several novel adaptations were attempted to the initial design for the MW processing unit and mechanism with the explicit purpose of reducing overheating methods. This included the use of solvents in which the samples were bathed before and during irradiation. This technique resulted in poor desorption and butane activities. Another technique used was alternating the irradiation over a set time, to which similar positive and negative effects of the initial study were replicated.

With the initial method it was found that using a MW power of 400 W from a 2-kW generator at 2.45 Ghz, over a period of 360s, was the most efficient at producing high butane activities. However, this did lead to destruction of carbon structure via localised overheating.

8.2 Low-density field

A low-density field environment was created by using a multimode waveguide cavity reactor as opposed to a single-mode reactor with the intention being that the chaotic way MWs would be dispersed would result in a slower rate of heating, reducing the localised overheating seen in the initial study. A systematic approach was followed in which MW power and irradiation times were analysed to establish whether the lower MW field density would provide a more adequate approach for retaining the carbon structure.

The first sets of experiments carried out acted as an initial comparison to the experiments carried out in the previous chapter which had used a single-mode waveguide reaction cavity. It was found that the use of a multimode cavity reduced the level of damage done to the overall carbon structure by reducing the rate of heating. However, the results from these initial studies also showed that the level of achievable butane activity was reduced compared to the analogous single-mode runs - 22.94 % (+/- 0.04 std) when using 400 W over 360s, compared to analogous single-mode run having achieved 33.43 % (+/- 0.87 std). This was due to the reduction in absorbed energy over the short relatively short periods of irradiation.

With the level of absorbed energy being lower when using a multimode waveguide cavity reactor for processing, it was theorised it would allow for exposure at higher MW powers. To analyse this, extended irradiation periods were analysed for a range of MW powers between 200-800 W. The best butane activity achieved was at 800 W over 360s at 32.78 % (+/- 0.03 std), comparable to that achieved using the single-mode waveguide cavity at 400 W for 360s. However, this led to a different heating profile than that seen in single-mode experiments where the concentration of sulphurous compounds around the edges of the AC were reduced dramatically, but the level around the interior of the AC remained like its pre-regeneration state. This irradiation of the AC using this method still led to significant damage to the carbon structure. It was theorised that this was being caused by a mass transfer related issue in which the desorbing material was not desorbing and exiting the AC at a rate fast enough to avoid the heat energy being emitted from the desorbing adsorbates from affecting the surroundings detrimentally. This informed the direction of the project going forward as mass and heat transfer manipulation would become a key path towards enhancing the technique.

Much like the high-density field experiments, the low-density field experiments also did not require a steam activation stage for the desorption of adsorbed material bonded to the surface via chemisorption. Thus, no sulphur-based acids were produced. The low-density field technique also didn't require long processing times. As such, two of the key criteria set out by CPL Ltd were still met – removing the steam activation phase which resulted in sulphurous and sulphuric acid production, and reducing the long processing time which can take upwards of 3 hours in on a laboratory scale.

The additional reasoning behind this study was to emulate what would be a typical design aspect were this process to be scaled up. Single-mode waveguide cavity reactors are single-mode owing to a single-mode of MW energy wavelength being transmitted from the cavity, along the waveguide, to the target. When a waveguide cavity is increased then the number of modes increase, thus multimode. Most industrial units used for MW processing use a multimode waveguide cavity set up as large targets are processing at a time to ensure that production of a product can be met to an industrial scale. With CPL Ltd, there current thermal regeneration unit processes several tonnes a day. A single-mode unit would not be viable to process such large target at a single time, but a multimode would if it were scaled up alongside a scaled-up generator. As such, even though the use of a multi-mode waveguide cavity

proved to not be as efficient as a single-mode unit, the research into how such a waveguide cavity effects the samples being processed would be key to a scale-up process.

8.3 Mass transfer manipulation mechanism

MW regeneration of spent sulphurous AC utilising inert gas flow directly over the target samples during was investigated as potential replacement for thermal regeneration processes currently in use by the research's sponsor, CPL Ltd.

The initial experiments of this study were conducted using ambient temperature inert gas (N_2) flowing directly over the target samples during the regeneration process. This was performed as a method by which mass transfer rates could be increased - attempting to reduce the damage to the surrounding carbon structure caused via heat energy emitted from desorbing materials as they desorb and exit the AC. These experiments (sections 7.4.1 and 7.4.2, respectively) resulted in levels of butane activity like those recorded for thermal regeneration, with the high-density field experiments reaching 40.73%, and the low-density field experiments reaching 38.72 % (+/- 0.24 std). However, the technique still led to slight damage to the interior of the AC during processing. It was believed that desorbing material had not left the AC at a rate fast enough for the heat energy to have not caused damage. Additionally, there were still increased levels of sulphurous compounds shown to be present across the ACs, and specifically more concentrated towards the interior. But, in terms of the unwanted by-products and reducing the processing time in comparison with thermal regeneration, the technique proved successful.

The second part of the study involved an in-depth analysis of gas flowrates, the effects of heating the gas flow, MW power, and irradiation time whilst using a high-density field provided by a single-mode waveguide cavity reactor. With regards to nitrogenous flowrate, it was discovered that lower gas flowrates resulted in a reduction in reliability, as well as decreased butane activity levels. A flowrate of 2.00 $L.min^{-1}$ was found to be optimum. When decreased flowrates were used it was also found that the variation in butane activity and mass change were increased, suggesting that the level of gas used could help to control overheating. When the inert gas flow was heated, it was found that increasing the temperature led to an increase in butane activity, with the mass transfer being more efficient at temperatures more than 160 ^{o}C. Marginal gains were seen when increasing the

temperature beyond 160 ^{o}C, but the increase was only slight and increasing the temperature represented an increase in financial cost for the process. Most importantly, it was found that when irradiating the sample for 360s or higher, the butane activity achieved was higher than that seen in thermal regeneration experiments in all but one temperature setting (100 ^{o}C). With increased irradiation time, the increase in butane activity was such that the levels seen in thermal regeneration could be surpassed in as little as 120s, with the longest experiments having surpassed the butane level by approximately 8% when regenerated for 1200s. In addition, the heating of the inert gas flow allowed for the MW power to be reduced to 200 W whilst still achieving up to 48.34 % (+/- 1.20 std) butane activity. Lower MW powers were tested, but optimal power was found to be 200 W.

The results of the second study also showed how heated inert gas flow over the samples during the regeneration process allowed for desorption to happen quicker for materials physiosorbed to the surface. And the gas flow also removed them from the AC pores quicker, resulting in less heat being transferred to the surrounding carbon. Additionally, the heating rate could also be controlled by the MW power – increasing MW power gave rise to higher internal pressure and vapor velocity, promoting more efficient removal of adsorbates from the carbon surface. Moreover, the increasing vapor velocity and internal pressure served to perpetuate removal of adsorbates with stronger chemical interactions. The increase in mass transfer rates also lead to less damage to the overall carbon structure, which increased the butane activity.

The heated inert gas flow paired with MW regeneration resulted in a more efficient process than the traditional thermal process, with a much-reduced processing time resulting in lower energy costs. And the lack of steam activation step had stopped the production of unwanted acidic by products.

8.4 Future work

At laboratory scale

Although the research being conducted at CPL will represent progression in industry when it comes to development of AC regeneration, the potential future work that could have been conducted in a research-focused setting would have been different.

In terms of optimising cavity size and design for a larger target load, a multimode waveguide cavity would be required for an industrial-scale version of the technology. For this, COSMOL software's RF module could be used to simulate 3D distribution of the electric field inside the waveguide cavity, within the load, and to determine the power loss density withing the load for various cavity dimensions. This would involve using the *Electromagnetic Waves Frequency Domain* physics outlined interface in the *RF model suite*. The governing equation for which being:

Equation 16:

$$\nabla \times \mu_r^{-1}(\nabla \times E) - k_o^2\left(\varepsilon_r - \frac{j\sigma}{\omega\varepsilon_o}\right)E = 0$$

Where: μ_r = The relative permeability of the material

E = The electric field strength which is a vector

k_o = The wave number given by $k_o = \omega/c$ (where ω is the wave angular frequency (rad.s^{-1}), c is the speed of light in a vacuum (3 x 10^8 m.s^{-1})

ε_r = Relative permittivity of the material

σ = The electric conductivity of the material, S.m^{-1}

j = Is the $\sqrt{-1}$

ε_0 = The permittivity of free space (8.854 x 10^{-12} F.m^{-1})

Using this could allow for optimal cavity height, cavity width, waveguide Y position and waveguide Z position to be found. Thus, a cavity optimised for the desired load size could be designed. However, investigations into the efficacy of penetration depth would still need to be evaluated before constructing physical designs – a larger load would likely reduce the effect when penetrating further.

In addition to this, the *RF module* of COSMOL could be coupled with other models such as the *Heat Transfer Module* to allow for an accurate temperature profile to be calculated through simulation as opposed to physical experiments. Using this combination of simulation techniques could allow for construction of waveguide cavities specific to each type of AC used and to specific adsorbates.

Current/future work at CPL Ltd.'s Immingham site

With the project having been moved to a pilot study at the CPL site in Immingham, a study on which I will be consulting for its projected 2-year runtime, work has already begun on constructing as pilot-scale MW processing unit. During this 2-year study there will be three main areas of study: optimising the gas mass transfer system; analysing the effects of the process on AC that has other kinds of contaminants adsorbed; taking the process to larger scales thus including the switch to a multimode system. Below is a brief description of the work underway:

- Optimisation of the gas flow system to incorporate a looped flow. The design of a looped gas flow will allow for nitrogen to be reused after it has passed through sulphur removal traps. The idea behind this being to reduce the amount of new gas being supplied to the system, thus reducing operational costs and the overall climate effects associated with the storage & supply of gas cylinders. Additionally, utilising a looped closed gas system like this reduces the likelihood of outside influence of moisture in the air reacting with the AC or adsorbed sulphurous compounds during the regeneration process.
- Following the projects implementation for sulphurous compound removal from AC, the next stage would be to use the technology to treat other spent AC that customers bring to CPL. Investigations into the usability of the technology on AC that has adsorbed other kind of contaminants initially started at the University, with experiments being conducted on AC used in oil spills and those used in cleaning water treatment systems struggling with high levels of calcium oxides. Both studies are continuing over at CPL, and both present their own individual challenges. The research in this area has already proved that the technology is not a one-method-fits-all approach. Instead, modifications to the current tech will be required for each new treatment plan. In turn, each would likely need a similar scale of research as has been conducted in this doctoral research project, but the building blocks of the technology developed here will already be in place.

- As the company would likely need to process large quantities daily, efforts have been made to investigate the ability to regenerate larger samples sizes than those which were regenerated throughout this research. There are two lines of thought: either increase the waveguide cavity dimensions (making it a multimode) to accommodate larger samples sizes as there would be more room for each processing load; or design a semi-batch style process in which smaller loads are processed. The latter of which would allow for a single-mode setup to be maintained as successive small loads could be processed at quick rate.

With this hands-on approach, CPL look to create a unit which can process at pilot-scale successfully. And, in time, the pilot unit will be scaled up and replace their industrial unit in its entirety, culminating in the end of the research presented in this thesis.

9. References

[1] Bansal, R., Donnet, J. and Stoeckli, F. (1988). *Active Carbons*. New York and Basel: Marcel Dekker Inc. pp. Introduction: vii-xii.

[2] Lozano-Castelló, D., Cazorla-Amorós, D., Linares-Solano, A. and Quinn, D. (2002). Activated Carbon Monoliths for Methane Storage: Influence of Binder. *Carbon*, 40(15), pp. 2817-2825.

[3] Jüntgen, H. (1986). Activated carbon as catalyst support. *Fuel*, 65(10), pp.1436-1446.

[4] Jiang, Q., Qu, M., Zhou, G., Zhang, B. and Yu, Z. (2002). A study of activated carbon nanotubes as electrochemical super capacitors electrode materials. *Materials Letters*, 57(4), pp.988-991.

[5] Moreno, N., Caballero, A., Hernán, L. and Morales, J. (2014). Lithium–sulfur batteries with activated carbons derived from olive stones. *Carbon*, 70, pp.241-248.

[6] Aoki, H., Ikeda, I., Kiriyama, T. and Kiyota, M. (2008). Industrial production and market of activated carbon. *Carbon*, 46(7), p.1111-1118.

[7] Odesola, I. and Daramola, N. (2010). Activated carbon production from wastes: profitability index and product cost reduction method. *American Journal of Scientific and Industrial Research*, 1(2), pp.332-341.

[8] Liu, P. and Wagner, N. (1985). Thermal regeneration of granular activated carbon. *Environmental Progress*, 4(2), pp.136-141.

[9] Martin, R. and Ng, W. (1987). The repeated exhaustion and chemical regeneration of activated carbon. *Water Research*, 21(8), pp.961-965.

[10] Van Vliet, B. M. (1991) The Regeneration of Activated Carbon. *Journal of the South African Institute of Mining and Metallurgy*. 91(5). pp. 159-167.

[11] Guo, Y. and Du, E. (2012). The Effects of Thermal Regeneration Conditions and Inorganic Compounds on the Characteristics of Activated Carbon Used in Power Plant. *Energy Procedia*, 17(1), pp.444-449.

[12] Leng, C. and Pinto, N. (1996). An Investigation of the Mechanisms of Chemical Regeneration of Activated Carbon. *Industrial & Engineering Chemistry Research*, 35(6), pp.2024-2031.

[13] Salvador, F., Martin-Sanchez, N., Sanchez-Hernandez, R., Sanchez-Montero, M. and Izquierdo, C. (2015). Regeneration of carbonaceous adsorbents. Part II: Chemical, Microbiological and Vacuum Regeneration. *Microporous and Mesoporous Materials*, 202, pp.277-296.

[14] Nasruddin, M., Fahmi, M., Abidin, C. and Yen, T. (2018). Regeneration of Spent Activated Carbon from Wastewater Treatment Plant Application. *Journal of Physics: Conference Series*, 1116, pp.1-8.

[15] Lee, Y., Park, J., Choung, J. and Choi, D. (2002). Adsorption Characteristics of SO_2 on Activated Carbon Prepared from Coconut Shell with Potassium Hydroxide Activation. *Environmental Science & Technology*, 36(5), pp.1086-1092.

[16] Chiang, H., Tsai, J., Tsai, C. and Hsu, Y. (2000). Adsorption Characteristics of Alkaline Activated Carbon Exemplified by Water Vapor, H_2S, and CH_3SH Gas. *Separation Science and Technology*, 35(6), pp.903-918.

[17] Margitan, J. (1984). ChemInform Abstract: Mechanism of the Atmospheric Oxidation of Sulfur Dioxide – Catalysis by Hydroxyl Radicals. *Journal of Physical Chemistry,* 88(15), pp. 3314-3318.

[18] Yamazaki, H. (1968). Microwave Heating. *SHINKU*, 11(3), pp.78-85.

[19] Ania, C., Menéndez, J., Parra, J. and Pis, J. (2004). Microwave-induced regeneration of activated carbons polluted with phenol. A comparison with conventional thermal regeneration. *Carbon*, 42(7), pp.1383-1387.

[20] Lee, G., Anand, S. C., Rajendran, S., Walker, I. (2010). Development of Odour (Volatile Molecule) Adsorbent Materials for Healthcare. *Medical and Healthcare Textiles*, pp. 206-214.

[21] Jadhav, A. S., (2014). Advancements in Drinking Water Treatments from Ancient Times. *International Journal of Science, Environment*, 3(4), pp. 1415-1418.

[22] Lapus, R. (2007). *Activated Charcoal for Pediatric Poisonings: The Universal Antidote?* Philadelphia: Lippincott Williams & Wilkins, pp.216-222.

[23] Partington, J. R., (1962, reprint 1966). *A History of Chemistry*. (3). New York: Martino Publishing. pp. 172-173.

[24] Partington, J. R., (1962, reprint 1966). *A History of Chemistry*. (3). New York: Martino Publishing. pp. 585-588

[25] Pendyal, B., Johns, M., Marshall, W., Ahmedna, M. and Rao, R. (1999). Removal of sugar colorants by granular activated carbons made from binders and agricultural by-products. *Bioresource Technology*, 69(1), pp.45-51.

[26] Wisniak, J., (2014). Gabriel Bertrand. *Revista CENIC Ciencias Biológicas,* 45(3), pp. 230-245.

[27] Woodhead, G. S., Cartwright-Wood, G. E., (1898). An Inquiry into the Relative Efficiency of Water Filters in the Prevention of Infectious Diseases. *The British Medical Journal*. (1). pp. 261-264.

[28] Baker, F., Miller, C., Repik, A. and Tolles, E. (2007). Carbon, Activated. *ChemInform*, 38(40), pp.741-757.

[29] Bansal, R. and Goyal, M. (2005). *Activated carbon adsorption*. Boca Raton: Taylor & Francis, pp.246-247.

[30] Alkhatib, A. J., Al Zailaey, K. (2015). Medical and Environmental Applications of Activated Charcoal: Review Article. *European Scientific Journal*. 11(3), pp. 50-56.

[31] Winchester, J. F., Ronco, C. (2010). Sorbent Augmented Hemodialysis Systems: Are We There Yet? *Journal of the American Society of Nephrology*. (21), pp. 209-211.

[32] Yamamoto, S., Zuo, Y., Ma, J., Yancey, P.G., Hunley, T.E., Motojima, M., Fogo, A.B., Linton, M.F., Fazio, S., Ichikawa, I., Kon, V. (2011). Oral Activated Charcoal Adsorbent (AST-120) Ameliorates Extent and Instability of Atheroscleros is Accelerated by Kidney Disease in Apolipoprotein E-deficient Mice. *Nephrology Dialysis Transplantation*. (26), pp. 2491–2497.

[33] Schulman, G. (2012). A Nexus of Progression of Chronic Kidney Disease: Tryptophan, Profibrotic Cytokines, and Charcoal. *Journal of Renal Nutrition*. (22). pp. 207-113.

[34] Foo, K. and Hameed, B. (2011). The environmental applications of activated carbon/zeolite composite materials. *Advances in Colloid and Interface Science*, 162(1-2), pp.22-28.

[35] Cukierman, A. (2013). Development and Environmental Applications of Activated Carbon Cloths. *ISRN Chemical Engineering*, 2013, pp.1-31.

[36] Onuki, S., Koziel, J., Jenks, W., Cai, L., Rice, S. and van Leeuwen, J. (2015). Ethanol purification with ozonation, activated carbon adsorption, and gas stripping. *Separation and Purification Technology*, 151, pp.165-171.

[37] Siříšťová, L., Přinosilová, Š., Riddellová, K., Hajšlová, J. and Melzoch, K. (2012). Changes in quality parameters of vodka filtered through activated charcoal. *Czech Journal of Food Sciences*, 30(5), pp.474-482.

[38] Zakaria, Z. and George, T. (2011). The Performance of Commercial Activated Carbon Adsorbent for Adsorbed Natural Gas Storage. *International Journal of Recent Research and Applied Studies*, 9(2), pp.225-230.

[39] Matranga, K., Myers, A. and Glandt, E. (1992). Storage of natural gas by adsorption on activated carbon. *Chemical Engineering Science*, 47(7), pp.1569-1579.

[40] Sun, J., Rood, M., Rostam-Abadi, M. and Lizzio, A. (1996). Natural gas storage with activated carbon from a bituminous coal. *Gas Separation & Purification*, 10(2), pp.91-96.

[41] Sevilla, M., Mokoya, R. (2014). Energy Storage Applications of Activated Carbons: Supercapacitors and Hydrogen Storage. *Energy & Environmental Science.* 4(7). pp. 1250-1280.

[42] Fierro, V., Zhao, W., Izquierdo, M., Aylon, E. and Celzard, A. (2010). Adsorption and compression contributions to hydrogen storage in activated anthracites. *International Journal of Hydrogen Energy*, 35(17), pp.9038-9045.

[43] Medinat, V., Webster, T., Ramaratnam, M. and Devinny, J. (1995). Treatment of Gasoline Residuals by Granular Activated Carbon Based Biological Filtration∗. *Journal of Environmental*

Science and Health . Part A: Environmental Science and Engineering and Toxicology, 30(2), pp.407-422.

[44] So, J. and Cho, H. (2017). Thermal Characteristics of Spent Activated Carbon Generated from Air Cleaning Units in Korean Nuclear Power Plants. *Nuclear Engineering and Technology*, 49(4), pp.873-880.

[45] Zhang, F., Nriagu, J., Itoh, H. (2005). Mercury removal from water using activated carbons derived from organic sewage sludge. *Water Research*, 39(2-3), pp.389-395.

[46] Zhu, Y., Frey, H. C. (2010). *Advanced Power Plant Materials, Design and Technology*. Sawston, Cambridge. Woodhead Publishing. pp. 54-88.

[47] Maulina, S. and Iriansyah, M. (2018). Characteristics of activated carbon resulted from pyrolysis of the oil palm fronds powder. *IOP Conference Series: Materials Science and Engineering*, 309, pp. 1-6.

[48] Liu, J., Liu, X., Sun, Y., Sun, C., Liu, H., Stevens, L., Li, K. and Snape, C. (2017). High Density and Super Ultra-Microporous-Activated Carbon Macrospheres with High Volumetric Capacity for CO2 Capture. *Advanced Sustainable Systems*, 2(2), pp.1700115 (1-8).

[49] Bansal, R., Donnet, J. and Stoeckli, F. (1988). *Active Carbons*. New York and Basel: Marcel Dekker Inc, pp. 3-7.

[50] Soo, Y., Chada, N., Beckner, M., Romanos, J., Burres, J., Pfiefer, P. (2013). Absorbed Methane Properties in Nanoporous Carbon Monoliths. *Bulletin of the American Physical Society.* 58(1) pp. 3-20.

[51] Dillon, E. C., Barlow. J., Jared, C., and Watson, W. (1989). Large Surface Area Activated Charcoal and the Inhibition of Aspirin Adsorption. *Annals of Emergency Medicine*. 18(5). pp. 547-552.

[52] Sulyman, M., Namiesnik, J., Gierak, A. (2017). Low-cost Adsorbents Derived from Agricultural By-products/Wastes for Enhancing Contaminant Uptakes from Wastewater: A Review. *Polish Journal of Environmental Studies*. 26(2). pp. 479-510.

[53] Saeidi, N. and Lotfollahi, M. (2015). Effects of powder activated carbon particle size on adsorption capacity and mechanical properties of the semi activated carbon fiber. *Fibers and Polymers*, 16(3), pp.543-549.

[54] Margot, J., Kienle, C., Magnet, A., Weil, M., Rossi, L., de Alencastro, L., Abegglen, C., Thonney, D., Chèvre, N., Schärer, M. and Barry, D. (2013). Treatment of micropollutants in municipal wastewater: Ozone or powdered activated carbon?. *Science of The Total Environment*, 461-462, pp.480-498.

[55] Najm, I., Snoeyink, V., Lykins, B. and Adams, J. (1991). Using Powdered Activated Carbon: A Critical Review. *Journal - American Water Works Association*, 83(1), pp.65-76.

[56] Walker, G. and Weatherley, L. (1997). Adsorption of acid dyes on to granular activated carbon in fixed beds. *Water Research*, 31(8), pp.2093-2101.

[57] Aygün, A., Yenisoy-Karakaş, S. and Duman, I. (2003). Production of granular activated carbon from fruit stones and nutshells and evaluation of their physical, chemical and adsorption properties. *Microporous and Mesoporous Materials*, 66(2-3), pp.189-195.

[58] Hagemann, N., Spokas, K., Schmidt, H., Kägi, R., Böhler, M. and Bucheli, T. (2018). Activated Carbon, Biochar and Charcoal: Linkages and Synergies across Pyrogenic Carbon's ABCs. *Water*, 10(2), pp.182-201.

[59] Herzberg, G. (1955). Heinrich Kayser 1853-1940. *Biographical Memoirs of Fellows of the Royal Society*. 1. pp. 135-143

[60] Gregg, S. J., Sing, K. S. W. (1982). *Adsorption, Surface Area and Porosity*. 2nd ed. London: Academic Press. p. 4

[61] Sharifan, S. (2013). *A Comparative Optimisation Study of Activated Carbon Production from Hazelnut Shells by Thermal and Microwave Heating Methods*. PhD Thesis. Imperial College London.

[62] Sing, K. S. W., Everett, D. H., Haul, R. A. W., Moscou, L., Pierotti, R. A., Rouquerol, J., and Siemieniewska, T. (1985). Reporting Physisorption Data For Gas/Solid Systems With Special Reference to the Determination of Surface Area and Porosity. *Pure and Applied Chemistry*. 57. pp. 603-619.

[63] Gill, A. (1998). Analysis of the Micropore Structure of Various Microporous Materials from Nitrogen at 77K. *Adsorption*, 4(3-4), pp. 197-206.

[64] Roquerol, J., and Rouquerol, F. (1999). *Adsorption by Powders and Porous Solids; Principles, Methodology and Applications.* London. Academic Press. pp. 82-98.

[65] Pendleton, P., and Zettlemoyer, A, C. (1984). A Study of the Mechanism of Micropore Filling: II. Pore Filling od Microporous Silica. *Journal od Colloid and Interface Science*, 98(2), pp. 439-446.

[66] Storck, S., Bretinger, H. and Maier, W. (1998). Characterization of micro- and mesoporous solids by physisorption methods and pore-size analysis. *Applied Catalysis A: General*, 174(1-2), pp.137-146.

[67] Soares Maia, D., de Oliveira, J., Toso, J., Sapag, K., López, R., Azevedo, D., Cavalcante, C. and Zgrablich, G. (2011). Characterization of the PSD of activated carbons from peach stones for separation of combustion gas mixtures. *Adsorption*, 17(5), pp.853-861.

[68] Spl.ethz.ch. (n.d.). *Capillary condensation and hysteresis in gas phase adsorption*. [online] Available at: http://www.spl.ethz.ch/research/fundamentals/hysteresis.html [Accessed 5 Jun. 2019].

[69] Wang, W., Liu, P., Zhang, M., Hu, J. and Xing, F. (2012). The Pore Structure of Phosphoaluminate Cement. *Open Journal of Composite Materials*, 02(03), pp.104-112.

[70] Vargas, D., Giraldo, L. and Moreno-Piraján, J. (2012). CO2 Adsorption on Activated Carbon Honeycomb-Monoliths: A Comparison of Langmuir and Tóth Models. *International Journal of Molecular Sciences*, 13(7), pp.8388-8397.

[71] Brunauer, S., and Emmet, P. H. (1938). Adsorption of Gases in Multimolecular Layers. *Journal of the American Chemical Society*. 60(2). pp. 309-319.

[72] Passe-Coutrin, N., Altenor, S., Cossement, D., Jean-Marius, C. and Gaspard, S. (2008). Comparison of parameters calculated from the BET and Freundlich isotherms obtained by nitrogen adsorption on activated carbons: A new method for calculating the specific surface area. *Microporous and Mesoporous Materials*, 111(1-3), pp.517-522.

[73] Ma, X., Yang, H., Yu, L., Chen, Y. and Li, Y. (2014). Preparation, Surface and Pore Structure of High Surface Area Activated Carbon Fibres from Bamboo by Steam Activation. *Materials*, 7(6), pp.4431-4441.

[74] Galarneau, A., Villemot, F., Rodriguez, J., Fajula, F. and Coasne, B. (2014). Validity of the t-plot Method to Assess Microporosity in Hierarchical Micro/Mesoporous Materials. *Langmuir*, 30(44), pp.13266-13274.

[75] Zhang, C., Wang, Y. and Yan, X. (2006). Liquid-phase adsorption: Characterization and use of activated carbon prepared from diosgenin production residue. *Colloids and Surfaces A: Physicochemical and Engineering Aspects*, 280(1-3), pp.9-16.

[76] Ng, C., Losso, J., Marshall, W. and Rao, R. (2002). Freundlich adsorption isotherms of agricultural by-product-based powdered activated carbons in a geosmin–water system. *Bioresource Technology*, 85(2), pp.131-135.

[77] Gholizadeh, A., Kermani, M., Gholami, M. and Farzadkia, M. (2013). Kinetic and isotherm studies of adsorption and biosorption processes in the removal of phenolic compounds from aqueous solutions: comparative study. *Journal of Environmental Health Science and Engineering*, 11(1), p.29.

[78] Demirbaş, A. (2004). Relationships between Carbonization Temperature and Pyrolysis Products from Biomass. *Energy Exploration & Exploitation*, 22(6), pp.411-419.

[79] Saha, B., Jribi, S., Koyama, S. and El-Sharkawy, I. (2011). Carbon Dioxide Adsorption Isotherms on Activated Carbons. *Journal of Chemical & Engineering Data*, 56(5), pp.1974-1981.

[80] Valix, M., Cheung, W. and McKay, G. (2004). Preparation of activated carbon using low temperature carbonisation and physical activation of high ash raw bagasse for acid dye adsorption. *Chemosphere*, 56(5), pp.493-501.

[81] Su, C. and Wang, C. (2007). Optimum manufacturing conditions of activated carbon fiber absorbents. II. Effect of carbonization and activation conditions. *Fibers and Polymers*, 8(5), pp.482-486.

[82] Jahangiri, M., Shahtaheri, S. J, Adl, J., Rashidi, A., Kakooei, H., Forushani, A. R., Nasiri, G., Ghorbanali. A., and Ganjali, M. R. (2012). Preparation of Activated Carbon from Walnut Shell and its Utilization for Manufacturing Organic-Vapour Respirator Cartridge. *Fresenius Environmental Bulletin*. 21(6a). pp. 1508-1514.

[83] Lamine, S., Ridha, C., Mahfoud, H., Mouad, C., Lotfi, B. and Al-Dujaili, A. (2014). Chemical Activation of an Activated Carbon Prepared from Coffee Residue. *Energy Procedia*, 50, pp.393-400.

[84] Wigmans, T. (1989). Industrial Aspects of Production and Use of Activated Carbons. *Carbon*. 27(1). pp. 13-22.

[85] Ahmadpour, A. and Do, D. (1996). The preparation of active carbons from coal by chemical and physical activation. *Carbon*, 34(4), pp.471-479.

[86] Ghouma, I., Jeguirim, M., Dorge, S., Limousy, L., Matei Ghimbeu, C. and Ouederni, A. (2015). Activated carbon prepared by physical activation of olive stones for the removal of NO2 at ambient temperature. *Comptes Rendus Chimie*, 18(1), pp.63-74.

[87] Stavropoulos, G. G., Zabaniotou, A. A. (2009). Minimizing Activated Carbons Production Costs. *Fuel Processing Technology,* 90. pp. 952-957.

[88] Santadkha, T., and Skolpap, W. (2017) Economic Comparative Evaluation of Combination of Activated Carbon Generation and Spent Activated Carbon Regeneration Plants. *Journal of Engineering Science and Technology*, 12(12), pp. 3329-3343.

[89] Pandey, B., Guautam, M. and Agrawal, M. (2017). *Environmental carbon footprints*. 1st ed. Amsterdam: Elsevier, pp.267-279.

[90] Krebs, C. and Smith, J. (1985). Kinetics of steam regeneration of virgin and phenol-loaded activated carbon. *Carbon*, 23(2), pp.223-235.

[91] Pawłowski, Ł., Lacy, W. and Dlugosz, J. (1991). *Chemistry for the Protection of the Environment*. 42nd vol. New York, NY: Plenum Press, pp.427-431.

[92] Sabio, E., González, E., González, J., González-García, C., Ramiro, A. and Gañan, J. (2004). Thermal regeneration of activated carbon saturated with p-nitrophenol. *Carbon*, 42(11), pp.2285-2293.

[93] Martin, R. J., Ng, W. J. (1984). Chemical Regeneration of Exhausted Carbon – I. *Water Research*, 1(18), pp. 59-73.

[94] Cooney, D., Nagerl, A. and Hines, A. (1983). Solvent regeneration of activated carbon. *Water Research*, 17(4), pp.403-410.

[95] Liu, D. (2015). *Water Treatment by Adsorption and Electrochemical Regeneration Development of a Liquid-Lift Reactor.* PhD. The University of Manchester. (Available at https://www.escholar.manchester.ac.uk/api/datastream?publicationPid=uk-ac-man-scw:283011&datastreamId=FULL-TEXT.PDF) [Accessed: 01 June 2019]

[96] Mehta, M. P., Flora, J. R. V. (1997). Effects of Electrochemical Treatment of Granular Activated Carbon on Surface Acid Groups and the Adsorptive Capacity for Phenol. *Water Research*, 31(9), pp. 2171-2176.

[97] Choi. J. J. (1997). Oxidative Removal of Malodorous Volatile Sulphur Compounds by Air Over an Activated Carbon Fibre. *Journal of Industrial and Engineering Chemistry*, 3(1), pp. 56-62.

[98] Narbaitz, R. M., and Karimi-Jashni, A. (1994). Removal of Volatile Organic Compounds by Activated Carbon Fibre. *Carbon*, 42(14), pp. 2949-2962.

[99] Zhang, H., Ye, L., and Zhong, H. (2002). Regeneration of Phenol-Saturated Activated Carbon in an Electrochemical Reactor. *Journal of Chemical Technology and Biochemical Technology,* 77, pp. 1246-1250.

[100] Narbaitz, R. M., and Karimi-Jashni, A. (2005) Electrochemical Reactivation of Granular Activated Carbon: pH Dependence. *Journal of Environmental Engineering Science*, 4, pp. 187-194.

[101] García-Otón, M., Lillo-Ródenas, M. A., Morallón, E., and Vazquez, J. L. (2005) Electrochemical Regeneration of Activated Carbon Saturated with Toluene. *Journal of Applicable Electrochemistry*, 35, pp. 319-325

[102] Reed, B., Vaughan, R. and Jiang, L. (2000). As(III), As(V), Hg, and Pb Removal by Fe-Oxide Impregnated Activated Carbon. *Journal of Environmental Engineering*, 126(9), pp.869-873.

[103] Gibson, J., Gromov, A., Brandani, S. and Campbell, E. (2015). The effect of pore structure on the CO2 adsorption efficiency of polyamine impregnated porous carbons. *Microporous and Mesoporous Materials*, 208, pp.129-139.

[104] Tanthana, J., and Chuang, S. S. C. (2010) In Situ Infrared Study of the Role of PEG in Stabilising Silica Supported Amines for CO_2 Capture. *ChemSusChem*, 3, pp. 957-964.

[105] Khalil, S. H. (2018). Effects on Surface Area, Intake Capacity and Regeneration of Impregnated Palm-Shell Activated Carbon with Monoethanolamide and 2-Amino-2-Methyl-1-Propanol Equipped For CO2 Adsorption. *Journal of Earth Science & Climatic Change*, 9(7), p. e1000484(1-10).

[106] Shah, I., Adnan, R., Wan Ngah, W. and Mohamed, N. (2015). Iron Impregnated Activated Carbon as an Efficient Adsorbent for the Removal of Methylene Blue: Regeneration and Kinetics Studies. *PLOS ONE*, 10(4), p. e0122603(1-23).

[107] Benhamed, I., Barthe, L., Kessas, R., Julcour, C. and Delmas, H. (2016). Effect of transition metal impregnation on oxidative regeneration of activated carbon by catalytic wet air oxidation. *Applied Catalysis B: Environmental*, 187, pp.228-237.

[108] Kostas, E., Beneroso, D. and Robinson, J. (2017). The application of microwave heating in bioenergy: A review on the microwave pre-treatment and upgrading technologies for biomass. *Renewable and Sustainable Energy Reviews*, 77, pp.12-27.

[109] Banik, S., Bandyopadhyay, S., and Ganguly, S. (2003) Bioeffects of Microwave – A Brief Review. *Bioresource Technology*, 82(2), pp. 115-124.

[110] Motasemi, F., and Ani, F. (2012) A Review On Microwave-assisted Production of Biodisel. *Renewable Sustainable Energy Review*, 16(7), pp. 4719-4733.

[111] Nüchter, M., Ondruschka, A., Bonrath, W., and Gum, A. (2004) Microwave Assisted Synthesis – A Critical Technology Overview. *Green Chemistry*, 6(3), pp. 128-141.

[112] Kumbhar, S. V., and Sonage, B. K. (2018) Enhancement of Thermal Efficiency and Cost Effectiveness by Devcelopment of Melting Furnace by Revamping and Troubleshooting Fuel-fired Furnace. *Heat Transfer – Asian Research*, 48(1), pp. 164-181.

[113] Tumpanuvatr, T., Juttanit, W., Kaewchutong, S., Jan-Ob, O., Pham, H., and Sajjaanatakul, T. (2015) Comparisons Between Ohmic and Conventional Heating of Pineapple and Longan in Sucrose Solution. *Natural Science*, 49, pp. 615-625.

[114] Irfan, M., Khan, M., and Khan, W. A. (2019) Impact of Non-uniform Heat Sink/Source and Convective Condistion in Radiative Heat Transfer to Oldroyd Nanofluid: A Revised Proposed Relation. *Physics Letters A,* 383(4), pp. 376-382.

[115] Wathen, R. L. (1953) Genesis of a Generator – The Early History of the Magnetron. *Journal of the Franklin Institute*, 255(4), pp. 271-287.

[116] Osepchuk, J. (1984). A History of Microwave Heating Applications. *IEEE Transactions on Microwave Theory and Techniques*, 32(9), pp.1200-1224.

[117] Sun, N., Jiang, H., Wang, Y. and Qi, A. (2018). A Comparative Research of Microwave, Conventional-Heating, and Microwave/Chemical Demulsification of Tahe Heavy-Oil-in-Water Emulsion. *SPE Production & Operations*, 33(2), pp.371-381.

[118] Menédez, J. A., and Inguanzo, M. (2002) Microwave-induced Pyrolysis of Sewage Sludge. *Water Research*, 36(13), pp. 3261-3264

[119] Punt, M. M., Raghavan, G. S. V., Bélanger, J. M. R., and Paré, J. R. J. (1999) Microwave-assisted Process (MAPTM) for the Extraction of Contaminants from Soil. *Journal of Soil Contamination*, 8(5), pp. 577-592

[120] Krieger-Brockett, B. (1994). Microwave Pyrolysis of Biomass. *Research on Chemical Intermediates*, 20(1), pp.39-49.

[121] Miura, M., Kaga, H., Sakurai, A., Kakuchi, T. and Takahashi, K. (2004). Rapid Pyrolysis of Wood Block by Microwave Heating. *Journal of Analytical and Applied Pyrolysis*, 71(1), pp.187-199.

[122] Robinson, J., Kingman, S., Snape, C. and Shang, H. (2007). Pyrolysis of Biodegradable Wastes Using Microwaves. *Proceedings of the Institution of Civil Engineers - Waste and Resource Management*, 160(3), pp.97-103.

[123] Grundas, S. (2011). *Advances in Induction and Microwave Heating of Mineral and Organic Materials*. 3rd ed. Rijeka, Croatia: Intech, pp.724-731.

[124] Moseley, J. and Woodman, E. (2009). Energy Efficiency of Microwave- and Conventionally Heated Reactors Compared at Meso Scale for Organic Reactions. *Energy & Fuels*, 23(11), pp.5438-5447.

[125] Berteli, M. and Marsaioli, A. (2005). Evaluation of Short Cut Pasta Air Dehydration Assisted by Microwaves as Compared to the Conventional Drying Process. *Journal of Food Engineering*, 68(2), pp.175-183.

[126] Pérez-Cid, B., Lavilla, I. and Bendicho, C. (1999). Application of Microwave Extraction for Partitioning of Heavy Metals in Sewage Sludge. *Analytica Chimica Acta*, 378(1-3), pp.201-210.

[127] Motasemi, F., and Afzal, M. T. (2013) A Review on the Microwave-Assisted Pyrolysis Technique. *Renewable and Sustainable Energy Reviews*, 28, pp. 317-330.

[128] Meredith, R. (1998). *Engineers' Handbook of industrial Microwave Heating*. 3rd ed. Stevenage: Institution of electrical engineers, pp.2-5, 54-56.

[129] Von Hippel, A. R. (1954) *Dielectrics and Waves*. 1st ed. Cambridge (Massachusetts), United States of America: The M.I.T Press, pp.95-96.

[130] Thostenson, E. and Chou, T. (1999). Microwave processing: fundamentals and applications. *Composites Part A: Applied Science and Manufacturing*, 30(9), pp.1055-1071.

[131] Lidström, P., Tierney, J., Wathey, B. and Westman, J. (2001). Microwave assisted organic synthesis—a review. *Tetrahedron*, 57(45), pp.9225-9283.

[132] Von Hippel, A. R. (1954) *Dielectrics and Waves*. 1st ed. Cambridge (Massachusetts), United States of America: The M.I.T Press, pp.26-28.

[133] Gabriel, C., Gabriel, S., H. Grant, E., H. Grant, E., S. J. Halstead, B. and Michael P. Mingos, D. (1998). Dielectric parameters relevant to microwave dielectric heating. *Chemical Society Reviews*, 27(3), p.213-223.

[134] Clark, D. E. and Sutton, W. H. (1996) Microwave Processing of Materials. *Annual Review of Materials Science,* 27, pp. 299-331.

[135] Huang, Y., Chiueh, P., and Lo, S. (2016) A Review on Microwave Pyrolysis of Lignocellulosic Biomass. *Sustainable Environment Research*, 26(3), pp. 103-109.

[136] Sazzat, H. (2015). *Welcome to E-Shop Presentation*. Available at: https://www.slideshare.net/sazzathossain39/home-appliances-54131617 [Accessed: 16 June 2019]

[137] Blanchard, Y., Galati, G. and van Genderen, P. (2013). The Cavity Magnetron: Not Just a British Invention [Historical Corner]. *IEEE Antennas and Propagation Magazine*, 55(5), pp.244-254.

[138] Vollmer, M. (2003). Physics of the Microwave Oven. *Physics Education*, 39(1), pp.74-81.

[139] Berishvili, Z., Gadakhabadze, I., Kordzakhia, I. and Dekanozishvili, G. (2017). Planar Magnetron Sputtering Device: A New Generation of Magnetron Sputtering Design and Technology. *Journal of Physical Science and Application*, 7(5), pp.38-45.

[140] Norström, H. (1980). The Electrical Characteristics of RF Magnetron and Non-Magnetron Planar Systems. *Vacuum*, 30(6), pp.225-226.

[141] Asmussen, J., Lin, H., Manring, B. and Fritz, R. (1987). Single-mode or controlled multimode microwave cavity applicators for precision materials processing. *Review of Scientific Instruments*, 58(8), pp.1477-1486.

[142] Metaxas, A. and Meredith, R. (1983). *Industrial microwave heating -Volume 1*. 1st ed. London: Peregrinus, pp.130-150.

[143] Bradshaw, S. M., Van Wyk, E. J., and De Swart, J. B. (1998) Microwave Heating Principles and the Application to the regeneration of Granular Activated Carbon. *The Journal of the South African Institute of Mining and Metallurgy*, 201, pp. 201-212.

[144] Ania, C., Parra, J., Menéndez, J. and Pis, J. (2005). Effect of Microwave and Conventional Regeneration on the Microporous and Mesoporous Network and on the Adsorptive Capacity of Activated Carbons. *Microporous and Mesoporous Materials*, 85(1-2), pp.7-15.

[145] Xia, H., Wu, J., Xia, Y., Zhang, L., Peng, J., Wang, S., Zheng, Z. and Zhang, S. (2014). Microwave Assisted Regeneration of Spent Activated Carbon From Petrochemical Plant Using Response Surface Methodology. *Journal of Porous Materials*, 22(1), pp.137-146.

[146] Coss, P. and Cha, C. (2000). Microwave Regeneration of Activated Carbon Used for Removal of Solvents from Vented Air. *Journal of the Air & Waste Management Association*, 50(4), pp.529-535.

[147] Foo, K. and Hameed, B. (2012). Microwave-assisted regeneration of activated carbon. *Bioresource Technology*, 119, pp.234-240.

[148] Muller, H. (1994). *Ullmann's Encyclopedia of Industrial Chemistry*. 2nd ed. Weinheim, Germany: Wiley-VCH, pp.635-639.

[149] Siedlewski, J. (1965) Mechanism of Catalytic Oxidation on Activated Carbon – V, the Contribution of Carbon Free Radicals in the SO_2 and SO_3 Oxidation Process. *Roczzniki Chemistry*, 39, pp 263-272.

[150] Siedlewski, J. (1965) Mechanism of Catalytic Oxidation on Activated Carbon – Vi, Determination of the Number of Active Centres on the Carbon Surface by the Electrochemical Method in Oxygen Chemisorption. *Roczzniki Chemistry*, 39, pp 425-430.

[151] Flagan, R. C, and Semfeld, J. H. (1988). *Fundamentals of Air Pollution Engineering*. 1st ed. New Jersey, USA: Prentice Hall, pp. 217-219.

[152] Lisovskii, A., Shter, G., Semiat, R. and Aharoni, C. (1997). Adsorption of sulfur dioxide by active carbon treated by nitric acid: II. Effect of preheating on the adsorption properties. *Carbon*, 35(10-11), pp.1645-1648.

[153] Mochida, I., Korai, Y., Shirahama, M., Kawano, S., Hada, T., Seo, Y., Yoshikawa, M. and Yasutake, A. (2000). Removal of SOx and NOx over activated carbon fibers. *Carbon*, 38(2), pp.227-239.

[154] Perry, R. H., Green, D. W., and Maloney, J. O. (1997) *Perry's Chemical Engineers' Handbook*, 7th ed. New York, USA: McGraw-Hill, pp. 2-25.

[155] Yan, R., Liang, D., Tsen, L. and Tay, J. (2002). Kinetics and Mechanisms of H_2S Adsorption by Alkaline Activated Carbon. *Environmental Science & Technology*, 36(20), pp.4460-4466.

[156] Shi, L., Yang, K., Zhao, Q., Wang, H. and Cui, Q. (2015). Characterization and Mechanisms of H2S and SO_2 Adsorption by Activated Carbon. *Energy & Fuels*, 29(10), pp.6678-6685.

[157] Bagreev, A., Bashkova, S., Locke, D. and Bandosz, T. (2001). Sewage Sludge-Derived Materials as Efficient Adsorbents for Removal of Hydrogen Sulfide. *Environmental Science & Technology*, 35(7), pp.1537-1543.

[158] Kalvia, A. N., and Smith, J. W. (1983). Oxidation of Low Concentration of Hydrogen Sulfide by Air on Fixed Activated Carbon Bed. *Canadian Jouranl of Chemical Engineering*, 61, pp. 208-212.

[159] Steijns, M., and Mars, P. (1974). The Role of Sulfur Trapped in Micropores in the Catalytic Partial Oxidation of Hydrogen Sulfide with Oxygen. *Journal of Catalysis*, 35, pp. 11-17.

[160] Merryman, E. and Levy, A. (1967). Kinetics of Sulfur-Oxide Formation in Flames: II. Low Pressure H2S Flames. *Journal of the Air Pollution Control Association*, 17(12), pp.800-806.

[161] Uzun, D., Razkazova-Velkova, E., Beschkov, V. and Petrov, K. (2016). A Method for the Simultaneous Cleansing of H2S and SO2. *International Journal of Electrochemistry*, 2016, pp.1-5.

[162] Wondyfraw, M. (2014). Mechanisms and Effects of Acid Rain on Environment. *Journal of Earth Science & Climatic Change*, 05(06), pp.1000204 (1-3).

[163] Tubingchina.com. (2018). *Sulfuric Acid Corrosion | H2SO4 Corrosion | Sulphuric Acids*. [online] Available at: https://tubingchina.com/Sulfuric-Acid-H2SO4-Corrosion.htm [Accessed 17 Jun. 2019].

[163] tantaline.com. (2017). *Corrosion in Sulfuric acid (H_2SO_4)* [online] Available at: https://tantaline.com/technology/corrosion-performance/ [Accessed 17 Jun. 2019]

[164] Smith, S., Brown, B. and Sun, W. (2011). Corrosion at Higher H2S Concentrations and Moderate Temperatures. In: *NACE International Corrosion Conference & Expo*. [online] Houston (Texas), USA: NACE International Publications Division, pp.1-18. Available at: https://www.researchgate.net/profile/Stephen_Smith21/publication/261174947_Corrosion_at_Higher_H2S_Concentrations_and_Moderate_Temperatures/links/0deec5346ea8fe0d57000000/Corrosion-at-Higher-H2S-Concentrations-and-Moderate-Temperatures.pdf [Accessed 2 Jul. 2019].

[165] Sylvester, O., Celestine, O., Rueben, I. and Okechukwu, C. (2012). Review of Corrosion Kinetics and Thermodynamics of CO2 and H2S Corrosion Effects and Associated Prediction/Evaluation on Oil and Gas Pipeline System. *International Journal of Scientific & Technology Research*, 1(4), pp.156-162.

[166] Khaksar, L. and Shirokoff, J. (2017). Effect of Elemental Sulfur and Sulfide on the Corrosion Behavior of Cr-Mo Low Alloy Steel for Tubing and Tubular Components in Oil and Gas Industry. *Materials*, 10(4), pp.430-442.

[167] Feng, W., Kwon, S., Borguet, E. and Vidic, R. (2005). Adsorption of Hydrogen Sulfide onto Activated Carbon Fibers: Effect of Pore Structure and Surface Chemistry. *Environmental Science & Technology*, 39(24), pp.9744-9749.

[168] Zain, H., Nasri, N., Sidik, U., Abdulrasheed, A., Moshin, R., Majid, Z., Rashid, N. and Sharer, Z. (2017). Sulphur Dioxide and Oxygen Adsorption Isotherm Breakthrough Time on Surface Porous Palm Shell Activated Carbon. *Chemical Engineering Transactions*, 56, pp.211-216.

[169] Bagreev, A., Rahman, H. and Bandosz, T. (2001). Thermal regeneration of a spent activated carbon previously used as hydrogen sulfide adsorbent. *Carbon*, 39(9), pp.1319-1326.

[170] ATSM (American Society for Testing and Materials) International (2005). Standard Test Method for Determination of Butane Activity of Activated Carbon. D5742 - 95.

[171] Roztocki, K., Rauche, M., Bon, V., Kaskel, S., Brunner, E., and Matoga, D. (2021) Combining *In situ* Techniques (XRD, IR, and ^{13}C NMR) and Gas Adsorption Measurements Reveals CO_2-Induced Structural Transitions and High CO_2/CH_4 Selectivity for a Flexible Metal-Organic Framework JUK-8, *ACS Appl. Mater. Interfaces*, 13, pp.28503-28513.

[172] Farma, R., Fatjan, D., Awitdrus, A., and Bin Deraman, M. (2016). 'Physical properties of activated carbon from fibers of oil palm empty fruit bunches by microwave assisted potassium hydroxide activation', *AIP Conference Proceedings*, *6th International Conference on Theoretical and Applied Physics (ICTAP 2016)*, Makassar, Indonesia, 19th-21st September.

[173] Ao, W., Fu, J., Mao, X., Kang, Q., Ran, C., Liu, Y., Zhang, H., Gao, Z., Li, J., Liu, G., and Dai. J. (2018). 'Microwave Assisted Preparation of Activated Carbon From Biomass: A Review', *Renewable and Sustainable Energy Reviews*, 92, pp.958-979.

[174] Liu, Z., Zhou, X., Wu, F., and Liu, Z. (2020). 'Microwave-Assisted Preparation of Activated Carbon Modified By Zinc Chloride As A Packing Material For Column Separation of Saccharides', *ACS Omega.* 5(17), pp.10106-10114.

[175] Jensen, W. and Slaughter, M. (1982) Elemental Mapping of Minerals by Electron Microprobe, *American Mineralogist*, 67(5), pp, 521-533.

[176] Donovan, J., Lowers, H. and Rus, B. (2011) Improved Electron Probe Microanalysis of Trace Elementals in Quartz, *American Mineralogist*, 96(2), pp, 274-282.

[177] Fukushima, S., Kimura, T., Ogiwara, T., Tsukamoto, K., Tazawa, T. and Tanuma, S. (2008) New Model Ultra-soft X-ray Spectrometer for Microanalysis, *Microchima Acta,* 161(3), pp. 388-404.

[178] Shamsuddin. M. S., Yusoff. N. R. R., and Sulaiman. M. A. (2015) 'Synthesis and Characterization of Activated Carbon Produced From Kenaf Core Fiber Using H_3PO_4 Activation'. *Procedia Chemistry*. 19, pp.558-565.

[179] Manoj. B., and Kunjomana. (2012). 'Study of Stacking Structure of Amorphous Carbon by X-Ray Diffraction Technique', *International Journal of Electrochemical Science*. 7, pp.3127-3134

[180] Young-Whan. L., Jin-Won. P., Jae-Hoon. C., and Dae-Ki. C. (2002). 'Adsorption Characteristics of SO_2 on Activated Carbon Prepared From Coconut Shell With Potassium Hydroxide Activation', *Envriomental Science & Technology*. 36(5), pp.1086-1092.

[181] Sitthikhankaew. R., Predapitakkun. S., Kiattikomol. R. W., Pumhiran. S., Assabumrungrat. S., and Laosiripojana. N. (2011). 'Comparative Study of Hydrogen Sulfide Adsorption by Using Alkaline Impregnated Activated Carbons for Hot Fuel Gas Purification', *Energy Procedia*. 9, pp.15-24.

[182] Sitthikhankaew. R., Chadwick. R., Assabumrungrat. S., and Laosiripojana. N. (2014). 'Effects of Humidity, O_2, and CO_2 on H_2S adsorption Onto Upgraded and KOH Impregnated Activated Carbons', *Fuel Process Technology.* 124, pp.249-257.

[183] Guo. B., Chang. L., and Xie. K. (2006). 'Study of the Behaviour of Adsorbing CS_2 by Activated Carbon', *Fuel Processing Technology*. 87(10), pp.873-881.

[184] Li. L., Zheng. S., Li. H., and Keener. T. (2012) 'Effects of Activated Carbon Surface Properties on the Adsorption of Volatile Organic Compounds', *Journal of the Air & Waste Management Association*. 62(10), pp.1196-1202.

[185] Zhang. G., Chang. H., Wang. L., and Chou. K. (2018) 'Study on reduction of MoS_2 Powders with Activated Carbon to Produce Mo_2S Under Vacuum Conditions', *International Journal of Minerals, Metallurgy, and Materials*. 25, pp,405-412.

[186] Ahn. Y., Koo. W., Yoo. K., and Alorro. R. (2022) 'Carbothermic Reduction Roasting of Cathode Active Materials Using Activated Carbon and Graphite to Enhance the Sulphuric-Acid-Leaching Efficiency of Nickel and Cobalt', *Materials*. 12(8), pp.1021

[187] Robinson, J., Kingman, S., Irvine, D., Licence, P., Smith, A., Dimitrakis. G., Obermayer, D., and Kappe, O. C. (2010) 'Understanding Microwave Heating Effects in Single Mode Type Cavities – Theory and Experiment', *Physical Chemistry Chemical Physics*. 18(12), pp4750-4758.

[188] Kappe, O. C., Dallinger, D., and Murphee, S. S. (2004) 'Practical Microwave Synthesis for Organic Chemists – Strategies, Instruments, and Protocols', *Angewandte Chemie*. 48(16), pp. 2828-2829.

[189] Kappe, O. C. (2004) 'Controlled Microwave Heating in Modern Organic Synthesis', *Angewandte Chemie.* 43(46), pp.6250-6584.

[190] Adam, M. 2017, ' Understanding Microwave Pyrolysis of Biomass Materials', PhD thesis, University of Nottingham, Nottingham, United Kingdom.

[191] Green, D.W. and Perry, R.H. (2007) Perry's Chemical Engineers' Handbook. 8th Edition, McGraw-Hill Professional, New York.

[192] Alfa Aesar (2020) *L14479 Kerosene, low odour,* Available at: https://www.alfa.com/en/catalog/L14479/ (Accessed: 12 April 2022).

[193] NIOSH (2014) *International Chemical Safety Cards (ICSC): Distillates (Petroleum), Hydrotreated Light* [Online]. The National Institute for Occupational Safety and Health (NIOSH). Available at: http://www.cdc.gov/niosh/ipcsneng/neng1379.html (Accessed: 12 April 2022).

[194] Cao, C., Chen, J., Islam, M. N., Xu, W., and Zhong, S. (2019) 'Effect of Intermittenet Microwave Volumetric Heating on Dehydration, Energy Consumption, Antioxidant Substances, and Sensory Qualities of Litchi Fruit during Vacuum Drying' , *Molecules*. 24(23), pp. 4291.

[195] Qiao, Z. and Xie, X. (2016). The Effects of Electric Field Intensification at Interparticle Contacts in Microwave Sintering. *Scientific Reports*, 6, pp. 32163.

[196] Kebsi, O, M., Rajabipour, A., Omid, M. and Goldansaz, S. (2019) Determination od Electric Field Intensity During Microwave Heating of Selected Vegetables and Fruits. *Journal od Microwave Power and Electromagnetic Energy*, 52(4), pp. 276-286.

[197] Hassani, Fe., Nekoovaght, P. M. and Gharib. N. (2016) The Influence of Microwave Irradiation on Rocks for Microwave-assisted Underground Excavation. *Journal of Rocl Mechanics and Geotechnical Engineering*, 8(1), pp. 1-15

[198] Anton Parr (2018) *Which Microwave Synthesis Reactor is the Best One For Your Research?* [Online]. Anton Parr Ltd. Available at: https://wiki.anton-paar.com/uk-en/which-microwave-synthesis-reactor-is-the-best-one-for-your-research/ (Accessed: 16 April 2022).

[199] Gaba, M. and Dhingra, N. (2011) Microwave Chemistry: General Features and Applications. *Indian Journal of Pharmacuetical Education and Research,* 45, pp. 175-183.

[200] Stadler, A., Yousefi, B. H., Dallinger, D., Walla, P., Van der Eycken, E., Kaval, N. and Kappe, C. O. (2003). Scalability of Microwave-Assisted Organic Synthesis. From Single-Mode to Multimode Parallel Batch From Single-Mode to Multimode Parallel Batch Reactors. *Organic Process Research Development*, 7, pp. 794-806.

[201] Stefanidis, G. D., Muñoz, A. N., Strum, G. S. J. and Stankiewicz, A. (2014). A Helicopter View of Microwave Application to Chemical Processes: Reactions, Separations, and Equipment Concepts. *Reviews in Chemical Engineering,* 30(3), pp. 233-259.

[202] Asmussen, J., Lin, H. H., Manring, B. and Fritz, R. (1987), Single-Mode or Controlled Multimode Microwave Cavity Applicators for Precision Materials Processing. *Review of Scientific Instruments*, 58, pp. 1477.

[203] DÍaz-Blancas, V., Aguilar-Madera, C. G., Flores-Cano, J. V., Leyva-Ramos, R., Padilla-Ortega, E. and Ocampo-Pérez. (2020). Evaluation of Mass Transfer Mechanisms Involved During the Adsorption of Metronidazole on Granular Activated Carbon in Fixed Bed Column, *Journal of Water Processing Engineering*, 36, pp. 101303.

[204] Eder, S., Müller, K., Azzari, P., Arcifa, P., Peydayesh, M. and Nyström. (2021) Mass Transfer Mechanism and Equilibrium Modelling of Hydroxytyrosal Adsorption on Olive Pit-Derived Activated Carbon, *Chemical Engineering Journal*, 404, pp. 126519.

[205] Junjie, G. and Hans-Jörg, B. (2005). Heat and Mass Transfer in Steam Desorption of and Activated Carbon Adsorber, *International Communications in Heta and Mass Transfer*, 32(4), pp. 296-304.

[206] Cai, Y., Liu, L., Tian, H., Yang, Z. and Luo, X. (2019) Adsorption Desorption Performance and Mechanism of Tetrcycline Hydrochloride by Activated Carbon -Based Adsorbents Derived from Sugar Cane Bagasse Activated with $ZnCl_2$, *Molecules*, 24(24), pp. 4535.

[207] Mao, Y., Robinson, J. and Binner, E. (2021). Understanding Heat and Mass Transfer Processes During Microwave-assisted and Conventional Solvent Extraction. *Chemical Engineering Science*. 223, pp. 116418

[208] Kostas, E. T., Williams, O. S. A., Duran-Jimenez, G., Tapper, A. J., Cooper, M., Meehan, R., & Robinson, J. P. (2019). Microwave pyrolysis of laminaria digitata to produce unique seaweed-derived bio-oils. *Biomass and Bioenergy,* 125, pp.41-49.

[209] Robinson, J., Binner, E. R., Vallejo, D. B., Diaz Perez, N., Al Mughairi, K., Ryan. J., Shepard, B., Adam, A., Budarin, V., Fan J., Gronnow, M., and Peneranda-Foix, F. (2022). Unravelling the mechanisms of microwave Pyrolysis of biomass, *Chemical Engineering Journal*, 430, pp. 132975.

[210] Ogunniran, O., Binner, E. R., Sklavounos A. H., and Robinson, J. P. (2017). Enhancing evaporative mass transfer and steam stripping using microwave heating, *Chemical Engineering Journal*, 165, pp.147-153.

[211] E. Worch, Adsorption kinetics, Adsorption Technology in Water Treatment, Fundamentals, Processes, and Modeling, De Gruyter, Berlin, Boston, 2012, pp. 123–168.

[212] Cooney, D. O. (1993) Comparison of Simple Adsorber Breakthrough Curve Method with Exact Solution, *American Institute of Chemical Engineering Journal*, 39, pp. 355-358.

[213] Leckner, B. (2021) Heat and Mass Transfer to/from Active Particles in a Fluidized bed Bed – An Analysis of the Baskakov-Palchonock Correlation, *International Journal of Heat and Mass Transfer*, 168, pp. 120860.

[214] Ma, F. and Shen, Z. -Q. (2004) Connective Heat Transfer Enhancement by Inert Gas Injection, *Dalian Ligong Daxue Xuebao / Journal of Dalian University of Technology*, 44(4), pp. 490-494.

[215] Christoph, R. E. and Turner, L. (1995) Heat Transfer in Granular Activated Carbon Beds in the Presence of Adsorbable Gases, *International Journal of Heat and Mass Transfer*, 38(9), pp. 1577-1585.

[216] Xiao, J., Tong, L. A., Deng, C. H., Bénard, P. and Chahine, R. (2010) Simulation of Heat and Mass Transfer in Activated Carbon Tank for Hydrogen Storage, *International Journal of Hydrogen Energy*, 35(15), pp. 8106-8116.

10. Appendix

10.1 Appendix A – Methods

Inserting gas calculations for single-mode microwave waveguide

The purpose of using purging gas, which is nitrogen, is to keep the oxygen concentration in the cavity and the waveguide below 5%v/v. This ensures that the contents of the cavity will not catch fire.

The following equation (adopted from PD CEN/TR 15281:2006) was used to estimate the quantity of the inert gas required to purge the system:

$$t = \frac{-V}{Q} \ln\left(\frac{c_f}{c_i}\right)$$

Where: t = Time

V = System volume

Q = Purge gas flowrate

C_F = Oxygen concentration after slow purging (fractional)

C_I = Concentration of oxygen in inert gas

Where t is the time required to reduce the oxygen concentration from an initial concentration c_i = 21% to a final concentration c_t = 5% applying an inert gas flow Q (taken as 200 mL/min) to the glass tube which has a volume V = 200 mL. Substituting these values gives:

$$t = \frac{-200[mL]}{200[\frac{mL}{min}]} \ln\left(\frac{5}{21}\right) = 1.435 \text{ min} = 86.1 \; second$$

For the experimental the reactor was purged for at least 2 mins at 200 mL/min before starting the microwave heating.

When running under wet conditions, the cavity would be purged with nitrogen at flowrate, Q, of 10L/min. The cavity has a volume, V, of 4.5 L. Substituting these values gives:

$$t = \frac{-4.5[L]}{10[\frac{L}{min}]} \ln\left(\frac{5}{21}\right) = 0.323 \text{ min} = 38.8 \; second$$

For the experiment the cavity would be purged for at least 60 seconds at 10L/min before starting the microwave heating.

Inserting gas calculations for multimode microwave waveguide

The purpose of using purging gas, which is nitrogen, was to keep the oxygen concentration in the cavity and the waveguide below 5%v/v. This ensures that the contents of the cavity will not catch fire in cases of failure such as broken glass and/or arcing.

The following equation (adopted from PD CEN/TR 15281:2006) wass used to estimate the quantity of the inert gas required to purge the system:

$$t = \frac{-V}{Q} \ln\left(\frac{c_f}{c_i}\right)$$

Where: t = Time

V = System volume

Q = Purge gas flowrate

C_F = Oxygen concentration after slow purging (fractional)

C_I = Concentration of oxygen in inert gas

Where t is the time required to reduce the oxygen concentration from an initial concentration c_i = 21% to a final concentration c_t = 5% applying an inert gas flow Q (taken as 10L/min) to the system which has a volume V = 17.5L. Substituting these values gives:

$$t = \frac{-17.5[L]}{10[\frac{L}{min}]} \ln\left(\frac{5}{21}\right) = 2.5 \text{ min} = 150 \; seconds$$

For the experiment the system will be purged for at least 3 mins at 10L/min before starting the microwave heating.

Calculation of Maximum and minimum Energy Input

With no heat losses, the energy required to heat the activated carbon (AC) sample can be calculated from:

$$Q = Cp\ (T - T_0)$$

Where: Q = Energy required to heat activated carbon, ^oC

C_p = Activated carbon's specific heat capacity, ~1.5 J/(g·K)

T = Sample's final temperature, with maximum 500 °C

T_o = Initial temperature, 20 °C

Thus the energy required to heat the AC sample to 500^{o}C with no heat losses is ~0.72 kJ/g
Taking into consideration the heat losses, an energy input in the range between 0.5 to 2 kJ/g was studied by varying the power input between 0 and 2 kW.

Liquid to solid sample ratio

A maximum energy input of 3 kJ/g is taken.

Hexane has a boiling point of 69 °C which suggested that part of it will be evaporated during the regeneration experiment. It is important to have enough liquid in the reactor to ensure the inert atmosphere during the heating. To calculate the minimum amount of liquid, it was assumed that all the energy absorbed by the solid sample material is transferred to the liquid (which was at room temperature, 20^{o}C) at the start of the experiment.

The energy required to evaporate the liquid molecules is the sum of the sensible heat and its latent heat of vaporisation = $0.00185\ kJ/(g.K)\ (69-20)K + 0.39\ \ kJ/g = 0.37\ kJ/g$

The minimum liquid to solid ratio = $3/0.37$ = 2.7:1 on a mass basis. This is equivalent to 8.1 ml liquid per each gram of the solid sample material.
As a safety margin a ration of 10ml hexane/1 g solid will be used.

Kerosene has a boiling point of 250 °C which suggested that part of it would be evaporated during the regeneration experiment. It was important to have enough liquid in the reactor to ensure the inert atmosphere during the heating. To calculate the minimum amount of liquid,

it will be assumed that all the energy absorbed by the solid sample material is transferred to the liquid which is at room temperature (20^{o}C) at the start of the experiment.

The energy required to evaporate the liquid molecules is the sum of the sensible heat and its latent heat of vaporisation = $0.00185\ kJ/(g.K)\ (250-20)K + 0.39\ \ kJ/g = 0.000083\ kJ/g$

The minimum liquid to solid ratio = $3/0.000083$ = 20:1 on a mass basis. This is equivalent to 36 ml liquid per each gram of the solid sample material.
As a safety margin a ration of 20ml hexane/1 g solid will be used.

10.2 Appendix B – All data for tables

The following tables show all the data collected to create the corresponding tables.

Table 4.

Time	Mass change (%)	Average (%)	Standard deviation	Butane activity (%)	Average (%)	Standard deviation	Specific energy input (kJ.g $^{-1}$)	Average (kJ.g -1)	Standard deviation
120	41.08 45.67 43.98	43.58	2.32	24.01 26.39 23.56	24.65	1.52	3.71 3.79 3.75	3.75	0.04
180	44.77 49.12 47.44	47.11	2.19	28.07 30.12 30.69	29.63	1.38	6.20 6.22 6.36	6.26	0.09
240	47.02 50.12 50.89	49.34	2.05	32.77 29.12 30.70	30.86	1.83	9.02 9.48 9.60	9.37	0.31
360	54.41 49.90 49.97	51.43	2.58	32.42 33.88 33.98	33.43	0.87	12.68 12.87 13.14	12.90	0.23

Table 5.

Power (W)	Time (s)	Mass change (%)	Average (%)	Standard deviation	Butane activity (%)	Average (%)	Standard deviation	Specific energy input (kJ.g $^{-1}$)	Average (kJ.g $^{-1}$)	Standard deviation
200	240	29.00 28.31 30.64	29.32	1.20	14.26 14.89 17.10	15.42	1.49	3.46 3.47 3.49	3.47	0.02
400	180	46.99 46.59 48.50	47.36	1.01	29.45 29.07 29.99	29.50	0.46	6.21 6.21 6.27	6.23	0.03
600	120	30.87 30.64 33.52	31.68	1.60	19.01 14.70 16.53	16.75	2.16	5.02 5.04 5.24	5.10	0.12
800	60	43.71 46.22 44.89	44.94	1.26	18.89 24.33 23.87	22.36	3.02	3.87 3.82 4.11	3.93	0.16

Table 7.

	Time (s)	Mass change (%)	Average mass change (%)	Standard deviation	Butane activity (%)	Average butane activity (%)	Standard deviation	Specific energy input (kJ.g $^{-1}$)	Average specific energy input (kJ.g $^{-1}$)	Standard deviation
Hexane	120	14.01 16.87 12.32	14.40	2.30	2.25 2.32 2.50	2.36	0.13	21.45 24.59 19.39	21.81	2.62
	180	15.23 15.00 17.54	15.92	1.40	2.36 2.36 2.79	2.50	0.25	33.50 33.10 42.33	36.31	5.22
	240	19.01 15.47 15.59	16.69	2.01	2.80 2.33 2.31	2.48	0.28	58.01 52.12 51.24	53.79	3.68
	360	16.92 18.44 16.83	17.40	0.90	2.39 2.33 2.46	2.39	0.07	60.89 70.12 61.13	64.05	5.26
Kerosene	120	12.36 13.40 17.08	14.28	2.48	2.09 2.08 2.11	2.09	0.02	18.87 19.32 22.30	20.16	1.86
	180	15.01 15.92 16.31	15.75	0.67	2.20 2.34 2.34	2.29	0.08	33.00 33.81 42.12	36.31	5.05
	240	14.60 18.55 18.27	17.14	2.20	2.27 2.34 2.35	2.32	0.04	58.72 69.12 68.01	65.28	5.71
	360	19.95 15.34 16.99	17.43	2.34	2.65 2.19 2.47	2.44	0.23	78.12 62.43 69.12	69.89	7.87

Table 8.

	Time (s)	Mass change (%)	Average mass change (%)	Standard deviation	Butane activity (%)	Average butane activity (%)	Standard deviation	Specific energy input (kJ.g $^{-1}$)	Average specific energy input (kJ.g $^{-1}$)	Standard deviation
Hexane	200	14.71 16.10 16.52	15.78	0.95	2.10 2.19 2.27	2.19	0.09	26.41 28.62 26.99	27.34	1.15
	400	12.31 17.71 18.69	16.24	3.44	2.22 2.44 2.45	2.37	0.13	38.34 36.12 39.49	37.98	1.71
	600	17.44 17.84 19.10	18.13	0.87	2.39 2.16 2.67	2.41	0.26	33.11 33.98 34.05	33.71	0.52
	800	20.11 14.16 17.95	17.41	3.01	2.29 2.21 2.34	2.28	0.07	20.99 23.74 23.12	22.62	1.44
Kerosene	200	19.51 13.32 18.49	17.11	3.32	2.22 2.28 2.24	2.25	0.03	21.44 23.12 24.47	23.01	1.52
	400	14.61 15.97 15.72	15.43	0.72	2.30 2.33 2.27	2.30	0.03	38.09 40.12 37.07	38.43	1.55
	600	21.05 16.42 17.74	18.40	2.39	2.30 2.38 2.32	2.33	0.04	35.99 35.71 37.07	36.26	0.72
	800	15.71 17.53 22.05	18.43	3.26	2.22 2.25 2.37	2.28	0.08	22.12 29.51 24.99	25.54	3.73

Table 9.

Time (s)	Mass change (%)	Average (%)	Standard deviation	Butane activity (%)	Average (%)	Standard deviation	Specific energy input (kJ.g $^{-1}$)	Average (kJ.g $^{-1}$)	Standard deviation
120	19.01 18.71 19.97	19.23	0.66	7.94 8.03 8.02	8.00	0.05	17.89 18.42 18.90	18.40	0.51
180	39.82 39.72 41.08	40.21	0.76	26.16 26.66 26.32	26.38	0.26	19.32 19.42 21.32	20.02	1.13
240	43.87 44.28 44.34	44.16	0.26	28.88 30.95 31.17	30.33	1.26	21.33 22.99 23.04	22.45	0.97
360	41.67 45.36 46.19	44.41	2.41	32.75 33.99 34.12	33.62	0.76	24.00 27.06 26.85	25.97	1.71

Table 10.

Power (W)	Mass change (%)	Average (%)	Standard deviation	Butane activity (%)	Average (%)	Standard deviation	Specific energy input ($kJ.g^{-1}$)	Average ($kJ.g^{-1}$)	Standard deviation
120	15.12 15.39 15.44	15.32	0.17	18.80 18.99 18.88	18.89	0.10	4.54 4.59 4.56	4.56	0.03
180	17.76 17.64 17.78	17.73	0.08	20.60 20.64 20.95	20.73	0.19	6.55 6.59 6.77	6.64	0.12
240	19.79 19.71 19.81	19.77	0.05	21.07 21.09 20.87	21.01	0.12	9.73 9.64 9.65	9.67	0.05
360	22.01 22.59 22.88	22.49	0.44	22.93 22.99 22.91	22.94	0.04	13.50 13.74 13.55	13.60	0.13

Table 11.

Power (W)	Mass change (%)	Average mass change (%)	Standard deviation	Butane activity (%)	Average butane activity (%)	Standard deviation	Specific energy input (kJ.g $^{-1}$)	Average specific energy input (kJ.g $^{-1}$)	Standard deviation
200	8.69 8.73 8.65	8.69	0.04	10.44 10.80 10.36	10.53	0.23	3.44 3.49 3.33	3.42	0.08
400	17.66 17.80 17.71	17.72	0.07	19.58 21.00 21.45	20.68	0.98	6.62 6.80 6.90	6.77	0.14
600	12.17 12.22 12.10	12.16	0.06	20.11 22.47 20.99	21.19	1.19	6.74 6.66 6.81	6.74	0.08
800	14.00 14.52 14.63	14.38	0.34	20.07 20.09 20.38	20.18	0.17	7.06 6.91 7.08	7.02	0.09

Table 12.

Power (W)	Time (s)	Mass change (%)	Average (%)	Standard deviation	Butane activity (%)	Average (%)	Standard deviation	Specific energy input (kJ.g -1)	Average (kJ.g -1)	Standard deviation
200	120	4.69 4.73 4.64	4.69	0.05	10.34 10.39 10.40	10.38	0.03	1.32 1.44 1.47	1.41	0.08
	240	5.62 5.81 5.86	5.76	0.13	12.30 12.44 12.22	12.32	0.11	3.55 3.53 3.72	3.60	0.10
400	120	17.02 17.99 17.91	17.64	0.54	19.55 19.41 19.67	19.54	0.13	4.70 4.59 4.88	4.72	0.15
	240	22.63 22.89 22.99	22.84	0.19	21.88 21.77 21.88	21.84	0.06	9.29 9.07 9.32	9.23	0.14
600	120	18.12 18.31 18.20	18.21	0.10	21.22 21.25 21.02	21.16	0.13	6.15 6.17 6.33	6.22	0.10
	240	28.00 28.17 28.47	28.21	0.24	24.01 24.01 24.07	24.03	0.03	12.59 12.51 12.77	12.62	0.13
800	120	18.88 18.87 18.52	18.76	0.21	21.28 21.14 21.32	21.25	0.09	8.00 8.06 8.07	8.04	0.04
	240	32.37 32.31 32.19	32.29	0.09	29.23 29.28 29.39	29.30	0.08	15.90 15.85 15.95	15.90	0.05

Table 13 (200 W, 400 W)

Power (W)	Time (s)	Mass change (%)	Average (%)	Standard deviation	Butane activity (%)	Average (%)	Standard deviation	Specific energy input (kJ.g -1)	Average (kJ.g -1)	Standard deviation
200	120	8.03 8.13 8.19	8.12	0.08	10.45 10.51 10.67	10.54	0.11	2.11 2.08 2.19	2.13	0.06
	180	9.87 9.91 10.09	9.96	0.12	11.22 11.13 11.36	11.24	0.12	3.01 3.00 3.18	3.06	0.10
	240	8.55 8.89 8.72	8.72	0.17	12.33 12.47 12.39	12.40	0.07	3.20 3.49 3.89	3.53	0.35
	360	10.33 10.39 10.56	10.43	0.12	13.00 13.33 13.12	13.15	0.17	5.05 5.49 5.51	5.35	0.26
400	120	15.88 15.02 15.82	15.57	0.48	18.82 18.14 18.93	18.63	0.43	4.87 4.33 4.34	4.51	0.31
	180	17.76 17.61 17.55	17.64	0.11	20.88 20.88 20.61	20.79	0.16	6.32 6.33 6.99	6.55	0.38
	240	19.77 19.88 19.82	19.82	0.06	21.00 21.34 20.87	21.07	0.24	7.30 7.77 7.52	7.53	0.24
	360	22.22 22.60 22.58	22.47	0.21	22.84 22.76 22.91	22.84	0.08	13.42 13.12 13.76	13.43	0.32

Table 13 (600 W, 800 W)

Power (W)	Time (s)	Mass change (%)	Average (%)	Standard deviation	Butane activity (%)	Average (%)	Standard deviation	Specific energy input (kJ.g -1)	Average (kJ.g -1)	Standard deviation
600	120	12.12 12.01 12.37	12.17	0.18	21.01 21.11 21.26	21.13	0.13	6.12 6.89 6.81	6.61	0.42
	180	18.88 18.22 18.33	18.48	0.35	22.32 22.57 22.40	22.43	0.13	7.65 8.74 9.11	8.50	0.76
	240	18.77 18.78 18.73	18.76	0.03	24.34 24.24 24.12	24.23	0.11	12.93 12.91 13.30	13.05	0.22
	360	22.82 23.07 23.01	22.97	0.13	27.11 27.19 27.16	27.15	0.04	18.01 18.34 18.56	18.30	0.28
800	120	16.44 16.32 16.57	16.44	0.13	21.49 21.67 21.70	21.62	0.11	7.41 7.77 7.69	7.62	0.19
	180	19.98 20.45 19.62	20.02	0.42	22.93 22.77 23.10	22.93	0.17	10.67 10.84 10.70	10.74	0.09
	240	22.20 22.67 22.21	22.36	0.27	29.42 29.91 29.56	29.63	0.25	14.35 14.36 14.89	14.53	0.31
	360	27.56 27.77 27.77	27.70	0.12	32.77 32.76 32.81	32.78	0.03	24.12 24.39 24.17	24.23	0.14

Table 14. (50 W – 100 W)

	Time (s)	Mass change (%)	Average (%)	Standard deviation	Butane activity (%)	Average (%)	Standard deviation	Specific energy input (kJ.g -1)	Average (kJ.g -1)	Standard deviation
50 W	360	4.98 5.05 5.12	5.05	0.07	5.44 5.46 5.49	5.46	0.03	1.39 1.67 1.72	1.59	0.18
	480	5.89 6.31 6.30	6.17	0.24	10.11 10.27 10.19	10.19	0.08	1.90 2.09 2.01	2.00	0.10
	960	7.22 7.22 7.69	7.38	0.27	12.94 12.99 12.77	12.90	0.12	4.23 4.10 4.35	4.23	0.13
	1200	8.01 8.23 7.67	7.97	0.28	13.01 13.11 13.00	13.04	0.06	5.03 5.37 5.89	5.43	0.43
100W	360	12.55 12.12 12.67	12.45	0.29	10.42 10.68 10.93	10.68	0.26	2.91 2.43 3.10	2.81	0.35
	480	14.01 14.88 14.12	14.34	0.47	16.20 16.67 16.61	16.49	0.26	3.44 3.66 3.57	3.56	0.11
	960	13.92 13.90 14.21	14.01	0.17	17.18 17.00 17.45	17.21	0.23	6.10 6.01 6.26	6.12	0.13
	1200	13.45 13.01 12.88	13.11	0.30	21.40 21.18 21.77	21.45	0.30	7.88 7.56 7.41	7.62	0.24

Table 14 (150 W – 200 W)

Power (W)	Time (s)	Mass change (%)	Average (%)	Standard deviation	Butane activity (%)	Average (%)	Standard deviation	Specific energy input (kJ.g -1)	Average (kJ.g -1)	Standard deviation
150 w	360	18.00 18.89 18.07	18.32	0.49	20.65 20.50 20.85	20.67	0.18	3.45 3.37 3.53	3.45	0.08
	480	20.67 20.66 20.42	20.58	0.14	27.00 27.20 27.19	27.13	0.11	4.70 4.75 4.78	4.74	0.04
	960	21.20 21.19 21.26	21.22	0.04	31.44 31.40 31.45	31.43	0.03	9.89 9.85 10.03	9.92	0.09
	1200	21.88 21.41 22.01	21.77	0.32	31.70 31.30 31.94	31.65	0.32	13.90 13.99 13.94	13.94	0.05
200 w	360	29.11 29.34 29.27	29.24	0.12	33.74 33.70 33.99	33.81	0.16	6.19 6.25 6.28	6.24	0.05
	480	24.77 24.64 24.76	24.72	0.07	34.01 34.25 34.00	34.09	0.14	7.45 8.21 8.01	7.89	0.39
	960	28.60 28.77 28.69	28.69	0.09	40.31 40.19 40.44	40.31	0.13	16.08 16.47 16.22	16.26	0.20
	1200	29.00 29.05 28.85	28.97	0.10	40.74 40.62 40.83	40.73	0.11	19.06 19.49 19.37	19.31	0.22

Table 15. (50 W – 100 W)

	Time (s)	Mass change (%)	Average (%)	Standard deviation	Butane activity (%)	Average (%)	Standard deviation	Specific energy input (kJ.g -1)	Average (kJ.g -1)	Standard deviation
50 W	360	3.55 3.75 3.62	3.64	0.10	3.82 3.99 4.11	3.97	0.15	1.19 1.22 1.17	1.19	0.03
	480	4.40 4.32 4.49	4.40	0.09	7.33 7.19 7.45	7.32	0.13	1.42 1.43 1.49	1.45	0.04
	960	5.35 5.29 5.42	5.35	0.07	9.44 9.67 9.66	9.59	0.13	3.06 3.09 3.10	3.08	0.02
	1200	5.71 5.88 5.81	5.80	0.09	9.61 9.63 9.74	9.66	0.07	3.70 3.65 3.80	3.72	0.08
100W	360	10.37 10.20 10.61	10.39	0.21	8.72 9.00 8.84	8.85	0.14	2.39 2.02 2.42	2.28	0.22
	480	11.38 11.55 11.67	11.53	0.15	13.22 13.45 13.71	13.46	0.25	2.88 2.87 2.96	2.90	0.05
	960	11.44 11.41 11.40	11.42	0.02	14.06 14.21 13.96	14.08	0.13	5.09 5.33 5.00	5.14	0.17
	1200	10.21 10.77 10.50	10.49	0.28	17.61 17.55 17.70	17.62	0.08	6.12 6.10 6.33	6.18	0.13

Table 15 (150 W – 200 W)

	Time (s)	Mass change (%)	Average (%)	Standard deviation	Butane activity (%)	Average (%)	Standard deviation	Specific energy input (kJ.g $^{-1}$)	Average (kJ.g $^{-1}$)	Standard deviation
150 w	360	15.55 15.92 15.87	15.78	0.20	18.07 18.00 18.22	18.10	0.11	3.07 3.11 2.98	3.05	0.07
	480	17.82 17.99 18.02	17.94	0.11	23.55 23.40 23.59	23.51	0.10	4.19 4.00 3.92	4.04	0.14
	960	18.20 18.57 18.52	18.43	0.20	27.22 27.88 27.50	27.53	0.33	8.59 8.81 8.67	8.69	0.11
	1200	19.06 18.85 19.02	18.98	0.11	27.45 27.71 27.60	27.59	0.13	12.10 12.10 12.81	12.34	0.41
200 w	360	20.48 20.22 20.49	20.40	0.15	25.29 25.49 22.45	24.41	1.70	5.19 5.11 5.26	5.19	0.08
	480	20.88 20.86 20.62	20.79	0.14	29.44 29.29 29.55	29.43	0.13	6.95 7.18 7.03	7.05	0.12
	960	22.31 22.19 22.44	22.31	0.13	35.47 35.00 35.88	35.45	0.44	13.70 13.72 13.85	13.76	0.08
	1200	24.97 24.99 24.90	24.95	0.05	38.45 38.79 38.92	38.72	0.24	17.05 17.40 17.10	17.18	0.19

Table 16.

N_2 flowrate (L.min $^{-1}$)	Mass change (%)	Average (%)	Standard deviation	Butane activity (%)	Average (%)	Standard deviation
0.25	19.31 25.11 21.59	22.00	2.92	29.11 33.71 32.12	31.65	2.34
0.50	22.01 26.82 25.97	24.93	2.57	39.21 38.12 32.16	36.50	3.80
0.75	21.36 22.81 22.05	22.07	0.73	35.22 35,81 37.03	36.13	1.28
1.00	23.42 22.87 23.14	23.14	0.28	36.41 37.00 36.11	36.51	0.45
2.00	24.34 24.67 24.62	24.54	0.18	42.31 42.66 42.54	42.50	0.18

Table 17. (360s)

Time (s)	Temperature (°C)	Mass change (%)	Average (%)	Standard deviation	Butane activity (%)	Average (%)	Standard deviation
360	100	26.87 28.24 29.12	28.08	1.13	37.87 40.71 40.28	39.62	1.53
	120	28.02 29.01 28.83	28.62	0.53	43.21 39.02 39.96	40.73	2.20
	140	29.12 29.45 29.47	29.35	0.20	42.66 42.03 42.11	42.27	0.34
	160	29.94 29.71 29.06	29.57	0.46	42.22 43.98 42.65	42.95	0.92
	180	28.66 28.65 28.99	28.77	0.19	43.66 43.29 43.71	43.55	0.23
	200	29.55 28.39 28.59	28.84	0.62	44.11 46.40 45.09	45.20	1.15

Table 17 (960s)

Time (s)	Temperature (°C)	Mass change (%)	Average (%)	Standard deviation	Butane activity (%)	Average (%)	Standard deviation
960	100	30.55	29.62	1.21	46.01	46.47	0.40
		30.06			46.77		
		28.26			46.63		
	120	29.37	29.73	0.32	45.72	45.74	0.04
		29.99			45.71		
		29.84			45.79		
	140	30.66	30.75	0.16	46.89	46.63	0.23
		30.65			46.55		
		30.94			46.46		
	160	30.49	30.38	0.10	47.01	47.08	0.12
		30.33			47.00		
		30.32			47.22		
	180	29.00	29.20	0.30	47.23	47.36	0.12
		29.06			47.40		
		29.55			47.45		
	200	30.69	30.89	0.17	47.59	47.50	0.10
		30.99			47.51		
		30.99			47.39		

Table 18.

Power (W)	Time (s)	Mass change (%)	Average (%)	Standard deviation	Butane activity (%)	Average (%)	Standard deviation	Specific energy input (kJ.g $^{-1}$)	Average (kJ.g $^{-1}$)	Standard deviation
200	120	28.32 28.77 29.25	28.78	0.47	40.60 40.21 40.90	40.57	0.35	2.26 2.27 2.37	2.30	0.06
	360	29.77 30.31 30.72	30.27	0.48	43.30 43.99 43.36	43.55	0.38	6.59 6.70 6.74	6.68	0.08
400	120	29.72 28.71 28.99	29.14	0.52	42.55 42.75 42.87	42.72	0.16	5.45 5.51 5.54	5.50	0.05
	360	30.77 31.02 30.27	30.69	0.38	45.27 46.07 45.21	45.52	0.48	14.77 14.82 14.21	14.60	0.34
600	120	33.03 32.46 32.87	32.79	0.29	42.72 42.63 41.22	42.19	0.84	7.67 7.82 7.83	7.77	0.09
	360	33.37 34.24 32.70	33.43	0.77	45.73 44.66 45.78	45.39	0.63	18.16 17.95 18.28	18.13	0.17
800	120	37.85 37.88 39.22	38.32	0.78	41.17 41.38 41.22	41.26	0.11	9.47 9.41 9.36	9.41	0.06
	360	40.28 40.70 40.34	40.44	0.23	40.28 40.27 40.26	40.27	0.01	22.73 22.64 22.88	22.75	0.12

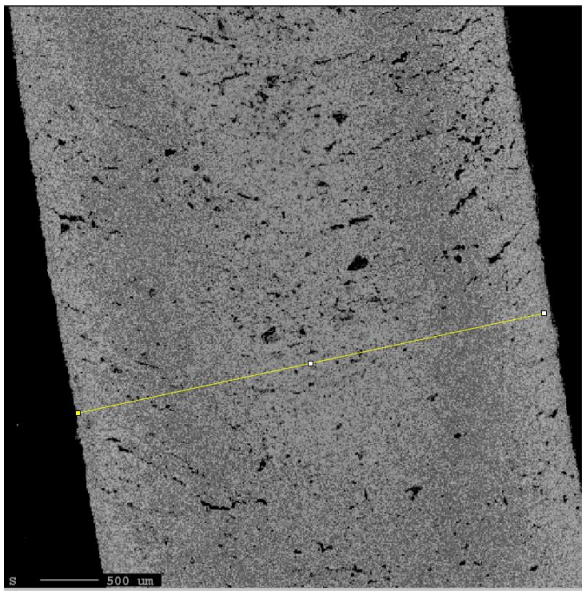
Table 19.

Time (s)	Mass change (%)	Average (%)	Standard deviation	Butane activity (%)	Average (%)	Standard deviation	Specific energy input (kJ.g -1)	Average (kJ.g -1)	Standard deviation
30	13.28 6.53 7.49	9.10	3.65	12.24 11.29 13.83	12.45	1.28	0.53 0.48 0.58	0.53	0.05
60	14.27 14.64 12.95	13.96	0.89	21.59 26.84 22.06	23.50	2.90	1.09 1.31 1.01	1.14	0.16
90	19.10 15.71 20.28	18.36	2.37	31.88 33.93 29.13	31.64	2.41	1.45 1.63 1.59	1.56	0.09
120	24.9004 24.78 24.17582	24.62	0.39	40.24 42.86 42.68	41.92	1.46	2.02 1.98 2.31	2.10	0.18
360	29.23 30.05 28.87	29.38	0.60	42.20 43.51 43.31	43.01	0.71	6.03 6.44 6.21	6.23	0.21
960	31.71 30.11 29.22	30.35	1.26	48.40 47.63 45.14	47.06	1.71	16.03 15.79 16.20	16.01	0.21
1200	33.27 32.70 32.05	32.67	0.61	49.44 47.07 48.52	48.34	1.20	20.33 20.00 20.56	20.30	0.28

10.3 Appendix C – Additional EPMA data

Figure 28

Grayscale image of AC cross section EPMA scan:



Profile intenisty plot of the greyscale changes across the draw line shown in above image:

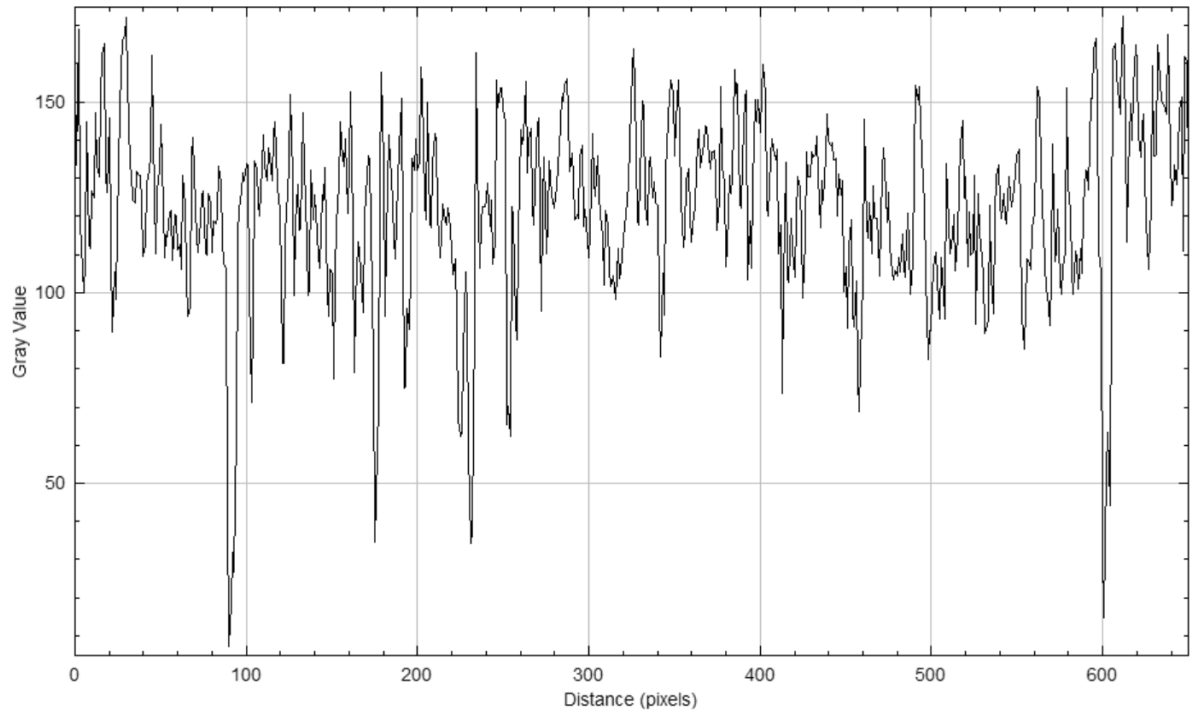
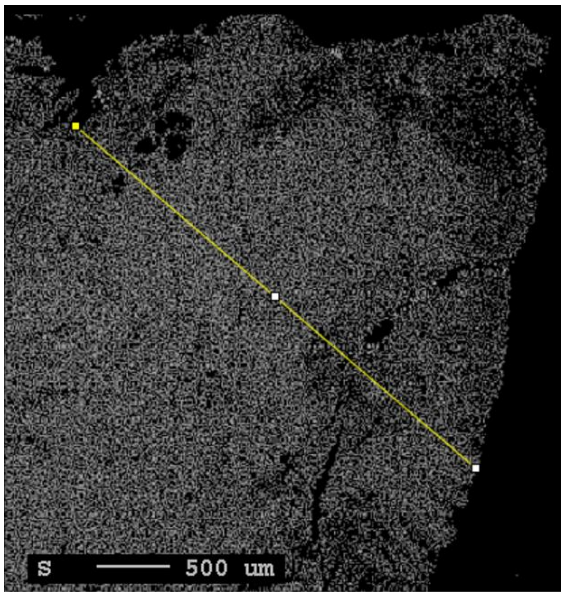
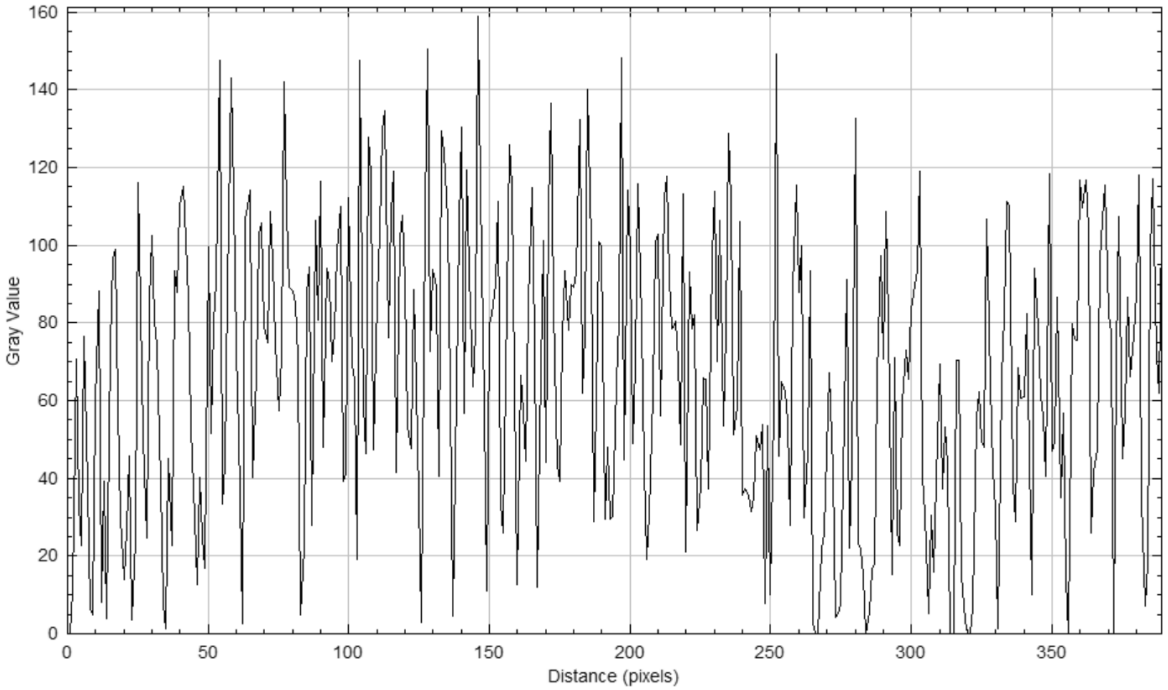


Figure 30

Grayscale image of AC cross section EPMA scan:



Profile intensity plot of the greyscale changes across the draw line shown in above image:



EPMA scan from repeat sample:

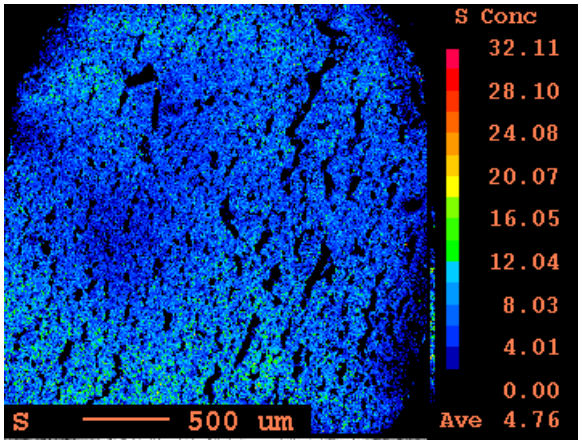
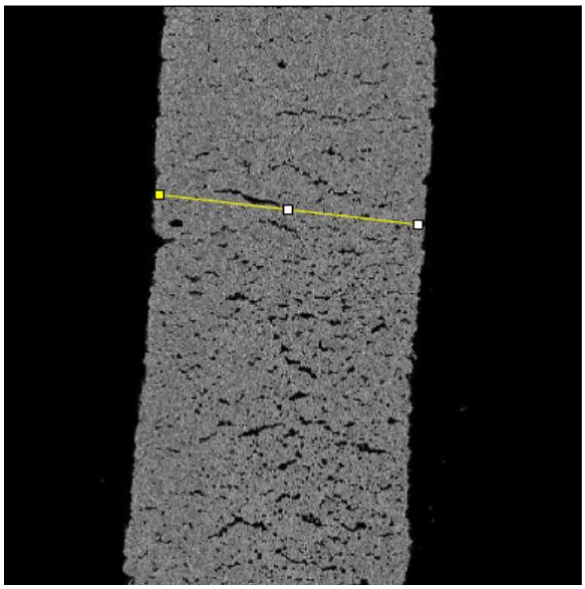
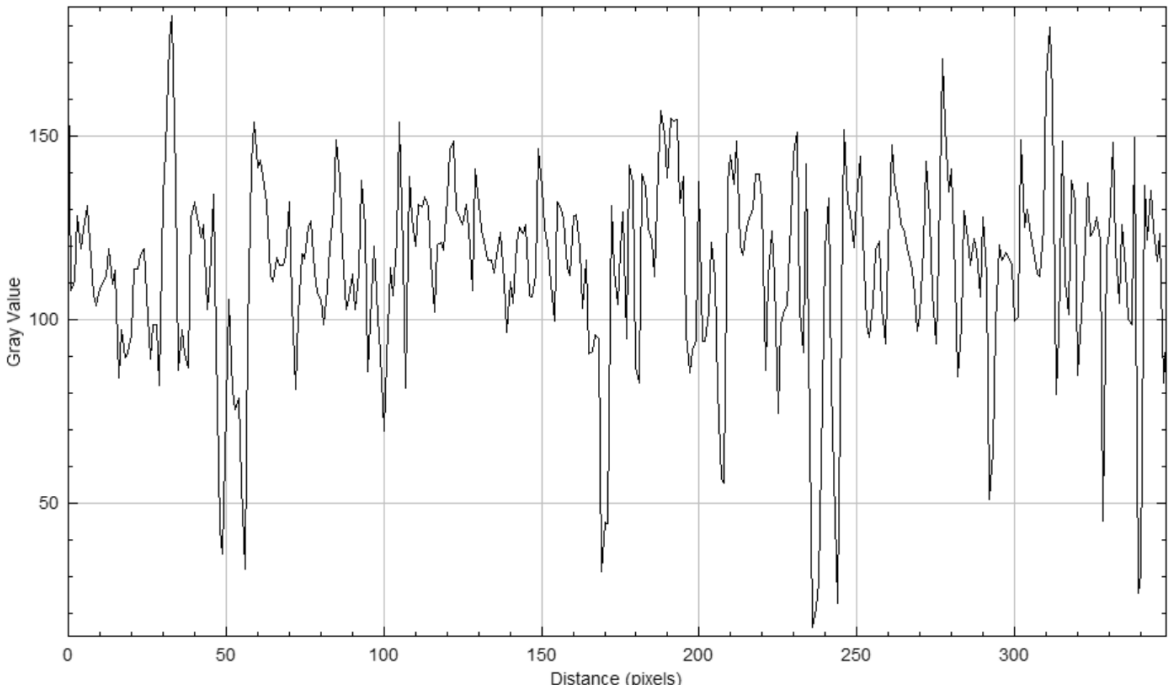


Figure 32

Grayscale image of AC cross section EPMA scan:



Profile intensity plot of the greyscale changes across the draw line shown in above image:



EPMA scan from repeat sample:

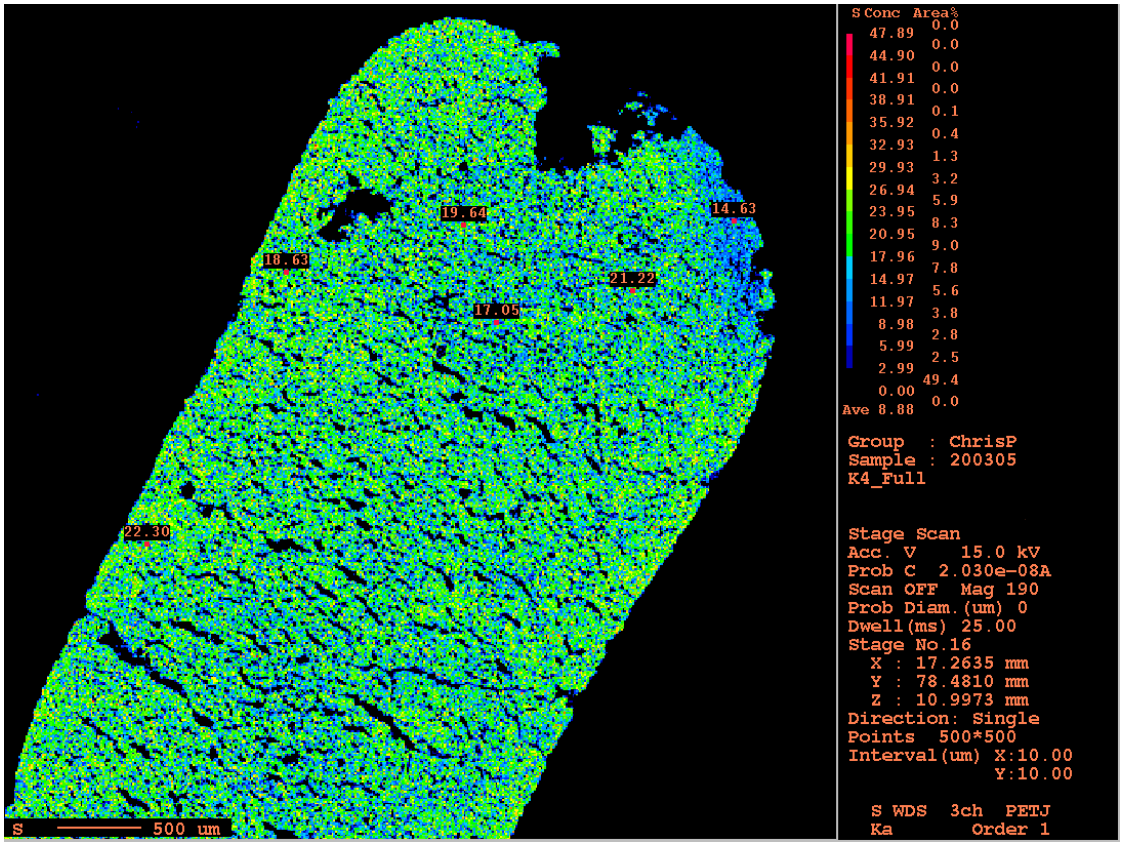
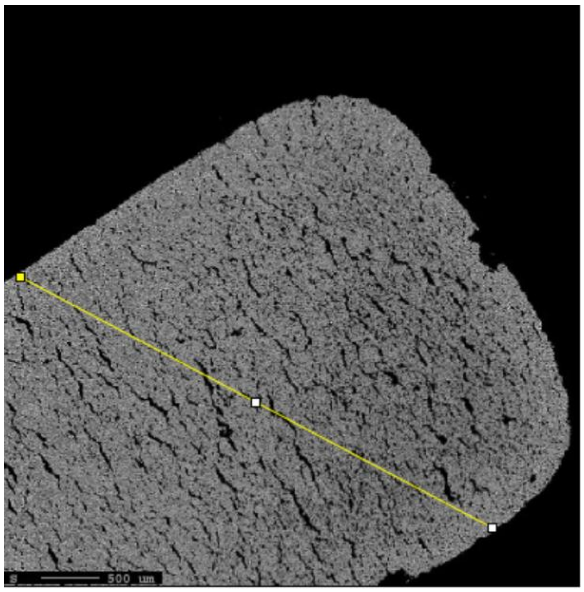


Figure 35

Grayscale image of AC cross section EPMA scan:



Profile intensity plot of the greyscale changes across the draw line shown in above image:

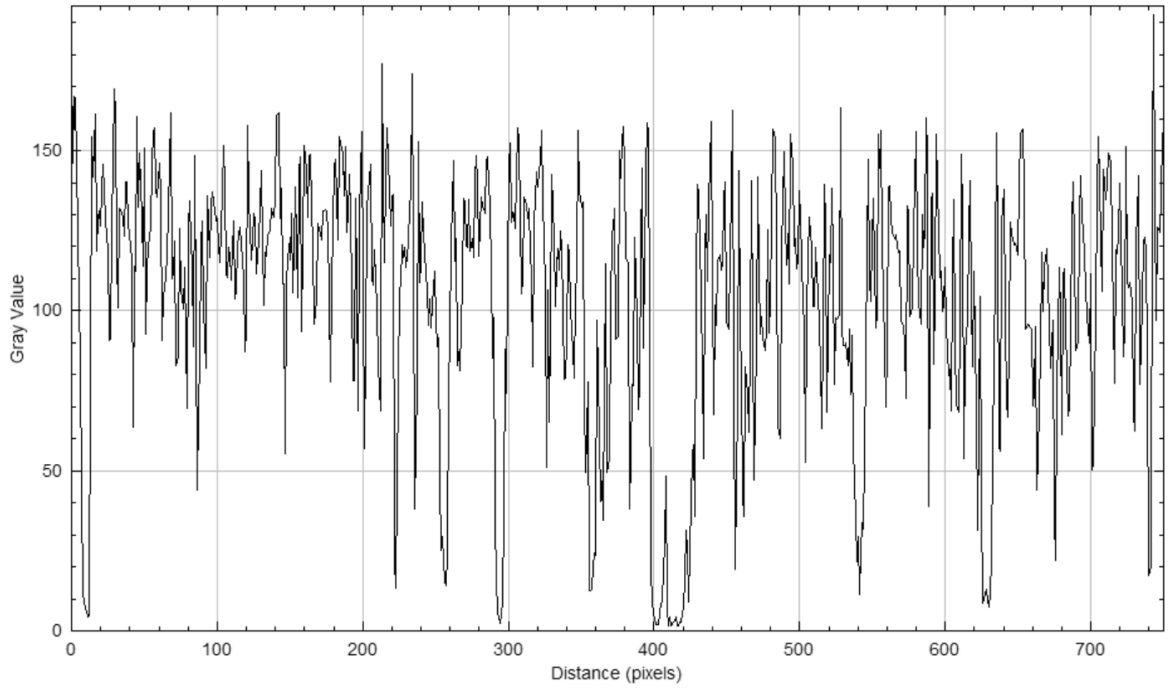
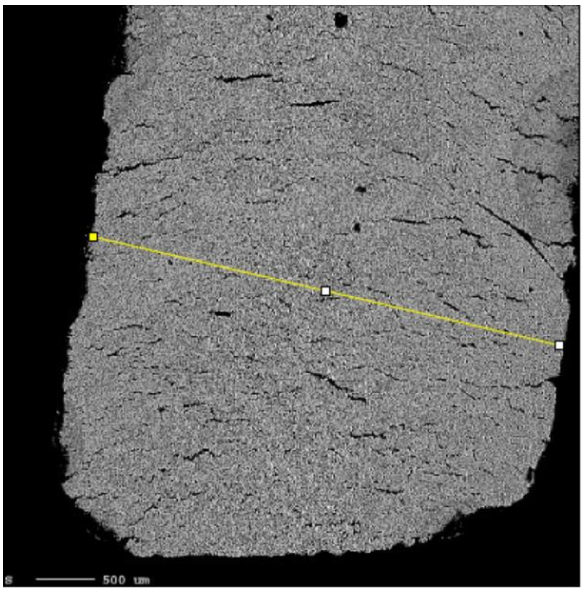
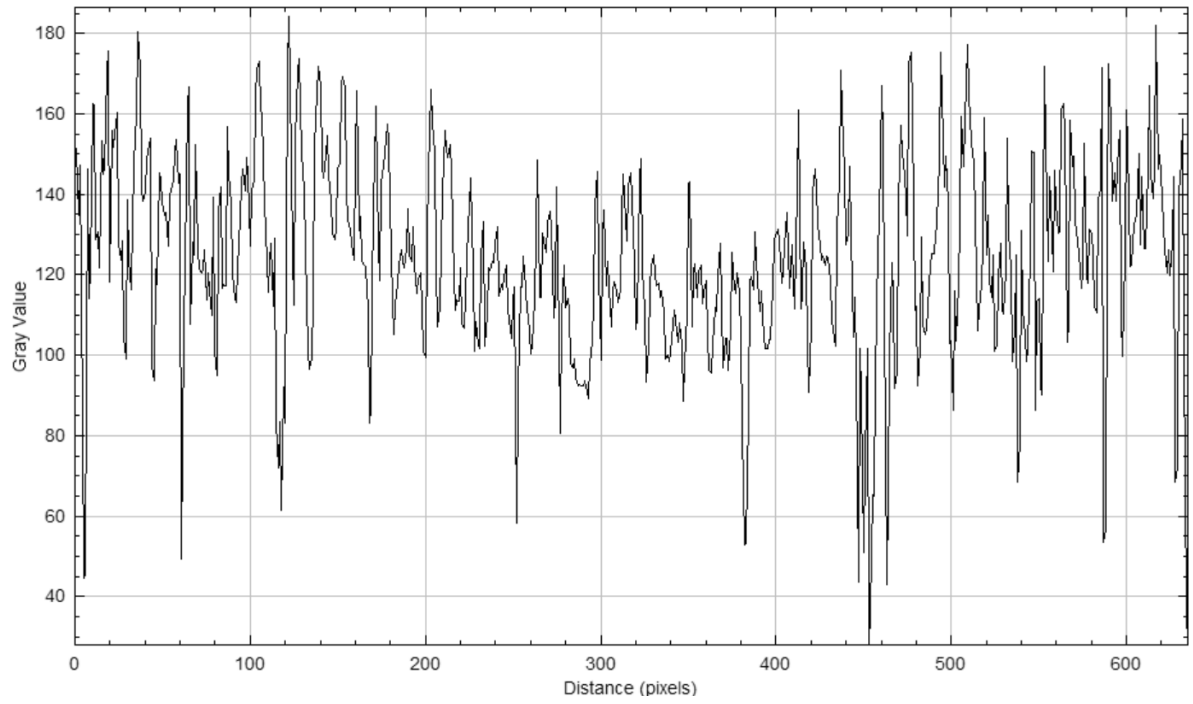


Figure 38

Grayscale image of AC cross section EPMA scan:



Profile intensity plot of the greyscale changes across the draw line shown in above image:



EPMA scan from repeat sample:

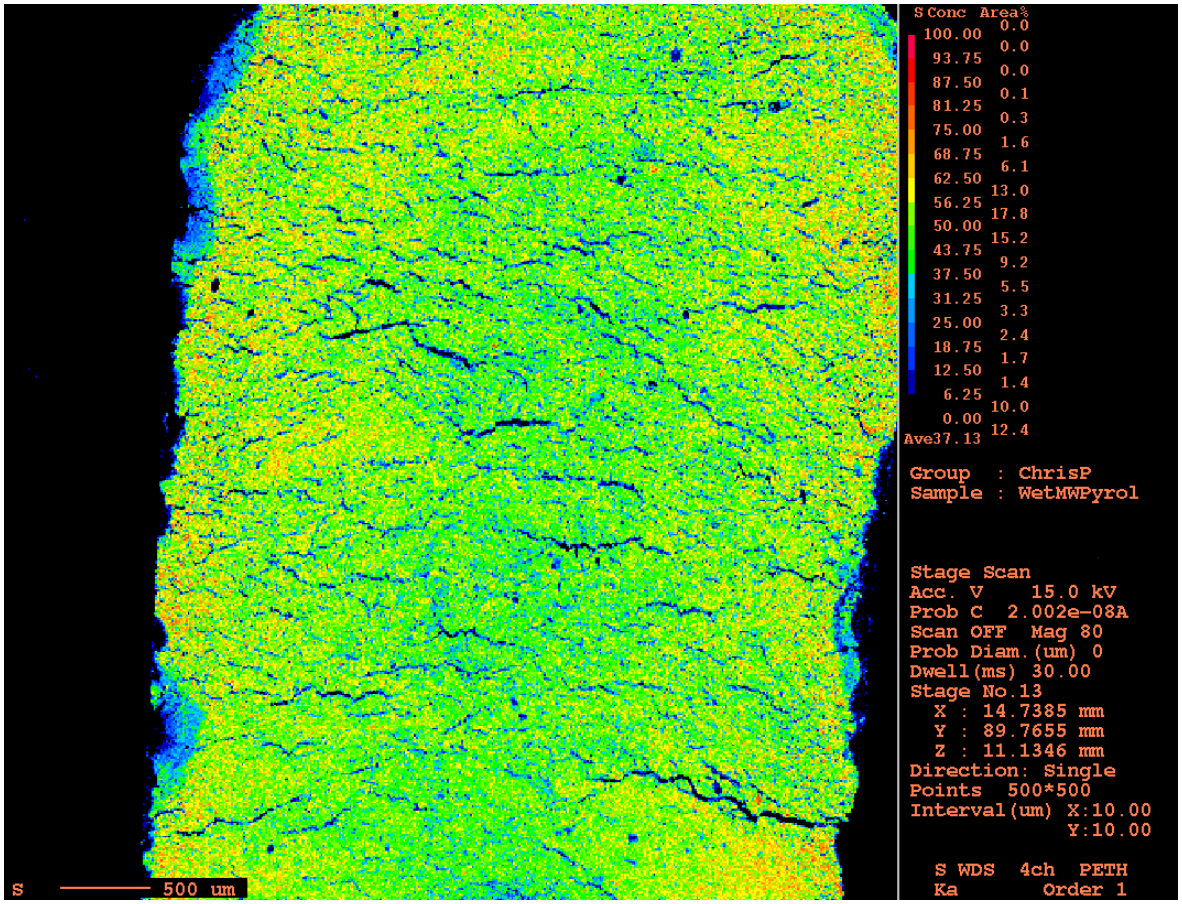
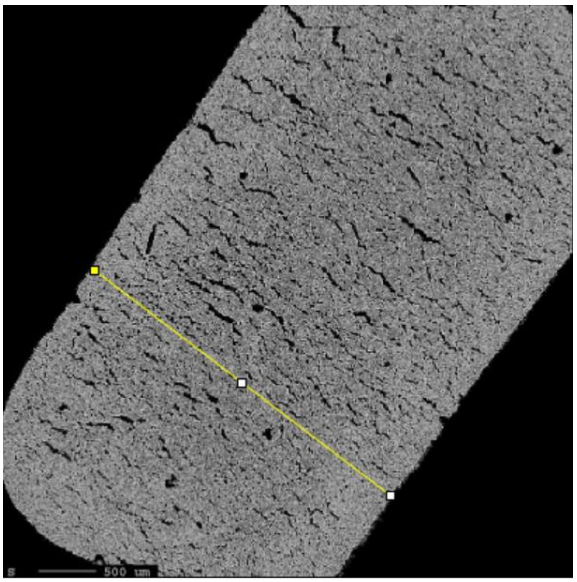
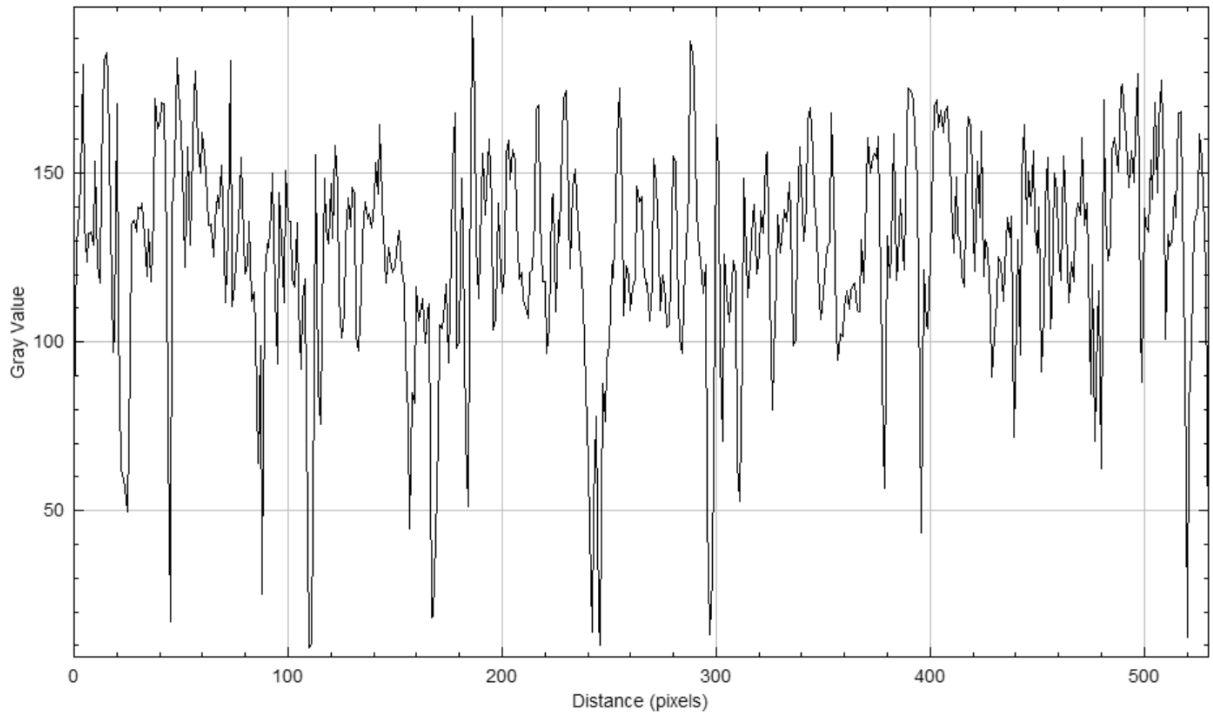


Figure 39

Grayscale image of AC cross section EPMA scan:



Profile intenisty plot of the greyscale changes across the draw line shown in above image:



EPMA scan from repeat sample:

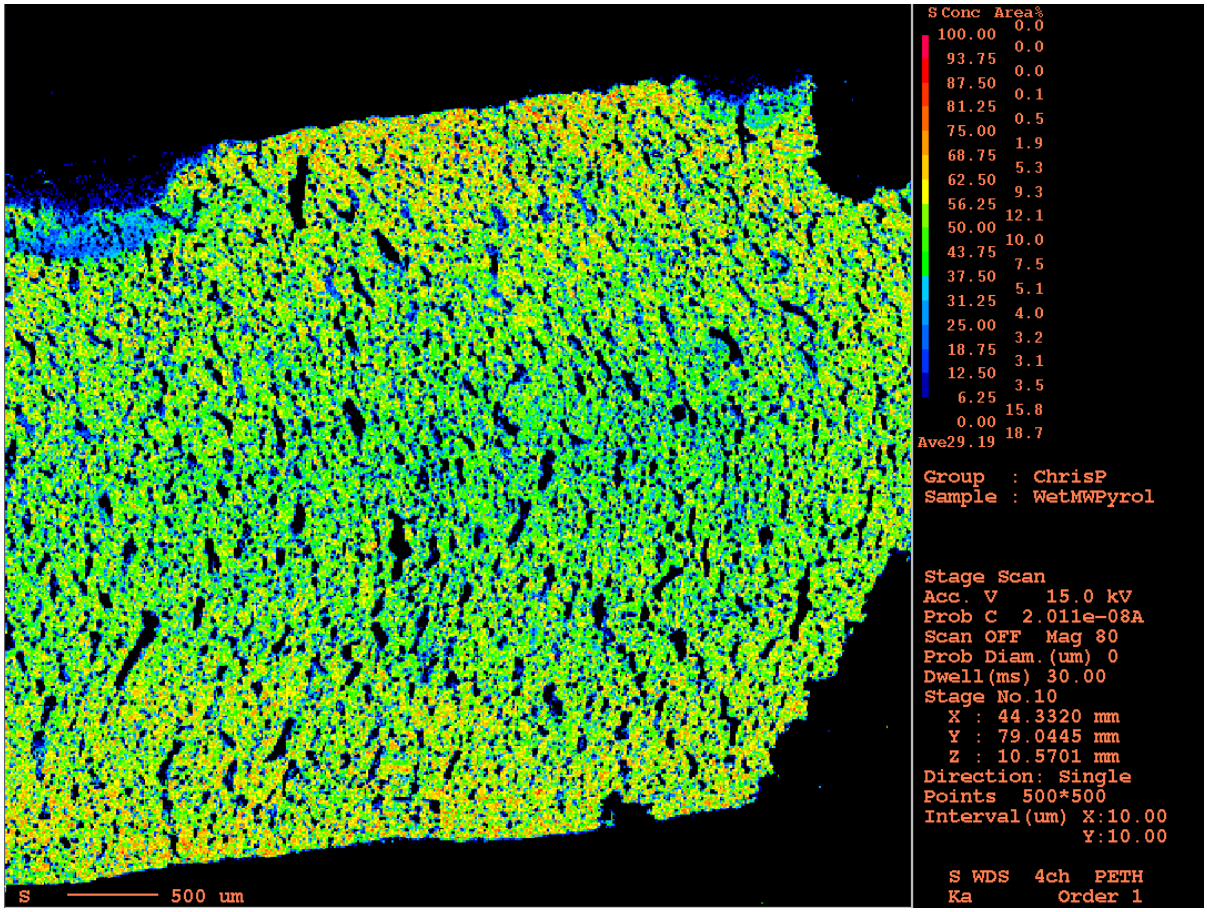
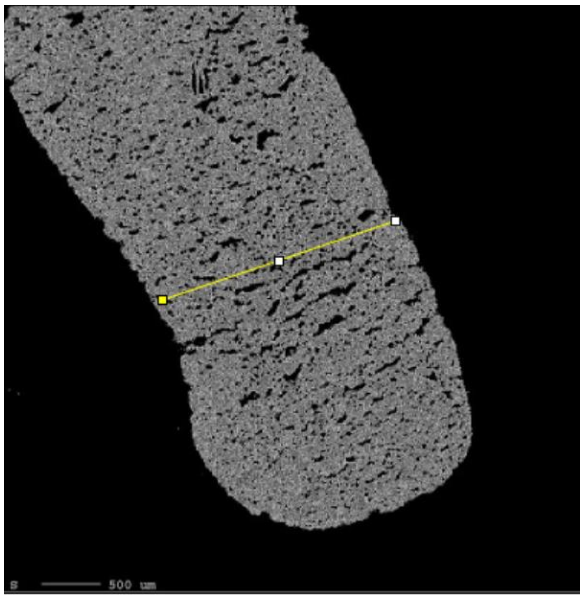


Figure 47

Grayscale image of AC cross section EPMA scan:



Profile intensity plot of the greyscale changes across the draw line shown in above image:

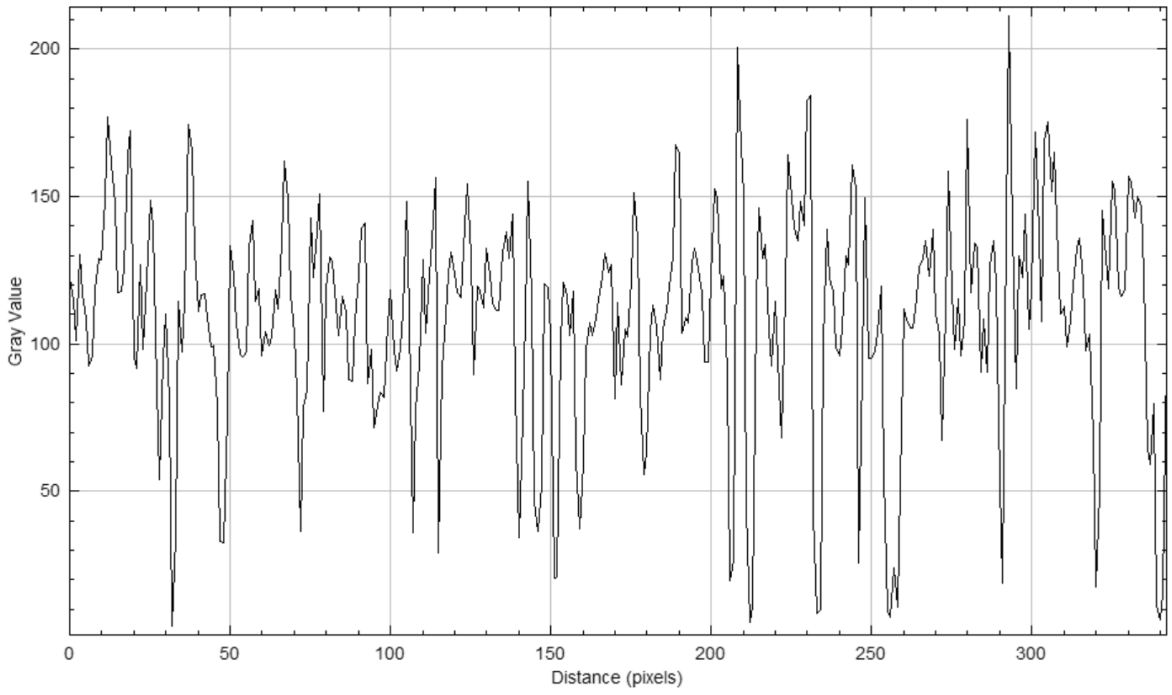
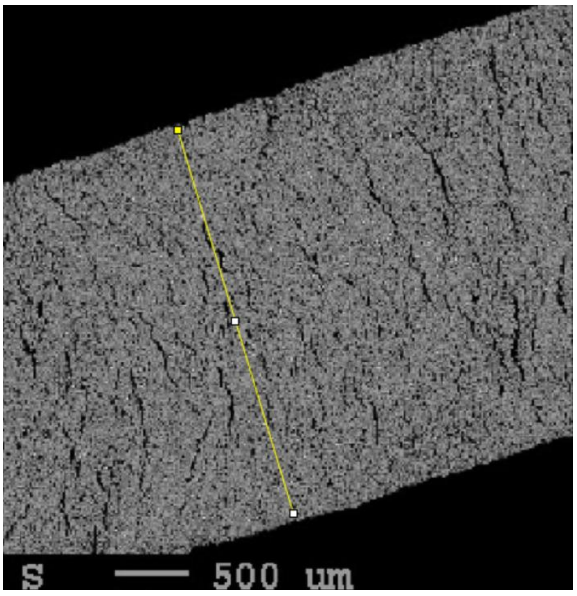
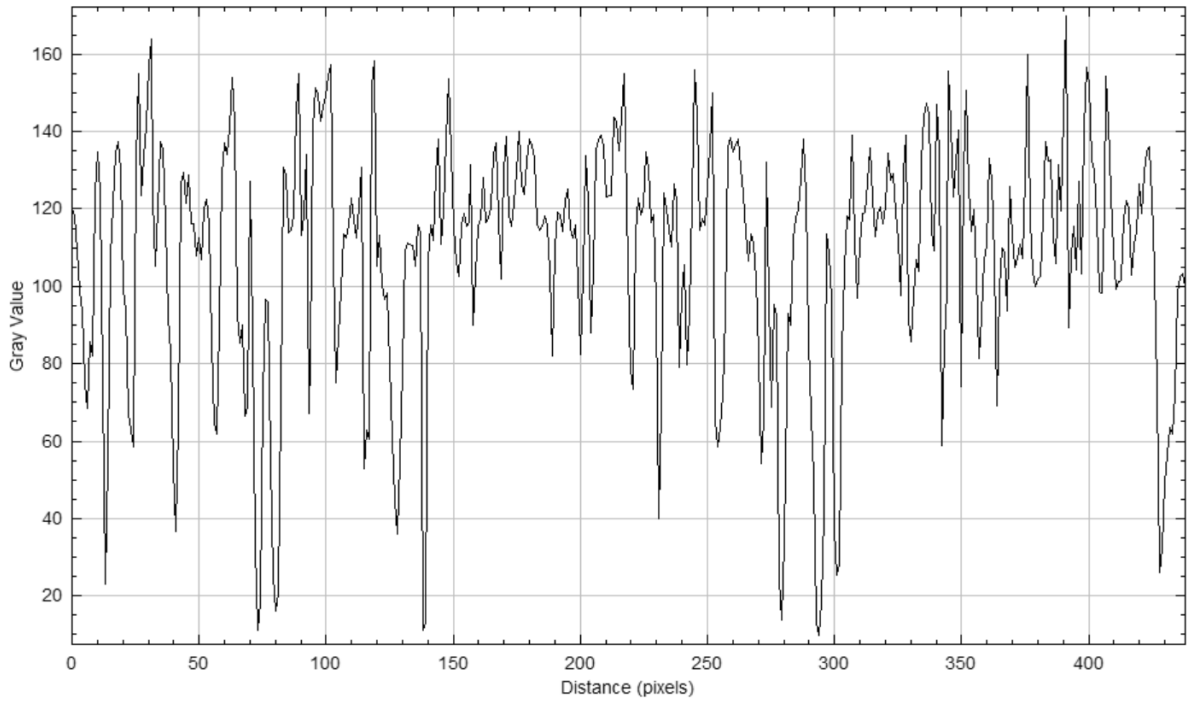


Figure 51

Grayscale image of AC cross section EPMA scan:



Profile intensity plot of the greyscale changes across the draw line shown in above image:



EPMA scan from repeat sample:

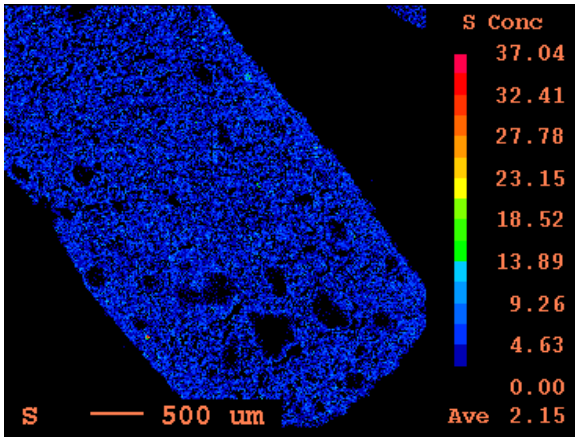
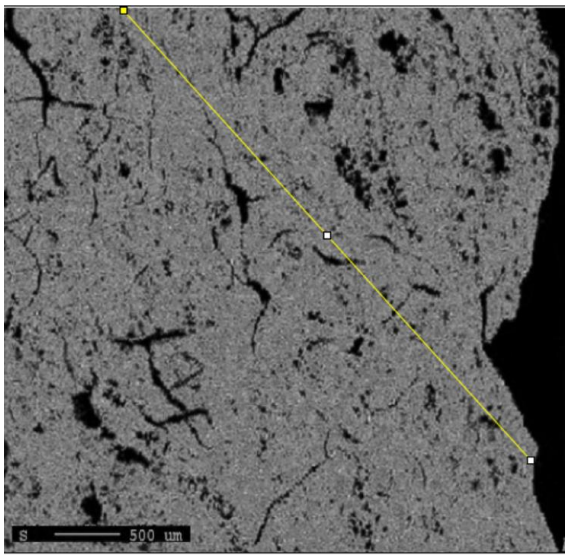
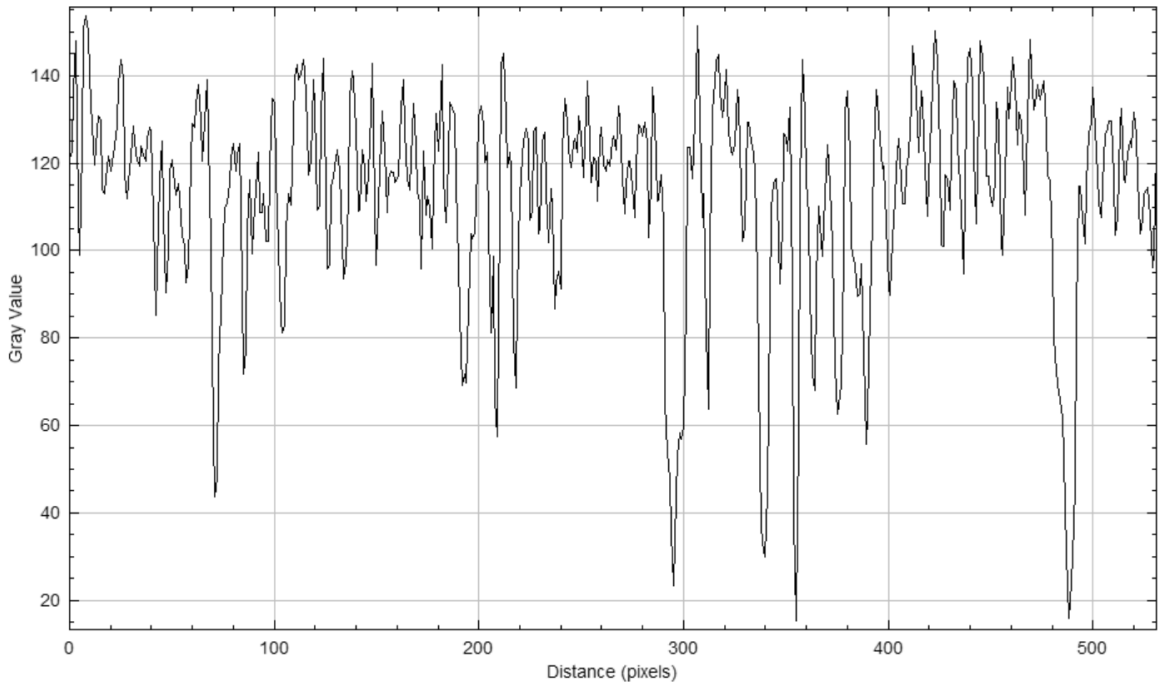


Figure 56

Grayscale image of AC cross section EPMA scan:



Profile intensity plot of the greyscale changes across the draw line shown in above image:



EPMA scan from repeat sample:

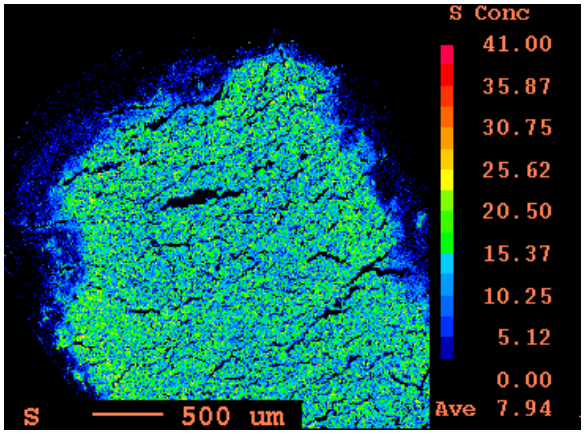
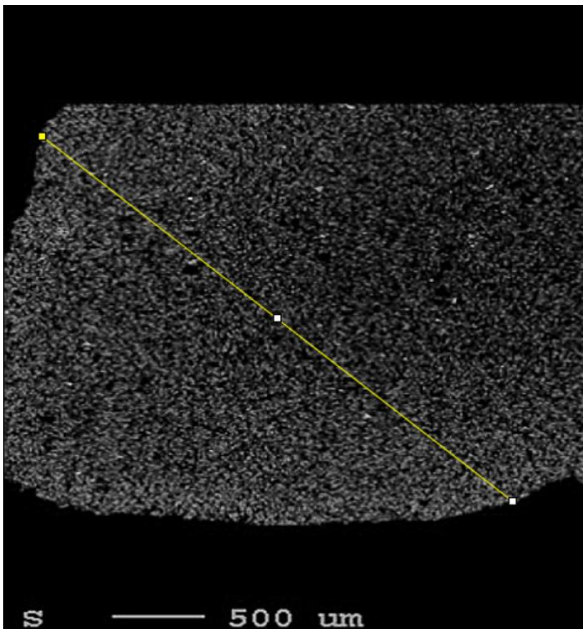
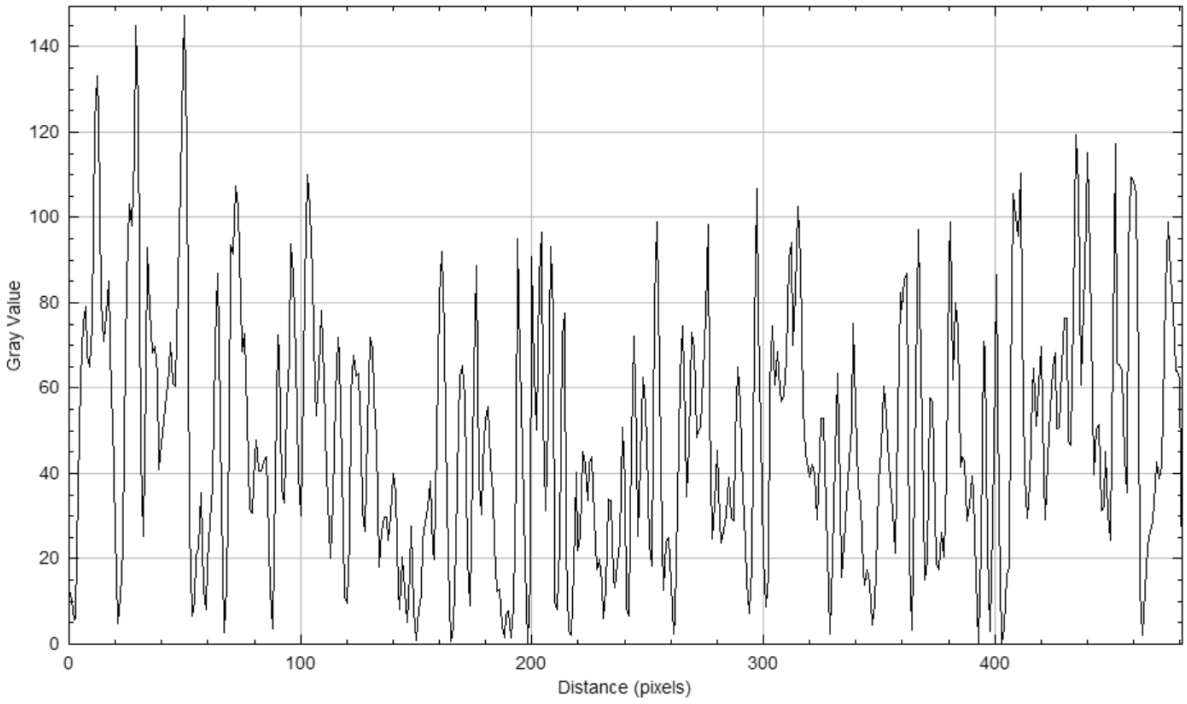


Figure 61

Grayscale image of AC cross section EPMA scan:



Profile intensity plot of the greyscale changes across the draw line shown in above image:



EPMA scan from repeat sample:

